

Journal of Polymer Science

Part A-2: Polymer Physics

Contents

C. W. PYUN: Some Probability Relations in Multicomponent Copolymers.....	577
S. OSAKI, S. UEMURA, and Y. ISHIDA: Effects of a Static Electric Field upon Dielectric Properties of Poly(vinylidene Fluoride) and Poly(vinyl Fluoride).....	585
T. P. WALLACE: Size-Distribution Analysis of Polymer Latex Systems by Use of the Extrema in the Angular Light-Scattering Pattern: II. The Polarization Ratio	595
R. E. KELCHNER and J. J. AKLONIS: Measurement of the Stress-Relaxation Modulus in the Primary Transition Region.....	609
C. W. PYUN and T. G. FOX: Polymerization Mechanisms and Stereosequence Distributions: A Monomer-Dimer Model.....	615
L. LAPČÍK and L. VALKO: Kinetic Study of Dissolution of Poly(vinyl Chloride) in Cyclohexanone.....	633
D. R. BUCHANAN: Analysis of Small-Angle X-Ray Diffraction from Polymers....	645
A. N. GENT and A. J. KINLOCH: Adhesion of Viscoelastic Materials to Rigid Substrates. III. Energy Criterion for Failure.....	659
O. YANO and Y. WADA: Dynamic Mechanical and Dielectric Relaxations of Polystyrene Below the Glass Temperature.....	669
G. C. BERRY: Thermodynamic and Conformational Properties of Polystyrene. III. Dilute Solution Studies on Branched Polymers.....	687
M. MEEKS and J. L. KOENIG: Laser-Raman Spectra of Vinyl Chloride-Vinylidene Chloride Copolymers.....	717
R. C. PENWELL, R. S. PORTER, and S. MIDDLEMAN: Determination of the Pressure Coefficient and Pressure Effects in Capillary Flow.....	731
A. H. BEGG and D. PUGH: Electronic States at Defects in Infinite Polyenes....	747
P. F. LESSE: Generalizations of the Diffusion Equation.....	755
NOTES	
L. H. TUNG: Calculation of Long-Chain Branching Distribution from Combined GPC, Sedimentation, and Intrinsic Viscosity Experiments.....	759
B. HARTMANN and J. JARZYNSKI: Ultrasonic Propagation in the Vicinity of the Glass Transition of a Poly(Carborane Siloxane).....	763
INFORMATION FOR CONTRIBUTORS.....	767

Journal of Polymer Science Part A-2: Polymer Physics

Board of Editors: H. Mark · C. G. Overberger · T. G. Fox

Advisory Editors:

R. M. Fuoss · J. J. Hermans · H. W. Melville · G. Smets

Editor: T. G. Fox **Associate Editors:** E. F. Casassa · H. Markovitz

Advisory Board:

G. Allen	G. Gee	S. Krimm	R. Simha
F. R. Anderson	A. N. Gent	M. Kurata	W. P. Slichter
W. O. Baker	W. E. Gibbs	R. F. Landel	T. L. Smith
H. Benoit	S. Gratch	P. H. Lindenmeyer	W. O. Statton
F. A. Bovey	C. A. J. Hoeve	L. Mandelkern	R. S. Stein
A. M. Bueche	J. D. Hoffman	B. Maxwell	W. H. Stockmayer
R. H. Cole	R. E. Hughes	L. Nielsen	M. Takayanagi
H. Eisenberg	H. D. Keith	A. Peterlin	A. V. Tobolsky
J. D. Ferry	A. Keller	R. S. Porter	K. Wolf
E. W. Fischer	A. J. Kovacs	F. Price	B. Wunderlich
P. J. Flory	G. Kraus	G. V. Schulz	
H. Fujita	W. R. Krigbaum	A. R. Shultz	

The Journal of Polymer Science is published in four sections as follows: Part A-1, Polymer Chemistry, monthly; Part A-2, Polymer Physics, monthly; Part B, Polymer Letters, monthly; Part C, Polymer Symposia, irregular.

Published monthly by Interscience Publishers, a Division of John Wiley & Sons, Inc., covering one volume annually. Publication Office at 20th and Northampton Sts., Easton, Pa. 18042. Executive, Editorial, and Circulation Offices at 605 Third Avenue, New York, N.Y. 10016. Second-class postage paid at Easton, Pa. Subscription price, \$325.00 per volume (including Parts A-1, B, and C). Foreign postage \$15.00 per volume (including Parts A-1, B, and C).

Copyright © 1971 by John Wiley & Sons, Inc. All rights reserved. No part of this publication may be reproduced by any means, nor transmitted, nor translated into a machine language without the written permission of the publisher.

Some Probability Relations in Multicomponent Copolymers

CHONG WHA PYUN, *Mellon Institute, Carnegie-Mellon University,
Pittsburgh, Pennsylvania 15213*

Synopsis

It was previously shown that for a stationary random copolymer of A, B, and C, we have in general $p(AB) + p(AC) = p(BA) + p(CA)$, etc., in place of $p(AB) = p(BA)$ which is valid for a stationary binary copolymer. Here, $p(AB)$ for example, is the probability that a randomly picked pair of consecutive comonomers in the polymer consists of an A followed by a B. For a stationary ternary copolymer produced by a first-order Markovian addition mechanism, we show that $P_{AB}P_{BC}P_{CA}/P_{AC}P_{CB}P_{BA} = \kappa$, where κ is a constant characteristic of a particular set of three monomers but independent of its composition. Here, P_{AB} is the conditional probability of finding a monomer of B given that its immediate predecessor is an A. We further show that if the individual rate constants of the monomer additions involved take a special form such as used in the Alfrey-Price $Q-e$ scheme, then we have $\kappa = 1$ irrespective of the kinds of monomers, and in addition we have $p(AB) = p(BA)$, $p(AC) = p(CA)$, etc. Thus, although these latter results were previously proposed by Ham as an alternative basis to supplant the $Q-e$ scheme, they may rather be regarded as mathematical consequences of special assumptions adopted for the form of the individual rate constants. For a stationary random copolymer of four components A, B, C, and D, we have $p(AB) + p(AC) + p(AD) = p(BA) + p(CA) + p(DA)$, etc., in general. For a first-order Markovian four-component copolymer, we show that there are seven different combinations of the conditional probabilities that are constants ($\kappa_1, \kappa_2, \dots, \kappa_7$) independent of the monomer composition. Again, if we assume the same special form for the rate constants involved, we find that all the seven constants $\kappa_1, \kappa_2, \dots, \kappa_7$ reduce to unity and $p(XY) = p(YX)$ for $X, Y, = A, B, C, D$.

The Alfrey-Price $Q-e$ scheme^{1,2} is often used to correlate monomer structure and reactivity in free-radical copolymerization. The central assumption of the scheme is that the rate constant k_{AB} of adding a monomer of the species B to the free-radical chain end of A monomer unit may be expressed as

$$k_{AB} = P_A Q_B \exp \{-e_A e_B\} \quad (1)$$

where the subscripted letters on the right side are the quantities characteristic of the monomer species denoted.

Recently, Ham proposed,³ for ternary copolymerization of the monomers A, B, and C, the following relation as "a more direct and possibly more precise means than the $Q-e$ scheme" and as based on "a logical and easily discernible concept,"

$$P_{AB}P_{BC}P_{CA} = P_{AC}P_{CB}P_{BA} \quad (2)$$

where P_{AB} , for example, is the conditional probability of adding a monomer B to the growing chain end given that the end consists of an A monomer unit. The conditional probabilities can be expressed in terms of the rate constants and the monomer concentrations in the feed.⁴ Denoting the concentration of A by [A] and so on, we have for, say P_{AB} ,

$$P_{AB} = \frac{k_{AB}[B]}{k_{AA}[A] + k_{AB}[B] + k_{AC}[C]} = \frac{k_{AB}[B]}{\sum_r k_{AX}[X]} \quad (3)$$

where the summation in the denominator extends over $X = A, B,$ and $C.$

Ham also proposed³ the following relations for ternary copolymerization

$$p(AB) = p(BA) \quad (4a)$$

$$p(BC) = p(CB) \quad (4b)$$

$$p(CA) = p(AC) \quad (4c)$$

where $p(AB)$, for example, is the probability that a randomly selected pair of consecutive monomers in the copolymer consists of an A followed by a B. This pair or doublet probability may also be expressed in terms of the singlet probability $p(A)$ and the conditional probability P_{AB} as follows

$$p(AB) = p(A)P_{AB} \quad (5)$$

Ham derived³ eqs. (4) using eq. (2). His derivation, therefore, depends on the validity of eq. (2). However, eq. (2) was given without a proof. Therefore, the question that whether eqs. (2) and (4) are more general than eq. (1) or not is not answered.

It is well known⁵ that for any stationary random binary copolymer of A and B, eq. (4a) holds. It has also been pointed out⁶ that the corresponding general relations applicable to any stationary random ternary copolymer of A, B, and C are not eqs. (4) but

$$p(AB) + p(AC) = p(BA) + p(CA) \quad (6a)$$

$$p(BA) + p(BC) = p(AB) + p(CB) \quad (6b)$$

$$p(CA) + p(CB) = p(AC) + p(BC) \quad (6c)$$

(Note that the sum of any two of these relations gives the third one.) These are consequences of the general properties⁵ of stationary random sequences of three-component systems and are valid for any stationary ternary comonomer distribution, whether Markovian or non-Markovian.

In the following, we restrict our discussion to stationary ternary copolymers formed by a first-order Markov addition mechanism as was implicitly assumed both in the Alfrey-Price $Q-e$ scheme and in the Ham relations. This is the case when the addition of a monomer to the growing polymer chain is controlled by the terminal monomer unit but not by the penultimate and other units in the chain. A further assumption is that the copolymer chain is sufficiently long so that the effects of the chain initiation and

termination steps are negligible compared that of the propagation step. In order to keep the conditional probabilities constant during the polymerization, the monomer composition in the feed is required to remain constant.

Under the circumstances, we have the following ternary copolymer composition⁷ in the copolymer:

$$\begin{aligned} p(A) &= d_A/d \\ p(B) &= d_B/d \\ p(C) &= d_C/d \end{aligned} \quad (7a)$$

where

$$\begin{aligned} d_A &= P_{BA}P_{CA} + P_{BA}P_{CB} + P_{BC}P_{CA} \\ d_B &= P_{AB}P_{CA} + P_{AB}P_{CB} + P_{AC}P_{CB} \\ d_C &= P_{AB}P_{BC} + P_{AC}P_{BA} + P_{AC}P_{BC} \\ d &= d_A + d_B + d_C \end{aligned} \quad (7b)$$

The singlet probability distribution $p(X)$, where $X = A, B,$ and C as given by eqs. (7), satisfies the normalization condition as expected

$$p(A) + p(B) + p(C) = 1$$

Another relation equally general as eqs. (7) is obtained by taking the ratio of $P_{AB}P_{BC}P_{CA}$ and $P_{AC}P_{CB}P_{BA}$ and by substituting eq. (3) and its analogs for the other conditional probabilities. We obtain

$$P_{AB}P_{BC}P_{CA}/P_{AC}P_{CB}P_{BA} = k_{AB}k_{BC}k_{CA}/k_{AC}k_{CB}k_{BA} \quad (8)$$

Or, in terms of the reactivity ratios as defined by

$$\begin{aligned} r_{AB} &= k_{AA}/k_{AB} \\ r_{BA} &= k_{BB}/k_{BA}, \text{ etc.}, \end{aligned}$$

we have

$$P_{AB}P_{BC}P_{CA}/P_{AC}P_{CB}P_{BA} = r_{AC}r_{CB}r_{BA}/r_{AB}r_{BC}r_{CA} \quad (9)$$

We note that eqs. (8) and (9) hold irrespective of the monomer composition and any special assumption such as that of the equimolar monomer concentrations is not necessary.

Although the conditional probabilities P_{XY} ($X, Y = A, B, C$) themselves are functions of the monomer composition in the feed or in the copolymer, the particular combination of six conditional probabilities as given on the left side of eq. (8) or (9) is independent of the monomer composition, that is, we have

$$\frac{P_{AB}P_{BC}P_{CA}}{P_{AC}P_{CB}P_{BA}} = \kappa \quad (10)$$

where κ is a constant characteristic of each ternary copolymerization system (and temperature) irrespective of its monomer composition. If one

of the rate constants in the numerator or in the denominator on the right side of eq. (8) is very small compared to the other five, κ can be very small or very large. The same conclusion can be reached with the left side of eq. (10). Since there are no other *a priori* restriction on the values of P_{XY} except the normalization conditions

$$P_{XA} + P_{XB} + P_{XC} = 1 \quad X = A, B, C \quad (11)$$

κ can have, in principle, any nonnegative value between zero and infinity. Mayo has previously proposed eq. (10) combined with eq. (9) as a potentially useful means of correlating copolymerization data.⁸

Now, Ham's relation as given by eq. (2) is very special in two respects: firstly, the value of κ does not change if one moves from one set of three monomers (A, B, C) to another set (X, Y, Z); secondly, this common value of κ is unity. In order to have this very special relation of Ham, we must obviously have some restriction on the form of the rate constants (or reactivity ratios) in view of eqs. (8) and (9). One such restriction presents itself in the form of the Alfrey-Price *Q-e* scheme.^{1,2} If this scheme is accepted, we can readily derive eq. (2) by substituting eq. (1) into eq. (8). More generally, if the rate constants take the form of

$$k_{AB} = f(I_A)g(J_B)h(K_AK_B), \quad (12)$$

then we get eq. (2). Here, $f(I_A)$ is a function of a property I of the monomer A and so forth. There are many other possible forms of k_{AB} which will also reduce κ to unity. An example is k_{AB} of eq. (12) with $h(K_AK_B)$ replaced by $h(K_AL_B + L_AK_B)$, where K and L are two different properties of the monomers. However, no physically meaningful scheme of such form other than the Alfrey-Price assumption has been proposed to our knowledge.

If we try a modified *Q-e* scheme,^{2,9}

$$k_{AB} = P_A Q_B \exp \{-e_A^* e_B\} \quad (13)$$

which takes into account the difference in the e factors of the free monomer and of the terminal monomer already incorporated in the chain, we see that κ is not equal to unity unless we happen to have

$$e_A^* e_B + e_B^* e_C + e_C^* e_A = e_A^* e_C + e_C^* e_B + e^*_{BEA} \quad (14)$$

Once eq. (2) is established, we see immediately that

$$p(ABCA) = p(ACBA) \quad (15a)$$

which results from eq. (2) by multiplying its both sides by $p(A)$. Similarly, multiplication by $p(B)$ yields

$$p(BCAB) = p(BACB) \quad (15b)$$

and so on. A further simplification which amounts to eliminating the both end letters in each parentheses is possible. For example, we take the ratio of $p(A)$ to $p(B)$ using Eq. (7):

$$\frac{p(A)}{p(B)} = \frac{P_{BA}}{P_{AB}} \left[\frac{1 + P_{BC}P_{CA}/P_{BA}(P_{CA} + P_{CB})}{1 + P_{AC}P_{CB}/P_{AB}(P_{CA} + P_{CB})} \right] \quad (16)$$

Now, if eq. (2) holds, we have

$$P_{BC}P_{CA}/P_{BA} = P_{AC}P_{CB}/P_{AB}$$

Identification of this equality in the second factor on the right side of eq. (16) reduces the factor to unity, yielding eq. (4a) in this example. Similarly eqs. (4b) and (4c) can be obtained from eqs. (7) and (2). A similar derivation was previously given³ by Ham.

We note here that eq. (2) can be readily derived if eqs. (4) are assumed. We first rewrite eqs. (4) as follows:

$$\begin{aligned} p(A)/p(B) &= P_{BA}/P_{AB} \\ p(B)/p(C) &= P_{CB}/P_{BC} \\ p(C)/p(A) &= P_{AC}/P_{CA} \end{aligned} \quad (17)$$

If we multiply each side of these three equations together, we obtain eq. (2).

To summarize, we first see that for any stationary ternary copolymer produced by a first-order Markovian monomer addition mechanism, we have in general eqs. (6) and (10) in addition to the composition equations [eqs. (7)]. However, if we impose special restrictions such as eq. (1) or eq. (12) on the form of the rate constants involved, then eq. (10) simplifies to eq. (2) and eqs. (6) reduce to eqs. (4). Thus, Ham's relations [eqs. (2) and (4)] may be considered as mathematical consequences of physical assumption as manifested by eq. (1) or eq. (12). Although Ham's relations are more general than the original assumption [eq. (1)] of the *Q-e* scheme in the sense that they can also be derived from Eq. (12) and its analogs, at present we have no physically significant examples of such forms other than eq. (1).

Similar conclusions can be drawn for higher multicomponent copolymers. For any stationary random comonomer sequence distribution in four-component copolymers of A, B, C, and D, we have

$$\begin{aligned} p(AB) + p(AC) + p(AD) &= p(BA) + p(CA) + p(DA) \\ p(BA) + p(BC) + p(BD) &= p(AB) + p(CB) + p(DB) \\ p(CA) + p(CB) + p(CD) &= p(AC) + p(BC) + p(DC) \\ p(DA) + p(DB) + p(DC) &= p(AD) + p(BD) + p(CD) \end{aligned} \quad (18)$$

any three of which are independent, corresponding to eqs. (6) for the three-component case.

If the comonomer sequence distribution is first-order Markovian, then by using the four-component analogs of eqs. (3) we have

$$P_{AB}P_{BC}P_{CD}P_{DA}/P_{AD}P_{DC}P_{CB}P_{BA} = \kappa_1 \quad (19a)$$

$$P_{AB}P_{BD}P_{DC}P_{CA}/P_{AC}P_{CD}P_{DB}P_{BA} = \kappa_2 \quad (19b)$$

$$P_{AC}P_{CB}P_{BD}P_{DA}/P_{AD}P_{DB}P_{BC}P_{CA} = \kappa_3 \quad (19c)$$

$$P_{AB}P_{BC}P_{CA}/P_{AC}P_{CB}P_{BA} = \kappa_4 \quad (19d)$$

$$P_{AB}P_{BD}P_{DA}/P_{AD}P_{DB}P_{BA} = \kappa_5 \quad (19e)$$

$$P_{AC}P_{CD}P_{DA}/P_{AD}P_{DC}P_{CA} = \kappa_6 \quad (19f)$$

$$P_{BC}P_{CD}P_{DB}/P_{BD}P_{DC}P_{CB} = \kappa_7 \quad (19g)$$

where κ_i ($i = 1, 2, \dots, 7$) are the constants expressing the appropriate ratios of the rate constants for individual monomer addition steps. These seven relations of eqs. (19) correspond to eq. (10) for the ternary copolymer. Again, if there is no restriction on the form of the rate constants involved, different κ_i will take different values ranging from zero to infinity. However, if we assume eq. (1) or eq. (12) for the rate constants, we have

$$\kappa_i = 1 \quad i = 1, 2, \dots, 7 \quad (20)$$

In order to see whether we can obtain the simple relations analogous to eqs. (4) under the assumption of eq. (1) or eq. (12), we first obtain the copolymer composition equations for the stationary first-order Markovian comonomer sequence distributions in general. The normalized singlet probability distribution for the four-component copolymer may be obtained, for example, by solving the set of eq. (21):

$$\begin{aligned} p(A) + p(B) + p(C) + p(D) &= 1 \\ p(A)P_{AA} + p(B)P_{BA} + p(C)P_{CA} + p(D)P_{DA} &= p(A) \\ p(A)P_{AB} + p(B)P_{BB} + p(C)P_{CB} + p(D)P_{DB} &= p(B) \\ p(A)P_{AC} + p(B)P_{BC} + p(C)P_{CC} + p(D)P_{DC} &= p(C) \end{aligned} \quad (21)$$

The solution may be written as follows:

$$\begin{aligned} p(A) &= d_A/d \\ p(B) &= d_B/d \\ p(C) &= d_C/d \end{aligned} \quad (22a)$$

$$p(D) = d_D/d \quad (22b)$$

$$d = d_A + d_B + d_C + d_D$$

where

$$d_A = \begin{vmatrix} P_{BA} & P_{CA} & P_{DA} \\ P_{BB}^{-1} & P_{CB} & P_{DB} \\ P_{BC} & P_{CC}^{-1} & P_{DC} \end{vmatrix} \quad (22c)$$

$$d_B = - \begin{vmatrix} P_{AA}^{-1} & P_{CA} & P_{DA} \\ P_{AB} & P_{CB} & P_{DB} \\ P_{AC} & P_{CC}^{-1} & P_{DC} \end{vmatrix} \quad (22d)$$

$$d_C = \begin{vmatrix} P_{AA}^{-1} & P_{BA} & P_{DA} \\ P_{AB} & P_{BB}^{-1} & P_{DB} \\ P_{AC} & P_{BC} & P_{DC} \end{vmatrix} \quad (22e)$$

$$d_D = - \begin{vmatrix} P_{AA}^{-1} & P_{CA} & P_{DA} \\ P_{AB} & P_{BB}^{-1} & P_{DB} \\ P_{AC} & P_{BC} & P_{DC} \end{vmatrix} \quad (22f)$$

As an example, let us calculate $p(A)/p(B)$:

$$\frac{p(A)}{p(B)} = \frac{d_A}{d_B} = \frac{P_{BA}(K + L)}{P_{AB}(K + M)} \quad (23a)$$

where

$$K = (P_{CA} + P_{CB})P_{DC} + (1 - P_{CC})(P_{DA} + P_{DC}) \quad (23b)$$

$$L = [P_{BC}P_{CA}(1 - P_{DD}) + P_{BD}P_{DA}(1 - P_{CC}) + P_{BC}P_{CD}P_{DA} + P_{BD}P_{DC}P_{CA}]/P_{BA} \quad (23c)$$

$$M = [P_{AC}P_{CB}(1 - P_{DD}) + P_{AD}P_{DB}(1 - P_{CC}) + P_{AD}P_{DC}P_{CB} + P_{AC}P_{CD}P_{DB}]/P_{AB} \quad (23d)$$

By using $\kappa_1 = 1$, $\kappa_5 = 1$, $\kappa_1 = 1$, and $\kappa_2 = 1$ successively to the four terms on the right sides of eqs. (23c) and (23d), we obtain

$$L = M \quad (24)$$

if the rate constants involved take the form of eq. (1) or eq. (12). Thus, within the framework of the Alfrey-Price $Q-e$ scheme, we have again

$$p(AB) = p(BA)$$

and similar calculations for all the other pairs lead to¹⁰

$$p(XY) = p(YX) \quad X, Y = A, B, C, D \quad (25)$$

corresponding to eqs. (4).

These special relations eqs. (2), (4), (20), and (25) also hold for any stationary "Bernoullian" copolymer with any number of components, since then we have

$$P_{AA} = P_{BA} = P_{CA} = \dots = P(A), \text{ etc.}$$

and

$$p(AB) = p(A)p(B) = p(BA), \text{ etc.}$$

In this case, however, the problem discussed above becomes rather trivial.

If we know that eq. (1) or (12) holds and therefore the relations of the type of Eqs. (4) or (25) are valid, we have the following simplification in ternary and higher-order multicomponent copolymers. It often happens

that experimental techniques do not allow us to distinguish $p(XY)$ and $p(YX)$ where $X, Y = A, B, C$, etc. and $X \neq Y$, and then what we observe is the sum of the two

$$p(XY_vYX) \equiv p(XY) + p(YX) \quad (26)$$

Even under these circumstances, however, if we have eqs. (4) or (25), we can immediately write

$$p(XY) = p(YX) = 1/2p(XY_vYX) \quad (27)$$

References

1. T. Alfrey and C. C. Price, *J. Polym. Sci.*, **2**, 101 (1947).
2. T. Alfrey and L. J. Young, in *Copolymerization*, G. E. Ham, Ed., Interscience, New York, 1964, Chap. 2.
3. G. E. Ham, in *Copolymerization*, G. E. Ham, Ed., Interscience, New York (1964). Chap. 1; *J. Polym. Sci. A*, **2**, 2735 (1964).
4. G. Goldfinger and T. Kane, *J. Polym. Sci.*, **3**, 462 (1948).
5. B. D. Coleman and T. G. Fox, *J. Polym. Sci. A*, **1**, 3183 (1963).
6. C. W. Pyun, *J. Polym. Sci. A-2*, **8**, 1111 (1970).
7. T. Alfrey and G. Goldfinger, *J. Chem. Phys.*, **12**, 322 (1944).
8. F. R. Mayo, *J. Polym. Sci. A*, **2**, 4207 (1964).
9. L. A. Wall, *J. Polym. Sci.*, **2**, 542 (1947).
10. G. E. Ham, *J. Polym. Sci. A*, **2**, 4181 (1964).

Received June 25, 1970

Revised August 6, 1970

Effects of a Static Electric Field upon Dielectric Properties of Poly(vinylidene Fluoride) and Poly(vinyl Fluoride)

SHIGEYOSHI OSAKI, SHINSAKU UEMURA,
and YŌICHI ISHIDA, *Department of Polymer Science,
Faculty of Science, Osaka University, Toyonaka, Osaka, Japan*

Synopsis

Dielectric measurements on poly(vinylidene fluoride) at higher temperatures result in anomalously large values of ϵ' and ϵ'' at lower frequencies. When a static field is applied, a drastic decrease of ϵ' and ϵ'' occurs. The effects of a static field can be summarized as follows: (1) the field effect upon ϵ' and ϵ'' is more significant at lower frequencies; (2) with increasing field strength, the rate of decrease of ϵ' and ϵ'' with time becomes greater and the ultimate values are smaller; (3) when the field is removed, ϵ' and ϵ'' recover but the ultimate recovery is incomplete; (4) the field effect depends strongly on temperature. Such behavior seems to be attributable to the displacement of ionic impurities and to their electrolysis. These results provided a method to remove the contribution of ionic impurities to ϵ' and ϵ'' and to measure the relaxation process due only to dipoles of a polymer. The application of this method revealed the dielectric high temperature absorption which had been masked by the ionic conduction in poly(vinyl fluoride).

Introduction

Dielectric measurements of polymers at higher temperatures result in anomalously large values of ϵ' and ϵ'' , the real and imaginary parts of the complex dielectric constant, at lower frequencies. Such a tendency is marked in some polymers,¹⁻³ for instance, poly(vinylidene fluoride). We have found that a drastic decrease of ϵ' and ϵ'' results when a static electric field is applied to poly(vinylidene fluoride). This has made it possible to measure unambiguously the highest temperature relaxation process. Furthermore, we have studied the effects of the electric field under various conditions and have made similar studies on poly(vinyl fluoride).

Experimental

Poly(vinylidene fluoride) film was supplied by Kureha Chemical Co., Ltd. The average degree of polymerization was 1000, and the head-to-head bonding content was determined to be about 5% by NMR. The material contained trace amounts of ionic impurities such as Na, Ca, Al, S, and Cl.

Specimens for dielectric measurements were prepared by remolding at 200°C and quenching into liquid nitrogen. The thickness of the specimens was about 0.1 mm. The density was determined to be 1.767 g/cm³ by the flotation method. For a quenched specimen the melting curve obtained by a differential scanning calorimeter (DSC) exhibited double peaks (at 167.0°C and 172.5°C). Annealing at 160°C for 24 hr changed the density to 1.779 g/cm³, and the DSC measurement showed a single peak (173°C). Longer annealing at the same temperature did not further raise the density and the melting point. The crystal form was identified as the α form by means of x-ray and infrared analysis.

The poly(vinyl fluoride) film used was Tedlar (manufactured by E. I. du Pont de Nemours and Co.). The specimens for dielectric measurements were prepared by annealing at 160°C for one day in order to avoid shrinkage. Their thickness was about 0.15 mm.

The surfaces of the specimens were sputtered with silver to form electrodes. The mutual inductance bridge was similar to that originally developed by Cole and Gross.⁴ Since it accommodated three terminal electrodes, the data were free from errors due to edge and surface effects as well as the stray capacity effect. Special care was taken to avoid the effect of humidity, by placing the specimen in a sealed cell with dry nitrogen. The design of the apparatus has been previously described in detail.⁵

After a static electric field had been applied to a specimen at constant temperature for a certain period, the field was removed and the dielectric measurement was carried out without delay. The field strength was varied from 0.1 kV/cm to 30 kV/cm.

Mechanical measurements for poly(vinyl fluoride) were carried out by means of the direct-reading dynamic viscoelastomer,⁶ which is similar to the Vibron instrument manufactured by Toyo Measuring Instrument Co., Ltd.

Results and Discussion

Poly(vinylidene fluoride) shows three kinds of dielectric relaxation processes.⁷ The highest temperature relaxation process is apt to be superimposed upon another process. As a result, the value of ϵ' or ϵ'' at lower frequencies is very large, as is shown in Figures 1 and 2. This process has been generally presumed to be due to ionic conduction. If such an inference is correct, the process should be affected by a static electric field.

When a static field of 25 kV/cm was applied to a specimen at 160°C for 40 hr, a significant change was observed, as is shown in Figures 3 and 4. For instance, ϵ' at 6.25 Hz was reduced to $1/2$ and ϵ'' at 6.25 Hz to $1/200$. As one of factors which cause the decrease of ϵ' and ϵ'' , the effect of annealing should be considered, because ϵ' and ϵ'' for crystalline polymers change generally upon annealing. When a specimen was annealed at 160°C, a small change (Figs. 5 and 6) was observed, while a large change was caused by the field. That is, the effect of annealing is negligible compared with that of the field.

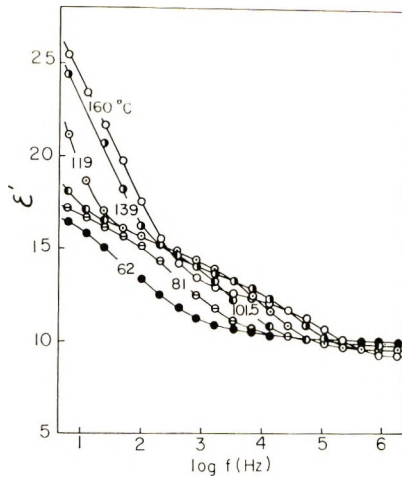


Fig. 1. Frequency dependence of ϵ' at various fixed temperatures for poly(vinylidene fluoride).

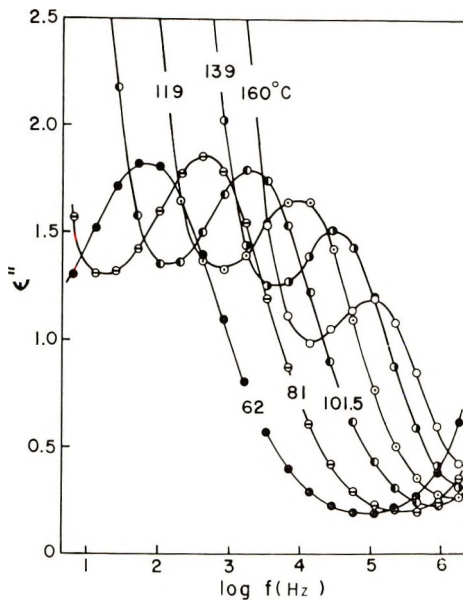


Fig. 2. Frequency dependence of ϵ'' at various fixed temperatures for poly(vinylidene fluoride).

On the other hand, the field effect is more significant at lower frequencies. This tendency can be clearly demonstrated by plotting $\Delta\epsilon''$, the decrease of ϵ'' in 25 hr, against frequency in Figure 7. This plot satisfies the equation:

$$\log \Delta\epsilon'' = A - B \log f$$

where A and B are constant. The constant B was nearly equal to unity and independent of temperature.

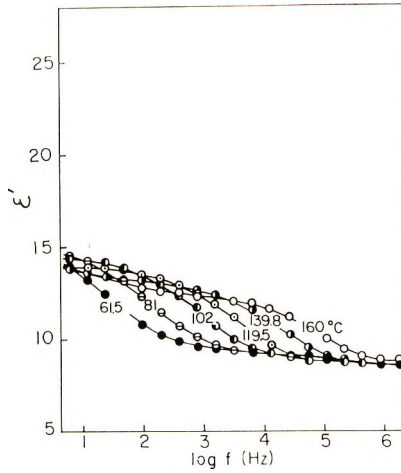


Fig. 3. Frequency dependence of ϵ' at various fixed temperatures for poly(vinylidene fluoride) to which a field of 25 kV/cm was applied at 160°C for 40 hr.

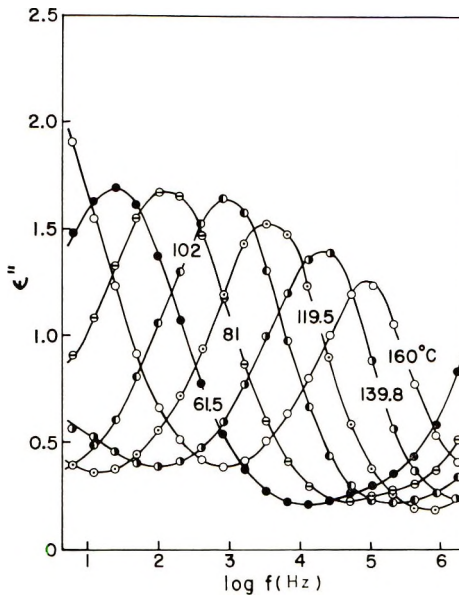


Fig. 4. Frequency dependence of ϵ'' at various fixed temperatures for poly(vinylidene fluoride) to which a field of 25 kV/cm was applied at 160°C for 40 hr.

It is expected that the rate of decrease of ϵ'' or ϵ' will be greater if the field strength is increased. The change of ϵ'' with time under three different field strengths was measured, as is shown in Figure 8. The highest field strength causes the most rapid change and gives the lowest asymptotic value.

When a static field is applied to a specimen, ϵ' and ϵ'' decrease rapidly, but increase again when the field is removed, as is shown in Figures 9 and 10.

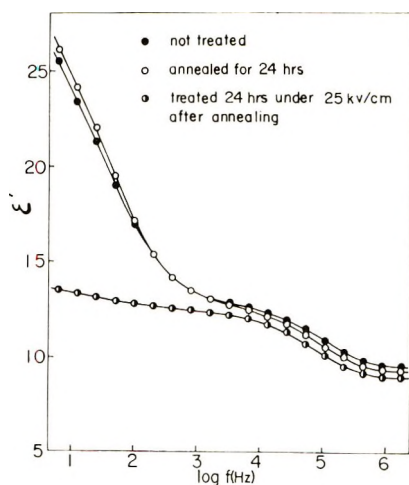


Fig. 5. Comparison between the effects of annealing and of a static electric field for ϵ' of poly(vinylidene fluoride) at 106°C .

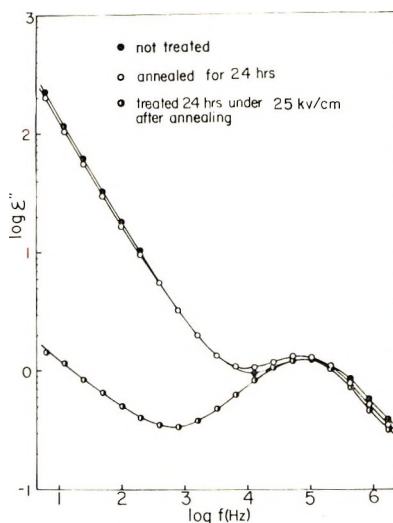


Fig. 6. Comparison between the effects of annealing and of a static electric field for ϵ'' of poly(vinylidene fluoride) at 160°C .

These changes appear to be interpretable in terms of the migration of ionic impurities. Ions initially distributed uniformly in the specimen are displaced towards the electrodes by a static field and concentrated. The concentration of ions results in reduction of their mobility. As a result, the contribution of the ions to complex dielectric constant diminishes, and hence ϵ' and ϵ'' decrease. The changes caused by the field cannot be instantaneous, since this process is due to the migration of ions.

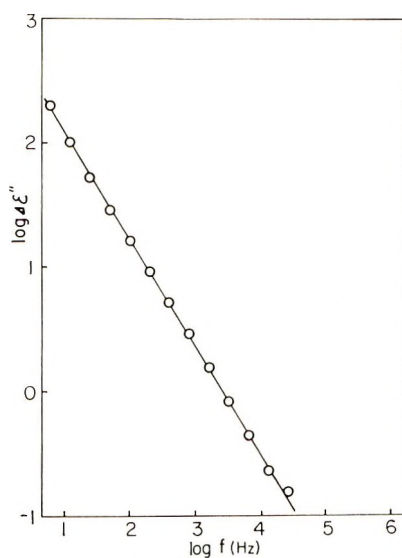


Fig. 7. Frequency dependence of decrease of ϵ'' caused by a static electric field; field, 25 kV/cm; 24 hr; 160°C.

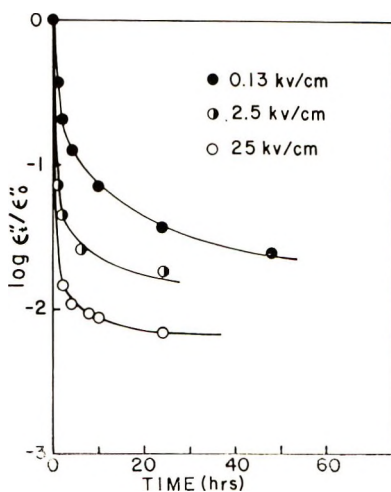


Fig. 8. Field strength dependence of the decrease of ϵ'' with time: ϵ_0'' , initial value; ϵ_t'' , value at time t ; 160°C.

If the decrease of ϵ' or ϵ'' is attributable to the migration of ions in a static electric field, the removal of the field should permit the diffusion of ions by thermal agitation and ϵ' or ϵ'' should again recover to the initial large value. When the static electric field is removed, the value of ϵ' or ϵ'' tends to increase, as is shown in Figures 9 and 10. The rate of recovery is very slow compared with the rate of decrease produced by the electric field. When the two rates are compared on the basis of the change in the first hour, the rate of recovery of ϵ'' owing to thermal agitation is only $1/20$ of

the rate of decrease caused by the field. The ultimate recovery is incomplete. The asymptotic values of ϵ' and ϵ'' in the recovery process depend on the strength of the static electric field and the temperature in the first step. The electrolysis of ionic impurities may account for this behavior. When a stronger field is applied at a higher temperature, the asymptotic

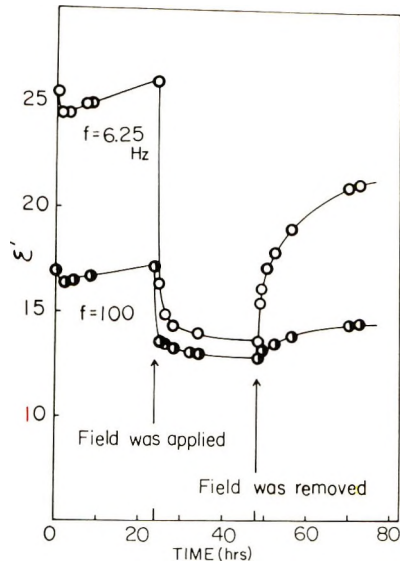


Fig. 9. Change of ϵ' with time. After the specimen was annealed at 160°C for 24 hr, a field of 25 kV/cm was applied for 24 hr at 160°C and then removed.

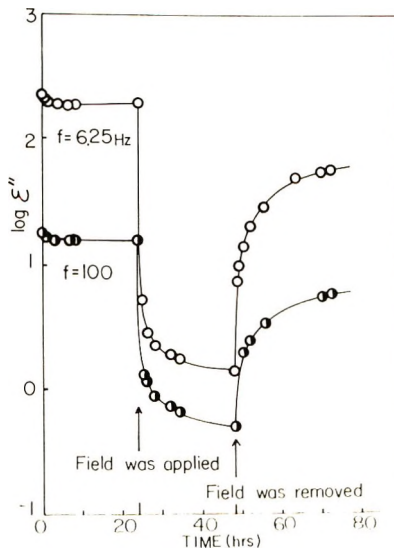


Fig. 10. Change of ϵ'' with time. After the specimen was annealed at 160°C for 24 hr, a field of 25 kV/cm was applied for 24 hr at 160°C and then removed.

value of ϵ'' or ϵ' in the recovery process is smaller, possibly because of more effective electrolysis.

We tried then to identify ionic impurities deposited on the silver electrodes. In order to remove the silver electrode without scratching the specimen, we made an amalgam by rolling a small mercury droplet over its surface. When this amalgam was analyzed by emission spectroscopy, the

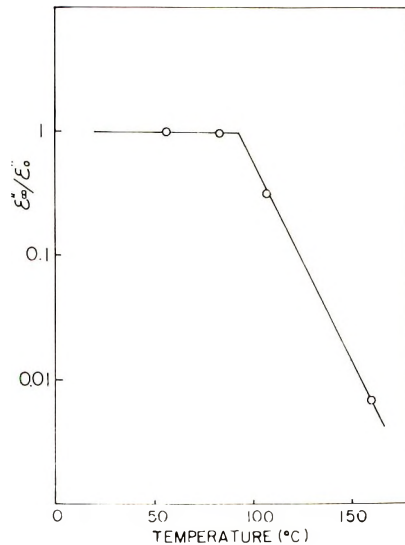


Fig. 11. Temperature dependence of decrease of ϵ'' caused by a static electric field. The ratio $\epsilon''_{\omega} / \epsilon''_0$ is used to represent the decrease of ϵ'' . ϵ''_{ω} , asymptotic value; ϵ''_0 , initial value; frequency, 6.25 Hz; field, 2.5 kv/cm.

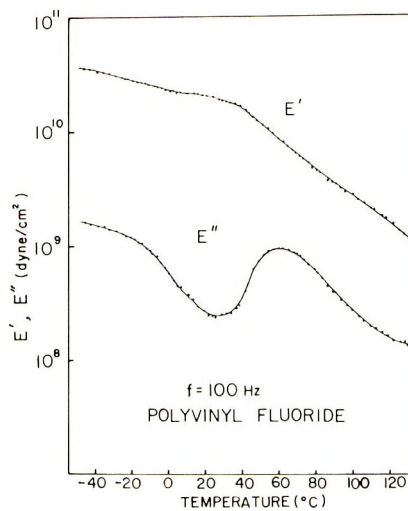


Fig. 12. Temperature dependence of the dynamic Young's moduli E' and E'' at 100 Hz for poly(vinyl fluoride).

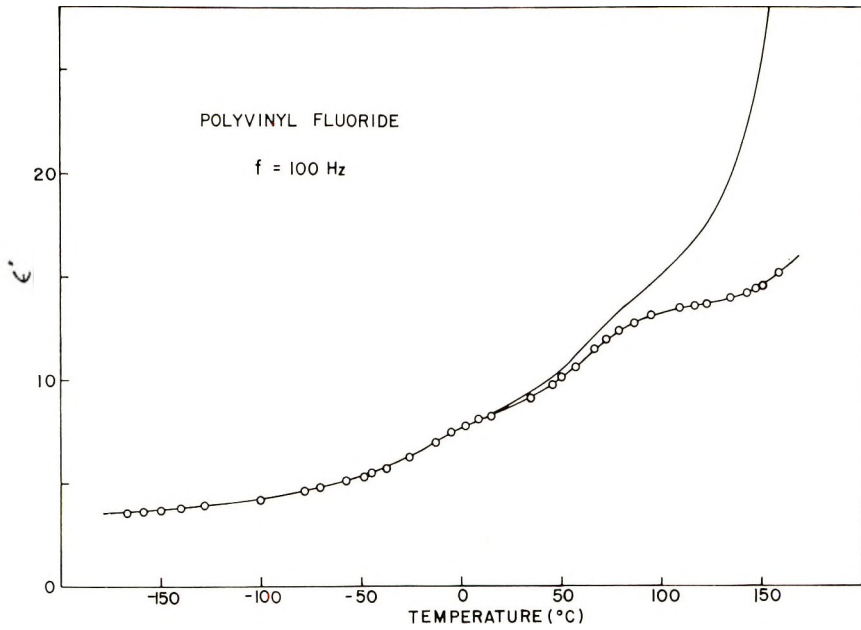


Fig. 13. Temperature dependence of ϵ' at 100 Hz for poly(vinyl fluoride): (—) original specimen; (—○—) after a field of 30 kV/cm had been applied for 36 hr at 155°C.

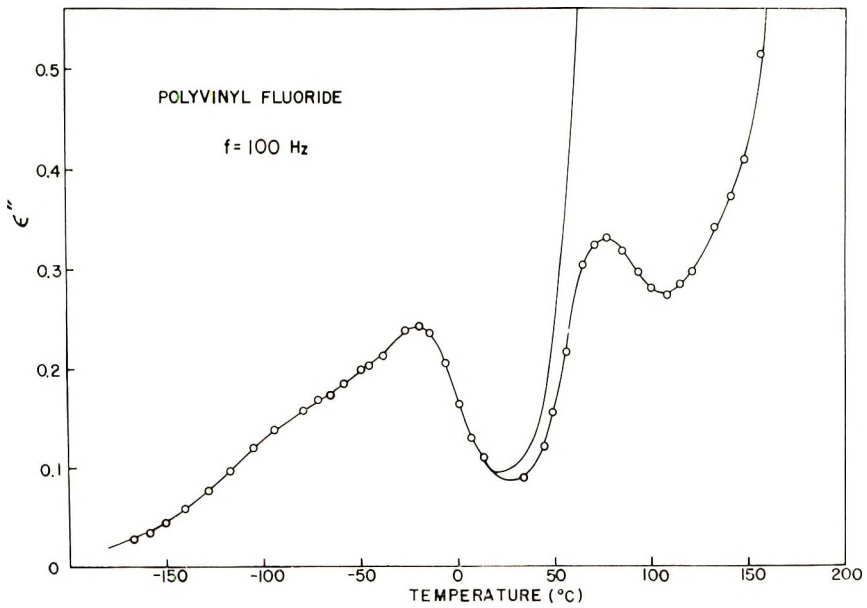


Fig. 14. Temperature dependence of ϵ'' at 100 Hz for poly(vinyl fluoride): (—) original specimen; (○) after a field of 30 kV/cm had been applied for 36 hr at 155°C.

presence of calcium was demonstrated. At present, other impurities have not been positively identified.

In order to test this conclusion further, we measured a specimen to which KCl had been added by the following way. After the film had been soaked in a saturated aqueous solution of KCl at 80°C for 3 days and dried at 100°C under vacuum for a day, it was remolded at 200°C. The values of ϵ' or ϵ'' at lower frequencies are much larger than those of the original specimen. The addition of NaCl or Na₂CO₃ caused a similar effect. When a static field was applied to the specimen containing added KCl, ϵ' and ϵ'' were reduced to values similar to those found for the original specimen when a static field was applied.

On the other hand, if the large values of ϵ' and ϵ'' at lower frequencies are caused by ionic impurities, the effect of the static electric field should depend strongly on temperature, since migration of ions requires large free volume. We measured the temperature dependence of the field effect. As is shown in Figure 11, the effect is obvious only above about 90°C, which seems to correspond to the onset of molecular motion in the crystalline regions of poly(vinylidene fluoride).

The high temperature dielectric absorption of poly(vinyl fluoride) previously could not be observed because of the predominant ionic conduction.^{3,8} On the other hand, as is shown in Figure 12, two kinds of absorptions were observed in mechanical measurements, as Schmieder and Wolf⁹ had found. We expected that the high-temperature absorption would appear in dielectric measurements when a static field was applied; and, in fact, application of a static field to poly(vinyl fluoride) revealed an absorption at the location corresponding to the high temperature absorption in mechanical measurements, as is shown in Figures 13 and 14.

We are grateful to Dr. M. Asahina and Miss H. Kakutani of Kureha Chemical Co., Ltd. for supplying the samples and to Dr. K. Hoashi for the measurement of poly(vinyl fluoride) by the viscoelastometer. We are also indebted to Prof. S. Seki for the use of the DSC and to Prof. H. Tadokoro for the use of the x-ray apparatus. Thanks are due to Prof. K. Yamafuji, Prof. Y. Yokoyama and Mr. N. Kawasaki for valuable discussion.

References

1. Y. Ishida, O. Amano, and M. Takayanagi, *Kolloid-Z.*, **172**, 129 (1960).
2. Y. Ishida, M. Watanabe, and K. Yamafuji, *Kolloid-Z.*, **200**, 48 (1964).
3. Y. Ishida and K. Yamafuji, *Kolloid-Z.*, **200**, 50 (1964).
4. R. H. Cole and P. M. Gross, *Rev. Sci. Instr.*, **20**, 252 (1949).
5. Y. Ishida, *Kolloid-Z.*, **168**, 29 (1960).
6. M. Takayanagi, *Mem. Fac. Eng. Kyushu Univ.*, **23**, 41 (1963).
7. H. Sasabe, S. Saito, M. Asahina, and H. Kakutani, *J. Polym. Sci.*, **7**, 1405 (1969).
8. R. Reddish, *Pure Appl. Chem.*, **5**, 723 (1962).
9. K. Schmieder and K. Wolf, *Kolloid-Z.*, **134**, 149 (1953).

Received July 13, 1970

Revised September 8, 1970

Size-Distribution Analysis of Polymer Latex Systems by Use of the Extrema in the Angular Light-Scattering Pattern: II. The Polarization Ratio

THOMAS P. WALLACE, *Department of Chemistry, Rochester Institute of Technology, Rochester, New York 14623*

Synopsis

Previously, the angular positions of the extrema of the polarization ratio have been utilized in light-scattering studies as a method of particle-size analysis under the assumption of monodisperse, spherical particles. Since the consequences of the existing finite polydispersity on this method of analysis was not assessed, the results are questionable. This work is concerned with (1) reporting the quantitative effects of a finite polydispersity on the method of analysis, (2) pointing out previous misuse of the method, and (3) revising the method of analysis to include polydispersity and the exact Mie calculations. The method will then permit the characterization of a scattering system in terms of a modal diameter and a distribution-width parameter by utilizing prepared diagrams for a particular relative refractive index.

INTRODUCTION

A number of literature reports¹⁻⁹ outline methods of particle size analysis based on the position of the extrema of a particular angular light-scattering function. Inherent in all of these methods (except that of Wallace and Kratochvil⁹) is the assumption that the scattering system is "monodisperse," and therefore the finite polydispersity that exists in real systems is disregarded. However, the sensitivity of the technique utilized in a particular experiment determines the validity of such an assumption. In many cases,¹⁰ the angular light scattering functions are extremely sensitive to small changes in polydispersity. The literature details numerous light-scattering studies^{3,7} of so-called monodisperse polymer latex systems where the polydispersity was sufficient to eliminate an extremum, or to shift the angular position of the extremum from the position calculated for the single-sphere situation. The influence of the polydispersity of these systems on the particle sizes reported was not quantitatively assessed. We have recently reported a study⁹ on the size-distribution analysis of latex systems based on the vertically polarized component of scattered light to illustrate this point and to outline a method of analysis which uses the exact Mie calculations^{11,12} and which permits evaluation of the distribution of particle sizes. The study reported here has the same basis but was designed to determine the feasibility of using the positions of the extrema of

the polarization ratio¹³⁻¹⁶ (i.e., the ratio of the intensities of the horizontal and vertical components of scattered light). The intensity of light scattered from an isotropic, spherical particle is dependent on the relative refractive index m (i.e., the ratio of the refractive indices of the sphere and the medium in which it is immersed) and the optical size $\alpha = \pi D/\lambda$, where D is the particle diameter and λ is the wavelength of light in the medium. The Mie angular intensity functions^{11,12} for either the vertically or horizontally polarized component of scattered light can be calculated for either a single sphere of diameter D or for a system of particles with a distribution of sizes characterized by an average diameter and a distribution-width parameter.

Maron et al.⁷ utilized the polarization ratio method to evaluate the particle size of polymer latex systems, whereas Kerker and La Mer¹ studied sulfur sols which have a higher relative refractive index than the latex systems. In a prelude to their paper dealing with this method of analysis, Maron et al.⁷ compared experimental polarization ratios at a scattering angle of 90° ρ_{90} from their laboratory and from the literature to ρ_{90} calculated from Mie theory for zero polydispersity, and $m = 1.20$ for polystyrene and $m = 1.17$ for 50:50 butadiene-styrene. The resulting lack of agreement between experiment and theory was attributed to optical anisotropy of polymer latex particles. However, the disagreement is not surprising since $m = 1.20$ was incorrectly used for polystyrene at all wavelengths of light from 271.1 nm to 519.3 nm (see Dezelic and Kratochvil³ for correct m values); and, likewise, the use of m of 1.17 at all wavelengths for 50:50 butadiene-styrene is of dubious validity. In addition, the latex systems possessed sufficient polydispersity for ρ_{90} to be appreciably different from values calculated for zero polydispersity. Table I illustrates the variation of ρ_{90} with the polydispersity factor σ_0 (defined below) and with small change (0.01) in the relative refractive index. The size-distribution parameters assigned¹⁸ to the Dow monodisperse polystyrene latex LS-057-A, based on computer analysis¹⁶ of ρ_θ for $\lambda = 409$ nm are $\alpha_m = 1.88$ and $\sigma_0 = 0.07$. Note that from Table I $(\rho_{90})_{\sigma_0=0.07}/(\rho_{90})_{\sigma_0=0}$ is 1.32 for $m = 1.20$ and that there are appreciable difference in ρ_{90} with changes in m . Therefore, the conclusion of Maron et al.⁷ that the latex particles are anisotropic because of the disagreement between theoretical $(\rho_{90})_{\sigma_0=0}$ and experimental $(\rho_{90})_{\sigma_0>0}$ (at incorrect or doubtful values of m in some cases) is without foundation. A detailed study¹⁹ of latexes has subsequently demonstrated that the particles are optically isotropic.

Maron et al.⁷ attempted to extend the method of particle size analysis based on the positions of the extrema of the vertically polarized component of scattered light to the use of the extrema of the polarization ratio ρ_θ .

$$\rho_\theta = \frac{(i_2)_\theta}{(i_1)_\theta} = \frac{H_{h,\theta}}{V_{r,\theta}} \quad (1)$$

where $V_{r,\theta}$ is the Rayleigh ratio for the vertically polarized component of the radiant scattered intensity per unit solid angle from an incident

TABLE I

σ_0	$\rho_\theta \times 10^2$	
	$m = 1.20,$ $\alpha_m = 1.88$	$m = 1.21,$ $\alpha_m = 1.88$
0.0	2.520	2.900
0.01	2.752	3.172
0.02	2.677	3.085
0.03	2.661	3.065
0.04	2.761	3.182
0.05	2.903	3.346
0.06	3.083	3.354
0.07	3.304	3.809
0.08	3.357	4.101
0.09	3.868	4.458
0.10	4.427	4.870
0.11	4.637	5.339
0.12	5.072	5.836
0.13	5.588	6.423
0.14	6.155	7.066
0.15	6.772	7.763

vertically (subscript v) polarized beam of unit irradiance; the definition of $H_{h,\theta}$ follows from that of $V_{v,\theta}$. The Mie angular intensity function^{11,12} $(i_1)_\theta$ for the vertically polarized component of scattered light from a scattering system of finite polydispersity is given by

$$(i_1)_\theta = \int_0^\infty (i_1')_\theta p(\alpha) d\alpha \tag{2}$$

where $(i_1')_\theta$ is the intensity function at angle θ for a single sphere of optical size α , and $p(\alpha)$ is the frequency function for the zeroth-order logarithmic distribution.²⁰ Therefore $p(\alpha)d\alpha$ gives the fraction of particles with sizes between α and $\alpha + d\alpha$. A similar expression exists for the horizontally polarized component of scattered light $(i_2)_\theta$. This distribution function has a slight positive skew and is expressed as

$$P(\alpha) = K \exp\left\{- (\ln \alpha - \ln \alpha_m)^2 / (2\sigma_0^2)\right\} \tag{3}$$

where K is a normalization constant, α_m is the modal optical size, and σ_0 is a distribution breadth parameter which is related to the standard deviation by

$$\sigma = \alpha_m \sigma_0 \left\{ 1 + \frac{7\sigma_0^2}{2!} + \frac{37\sigma_0^4}{3!} + \dots \right\}^{1/2} \tag{4}$$

A number of other size distribution functions (e.g., Gaussian) would be equally suitable.²¹ Therefore, ρ_θ is considered to be a function of $m, \theta, \alpha_m,$ and σ_0 whereas the previous treatments^{1-3,7,17} of this method considered ρ_θ to be a function of only $m, \alpha,$ and θ . In addition, ρ_θ may be expressed as either $H_{u,\theta}/V_{u,\theta}$ (subscript u denoting unpolarized incident light) or $H_{h,\theta}/-$

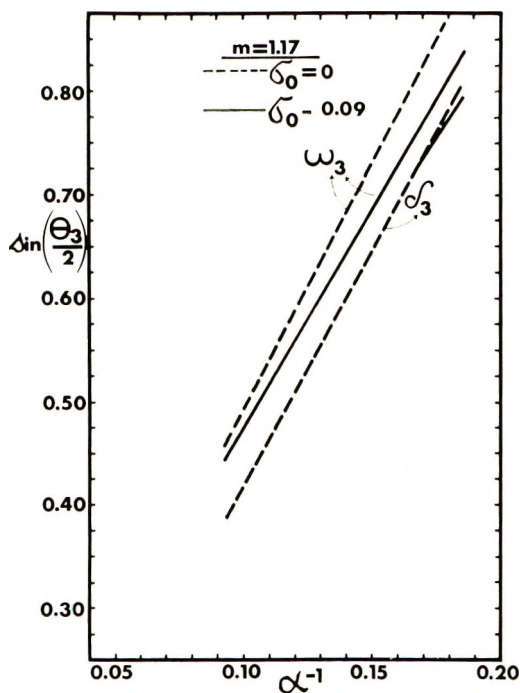


Fig. 1. Theoretical values of $\sin(\theta_3/2)$ vs. α^{-1} for $m = 1.17$: (---) $\sigma_0 = 0$; (—) $\sigma_0 = 0.09$.

$V_{v,\theta}$ since $H_{u,\theta} = (H_{h,\theta} + H_{v,\theta})/2$ and $V_{u,\theta} = (V_{v,\theta} + V_{h,\theta})/2$ with $H_{v,\theta}$ and $V_{h,\theta}$ both zero for optically isotropic spheres.

Maron *et al.*⁷ used

$$\alpha \sin (\delta_i/2) = l_i' \tag{5a}$$

or

$$(D/\lambda) \sin (\delta_i/2) = l_i \tag{5b}$$

to evaluate particle size from the location of the position of the minima δ_i in the angular ρ_θ scattering pattern while the angular positions of the maxima ω_i were related to particle size by

$$\alpha \sin (\omega_i/2) = L_i' \tag{6a}$$

or

$$(D/\lambda) \sin (\omega_i/2) = L_i \tag{6b}$$

In eqs. (5) and (6) l_i' , l_i , L_i' and L_i were considered constant for a given m and i and were experimentally evaluated from plots of α^{-1} versus $\sin (\delta_i/2)$ and $\sin (\omega_i/2)$ by using electron microscopy to evaluate particle size. These constants were also evaluated theoretically from Mie calculations for $\sigma_0 = 0$. The comparison of the experimentally ($\sigma_0 > 0$) and theoretically ($\sigma_0 = 0$) determined constants, again on ignoring the change in m with

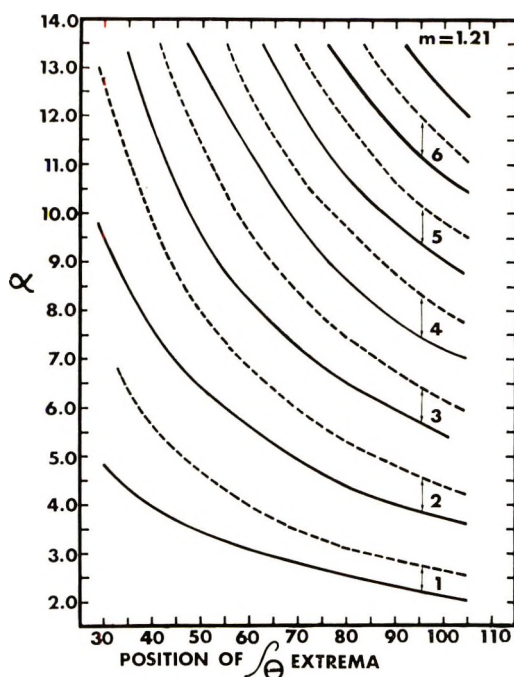


Fig. 2. Angular position of the extrema in ρ_θ , $i = 1$ to $i = 7$, calculated from the Mie theory for $\sigma_0 = 0$, $m = 1.21$: (—) minima; (---) maxima.

variation in λ , was reported⁷ as satisfactory only for the first minimum. It was further stated by Maron et al.⁷ that the lack of agreement could not be due to polydispersity as both monodisperse and polydisperse samples behaved in a similar manner and that, therefore, the disagreement must be due to anisotropy. For reasons discussed above, the disagreement between experiment and theory is reasonable and to be expected. Figure 1, based on Mie calculations, illustrates that for ω_3 different slopes and therefore different values of L_3' are obtained for $\sigma_0 = 0$ and $\sigma_0 = 0.09$. In addition, for an observed ω_3 from a sample of finite polydispersity (e.g., $\sigma_0 = 0.09$), the erroneous assumption of $\sigma_0 = 0$ results in a diameter larger than the true diameter. This same figure illustrates the negligible effect of polydispersity on the angular position of δ_i .

EVALUATION OF SIZE-DISTRIBUTION PARAMETERS

The position of the extrema and the corresponding value of ρ_θ [i.e., $(i_2)_\theta / (i_1)_\theta$] were determined by use of an IBM 360/65 computer from Mie calculations for various size distribution parameters [$\alpha_m = 2.0$ (0.2) 13.5 and $\sigma_0 = 0$ (0.02) 0.15] at angles 1° (1°) 140° for $m = 1.21$ and 1.17.

At a fixed α_m , the shifting of the minima with increased polydispersity is limited to 3° or less in the forward direction if the angular range is restricted to less than 105° , whereas the maxima shift as much as 10° in the forward

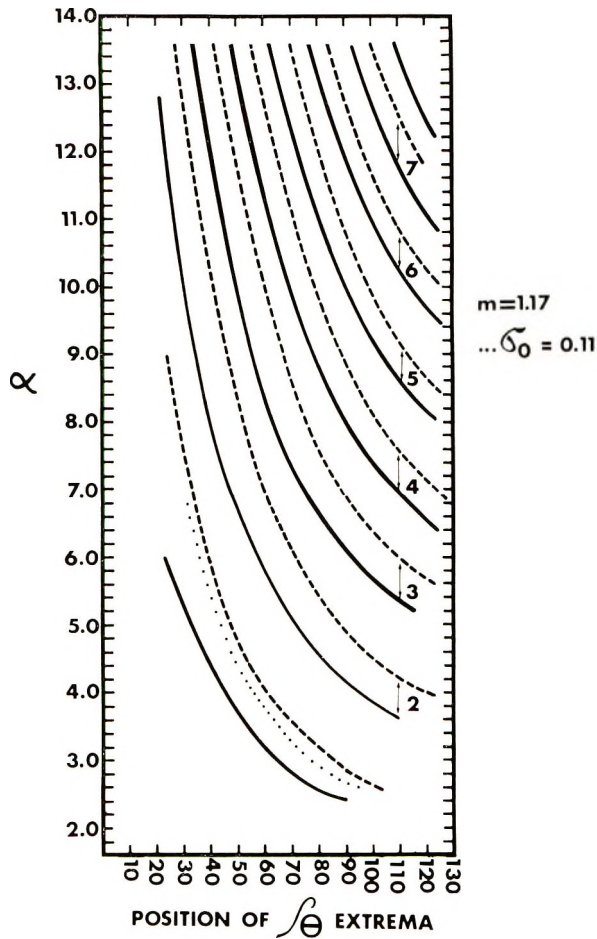


Fig. 3. Angular position of the extreme in ρ_θ as in Fig. 2 except that $m = 1.17$: (—) minima, (---) maxima; (···) maximum for $i = 1$ and $\sigma_0 = 0.11$.

TABLE II
Calculated Diameters from Eqs. (5) and (6) and the Extrema Positions from Mie Theory

σ_0	Extrema position from Mie theory ^a		D from eqs. (5) and (6), nm	
	δ_1	ω_1	From δ_1	From ω_1
0.01	46	68	373	373
0.03	46	67	373	378
0.05	46	67	373	378
0.07	46	65	373	388
0.09	45	64	381	394
0.11	44	62	389	405
0.13	44	60	389	417
0.15	43	58	398	430

^a $m = 1.21$ ($\lambda = 325$ nm), $\alpha_m = 3.6$ ($D_m = 373$ nm).

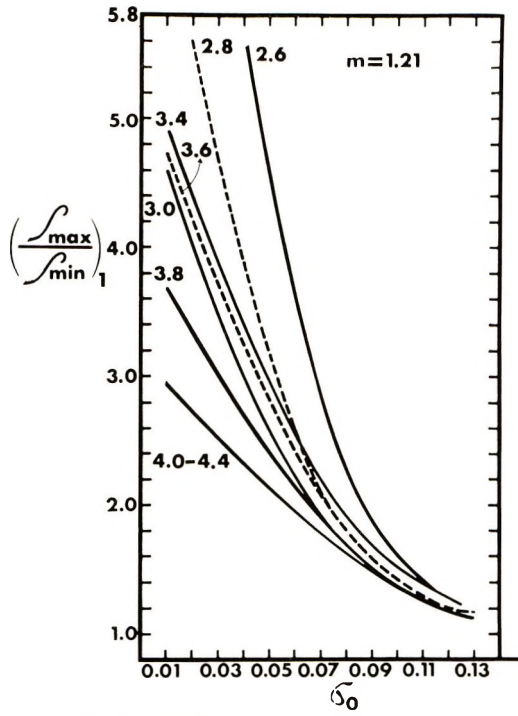


Fig. 4. Effect of the distribution-width parameter σ_0 on the extrema rho ratio for $i = 1$, $m = 1.21$.

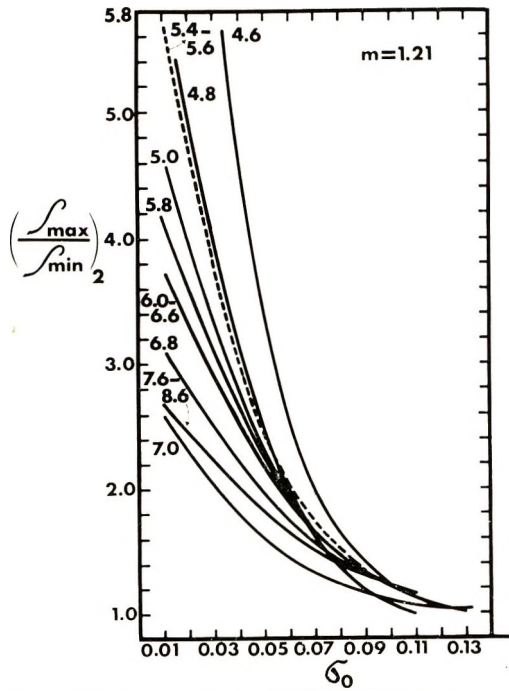


Fig. 5. Effect of the distribution width parameter σ_0 on the extrema rho ratio for $i = 2$, $m = 1.21$.

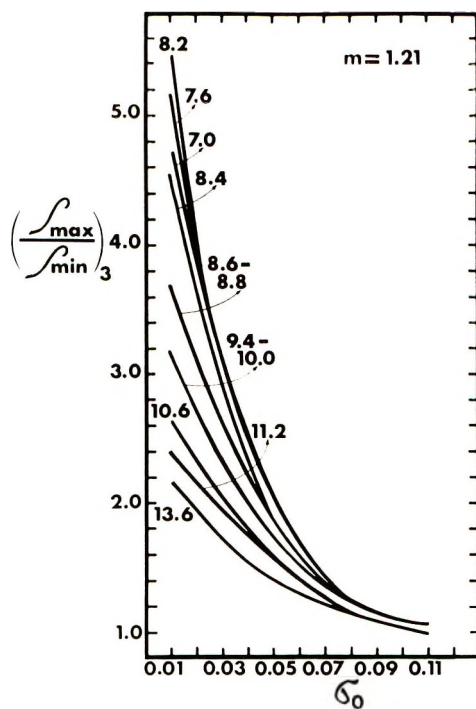


Fig. 6. Effect of the distribution width parameter σ_0 on the extrema rho ratio for $i = 3, m = 1.21$.

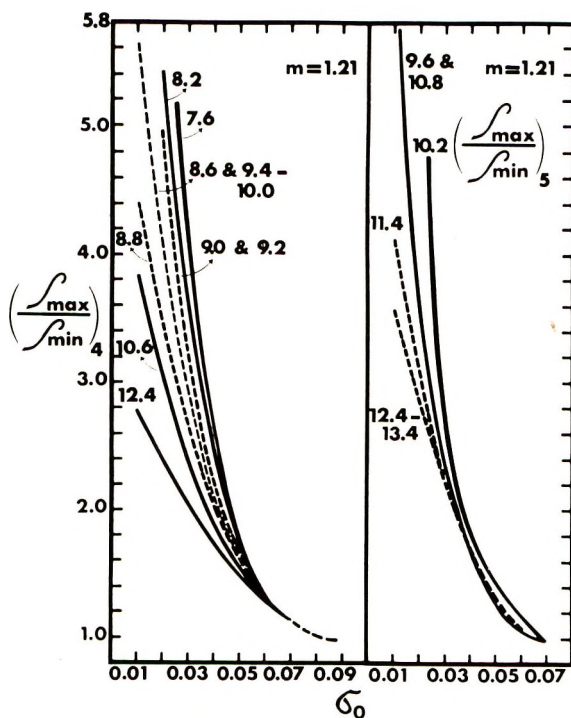


Fig. 7. Effect of the distribution width parameter σ_0 on the extrema rho ratio for $i = 4$ and $i = 5, m = 1.21$.

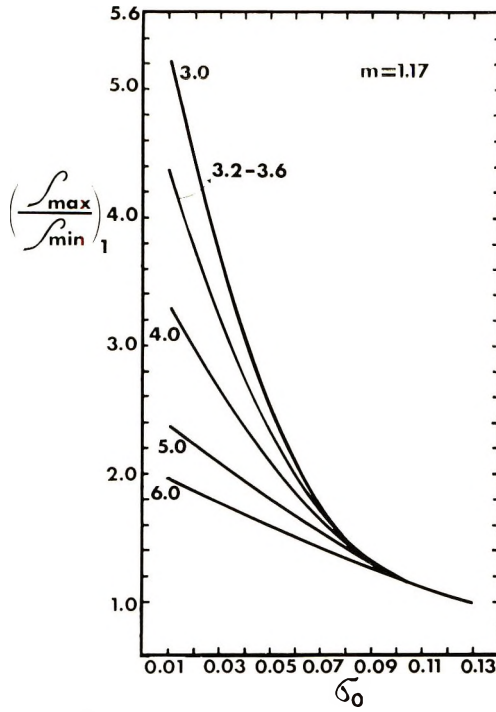


Fig. 8. Effect of the distribution width parameter σ_0 on the extrema rho ratio for $i = 1$, $m = 1.17$.

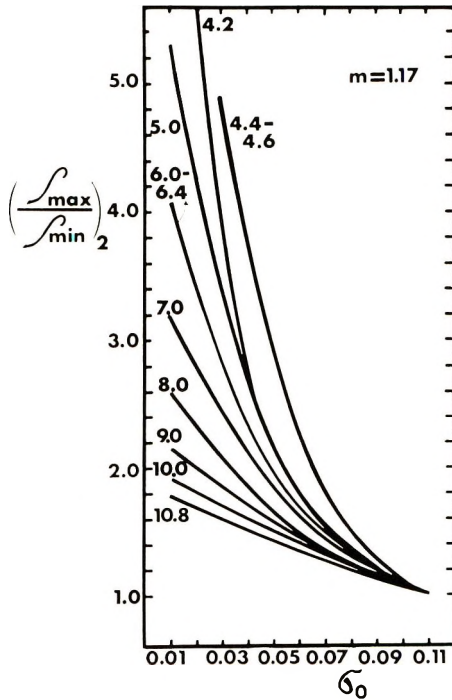


Fig. 9. Effect of the distribution width parameter σ_0 on the extrema rho ratio for $i = 2$, $m = 1.17$.

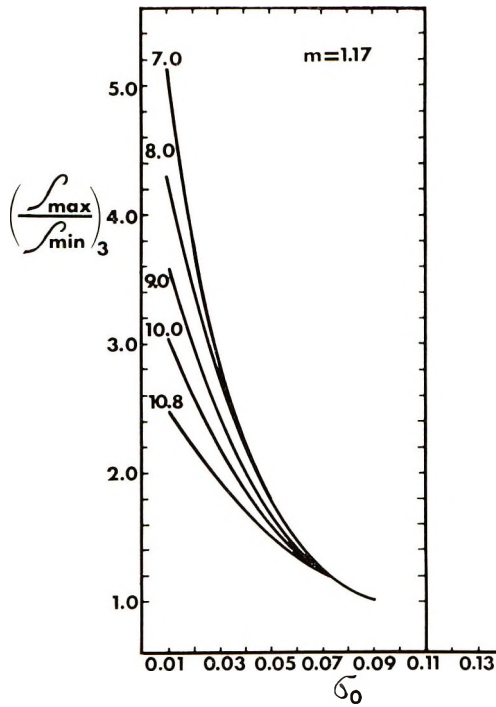


Fig. 10. Effect of the distribution width parameter σ_0 on the extrema rho ratio for $i = 3$, $m = 1.17$.

direction. The insensitivity to polydispersity of the position of the minima in the angular ρ_θ pattern may be utilized for particle-size determination in an analogous manner to the recently reported method⁹ based on $(i_1)_\theta$. Figures 2 and 3 are plots of the position of the extrema in ρ_θ versus α_m for $\sigma_0 = 0$ and m equal to 1.21 and 1.17, respectively. Such plots can be used for evaluation of α_m from observed δ_i for systems of low polydispersity. The relation $180/(\delta_{i+1} - \delta_i) \approx \alpha_m$ (with angles in degrees) previously suggested⁹ in the $(i_1)_\theta$ method for the estimation of α_m , and therefore of the index i , is also satisfactory for ρ_θ . That is, if the angular separation of two consecutive minima ($\Delta\delta$) is known, α_m can be estimated and $i = \delta_i/\Delta\delta$. Since in many cases, the maxima shift appreciably as polydispersity increases, the calculation of particle size based on the observed maxima (i.e., ω_i) and eq. (6) can lead to erroneous results which can contradict the results obtained from δ_i and eq. (5). This is illustrated in Table II, which lists the diameters calculated from these two equations and the positions of the extrema from Mie calculations. Once α_m is evaluated from the minima, σ_0 can be determined by comparison of the experimental extrema rho ratio $(\rho_{\max}/\rho_{\min})_t$ to theoretical curves of the extrema rho ratio versus σ_0 for a given α_m and m (Figs. 4-11). These curves are similar to those used in the method⁹ based on the vertically polarized component of scattered light but differ in one respect. The extrema intensity ratio⁹ was found to decrease

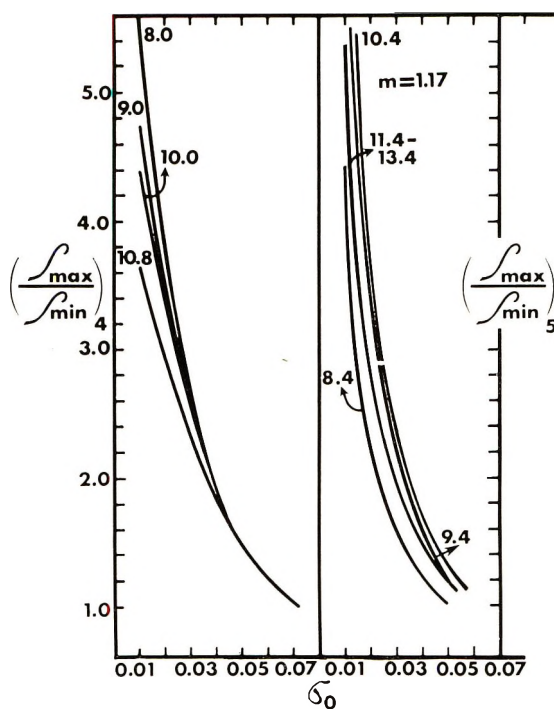


Fig. 11. Effect of the distribution width parameter σ_0 on the extreme rho ratio for $i = 4$ and $i = 5$, $m = 1.17$.

steadily with increasing α_m at a fixed σ_0 while $(\rho_{\max}/\rho_{\min})_i$ may go through a minimum and a maximum. An example of this behavior can be found in Figure 4 between $\alpha_m = 2.8$ and $\alpha_m = 3.8$. This complicates somewhat the use of such curves which must be obtained at close intervals if interpolation procedures are to be used.

APPLICATION OF METHOD

Polystyrene Latex, $m = 1.21$ ($\lambda = 325$ nm)

Dow polystyrene latexes LS-1138-B and LS-449-E were used as model scattering systems. The electron microscopy results (EM), obtained by the Dow Company, are $D_{EM} = 1011$ nm ($\alpha_{EM} = 9.75$), $(\sigma_0)_{EM} = 0.005$; and $D_{EM} = 796$ nm ($\alpha_{EM} = 7.68$), $(\sigma_0)_{EM} = 0.004$, respectively.

A Sofica light-scattering photometer was used to measure the polarization ratio which is experimentally defined as the ratio of the galvanometer deflections for the two states of polarization corrected for scattering of the water medium. The effects of multiple scattering at the concentrations of ca. 10^{-7} g/g and the reflection corrections for this instrument were found to be negligible. The experimental details are given elsewhere⁹ and in the literature cited. Based on the data and the results of the analyses of the three extrema given in Table III for LS-1138-B, the size distribution param-

TABLE III
 Size-Distribution Analysis

Sample	i	δ_i	α_m	$(\rho_{\max}/\rho_{\min})_i$	σ_0
Dow polystyrene latex LS-1138-B:	3	50°	9.55	1.7	0.05
$D_{EM} = 1011$ nm, $C = 5.18 \times 10^{-7}$ g/g	4	68°	10.0	2.1	0.04
	5	90°	9.75	1.9	0.04
Dow polystyrene latex LS-449-E:	2	42°	7.4	1.7	0.05
$D_{EM} = 796$ nm, $C = 2.26 \times 10^{-7}$ g/g	3	68°	7.4	1.8	0.055
	4	94°	7.5	2.5	0.045
50:50 Butadiene-styrene latex ^a	2	49°	6.8	1.3	0.08
	3	79°	6.7	1.3	0.07

^a Data from Maron et al.⁷

eters assigned to this sample are $\alpha_m = 9.8 \pm 0.2$ and $\sigma_0 = 0.040 \pm 0.015$.^{*} Previous results⁹ for this sample based on the use of the extrema in $(i_1)_\theta$ were reported as $\alpha_m = 9.7 \pm 0.1$ and $\sigma_0 = 0.05 \pm 0.01$. The large discrepancies between these σ_0 and $(\sigma_0)_{EM}$ are discussed elsewhere.²² The results for sample LS-449-E indicate size-distribution parameters of $\alpha_m = 7.4 \pm 0.10$ and $\sigma_0 = 0.05 \pm 0.015$. Since the fourth minimum at about 94° is considerably more shallow than the two minima in the more forward direction, there is a larger uncertainty in δ_4 and therefore in α_m , based on $i = 4$.

50:50 Butadiene-Styrene Latex

Experimental values of ρ_θ were obtained for $\lambda = 271.1$ nm from Figure 2 of reference 7 (Sample 2713). The results from the analysis of the data by the extrema method are given in Table III and indicate average size-distribution parameters of $\alpha_m = 6.75 \pm 0.10$ ($D_m = 583$ nm) and $\sigma_0 = 0.075 \pm 0.015$. Maron et al.,⁷ utilizing four wavelengths of light, obtained an average diameter of 541 nm based on evaluation of eleven minima and ten maxima by eqs. (5) and (6). The 21 diameters ranged from 497 nm to 590 nm.

Because of the questionable validity of $m = 1.17$ at $\lambda = 271.1$ nm, values of ρ_θ at 19 angles were compared by computer with theoretical values for $m = 1.15$ (0.01) 1.19 and a wide range of α_m and σ_0 in order to find the best fit of experiment and theory. This fitting procedure is described elsewhere,¹⁶ except that the previous procedure was extended to a third variable m to produce a three-dimensional contour error map of α_m versus σ_0 versus m . The best fit of experiment and theory was found at $\alpha_m = 6.6$; $\sigma_0 = 0.08$ for $1.17 \leq m \leq 1.19$ with the agreement improving at higher m ; however, the deviation of experiment from theory even for the best fit ($m = 1.19$) was too high to place confidence in the results. That is, the volume

* The \pm quantities represent subjective estimates of the uncertainty in assigning the size-distribution parameters.

of minimum error in the three-dimensional contour error map was so abnormally large for this set of data that the uncertainty in the assignment of m , α_m , and σ_0 was unacceptably large.

CONCLUSION

Since at least one maximum and one minimum are required for analysis, this method is restricted to $\alpha_m > 4$ for m values considered here. The limiting value of σ_0 decreases with increasing i from about 0.13 for $i = 1$ to 0.07 for $i = 5$. A detailed discussion of the strengths and limitations of this type of extrema method was given previously.⁹

This study was initiated as a result of exposure to and discussions with Professor J. P. Kratochvil of Clarkson College of Technology, Potsdam, New York. The author is grateful to Bausch and Lomb for the generosity in providing the Sofica light scattering photometer and to the University of Rochester for the use of their computing facilities.

References

1. M. Kerker and V. K. LaMer, *J. Amer. Chem. Soc.*, **72**, 3516 (1950).
2. M. Nakagaki and W. Heller, *J. Chem. Phys.*, **32**, 835 (1960).
3. G. Dezelic and J. P. Kratochvil, *J. Colloid Sci.*, **16**, 561 (1961).
4. S. H. Maron and M. E. Elder, *J. Colloid Sci.*, **18**, 107 (1963).
5. S. H. Maron, P. E. Pierce, and M. E. Elder, *J. Colloid Sci.*, **18**, 391 (1963).
6. S. H. Maron and M. E. Elder, *J. Colloid Sci.*, **18**, 199 (1963).
7. S. H. Maron, P. E. Pierce, and M. E. Elder, *J. Colloid Sci.*, **19**, 591 (1964).
8. M. Kerker, W. A. Farone, L. B. Smith, and E. Matijević, *J. Colloid Sci.*, **19**, 193 (1964).
9. T. P. Wallace and J. P. Kratochvil, *J. Polym. Sci. A-2*, **8**, 1425 (1970).
10. T. P. Wallace and J. P. Kratochvil, *Appl. Opt.*, **8**, 824 (1969).
11. M. Kerker, *The Scattering of Light and Other Electromagnetic Radiation*, Academic Press, New York, 1969.
12. H. C. van de Hulst, *Light Scattering by Small Particles*, Wiley, New York, 1957.
13. M. Kerker, E. Dabey, G. Cohen, J. P. Kratochvil, and E. Matijević, *J. Phys. Chem.*, **67**, 2105 (1963).
14. M. Kerker, E. Matijević, W. F. Espenscheid, W. A. Farone, and S. Kitani, *J. Colloid Sci.*, **19**, 213 (1964).
15. R. T. Jacobsen, M. Kerker, and E. Matijević, *J. Phys. Chem.*, **71**, 514 (1967).
16. T. P. Wallace and J. P. Kratochvil, in *The Computer in Polymer Science (J. Polym. Sci., C, 25)*, J. B. Kinsinger, Ed., Interscience, New York, 1968, p. 89.
17. S. H. Maron, M. E. Elder, and P. E. Pierce, *J. Colloid Sci.*, **18**, 733 (1963).
18. J. P. Kratochvil and T. P. Wallace, *J. Phys. Appl. Phys.*, **D3**, 221 (1970).
19. T. P. Wallace, Ph.D., *Thesis, Clarkson College of Technology, Potsdam, New York* (1976).
20. W. F. Espenscheid, M. Kerker and E. Matijević, *J. Phys. Chem.*, **68**, 3093 (1964).
21. T. P. Wallace and J. P. Kratochvil, paper presented at American Chemical Society Meeting, Minneapolis, April 1969; *Polym. Preprints*, **10**, No. 1, 343 (1969).
22. J. P. Kratochvil and T. P. Wallace, *Anal. Chem.*, in press.

Received July 22, 1970

Revised October 5, 1970

Measurement of the Stress-Relaxation Modulus in the Primary Transition Region

R. E. KELCHNER and J. J. AKLONIS, *Department of Chemistry,
University of Southern California, Los Angeles, California 90007*

Synopsis

Difficulties have been encountered in experimentally measuring the stress-relaxation modulus for systems with steep slopes in the primary transition region. The usually applied "factor-of-ten" rule is shown to apply in these cases as well as in cases where the relaxation is slower; with the steep slope, however, the rule offers little help, since the decay in the modulus is so fast that stresses are usually very small at times when direct modulus calculations may be made. A technique is suggested which allows calculation of the modulus in this difficult region. A slow constant strain-rate deformation is followed by a constant strain period. Modulus values for times during the constant strain rate period are calculated using well known relationships. Long-time values are calculated from the definition of the modulus (the factor-of-ten rule being employed) and a recursion relation is developed which is used for modulus calculations during the constant strain period at relatively short times where effects of strain rate are important. Starting values for the recursion relation are long-time moduli which can be calculated directly.

Experimental investigations¹⁻⁴ of the stress-relaxation behavior of amorphous polymers in the primary transition region have demonstrated at least one very interesting fact. The maximum value of the negative slope of the stress-relaxation master curve in this region is not the same for all polymers. For example, when comparing the relaxation behavior of polyisobutylene (PIB) with that of polystyrene (PS), one notices that maximum slopes on the usual log-log scales are about $1/2$ for PIB¹ and $3/2$ for PS.² In experimental time, account having been made for differences in glass transition temperatures, PS experiences its glass-to-rubber transition about 10,000 times as rapidly as PIB. The molecular reasons for these very differing behaviors are not yet understood. Thus, it seems clear that additional measurements of the behavior of other polymers in the primary transition region would be useful although such experiments, are usually relatively difficult. We present here a technique which can be used to measure the stress relaxation of polymers in the primary transition region rather easily.

A short discussion of the complications which arise in attempting direct

$$E(t) = \sigma(t)/\epsilon_0 \quad (1)$$

measurement of this behavior may be beneficial. The tensile stress-relaxation modulus $E(t)$ may be defined by the equation

where $\sigma(t)$ is the stress at time t and ϵ_0 is the strain applied instantaneously at zero time. In actual experiments, however, instantaneous strain application is impossible. Usually, the strain is applied rapidly and, as a rule, one uses eq. (1) with data obtained at times greater than the strain time by a factor of ten. Thus, for a one-second strain, the first experimental modulus would be calculated at 10 sec.

When attempting measurements in the primary transition region, however, the application of the "factor-of-ten" rule becomes impossible. Consider attempting to measure a modulus value in the range of 10^9 dyne/cm², at a time 10 sec after the initial strain application. In order to do this, the strain rate must vanish before one second has elapsed. But, if the 10-second modulus is about 10^9 dyne/cm², the modulus at times < 1 sec will be correspondingly higher, perhaps in the neighborhood of 10^{10} dyne/cm², i.e., approaching a glassy modulus value. Clearly, finite strains applied to glassy materials are not desirable. Among other drawbacks the possibilities of slippage from the clamps or fracture are maximized under these conditions, since very high forces must be employed to obtain measurable strains.

Since we are interested in examining the behavior of polymers with different slopes in the primary transition region, the factor-of-ten rule should be examined in this light. Perhaps the factor can be decreased for materials with slopes within certain bounds. One form of the Boltzmann superposition principle⁵ allows the calculation of the time-dependent stress from a knowledge of the strain history and the modulus:

$$\sigma(t) = \int_0^t \frac{d\epsilon(\mu)}{d\mu} E(t - \mu) d\mu \quad (2)$$

A functional form for $E(t)$ which will simplify this analysis is:

$$E(t) = E_1[1 + (t/\tau)]^{-m} + E_2 \quad (3)$$

where E_1 is the glassy modulus, E_2 is the rubbery plateau modulus, τ is a parameter which places the transition on the time axis, and m is the maximum value of the negative slope in this primary transition region. If m has a value of $3/2$, eq. (2) will generate a PS-like master curve, while a value of $1/2$ for m will result in a PIB-like response. The solid line in Figure 1 was calculated with $E_1 = 3.0 \times 10^{10}$ dyne/cm², $E_2 = 1.0 \times 10^7$ dyne/cm², $\tau = 3.0 \times 10^{-2}$ sec, and $m = 3/2$.

Next, eq. (2) was utilized to calculate the stress for a sample subjected to a constant strain rate for 3 sec. This calculated stress was then incorrectly substituted into eq. (1) in an attempt to calculate the modulus at times greater than 3 sec. These modulus values we show as the dashed line in Figure 1. It is apparent that eq. (1) is useful only at times greater than 30 sec, the difference between the true modulus and that calculated

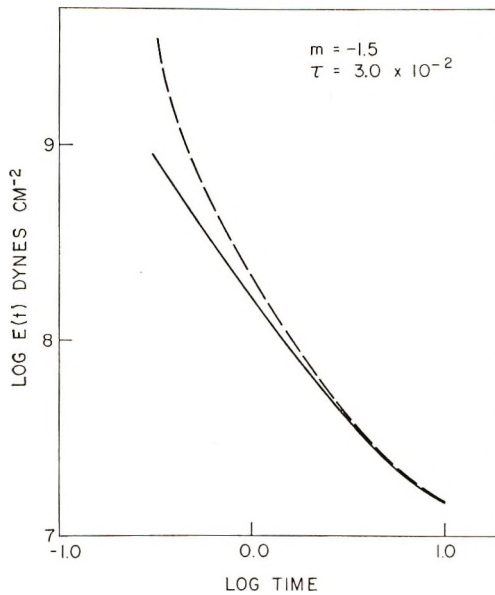


Fig. 1. Examination of the factor-of-ten rule: (—) calculated by eq. (3) with $E_1 = 3.0 \times 10^{10}$ dyne/cm², $E_2 = 1.0 \times 10^7$ dyne/cm², $\tau = 3.0 \times 10^{-2}$ sec, $m = 3/2$; (---) calculated by eqs. (1), (2), and (3) for a 0.3 sec constant-strain-rate experiment.

via eq. (1) at times shorter than this being in excess of 5%. Similar results are obtained if values other than $3/2$ are used for the parameter m in eq. (3); thus the factor-of-ten rule holds rather well, irrespective of the exact shape of the curve in this area.

It is well known that $E(t)$ may be computed from the slope of a stress-strain experiment carried out at constant strain rate. The equation⁶

$$E(t) = \sigma d \log \sigma / \epsilon d \log \epsilon \quad (4)$$

represents a particularly suitable expression to use in carrying out this calculation. To limit stress so as to avoid the experimental difficulties mentioned above, it is clear that very slow strain rates are necessary. Yet the extension must result in a measurable stress at short times. A strain rate in the region of 1×10^{-2} /min is the best compromise to satisfy both these considerations. To deal with linear viscoelastic materials, one should limit the overall strain as much as possible. In the lower transition region, for example, strains of the order of 5% appear to be within the region of linear viscoelasticity. Thus, to limit overall strain to 5% at a strain rate of 10^{-2} /min indicates an experiment of 5 min duration and a calculation of a 5-min modulus. Even smaller extensions, i.e., shorter experiments, would be necessary in the upper transition region. So although this technique can be used, its inability to measure long-time modulus values is definitely a limitation. Normally, stress relaxation experiments are carried out to yield modulus values at about an hour.

In Figure 2 the results of a constant strain-rate experiment are presented.

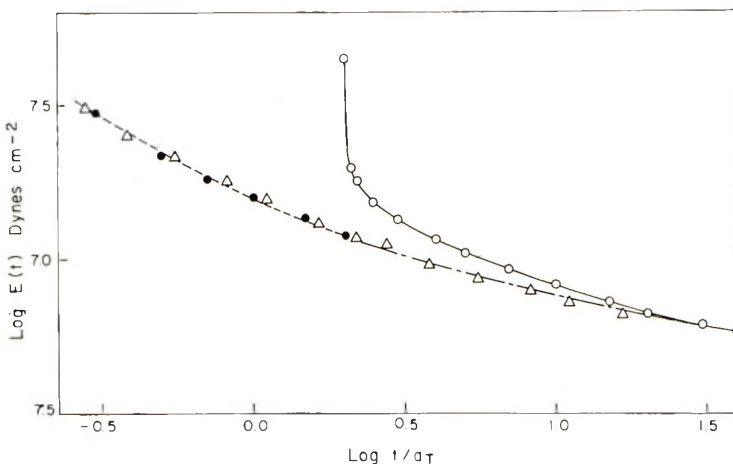


Fig. 2. Relaxation behavior of polystyrene reduced to 106°C: See text for explanation of curves.

A polystyrene sample with $\bar{M}_w = 2.74 \times 10^5$, furnished by Mr. R. F. Kratz of the Koppers Company, Inc., Monroeville, Pa., was elongated at the constant strain rate of $1.74 \times 10^{-2}/\text{min}$ at 106°C. The constant strain rate was imposed for 2 min, after which constant strain was maintained. Equation (4) was used to calculate the modulus during the constant strain-rate portion of the experiment and resulted in the filled circles connected by the dashed line at times shorter than two minutes. The data measured at constant strain were utilized for modulus calculations by use of eq. (1) the factor-of-ten rule being ignored. These data are represented by open circles and the solid line. The previous discussion indicates that modulus values calculated for times greater than 20 min are within experimental error while those calculated for times between 2 and 20 min are much too high. Clearly, then, a relaxation curve may be measured; but approximately one decade of time in the central portion of the curve must be discarded. Although the data measured do contain information about the $E(t)$ through this region, neither eq. (1) nor eq. (4) is suitable for the calculation of $E(t)$ from these data.

In the light of this gap, further examination of the Boltzmann principle is interesting. Under the condition of a constant strain rate applied for a time c , eq. (2) becomes

$$\sigma(t) = \dot{\epsilon} \int_0^c E(t - \mu) d\mu \quad t \geq c \quad (5)$$

Approximation of the integral by a sum and subsequent rearrangement yields:

$$E(t - c) = \frac{\sigma(t)}{\dot{\epsilon}\Delta} - \sum_{i=1}^{n-1} E(t - i\Delta) \quad t > c \quad (6)$$

where $n\Delta = c$. Thus, if one were to know the $n - 1$ modulus values at the relatively long times $t - i\Delta$, as well as ϵ and $\sigma(t)$, one could calculate the modulus value at the shorter time $t - c$. Now with a value for $E(t - c)$, one could rewrite eq. (6) for a still shorter time and again calculate the modulus, but now at an even shorter time. Thus one has a recursion relation for modulus values in terms of moduli which obtain at longer times. The starting $n - 1$ modulus values at long times are calculated where eq. (1) is correct, and the recursion relation is then applied over and over to regress back to short times where eq. (1) is no longer applicable. Such a regression is easily carried out on a computer.

This technique has been applied to synthesized data generated by using eqs. (2) and (3) and is essentially exact. Such synthesized data, however, are not subject to the scatter inherent in experimental data, and such a test is not conclusive proof of the applicability of this technique to real experiments. Still, the complete success of this technique should be contrasted with more limited success of previously suggested approximation techniques,⁷ even in such an idealized situation.

A critical test of eq. (6) may be realized by calculating from the experimental data the modulus values in the interval 2–20 min in Figure 2. Equation (6) is strictly correct in the limit of infinitely small Δ . Thus, this technique should be most satisfactory for closely spaced data points. Rather than introduce roughly a thousand measured data points $\sigma(t)$ into the computer for this experimental run, we have introduced about 30 data points and used these to calculate the coefficients of a three-term power series over small segments of the experimental run:

$$\sigma(t) = C_1 + C_2t + C_3t^2 \quad (7)$$

Ten sets of coefficients were used for the relaxation curve. These functions were then used internally to generate the closely spaced data points needed. The values of the modulus at long times, which are the necessary input for the recursion relation, are obtained by using eq. (1) well within its range of applicability.

The results of this calculation are presented as the dash-dot line in Figure 2. It is reassuring that the modulus values calculated with eq. (6) in the region of 2 min match so well with the modulus values calculated with eq. (4).

As a final examination of the validity of this procedure for calculating the stress relaxation modulus, we have measured the modulus directly, using a rapid strain application and the factor-of-ten rule. In this experiment the temperature was decreased to 104°C to enable modulus values above 10^7 dyne/cm² to be measured. It should be pointed out, however, that this rapid-strain, low-temperature measurement is just the experiment which is not feasible when measuring the main portion of the primary transition region. In this case however, the temperature of the original run was selected to be high enough so that a rapid strain experiment could be done as a final test. The 1% strain was applied in 0.02 min, and eq. (1) could then be em-

ployed for times longer than 0.2 min. A horizontal shift factor ($a_T = 1.81$) was applied to the 104°C data to reduce them to 106°C. The superposition of these two curves over four decades of time is good, indicating the validity of the three-part modulus calculation.

This regression is not limited to experiments where $\dot{\epsilon}$ is a constant; non-linear strains can be straightforwardly handled within this formalism.

The techniques outlined here enable one to measure the stress relaxation modulus well up into the primary transition region;⁴ modulus values of 10^9 dyne/cm² and higher are easily accessible. This measuring capacity exists since one is neither forced to attempt rapid finite strain on glassy materials (slow constant strain rates are employed) nor to work at temperatures too close to the glass transition temperature (in Fig. 2 a 106°C experiment at a constant strain rate resulted in modulus values equal in magnitude to those measured at rapid strain at a test temperature of 104°C).

Acknowledgment is made to the Petroleum Research Fund, administered by the American Chemical Society, as well as the Research Corporation for the partial support of this research. We are grateful for the services of the Computer Sciences Laboratory of the University of Southern California.

References

1. A. V. Tobolsky, *Properties and Structure of Polymers*, Wiley, New York, 1960, p 154.
2. A. V. Tobolsky, J. J. Aklonis, and G. Akovali, *J. Chem. Phys.*, **42**, 723 (1965).
3. T. Fujimoto, N. Ozaki, and M. Nagasawa, *J. Polym. Sci. A-2*, **6**, 129 (1968).
4. R. E. Kelchner and J. J. Aklonis, *J. Polym. Sci. A-2*, **8**, 799 (1970).
5. J. D. Ferry, *Viscoelastic Properties of Polymers*, Wiley, New York, 1961, p. 15.
6. T. L. Smith, *J. Polym. Sci.*, **20**, 89 (1956).
7. R. J. Farris, JANNAF Meeting, U.S. Naval Weapons Center, China Lake, California, Nov. 1969.

Received March 12, 1970

Revised August 12, 1970

Polymerization Mechanisms and Stereosequence Distributions: A Monomer-Dimer Model

CHONG WHA PYUN* and THOMAS G FOX
*Mellon Institute, Carnegie-Mellon University,
Pittsburgh, Pennsylvania 15213*

Synopsis

A polymerization mechanism in which monomers and dimers add to a growing polymer chain with different rate constants and different stereospecificity is considered. A fraction of the dimers are in isotactic placement internally, and low conversion to polymer is assumed. The stereosequence distribution generated by this monomer-dimer model is calculated and found to be non-Markovian in general. A method of determining kinetic parameters of the mechanism from experimentally obtained placement sequence probabilities and related experimental tests for the applicability of the mechanism are also described. A few ramifications of the general monomer-dimer model are then discussed. A case of special interest is the one in which all the dimers have a single internal tacticity, a model recently proposed by Blumstein, et al., for a polymerization involving the surface of certain aluminosilicate minerals. For the case where all dimers are isotactic, it is found that although the propagation of consecutive syndiotactic placements alone is simple Markovian, the overall stereosequence distribution is non-Markovian. Another special case of interest is the limiting case with dimers only in the feed. This case turns out to correspond to a special case of the cyclopolymerization mechanism proposed previously by Reinmöller and Fox. Although the tacticity distribution of the placements created by the head (or tail) monomer units alone of the dimers is Bernoullian, the composite stereosequence distribution is again non-Markovian.

Introduction

The stereochemical structure of a polymer chain is determined by the polymerization mechanism by which it is produced. The polymer chain stereoisomerism or configuration is completely described by the stereosequence distribution, that is, by the specification of the probability of occurrence of every possible sequence of tacticity placements formed by consecutive monomer units. In a polymer chain formed by head-to-tail addition polymerization of an unsymmetrical α -olefin (a typical vinyl polymer chain), the adjacent monomer units m and $m + 1$ constitute the m th placement, which is called isotactic (I) or syndiotactic (S) accordingly as the two monomer units are in the same or opposite relative stereoconfigurations.^{1,2}

If the probability of a given placement being I or S depends on the tac-

* Present address: Department of Chemistry, Lowell Technological Institute, Lowell, Massachusetts 01854.

ticity of a finite number n of immediately preceding placements but is independent of the tacticity of any farther placements, the resulting stereosequence is termed Markovian of n th order. A special case of a Markovian distribution is given by a simple (i.e., first-order) Markov chain ($n = 1$), in which the tacticity of a given placement is affected only by that of the immediately preceding placement. Another special case is the Bernoulli trial distribution (i.e., zeroth-order Markovian distribution; $n = 0$), in which the tacticity of a given placement is completely independent of the tacticity of all other placements. If a stereosequence distribution is not finite-order Markovian, it is called non-Markovian.

At present, the probability of occurrence of relatively short sequences of placements can be determined by high-resolution nuclear magnetic resonance spectroscopy. Comparison of experimental placement sequence concentrations with those predicted by assumed polymerization mechanisms plays a central role in elucidation of polymerization kinetics.

In this paper, we consider a simplified mechanism in which monomers and dimers in the feed add to a growing polymer chain with different rate constants and different stereospecificity. A given fraction of the dimers are in preformed I placements internally. The individual steps are all assumed to be Bernoullian. The ratio of the monomer and dimer concentrations is taken to be constant by assuming that either concentration is much larger than the polymer concentration throughout the polymerization.

By the word "dimer" we do not necessarily mean a chemical compound formed from two monomer units. Any association of two monomers in the feed may be regarded as a dimer for our purpose if the pair behave in the following way. A monomer associated in a "dimer" adds to the growing polymer chain end with a rate constant and stereospecificity different from those for a "free" monomer, and once this addition is completed the other monomer in the pair is attached to the chain end without fail with its own stereospecificity. Thus, a dimer can be, for example, a pair of loosely held monomers adsorbed on a surface, or it can be a divinyl monomer, as discussed below.

We calculate the stereosequence distribution generated by this monomer-dimer mechanism and then characterize the distribution using the persistence ratio² ρ , the Ω factors,³ and the generalized Ω factors. We also describe a method of determining the kinetic parameters of the model from a few experimentally observed placement sequence probabilities and experimental tests for physical applicability of the mechanism. Subsequently, we discuss some special cases of the general monomer-dimer mechanism including two specific mechanisms previously proposed for cyclopolymerization⁴ and for insertion polymerization.⁵

Model and Assumptions

We denote the concentrations of the monomeric and dimeric feed molecules by $[M_1]$ and $[M_2]$, respectively. We make the usual low-conversion

hypothesis and assume that the monomer-dimer concentration ratio is substantially constant as the polymerization proceeds. A fraction δ of the internal placements in the dimers is taken to be isotactic and $1 - \delta$, syndiotactic. The rate constants for adding species M_1 and M_2 to the growing polymer chains are denoted by k_1 and k_2 , respectively. If we use k_{ni} and k_{ns} ($n = 1, 2$) to denote the rate constants for adding M_n to the polymer chain ends to form an I or S placement respectively (in the case of M_2 , for example, we refer to the placement formed by the monomer unit originally at the chain end and the monomer unit in the dimer directly connected to it), we have

$$k_{ni} + k_{ns} = k_n \quad n = 1, 2 \quad (1)$$

All these rate constants are assumed to be independent of the length of the growing chain, end effects being neglected. In adopting this notation, we have also implicitly assumed that k_{ni} and k_{ns} are not affected by the tacticity of the chain-end placement, that is, the individual stereoaddition steps are taken to be Bernoullian.

If by σ_n we denote the fraction of M_n being added to the polymer chain ends forming I placements, then the fraction forming S placements is $1 - \sigma_n$. In terms of the rate constants, we write

$$\begin{aligned} \sigma_n &= k_{ni}/k_n \\ 1 - \sigma_n &= k_{ns}/k_n \end{aligned} \quad n = 1, 2 \quad (2)$$

Further, we introduce the following notation

$$\begin{aligned} f_1 &= \frac{k_1[M_1]}{k_1[M_1] + k_2[M_2]} \\ f_2 &= \frac{k_2[M_2]}{k_1[M_1] + k_2[M_2]} = 1 - f_1 \end{aligned} \quad (3)$$

for the mole fractions of M_1 and M_2 consumed, i.e., for the mole fractions of monomers and dimers incorporated into the polymer chain. If $k_1 = k_2$, then f_1 and f_2 are also the mole fractions of M_1 and M_2 in the feed.

We represent, for example, the probability that a randomly picked pair of successive placements along the chain form a sequence of X_2X_1 , X_1 followed by X_2 (where $X_k = I$ or S ; $k = 1, 2$), by $p(X_2X_1)$, following the convention used previously.^{2,6} It is presumed that the chain is statistically stationary, i.e., that the occurrence of any placement sequence of finite length is independent of its position along the chain provided the chain is sufficiently long to permit neglect of end effects.

Singlet and Pair Placements

Suppose that we pick a monomer unit at random in the polymer chain and consider the placement formed by this monomer unit and the succeeding unit. The probability that a randomly chosen monomer unit came

from the first unit of a dimer (to be called a unit of type B) is ϕ_b . The probability that it came from the other sources (monomer or the second unit of a dimer; to be collectively called as units of type A) is then

$$\phi_a = 1 - \phi_b \quad (4)$$

If the monomer unit picked at random from the polymer chains is of type A, then it can be succeeded either by an M_1 with the (conditional) probability f_1 or by an M_2 with the probability f_2 . In case the monomer unit picked is of type B, it is certainly succeeded by the second unit of the dimer. Therefore, the probability of occurrence of either tacticity in the placement formed between a randomly picked monomer unit and the succeeding one is, respectively,

$$p(I) = \phi_a(f_1\sigma_1 + f_2\sigma_2) + \phi_b\delta \quad (5)$$

$$p(S) = \phi_a[f_1(1 - \sigma_1) + f_2(1 - \sigma_2)] + \phi_b(1 - \delta) \quad (6)$$

The singlet tacticity distribution [eqs. (5) and (6)] satisfies the normalization condition

$$p(I) + p(S) = 1 \quad (7)$$

It can be easily shown that

$$\phi_a = 1/(1 + f_2) \quad (8)$$

$$\phi_b = f_2/(1 + f_2)$$

With eqs. (8), we rewrite eqs. (5) and (6) as follows

$$p(I) = (F_1 + F_2 + f_2\delta)/(1 + f_2) \quad (9)$$

$$p(S) = (F_1' + F_2' + f_2\delta')/(1 + f_2) \quad (10)$$

in which we have used the following notation:

$$\begin{aligned} F_1 &\equiv f_1\sigma_1 \\ F_1' &\equiv f_1(1 - \sigma_1) \\ F_2 &\equiv f_2\sigma_2 \\ F_2' &\equiv f_2(1 - \sigma_2), \delta' \equiv 1 - \delta. \end{aligned} \quad (11)$$

Note that

$$\begin{aligned} F_1 + F_1' &= f_1 \\ F_2 + F_2' &= f_2 \end{aligned} \quad (12)$$

In a similar way, we obtain the probability distribution for pairs of placements:

$$p(II) = [(F_1 + F_2)(F_1 + f_2\delta) + F_2\delta]/(1 + f_2) \quad (13)$$

$$p(SS) = [(F_1' + F_2')(F_1' + f_2\delta') + F_2'\delta']/(1 + f_2) \quad (14)$$

$$p(SI) = [(F_1 + f_2\delta)(F_1' + F_2') + F_2\delta]/(1 + f_2) \quad (15)$$

$$p(IS) = [(F_1' + f_2\delta')(F_1 + F_2) + F_2'\delta]/(1 + f_2) \quad (16)$$

As expected for any stationary random sequences,² we can easily verify with eqs. (15) and (16) that

$$p(\text{SI}) = p(\text{IS}) = 1/2 p(\text{SI,IS})$$

where $p(\text{SI,IS}) \equiv p(\text{SI}) + p(\text{IS})$ is the probability that a randomly selected pair of consecutive placements is heterotactic (irrespective of the order).

Stereosequence Distribution

The above method of calculating $p(X_1)$ and $p(X_2X_1)$ where $X_k = \text{I}$ or S ($k = 1, 2$) can be extended to the calculation of $p(X_n \dots X_2X_1)$, the probability that a randomly selected sequence of n consecutive placements is such that the first placement is of type X_1 , the second of type X_2 , etc., for any positive integer n . In matrix notation, we have, denoting the trace by Tr ,

$$p(X_n \dots X_2X_1) = \text{Tr}(\mathbf{X}_n \dots \mathbf{X}_2 \mathbf{X}_1 \phi) \quad (17)$$

or alternatively

$$p(X_n \dots X_2X_1) = (1, 1) \mathbf{X}_n \dots \mathbf{X}_2 \mathbf{X}_1 \begin{pmatrix} \phi_a & 0 \\ 0 & \phi_b \end{pmatrix} \begin{pmatrix} 1 \\ 1 \end{pmatrix}$$

If $X_k = \text{I}$, the matrix \mathbf{X}_k ($k = 1, 2, \dots, n$) is \mathbf{I}

$$\mathbf{I} = \begin{pmatrix} F_1 & \delta \\ F_2 & 0 \end{pmatrix} = \begin{pmatrix} f_1 \sigma_1 & \delta \\ f_2 \sigma_2 & 0 \end{pmatrix} \quad (18)$$

If $X_k = \text{S}$, it becomes \mathbf{S}

$$\mathbf{S} = \begin{pmatrix} F_1' & \delta' \\ F_2' & 0 \end{pmatrix} = \begin{pmatrix} f_1(1 - \sigma_1) & 1 - \delta \\ f_2(1 - \sigma_2) & 0 \end{pmatrix} \quad (19)$$

And the matrix ϕ is given by

$$\phi = \begin{pmatrix} \phi_a & \phi_a \\ \phi_b & \phi_b \end{pmatrix} = \frac{1}{1 + f_2} \begin{pmatrix} 1 & 1 \\ f_2 & f_2 \end{pmatrix} \quad (20)$$

The matrix elements of \mathbf{I} and \mathbf{S} have simple physical meaning. For example, I_{ab} , the 1,2 element of matrix \mathbf{I} , is simply the probability of adding a monomer unit of type A in I placement to the immediately preceding monomer unit of type B. This type of matrix notation was first used in a study of the two-state mechanism⁶ for homogeneous ionic polymerization and allows compact and convenient manipulation of stereosequence distributions.

With eqs. (18)–(20), we have

$$(\mathbf{I} + \mathbf{S})\phi = \phi(\mathbf{I} + \mathbf{S}) = \phi \quad (21)$$

With this and the obvious relations

$$\text{Tr}\mathbf{A} + \text{Tr}\mathbf{B} = \text{Tr}(\mathbf{A} + \mathbf{B})$$

$$\text{Tr}(\mathbf{AB}) = \text{Tr}(\mathbf{BA})$$

we can easily verify that for a given sequence of placements U of any length,

$$p(\text{UI}) + p(\text{US}) = p(U) \quad (22)$$

$$p(\text{IU}) + p(\text{SU}) = p(U) \quad (23)$$

Derivations of eqs. (22) and (23) follows:

$$\begin{aligned} p(\text{UI}) + p(\text{US}) &= \text{Tr}(\mathbf{UI}\phi) + \text{Tr}(\mathbf{US}\phi) \\ &= \text{Tr}[\mathbf{U}(\mathbf{I} + \mathbf{S})\phi] = \text{Tr}(\mathbf{U}\phi) = p(U) \\ p(\text{IU}) + p(\text{SU}) &= \text{Tr}[(\mathbf{I} + \mathbf{S})\mathbf{U}\phi] \\ &= \text{Tr}[\mathbf{U}\phi(\mathbf{I} + \mathbf{S})] = \text{Tr}(\mathbf{U}\phi) = p(U) \end{aligned}$$

Equations (22) and (23) together with eq. (7) verify that the stereosequence distribution generated by eqs. (17)–(20) is indeed statistically stationary.²

Using the matrix formulation of the stereosequence probability distribution, we can also readily derive a recursion formula for $p(\mathbf{I}^n)$, the probability of finding n consecutive I placements and its counterpart $p(\mathbf{S}^n)$ for S placements. Since ϕ has identical columns, $\mathbf{X}\phi$ has identical rows for any 2×2 matrix \mathbf{X} with all different elements. Therefore, we write

$$\mathbf{I}^n\phi = \begin{pmatrix} A_1 & A_2 \\ A_1 & A_2 \end{pmatrix}$$

Then, by multiplying this with \mathbf{I} of eq. (18) from the left, we obtain successively

$$\begin{aligned} \mathbf{I}^{n+1}\phi &= \begin{pmatrix} F_1A_1 + \delta A_2 & F_1A_1 + \delta A_2 \\ F_2A_1 & F_2A_1 \end{pmatrix} \\ \mathbf{I}^{n+2}\phi &= \begin{pmatrix} F_1(F_1A_1 + \delta A_2) + F_2\delta A_1 & F_1(F_1A_1 + \delta A_2) + F_2\delta A_1 \\ F_2(F_1A_1 + \delta A_2) & F_2(F_1A_1 + \delta A_2) \end{pmatrix} \end{aligned}$$

From the above three equalities, we see that

$$\text{Tr}(\mathbf{I}^{n+2}\phi) = F_1\text{Tr}(\mathbf{I}^{n+1}\phi) + F_2\delta\text{Tr}(\mathbf{I}^n\phi)$$

Thus, we obtain

$$p(\mathbf{I}^{n+2}) = f_1\sigma_1p(\mathbf{I}^{n+1}) + f_2\sigma_2\delta p(\mathbf{I}^n) \quad (24)$$

for any positive integer n . From eqs. (9) and (13), we see that for $n = 0$

$$p(\text{II}) = f_1\sigma_1p(\text{I}) + f_2\sigma_2\delta \quad (25)$$

The recursion formula, eq. (24) states that $n + 2$ consecutive I placements may be obtained by adding a monomer in I placement to a sequence of $n + 1$ consecutive I placements or by adding an internally isotactic dimer in

I placement to a sequence of n consecutive I placements. A parallel calculation gives

$$p(S^{n+2}) = f_1(1 - \sigma_1)p(S^{n+1}) + f_2(1 - \sigma_2)(1 - \delta)p(S^n) \quad (26)$$

$$p(SS) = f_1(1 - \sigma_1)p(S) + f_2(1 - \sigma_2)(1 - \delta) \quad (27)$$

with analogous implications.

Characterization of the Distribution

The probability distributions of the pair and triplet placements may be conveniently characterized by the persistence ratio² ρ and the Ω factors^{3,7} (Ω_i and Ω_s), respectively. The former compares $p(X_2X_1) = p(X_2|X_1)p(X_1)$ with $p(X_2)p(X_1)$, that is, the actual pair distribution versus a hypothetical Bernoullian pair distribution with the actual $p(X_1)$ and $p(X_2)$. In the above, we have used $p(X_2|X_1)$ to denote the conditional probability of occurrence of placement X_2 given that the placement immediately preceding is X_1 . The Ω factors contrast $p(XXX) = p(X|XX)p(XX)$ against $[p(XX)/p(X)]p(XX) = p(X|X)p(XX)$, that is, the actual triplet distribution versus a hypothetical first-order Markovian triplet distribution with given $p(XX)$ and $p(X)$. The persistence ratio and the Ω factors may be expressed as^{2,3}

$$\rho = \frac{2p(I)p(S)}{p(SI \vee IS)} = \frac{p(I)[1 - p(I)]}{p(I) - p(II)} = \frac{p(S)[1 - p(S)]}{p(S) - p(SS)} \quad (28)$$

$$\Omega_i = \frac{p(III)p(I)}{[p(II)]^2} \quad (29)$$

$$\Omega_s = \frac{p(SSS)p(S)}{[p(SS)]^2}$$

For the monomer-dimer mechanism under consideration, we find, for example, by using the second expression for ρ in eqs. (28) with eqs. (9) and (13).

$$\rho = \frac{1 - (F_1 + F_2 + f_2\delta)/(1 + f_2)}{1 - [(F_1 + F_2)(F_1 + f_2\delta) - F_2\delta]/(F_1 + F_2 + f_2\delta)} \quad (30)$$

This indicates that $\rho > 1$ or not according to whether

$$(1 + f_2)[(F_1 + F_2)(F_1 + f_2\delta) - F_2\delta] > (F_1 + F_2 + f_2\delta)^2$$

or not. Therefore, except for special cases, we have $\rho \neq 1$ in general; that is, the stereosequence distribution is generally not Bernoullian.

As for the Ω factors, we need $p(III)$ and $p(SSS)$ in addition, which may be obtained from eqs. (17)–(20) or from eqs. (24)–(27)

$$p(III) = [(F_1^2 + F_2\delta)(F_1 + F_2 + f_2\delta) + (1 + f_2)F_1F_2\delta]/(1 + f_2) \quad (31)$$

$$p(SSS) = [(F_1'\delta + F_2'\delta)(F_1' + F_2' + f_2\delta') + (1 + f_2)F_1'F_2'\delta']/(1 + f_2) \quad (32)$$

We find

$$\Omega_i = 1 + F_2\delta \frac{(F_1 + F_2 + f_2\delta)(F_2 + f_2\delta - F_1f_2) - (1 + f_2)^2F_2\delta}{[F_1(F_1 + F_2 + f_2\delta) + (1 + f_2)F_2\delta]^2} \quad (33)$$

and a similar expression for Ω_s by replacing F_1 , F_2 , and δ in eq. (33) by F_1' , F_2' , and δ' , respectively. It can also be seen that Ω_i , for example, can be larger or smaller than unity according to whether $(F_1 + F_2 + f_2\delta)(F_2 + f_2\delta - F_1f_2)$ is larger or smaller than $(1 + f_2)^2F_2\delta$, and therefore $\Omega_i \neq 1$ and $\Omega_s \neq 1$, in general. This signifies that the stereosequence distribution is generally not simple Markovian.

Thus, we have seen that the stereosequence distribution generated by the general monomer-dimer mechanism is neither Bernoullian nor simple Markovian. We now further show that the stereosequence distribution does not in fact obey Markovian statistics of any finite order. For this purpose, we define the following generalized Ω factors

$$\Omega_i^{(n)} = \frac{p(I|I^{n+1})}{p(I|I^n)} = \frac{p(I^{n+2})p(I^n)}{[p(I^{n+1})]^2} \quad (34)$$

Since $\Omega_i^{(n)} = 1$ signifies that $p(I|I^{n+1}) = p(I|I^n)$, $\rho = 1$ and $\Omega_i^{(n)} = 1$ for $n = 1, 2, \dots, k$ is a necessary but not sufficient condition for the distribution to be k th-order Markovian, but $\Omega_i^{(n)} \neq 1$ is a sufficient condition that the distribution is not n th-order Markovian. Using the recursion formula, eq. (24), we have

$$\Omega_i^{(n)} = 1 + F_2\delta \frac{[p(I^n)]^2 - F_1p(I^n)p(I^{n-1}) - F_2\delta[p(I^{n-1})]^2}{[F_1p(I^n) + F_2\delta p(I^{n-1})]^2} \quad (35)$$

for any positive integer n . Since the second term on the right side of eq. (35) does not vanish except for special cases, we see that the stereosequence is non-Markovian. Since $F_2 = f_2\sigma_2$ [eq. (11)], we see from eq. (35) that $\Omega_i^{(n)} = 1$ if there are no dimers ($f_2 = 0$), or if the dimers can add to the polymer chains only in S placement ($\sigma_2 = 0$), or if all the dimers are syndiotactic internally ($\delta = 0$). Similar conclusions may be drawn by considering $\Omega_s^{(n)}$.

Determination of the Parameters and Test of the Mechanism

There are four independent parameters f_1 (or $f_2 = 1 - f_1$), σ_1 , σ_2 , and δ in the general monomer-dimer mechanism and these can be determined at least in principle if we have four independent probabilities obtained from NMR spectra. Suppose that we are given $p(II)$, $p(SS)$, $p(III)$, and $p(SSS)$. The first two give $p(SI \vee IS)$, $p(I)$, and $p(S)$. From eqs. (24) and (26) for $n = 1$ with eqs. (25) and (27), we obtain

$$F_1 = \frac{p(\text{I})p(\text{II}) - p(\text{III})}{[p(\text{I})]^2 - p(\text{II})} \quad (36)$$

$$F_2\delta = \frac{p(\text{I})p(\text{III}) - [p(\text{II})]^2}{[p(\text{I})]^2 - p(\text{II})}$$

$$F_1' = \frac{p(\text{S})p(\text{SS}) - p(\text{SSS})}{[p(\text{S})]^2 - p(\text{SS})} \quad (37)$$

$$F_2'\delta' = \frac{p(\text{S})p(\text{SSS}) - [p(\text{SS})]^2}{[p(\text{S})]^2 - p(\text{SS})}$$

From these relations, we immediately obtain f_1 , f_2 , and σ_1 through

$$f_1 = F_1 + F_1' \quad (38)$$

$$f_2 = 1 - (F_1 + F_1')$$

$$\sigma_1 = F_1/(F_1 + F_1') \quad (39)$$

Furthermore, σ_2 and δ may be obtained by solving

$$\sigma_2\delta = B_1 \quad (40)$$

and

$$(1 - \sigma_2)(1 - \delta) = B_2$$

where

$$B_1 = F_2\delta/(1 - F_1 - F_1') \quad (41)$$

$$B_2 = F_2'\delta'/(1 - F_1 - F_1')$$

Solution of eqs. (40) gives

$$\sigma_2, \delta = \frac{1}{2}[1 + B_1 - B_2 \pm \sqrt{(1 + B_1 - B_2)^2 - 4B_1}] \quad (42)$$

which indicates that the roles played by σ_2 and δ are interchangeable, that is, interchanging σ_2 and δ in all the expressions for the sequence probabilities gives back the same expressions. This conclusion is also expected from the nature of the model itself. The four parameters thus obtained must of course have positive values not exceeding unity.

Suppose that we alter the monomer-dimer composition of the feed without changing the various rate constants. If we assume an equilibrium between M_1 and M_2 , this condition may be realized by simply changing the monomer-feed concentration, since then we have

$$[M_2]/[M_1] = K[M_1] \quad (43)$$

where K is the monomer-dimer equilibrium constant. In the case of insertion polymerization,⁵ this is achieved by controlling the concentration of exchangeable cations on the mineral surface responsible for the formation of dimeric sorption complex. Therefore, if the sequence concentrations of the polymer prepared at different monomer-dimer compositions yield substantially the same values for the parameters σ_1 , σ_2 , and δ and

different values for f_1 and $f_2 = 1 - f_1$, this will serve as a convincing evidence for the applicability of the monomer-dimer mechanism.

Although the above method by itself provides a decisive test for the applicability of the mechanism, we can proceed further under some favorable circumstances. From the definition of f_1 and f_2 given by eqs. (3), it is obvious that these involve only two ratios, $\kappa \equiv k_2/k_1$ and $\mu \equiv [M_2]/[M_1]$:

$$\begin{aligned} f_1 &= 1/(1 + \kappa\mu) \\ f_2 &= \kappa\mu/(1 + \kappa\mu) \end{aligned} \quad (44)$$

Therefore, in addition to the values of the parameters given by eqs. (38), (39), and (42), if we have knowledge of one of the two ratios, say μ , from an independent source, this will determine the other ratio κ .

So far we have concerned ourselves with the general monomer-dimer mechanism. In the following, we will consider a few special cases of the general model.

Monomers Only in the Feed

In the limit with the dimeric species present in the feed in negligible concentration, we expect to recover a completely Bernoullian stereosequence distribution since the monomers are assumed to add to the polymer chains by a Bernoulli trial process. In this almost trivial case with $f_2 = 0$ (and therefore $f_1 = 1$), eqs. (18)–(20) reduce to

$$\begin{aligned} \mathbf{I} &= \begin{pmatrix} \sigma_1 & 0 \\ 0 & 0 \end{pmatrix} \\ \mathbf{S} &= \begin{pmatrix} 1 - \sigma_1 & 0 \\ 0 & 0 \end{pmatrix} \\ \Phi &= \begin{pmatrix} 1 & 1 \\ 0 & 0 \end{pmatrix} \end{aligned} \quad (45)$$

and we recover indeed a Bernoullian sequence distribution with

$$\begin{aligned} p(\text{I}) &= \sigma_1 \\ p(\text{S}) &= 1 - \sigma_1 \end{aligned} \quad (46)$$

and, of course,

$$\rho = \Omega_i = \Omega_s = \Omega_i^{(n)} = \Omega_s^{(n)} = 1 \quad (47)$$

As is well known, this mechanism is consistent with free-radical homopolymerizations.

In this connection, we also note that even if both monomers and dimers are present in the feed, we get a Bernoullian stereosequence distribution

if the highly artificial assumption $\sigma_1 = \sigma_2 = \delta$ is made. If we denote $\sigma_1 = \sigma_2 = \delta$ by x , **I** and **S** now read

$$\mathbf{I} = x \begin{pmatrix} f_1 & 1 \\ f_2 & 0 \end{pmatrix}, \mathbf{S} = (1 - x) \begin{pmatrix} f_1 & 1 \\ f_2 & 0 \end{pmatrix} \quad (48)$$

with ϕ as given by eq. (20), which lead to a Bernoullian stereosequence distribution with $p(\mathbf{I}) = x$ and $p(\mathbf{S}) = 1 - x$, regardless of the value of f_2 (or f_1). That this should be so is obvious if we consider the physical significance of the assumption.

Dimers Only in the Feed

If all the feed molecules are in the dimeric form, we have the opposite extreme. Interestingly, this case corresponds to a special case of a completely different polymerization mechanism proposed for cyclopolymerization.⁴ If the intramolecular cyclization step is Bernoullian, it is immaterial whether the cyclization step occurs prior to or after the intermolecular addition, as far as the resulting stereosequence distribution is concerned. When the addition step is also Bernoullian, the cyclopolymerization mechanism becomes indistinguishable from the dimers-only case of the monomer-dimer mechanism. Stereosequence concentration data obtained by NMR measurements on the poly(methyl methacrylate) derived by hydrolysis of poly(methacrylic anhydride) indicate the consistency of this mechanism for the cyclopolymerization of methacrylic anhydride, except at low temperatures.⁴

In this limit of no monomer in the feed, we set $f_2 = 1$ in eqs. (18)–(20) and obtain

$$\begin{aligned} \mathbf{I} &= \begin{pmatrix} 0 & \delta \\ \sigma_2 & 0 \end{pmatrix} \\ \mathbf{S} &= \begin{pmatrix} 0 & 1 - \delta \\ 1 - \sigma_2 & 0 \end{pmatrix} \\ \phi &= \frac{1}{2} \begin{pmatrix} 1 & 1 \\ 1 & 1 \end{pmatrix} \end{aligned} \quad (49)$$

For any positive integer n , this leads to

$$p(\mathbf{I}^{2n-1}) = [p(\mathbf{II})]^{n-1} p(\mathbf{I}), \quad p(\mathbf{I}^{2n}) = [p(\mathbf{II})]^n \quad (50)$$

$$\begin{aligned} p(\mathbf{I}) &= \frac{1}{2}(\sigma_2 + \delta) \\ p(\mathbf{II}) &= \sigma_2 \delta \end{aligned} \quad (51)$$

Relations analogous to eqs. (50) and (51) hold for $p(\mathbf{S}^k)$ ($k = 1, 2, \dots$), the only difference being replacement of σ_2 and δ by $1 - \sigma_2$ and $1 - \delta$, respectively. We have also

$$p(\mathbf{SI}) = p(\mathbf{IS}) = \frac{1}{2}[\sigma_2(1 - \delta) + (1 - \sigma_2)\delta] \quad (52)$$

The physical meaning of eqs. (50)–(52) is obvious. For example, $p(I)$ may be explained as follows. If we pick a monomer unit in the polymer at random, the probability that it belongs to the head or the tail of the dimer is $1/2$ for each case. The (conditional) probability that a head of the dimer is placed in I placement is σ_2 and that for the tail is δ . Therefore, $p(I)$ is obtained by adding $(1/2)\sigma_2$ and $(1/2)\delta$.

The persistence ratio for this special case turns out to be⁴

$$\rho = \frac{(\sigma_2 + \delta)[(1 - \sigma_2) + (1 - \delta)]}{2[\sigma_2(1 - \delta) + (1 - \sigma_2)\delta]} \quad (53)$$

It can be shown⁴ that

$$1/2 \leq \rho \leq 1 \quad (54)$$

$$\rho = 1 \text{ if } \sigma_2 = \delta \quad (55)$$

$$\rho \rightarrow 1/2 \text{ if } \sigma_2 \rightarrow 0, \delta \rightarrow 1 \text{ or } \sigma_2 \rightarrow 1, \delta \rightarrow 0 \quad (56)$$

In general,⁷ the lower bound to ρ is $1/2$ and there is no upper bound. In this respect, the upper bound of unity obtained for this case is of special interest. Suppose that instead of regularly alternating the head and tail monomer units of dimers, we generate a hypothetical polymer chain by adding broken-off heads and tails at random with equal numbers of heads and tails, but still requiring the heads to connect the chain end with probability σ_2 and the tails with probability δ for I placement. Then, $p(I)$ for this hypothetical chain is the same as that given in eq. (51), but $p(II)$ is no longer $\sigma_2\delta$ but $(1/4)(\sigma_2 + \delta)^2$ or $[p(I)]^2$. Thus we have a Bernoullian sequence distribution with $p(I) = (\sigma_2 + \delta)/2$. Since the persistence ratio is² the ratio of the actual mean length of closed I (or S) sequences calculated on the assumption of the Bernoullian distribution with the same actual $p(I)$, eq. (54) indicates that the regular alternation of heads and tails of the dimers tends to shorten the mean length of closed sequences.

The Ω factors for this special case are

$$\Omega_i = (\sigma_2 + \delta)^2/4\sigma_2\delta \quad (57)$$

$$\Omega_s = [(1 - \sigma_2) + (1 - \delta)]^2/4(1 - \sigma_2)(1 - \delta)$$

$$1 \leq \Omega_i, \Omega_s < \infty \quad (58)$$

$$\Omega_i, \Omega_s = 1 \text{ if } \sigma_2 = \delta \quad (59)$$

$$\Omega_i, \Omega_s \rightarrow \infty \text{ if } \sigma_2 \rightarrow 0, \delta \rightarrow 1 \text{ or } \sigma_2 \rightarrow 1, \delta \rightarrow 0 \quad (60)$$

Again, the regular alternation of heads and tails makes the Ω factors larger than the corresponding value of unity for Bernoullian distributions. The generalized Ω factors defined by eq. (34) reduce to the following for $m = 1, 2, \dots$

$$\Omega_i^{(2m-1)} = (\sigma_2 + \delta)^2/4\sigma_2\delta \quad (61)$$

$$\Omega_i^{(2m)} = 4\sigma_2\delta/(\sigma_2 + \delta)^2$$

These generalized Ω factors are not equal to unity unless $\sigma_2 = \delta$. This shows that regular alternation of two Bernoullian trials leads to a non-Markovian distribution. We note that from eqs. (61) we have

$$\Omega_1^{(2m-1)}\Omega_1^{(2m)} = \Omega^{(2m)}\Omega_1^{(2m+1)} = 1 \quad (62)$$

or

$$p(\text{I}|\text{I}^{2m+1})/p(\text{I}|\text{I}^{2m-1}) = p(\text{I}|\text{I}^{2m+2})/p(\text{I}|\text{I}^{2m}) = 1 \quad (63)$$

which apparently results from the fact that when we consider the stereo-sequence distribution of placements created by the head (or tail) monomer units of the dimers only, it is Bernoullian.

Finally the two parameters σ_2 and δ of this special model may be determined⁴ if two independent sequence probabilities such as $p(\text{I})$ and $p(\text{II})$ are given:

$$\sigma_2, \delta = p(\text{I}) \pm \{ [p(\text{I})]^2 - p(\text{II}) \}^{1/2} \quad (64)$$

As noted previously, σ_2 and δ play interchangeable roles in this model and for unique assignment of each, additional information besides the stereo-sequence distribution is required.

Monomers and Dimers with Single Internal Tacticity

When all the dimers have the same internal tacticity (either $\delta = 1$ or $\delta = 0$), the complete regularity in the internal tacticity of dimer is sharply contrasted to the Bernoullian nature of the tacticity propagation resulting from the addition step of the monomers and dimers to the growing polymer chain. Since the algebra is parallel for $\delta = 1$ and $\delta = 0$, we report here only the results for the case $\delta = 1$. Recently, Blumstein, et al.,⁵ proposed a monomer-dimer model (the BMW model) in which all the dimers are in isotactic internal placements for the insertion polymerization of methyl methacrylate involving the surface of an aluminosilicate mineral.

Substituting $\delta = 1$ into eqs. (18) and (19), we have

$$\begin{aligned} \mathbf{I} &= \begin{pmatrix} F_1 & 1 \\ F_2 & 0 \end{pmatrix} = \begin{pmatrix} f_1\sigma_1 & 1 \\ f_2\sigma_2 & 0 \end{pmatrix} \\ \mathbf{S} &= \begin{pmatrix} F_1' & 0 \\ F_2' & 0 \end{pmatrix} = \begin{pmatrix} f_1(1 - \sigma_1) & 0 \\ f_2(1 - \sigma_2) & 0 \end{pmatrix} \end{aligned} \quad (65)$$

The matrix ϕ is the same as given by eq. (20). The singlet, pair, and triplet probability distributions are

$$p(\text{I}) = (F_1 + F_2 + f_2)/(1 + f_2) \quad (66)$$

$$p(\text{S}) = (F_1' + F_2')/(1 + f_2) \quad (67)$$

$$\begin{aligned} p(\text{II}) &= F_1(F_1 + F_2 + f_2)/(1 + f_2) + F_2 \\ &= F_1p(\text{I}) + F_2 \end{aligned} \quad (68)$$

$$\begin{aligned} p(\text{SS}) &= F_1'(F_1' + F_2')/(1 + f_2) \\ &= F_1'p(\text{S}) \end{aligned} \quad (69)$$

$$\begin{aligned} p(\text{SI}) &= p(\text{IS}) \\ &= {}^{1/2}p(\text{SI} \downarrow \text{IS}) \\ &= (F_1 + f_2)(F_1' + F_2')/(1 + f_2) \\ &= (F_1 + f_2)p(\text{S}) \end{aligned} \quad (70)$$

$$\begin{aligned} p(\text{III}) &= (F_1^2 + F_2)(F_1 + F_2 + f_2)/(1 + f_2) + F_1F_2 \\ &= F_1p(\text{II}) + F_2p(\text{I}) \end{aligned} \quad (71)$$

$$\begin{aligned} p(\text{SSS}) &= F_1'^2(F_1' + F_2')/(1 + f_2) \\ &= F_1'p(\text{SS}) = F_1'^2p(\text{S}) \end{aligned} \quad (72)$$

$$\begin{aligned} p(\text{SII}) &= p(\text{IIS}) \\ &= {}^{1/2}p(\text{SII} \downarrow \text{IIS}) \\ &= [F_1(F_1 + f_2) + F_2](F_1' + F_2')/(1 + f_2) \\ &= [F_1(F_1 + f_2) + F_2]p(\text{S}) \end{aligned} \quad (73)$$

$$\begin{aligned} p(\text{SSI}) &= p(\text{ISS}) \\ &= {}^{1/2}p(\text{SSI} \downarrow \text{ISS}) \\ &= F_1'(F_1 + f_2)(F_1' + F_2')/(1 + f_2) \\ &= (F_1 + f_2)p(\text{SS}) \\ &= F_1'p(\text{IS}) = F_1'(F_1 + f_2)p(\text{S}) \end{aligned} \quad (74)$$

$$\begin{aligned} p(\text{ISI}) &= (F_1 + f_2)^2(F_1' + F_2')/(1 + f_2) \\ &= (F_1 + f_2)p(\text{IS}) = (F_1 + f_2)^2p(\text{S}) \end{aligned} \quad (75)$$

$$\begin{aligned} p(\text{SIS}) &= (F_1F_1' + F_2')(F_1' + F_2')/(1 + f_2) \\ &= (F_1F_1' + F_2')p(\text{S}) \end{aligned} \quad (76)$$

Further, for any sequence length n , we have (since $\mathbf{S}^n = (F_1')^{n-1}\mathbf{S}$)

$$p(\mathbf{S}^n) = [f_1(1 - \sigma_1)]^{n-1}p(\text{S}) \quad n = 1, 2, \dots \quad (77)$$

which indicates that as far as S-S propagation is concerned, the BMW model behaves as a simple Markov process. Equation (77) also conforms to the obvious requirement that for the occurrence of n consecutive S placements, successive addition of at least $n - 1$ monomers is necessary. On the other hand, for $p(\mathbf{I}^n)$ we have

$$p(\mathbf{I}^{n+2}) = f_1\sigma_1p(\mathbf{I}^{n+1}) + f_2\sigma_2p(\mathbf{I}^n) \quad (78)$$

with physical significance analogous to that of eq. (24).

The persistence ratio ρ is found to be

$$\rho = (f_1\sigma_1 + f_2\sigma_2 + f_2)/(1 + f_2)(f_1\sigma_1 + f_2) \tag{79}$$

and it can be seen that

$$1/2 < \rho < 2 \tag{80}$$

$$\rho \geq 1 \text{ if } \sigma_2 \geq f_1\sigma_1 + f_2 \tag{81}$$

$$\rho < 1 \text{ if } \sigma_2 < f_1\sigma_1 + f_2 \tag{82}$$

From eq. (79) it can be seen that ρ is a monotonically decreasing function of σ_1 for fixed σ_2 and f_2 , and a monotonically increasing function of σ_2 for fixed σ_1 and f_2 . And, in the limits of $\sigma_1 \rightarrow 0$ and $\sigma_2 \rightarrow 1$, we have $\rho = 2/(1 + f_2)$. When $f_2 \rightarrow 0$ ($f_2 \gg \sigma_1, 1 - \sigma_2$), then ρ approaches its upper bound 2. This limiting case may be visualized as an almost continuous S sequence arising from the monomer addition occasionally interrupted by an II sequence coming from rare dimer additions. Here, we have $\mu_i \rightarrow 2$ and $\mu_s \rightarrow \infty$, where μ_i and μ_s are the mean lengths of closed I and S sequences, respectively. Thus, we obtain⁷

$$\rho = \mu_i\mu_s/(\mu_i + \mu_s) \approx \mu_i \approx 2$$

It is true that if σ_1 is nonvanishingly small, then μ_i gets longer than 2. However, this is more than compensated by much shortened, finite value of μ_s , together leading to $\rho < 2$. For example, if $\sigma_1 = 0.01$, we have $\mu_i = 2.01$ and $\mu_s = 43.9$, yielding the maximum value of $\rho = 1.92$ at $f_2 = 0.0218$. On the other hand, if we consider the limit of $f_2 \rightarrow 1$, we have $\rho = (1 + \sigma_2)/2$, corresponding to the case of dimers only in the feed [Eq. (53)] with $\delta = 1$. Thus, as $\sigma_2 \rightarrow 0$ ($\sigma_2 \gg f_2$), ρ approaches its lower bound of $1/2$. Here we have almost regularly repeating sequence of SI occasionally interrupted by an II sequence. Obviously, we have $\mu_i \approx \mu_s \approx 1$ and hence $\rho \approx 1/2$.

The Ω factors are given as follows

$$\Omega_i = 1 + f_2\sigma_2 \frac{[f_1(1 - \sigma_1) + f_2(1 - \sigma_2)][f_2(f_1\sigma_1 + f_2) - f_2\sigma_2]}{[f_1\sigma_1(f_1\sigma_1 + f_2\sigma_2 + f_2) + (1 + f_2)f_2\sigma_2]^2} \tag{83}$$

$$\Omega_s = 1 \tag{84}$$

For Ω_i , we have further

$$0 < \Omega_i < \infty \tag{85}$$

$$\Omega_i \geq 1 \text{ if } f_1\sigma_1 + f_2 \geq \sigma_2 \tag{86}$$

$$\Omega_i < 1 \text{ if } f_1\sigma_1 + f_2 < \sigma_2 \tag{87}$$

Again, in the limit of $\sigma_1 \rightarrow 0$, $\sigma_2 \rightarrow 1$ and $f_2 \rightarrow 0$, we see that although $p(\text{I}) \approx 0$, $p(\text{II}) \approx 0$, $p(\text{I}|\text{I}) \approx 1/2$ but $p(\text{I}|\text{II}) \approx 0$, which lead to $\Omega_i \approx 0$. If $f_2 \rightarrow 1$, $\sigma_2 \rightarrow 0$, then $p(\text{I}) \approx 1/2$, $p(\text{II}) \approx 0$, $p(\text{I}|\text{I}) \approx 0$, $p(\text{I}|\text{II}) \approx 1/2$

which lead to $\Omega_i = p(\text{I}|\text{II})/p(\text{I}|\text{I}) \rightarrow \infty$. As for $\Omega_s = 1$, we note that this ensures⁷

$$\frac{p(\text{S}|\text{SS})}{p(\text{S}|\text{S})} = \frac{p(\text{I}|\text{SS})}{p(\text{I}|\text{S})} = \frac{p(\text{S}|\text{SI})}{p(\text{S}|\text{S})} = \frac{p(\text{I}|\text{SI})}{p(\text{I}|\text{S})} = 1 \quad (88)$$

The other ratios $p(\text{X}_2|\text{IX}_1)/p(\text{X}_2|\text{I})$ in terms of Ω_i and $p(\text{X}_2|\text{I})$ are⁷

$$\begin{aligned} \frac{p(\text{S}|\text{II})}{p(\text{S}|\text{I})} &= \frac{p(\text{I}|\text{IS})}{p(\text{I}|\text{I})} = \frac{1 - p(\text{I}|\text{I})\Omega_i}{p(\text{S}|\text{I})} \\ \frac{p(\text{S}|\text{IS})}{p(\text{S}|\text{I})} &= \frac{1 - 2p(\text{I}|\text{I}) + [p(\text{I}|\text{I})]^2\Omega_i}{[p(\text{S}|\text{I})]^2} \end{aligned} \quad (89)$$

The generalized Ω factors are, for any positive integer n ,

$$\Omega_s^{(n)} = 1 \quad (90)$$

$$\Omega_i^{(n)} = 1 + F_2 \frac{[p(\text{I}^n)]^2 - F_1 p(\text{I}^n) p(\text{I}^{n-1}) - F_2 [p(\text{I}^{n-1})]^2}{[F_1 p(\text{I}^n) + F_2 p(\text{I}^{n-1})]^2} \quad (91)$$

Thus, the BMW mechanism⁵ generates a stereosequence distribution which is partially simple Markovian in the sense of eqs. (84) and (90) but the overall distribution is non-Markovian in general, as can be seen from eq. (91). Obviously, if $\delta = 0$, then we have $\Omega_i^{(n)} = 1$ and $\Omega_s^{(n)} \neq 1$, in general.

There are three independent parameters f_1 , σ_1 , and σ_2 in the BMW model, which can be uniquely determined, at least in principle, if we have three independent sequence probabilities such as $p(\text{II})$, $p(\text{SS})$, and $p(\text{III})$. Again, $p(\text{II})$ and $p(\text{SS})$ completely determine $p(\text{IS}, \text{SI})$, $p(\text{I})$, and $p(\text{S})$. If we solve eqs. (68) and (71), we obtain the expressions for F_1 and F_2 as given by eq. (36) with δ replaced by unity. As for F_1' , eq. (69) gives

$$F_1' = p(\text{SS})/p(\text{S}) \quad (92)$$

From these, we obtain

$$f_1 = F_1 + F_1' \quad (93)$$

$$f_2 = 1 - F_1 - F_1' \quad (94)$$

$$\sigma_1 = F_1/(F_1 + F_1') \quad (95)$$

$$\sigma_2 = F_2/(1 - F_1 - F_1') \quad (96)$$

We can also subject the model to a stringent test if we have sequence probability data for different monomer-dimer concentration ratios, as discussed in a previous sections.

Concluding Remarks

In the above, we have considered the monomer-dimer mechanism of polymerization and the resulting stereosequence distribution (see Appendix). It is shown by means of the generalized Ω factors (and by other results as well) that although the individual steps involved in the mechanism are all Bernoullian, the composite overall stereosequence distribution is, in general, non-Markovian. A similar situation has already been found in

the two-state mechanism⁶ for ionic polymerization. We have also shown how the four independent kinetic parameters of the monomer-dimer mechanism can be determined from four experimentally observed placement sequence concentrations. A convincing experimental test for physical applicability of the mechanism is also described.

We recover a Bernoullian stereosequence distribution, as expected, in the limit of monomers only in the feed. Even when the dimer concentration is not negligible, we obtain a Bernoullian distribution indistinguishable from that generated by the case of monomers only in the feed, if a highly artificial assumption is made that all three modes of forming placements yield the same fraction of I (or S) placement.

Another special case discussed is the limiting case with dimers only in the feed, which is equivalent to a special mechanism for cyclopolymerization proposed previously by Reinmüller and Fox.⁴ Although the tacticity distribution of the heads (and tails) alone of the dimers is Bernoullian, the overall stereosequence distribution is non-Markovian.

Other cases of special interest arise if all the dimers in the monomer-dimer mixture have a single internal tacticity. For the case where the preformed dimer tacticity is isotactic as proposed by Blumstein, et al.⁵ in connection with the insertion polymerization involving a mineral surface, we have seen that, although the propagation of consecutive syndiotactic placements alone is simple Markovian, the stereosequence distribution as a whole is non-Markovian.

It is seen in the above discussions that the persistence ratio and the Ω factors sometimes serve as convenient criteria for ruling out certain mechanisms. For example if one of the following is found to hold, the limiting case of dimers only is ruled out: (1) $\rho > 1$, (2) $\Omega_i < 1$, (3) $\Omega_s < 1$, (4) $\Omega_i^{(2)} > 1$, (5) $\Omega_s^{(2)} > 1$, (6) $\Omega_i \Omega_i^{(2)} \neq 1$, (7) $\Omega_s \Omega_s^{(2)} \neq 1$, etc. Similarly, if we find experimentally either $\rho > 2$ or $\Omega_s \neq 1$, then the BMW model cannot account for the stereosequence distribution.

Further generalization of the monomer-dimer model in a few directions is conceivable. For example, the individual addition steps might be assumed to be simple Markovian instead of Bernoullian. Effects of relatively slow monomer-dimer equilibration may be required to be taken into account in some cases. Perhaps a practically more important extension would be the removal of the low-conversion hypothesis.

APPENDIX

To illuminate the nature of the statistical processes involved in the monomer-dimer mechanism, we present in this Appendix a simple analogue in the form of a card game.

The stereosequence distribution resulting from the monomer-dimer mechanism may be reproduced by shuffling and drawing cards in four decks each containing a large number of cards. Three decks are related to three different types of monomer units (or placements formed by adding three different types of monomer units) in the polymer chain and each contains

two kinds of cards labeled I and S. Deck 1 is for the placement coming from the addition of monomer molecules in the feed and a fraction σ_1 of these cards are I. Deck 2 is for the placement coming from the addition of the head monomer units of the dimers in the feed and fraction σ_2 of these are I. Deck 3 is for the internal placement in the dimer molecules and accordingly a fraction δ are labeled I.

Drawing a card from deck 4 decides which of the two decks (decks 1 and 2) to use at one time. Naturally, a fraction f_1 of the cards in deck 4 are labeled M and the remainder D. If a card drawn from deck 4 is an M, we draw a card from deck 1. If it is I (or S), we add a monomer unit to the polymer chain in I (or S) placement. Then we go back to deck 4 and draw another card. If it is a D, we draw a card from deck 2. We add a monomer unit in I or S placement according to this outcome. Drawing of a card from deck 2 is automatically followed by drawing a card from deck 3 without consulting deck 4. Again a monomer unit is added to the polymer chain in the tacticity specified by the card drawn from deck 3. Then we go back to deck 4 to decide which of the two decks 1 and 2 is to be used next. After each drawing of a card from a deck, it is replaced in the deck which is then shuffled.

In the special case of no dimers in the feed, deck 4 consists of M cards only and only deck 1 is used to decide successive placements produced by the addition of monomer units. If decks 1 through 3 have the same I-S composition, we may use any one of them disregarding all the other decks including deck 4 (irrespective of its M-D composition). In the dimers-only case, there are no M cards in deck 4 and we draw cards alternately from decks 2 and 3. Therefore, only two decks are used in this case. In the special case of the BMW model, deck 3 contains only I cards. Therefore, in this case, after drawing a card from deck 2 and adding a monomer unit according to the outcome of the drawing, we automatically add another monomer unit always in I placement. Thus we can play the game with these three decks eliminating deck 3.

This development was motivated by the work of Drs. A. Blumstein, S. L. Malhotra and A. C. Watterson. The present authors are greatly indebted to them for the opportunity of seeing their manuscript prior to publication.

References

1. B. D. Coleman, *J. Polym. Sci.*, **31**, 155 (1958).
2. B. D. Coleman and T. G. Fox, *J. Polym. Sci. A*, **1**, 3183 (1963).
3. B. D. Coleman, T. G. Fox, and M. Reinmüller, *J. Polym. Sci. B*, **4**, 1029 (1966).
4. M. Reinmüller and T. G. Fox, paper presented at American Chemical Society Meeting, 1966; *Polym. Preprints*, **7**, 1005 (1966); M. Reinmüller, C. W. Pyun, and T. G. Fox, to be published.
5. A. Blumstein, S. L. Malhotra, and A. C. Watterson, *J. Polym. Sci. A-2*, **8**, 1599 (1970).
6. B. D. Coleman and T. G. Fox, *J. Chem. Phys.*, **38**, 1065 (1963).
7. C. W. Pyun, *J. Polym. Sci. A-2*, **8**, 1111 (1970).

Received May 15, 1970

Kinetic Study of Dissolution of Poly(vinyl Chloride) in Cyclohexanone

LUBOMÍR LAPČÍK and LADISLAV VALKO, *Institute of Physical Chemistry, Slovak Technical University, Bratislava, Czechoslovakia*

Synopsis

The kinetics of dissolution of five fractions of commercial poly(vinyl chloride) in cyclohexanone was studied at temperatures from 20 to 70°C. Good agreement was observed between the experimental results and equations expressing the dependence of the induction periods and the rates of dissolution on temperature and molecular weight. It was found that the apparent activation energy for the swelling process lies in the range 9–14 kcal/mole and the apparent activation energy for the dissolution diffusion process in the range 8–12 kcal/mole. The apparent dependence of activation energies on number-average molecular weight indicates that the chain ends are more important in determining the dissolution rate than the centers of the polymer chains.

Introduction

If a solid macromolecular film is in contact with a liquid solvent, the movement of the optical boundary of solvent into the sample and the "solid"–liquid interface in the opposite direction can be observed.¹ The latter movement can be viewed as an intrinsic swelling and is known as Kirkendall's effect.² The forward velocity of the optical boundary determines the rate of dissolution.³ The diffusion of solvent molecules into the polymer is caused by a gradient of chemical potential which depends on the molecular size and chemical composition of the solvent.

The dissolution of macromolecular compounds usually does not take place immediately after they come into contact with the solvent, but after a definite induction period, t_0 ,⁴ which depends on temperature, molecular weight of polymer, kinetic properties of solvent, and also on the method of preparation of the film.

Induction Period for Dissolution

After the initial induction period a steady state is reached in which the dissolution process becomes stationary. According to Eyring's transition-state theory⁵ of diffusion processes, the movement of the solvent molecules takes place through local density fluctuations or "holes" which are produced as a result of polymer segmental mobility. The movement of the optical interface between solvent and polymer determines the rate of dissolution.

For the induction period, eq. (1) is valid:⁶

$$t_Q - \tau = \delta^2/4\kappa D \quad (1)$$

where δ is the total thickness of the swollen layer on the film surface, κ is a parameter appearing in the expression for the rate of movement of the optical interface, D is the diffusion coefficient of solvent, and τ is the time at which diffusion begins, which we set equal to zero. We discuss the kinetic phenomena connected with the swelling and dissolution of polymers formally in terms of the simple classical model of an activated process.

According to Eyring and co-workers,⁵ the diffusion coefficient for solvent may be expressed as

$$D = K\lambda^2 e(kT/h) \exp\{\Delta S^\ddagger/R\} \exp\{-\Delta E_D/RT\} \quad (2)$$

where K is the transition coefficient; λ is the average distance between two consecutive equilibrium positions of solvent molecules; k , T , e , and R have their usual significance; ΔE_D is the activation energy and ΔS^\ddagger is the activation entropy for diffusion.

Ueberreiter and Asmussen,⁴ studying the dissolution of polystyrene in various solvents, have found that the effective thickness of the swollen surface layer is temperature-dependent according to the empirical equation (3):

$$\delta = \delta_0 \exp\{-A_\delta/T\} \quad (3)$$

where δ_0 is the thickness of the total swollen surface layer at infinite temperature and A_δ is an empirical constant.

The thickness of the swollen surface layer plays a larger role in the dissolution and fractional dissolution of polymers. Assuming that eq. (3) is valid for our case and taking account of Eyring's transition state theory of diffusion, we may rewrite eq. (1) in the form

$$t_Q = t_Q^0 \exp\{\Delta E_s/RT\} \quad (4)$$

where t_Q^0 is given by

$$t_Q^0 = \delta_0^2 \exp\{-\Delta S^\ddagger/R\} / [4\kappa K\lambda^2 e(kT/h)] \quad (5)$$

and ΔE_s is the apparent activation energy of swelling defined as

$$\Delta E_s = \Delta E_{D,s} - 2RA_{\delta,s} \quad (6)$$

Here $\Delta E_{D,s}$ and $A_{\delta,s}$ are, respectively, the apparent activation energy of diffusion connected with swelling and an empirical constant. The physical meaning of $A_{\delta,s}$ was explained in our previous work.⁷

The dependence of swelling time t_Q on molecular weight can be derived from eq. (1) on the assumption that the total thickness of the swollen surface layer can be represented by a uniform layer⁴ of polymer coils of effective mean-square radius of gyration $\langle s^2 \rangle^{1/2}$. Then, we have

$$\delta \approx 2n\langle s^2 \rangle^{1/2} \approx n\varphi_{\text{eff}} \quad (7)$$

where n is the effective number of polymer coils across of the swollen surface layer and φ_{eff} is the effective diameter of a coil.

For randomly coiled linear polymer molecules, the mean square radius of gyration is directly proportional to the molecular weight. In good solvents this proportionality is lost. This is due to expansion of the coils resulting from strong solvent-solute interactions. Then, the relation between the mean-square radius of gyration and molecular weight can be expressed by⁸

$$\langle s^2 \rangle = k' M^{1+\epsilon} \quad (8)$$

where ϵ is a measure of the deviation from random coil statistics.

It can be supposed that the number of polymer coils included in the swollen surface layer increases with increasing molecular weight as a consequence of entanglement and then that

$$\delta \approx k'' M^{\beta+1/2(\epsilon+1)} = k'' M^{\alpha/2} \quad (9)$$

where k'' , α , and β are constants independent of molecular weight.

By substituting eqs. (7), (8), and (9) in eq. (1) the expression (10) for the dependence of the induction period on molecular weight is obtained:

$$t_Q = [(k'')^2/4\kappa D] M^\alpha \quad (10)$$

Rate of Dissolution

The rate of dissolution of macromolecular substances is determined primarily by the diffusion of solvent molecules inside the polymer sample. The diffusion rate depends on the molecular volume and the chemical structure of the solvent.

In the following, a polymer solution is considered as a binary system in which the first component consists of macromolecular coils solvated to different degrees and the second component is the solvent. Throughout, J denotes the local flow of solvent (expressed as grams per square centimeter per second) crossing a plane parallel to the film surface, and c denotes the local concentration of this component (in grams per cubic centimeter). The flux density of solvent molecules in the laboratory coordinate system $(J)_C$ is related to the flux density $(J)_O$ referred to the optical plane, which is defined by the maximum value of the refractive index gradient at the boundary between the gel and infiltration layers, by eq. (11):⁹

$$(J)_C = (J)_O + u_{OC}c \quad (11)$$

Here, u_{OC} is the velocity of frame O with respect to frame C, and c is the concentration of solvent molecules at the position and time considered. For the steady state, the net flux density through the optical plane is zero; i.e. $(J)_O = 0$, and the equation for the rate of dissolution can be obtained as

$$u_{OC} = (J)_C/c_\xi \quad (c = c_\xi; x = \xi) \quad (12)$$

With the assumption that the system does not change volume during mixing, the flux density can be expressed as

$$(J)_C = (J)_V = -D_V(dc/dx) \quad (13)$$

where $(J)_V$ and D_V are the flux density and the mutual diffusion coefficient with respect to the fixed frame. By continuity $(J)_C$ must now be independent of x ; thus eq. (13) may be immediately integrated:

$$u_{OC} = \bar{D}_V(c_1 - c_2)/\delta_e c_\xi \quad (14)$$

or

$$u_{OC} = \bar{D}_V(\varphi_1 - \varphi_2)/\delta_e \varphi_\xi \quad (15)$$

where

$$\bar{D}_V = \bar{D} = [1/(c_1 - c_2)] \int_{c_1}^{c_2} D_V(c) dc \quad (16)$$

δ_e is the effective value of the thickness of the swollen surface layer, c and φ are concentrations and volume fractions of solvent molecules, and the subscripts 1 and 2 refer to the outer and inner boundaries of the surface layer, respectively. In the case of polymer dissolution with high polymer concentration in the swollen surface layer we can further assume $\varphi_1 = 1$ and $\varphi_2 = 0$, and obtain from eqs. (15) and (16)

$$u_{OC} = \bar{D}/\delta_e \varphi_\xi \quad (17)$$

which is identical with the equation derived by Ueberreiter and Asmussen.¹⁰

The rate of dissolution obtained from the application of the absolute rate theory and eq. (3) can be expressed as

$$u_{OC} = u_{OC}^0 \exp\{-\Delta E_d/RT\} \quad (18)$$

where ΔE_d is the activation energy for dissolution and u_{OC}^0 is the pre-exponential factor defined by¹¹

$$u_{OC}^0 = K\lambda^2 e(kT/h\delta_0) \exp\{\Delta S^\ddagger/R\} \quad (19)$$

where δ_0 is the thickness of swollen surface layer at infinite temperature and the other symbols have their usual significance.

Equation (17) can be rewritten by means of eq. (7) in the form

$$u_{OC} = \bar{D}/2n\langle s^2 \rangle^{1/2} \varphi_\xi \quad (20)$$

provided that \bar{D} and φ_ξ are independent of the molecular weight of the polymer. With eq. (9), eq. (20) can be written

$$u_{OC} = (\bar{D}/k'' \varphi_\xi) M^{-\alpha/2} \quad (21)$$

which expresses the dependence of the rate of dissolution at a given temperature on the molecular weight.

Experimental

For an investigation of the dissolution process it is necessary to follow continuously the increase in concentration of dissolved macromolecules in the solvent without disturbing the process. As Ueberreiter and Asmussen^{3,4} pointed out, this seems to be best done by measuring the increase in refractive index of the solution. It is possible to measure changes in concentration so small that one can regard the solution as a pure solvent.

The apparatus used in this work is shown in Figure 1. The solvent is supplied from a buret into the thermostatted vessel (A) and at the same time the polymer sample is fixed in the dissolution chamber (B). The immersion refractometer (D) is sealed in the measuring chamber (C). After 1 hr all the internal parts of the apparatus have come into thermal equilibrium and the kinetic measurement can be begun.

The solvent is supplied from vessel (A) to the dissolution chamber and is circulated by means of a stirring device.

Kinetic studies were made on five fractions of PVC prepared by fractional precipitation of a Czechoslovak commercial product. The samples studied were rectangular in shape (1.0 cm × 5.0 cm) and about 1 mm thick. The samples were cut from films cast from tetrahydrofuran. The PVC films were baked for several weeks (in a vacuum thermostat) at 50°C to remove residual solvent.

The limiting viscosity numbers for individual fractions and corresponding values of \bar{M}_n computed from the Mark-Houwink equation,¹² $[\eta] = 2.4 \times 10^{-5} M^{0.77}$ (cyclohexanone, 25.0°C), are listed in Table I.

TABLE I
Intrinsic Viscosities and Number-Average Molecular Weights of PVC Fractions

Fraction	Intrinsic viscosity [η], dl/g	\bar{M}_n
1	1.50	85,000
2	1.16	60,000
3	0.93	47,000
4	0.80	38,000
5	0.60	31,000

The velocity of movement of the optical boundary was calculated from eq. (22):

$$u_{OC} = (1/\rho S)(dm/dt) \quad (22)$$

where dm/dt is the rate of dissolution expressed as a quantity of material dissolved in grams per second from a surface of area S . The density ρ of the polymer and the surface area are temperature-independent in this narrow temperature interval. For dilute polymer solutions (our case) one can write:

$$dm/dt = k_n(dn_D/dt) \quad (23)$$

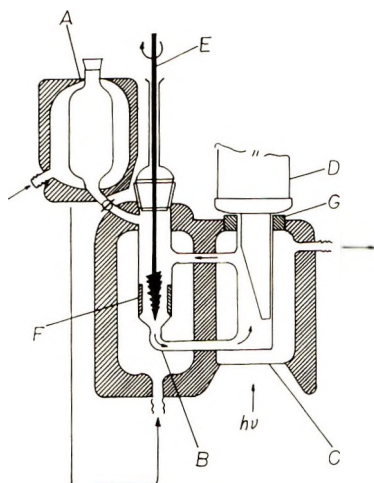


Fig. 1. Schematic drawing of equipment: (A) thermostatted vessel; (B) dissolution chamber; (C) measuring chamber; (D) immersion refractometer; (E) stirring device; (F) polymeric sample; (G) rubber ring.

where dn_D/dt is the rate of change of the refractive index of the solution (Na_D line). The numerical value of the constant k_n was determined from experimental measurements.

Freshly distilled cyclohexanone (Lachema, analytical grade) was used.

Results and Discussion

Relatively little information is available from the literature about swelling and dissolution of PVC, especially with respect to the influence of molecular weight and molecular weight distribution. Corbiere et al.¹³ studied the kinetics of dissolution of PVC in several solvents, but only from a qualitative point of view. The first quantitative kinetic study of dissolution of PVC was described in 1966.¹¹

Swelling and dissolution of polymers are likely to be controlled by the diffusion of solvent molecules. Hence knowledge of the dependence of induction periods and dissolution rates on temperature, molecular weight, and molecular structure of solvent and polymer will be valuable in promoting understanding of the swelling and dissolution mechanism. The appearance of an induction period and the apparent dependence of the dissolution rate on the swelling of a polymer film both imply that the rate-determining process is the movement of segments of the polymer chain. The rate of diffusion is slow until polymer molecules on the surface have been solvated by the solvent.

Plots of the dissolution data, obtained as the change of refractive index of the solution with time, gave the results illustrated in Figures 2 and 3. After an initial induction period, which is dependent on molecular weight, solvent activity, and temperature, linear plots were obtained. These are

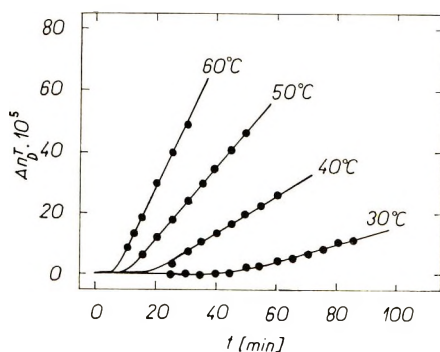


Fig. 2. Kinetic curves of dissolution of PVC in cyclohexanone (fraction 1).

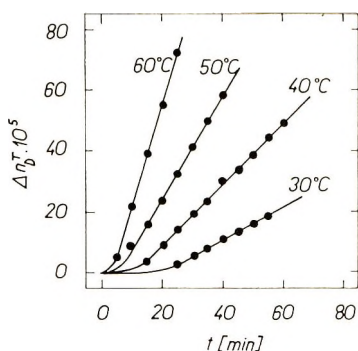


Fig. 3. Kinetic curves of dissolution of PVC in cyclohexanone (fraction 2).

in good agreement with results obtained by Ueberreiter and Asmussen⁴ for the dissolution of polystyrene in amylacetate.

During the induction period the change of the end-to-end distances of macromolecular coils becomes large enough for macromolecular coils to leave the rubberlike layer of amorphous polymer and go through the polymer-solvent interface into the solution. In order to understand swelling and dissolution of polymers, it is important to distinguish between molecular vibrations and rotations. Since many modes of oscillation exist, there are many types of vibrational energy governed by the force constants and mass concentrations in the system. In accordance with Bueche¹⁴ we shall assume that a polymer segment will be able to jump or rotate whenever the density of segments becomes smaller than a certain critical value. A rotational reorientation process of macromolecular segments during swelling includes local lattice expansion against the internal pressure. The work associated with the activation volume is included in the activation enthalpy of swelling or dissolution of the polymer.⁷ The activation enthalpy includes the energy differences between the original and activated states due to very many bonds in the molecule.

The induction period can be expected to disappear at a temperature somewhere near the glass transition temperature of the polymer, i.e., above

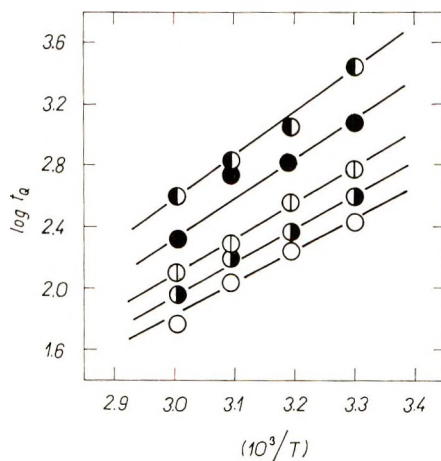


Fig. 4. Induction period of dissolution of PVC in cyclohexanone as a function of temperature: (●) fraction 1; (●) fraction 2; (⊙) fraction 3; (●) fraction 4; (○) fraction 5.

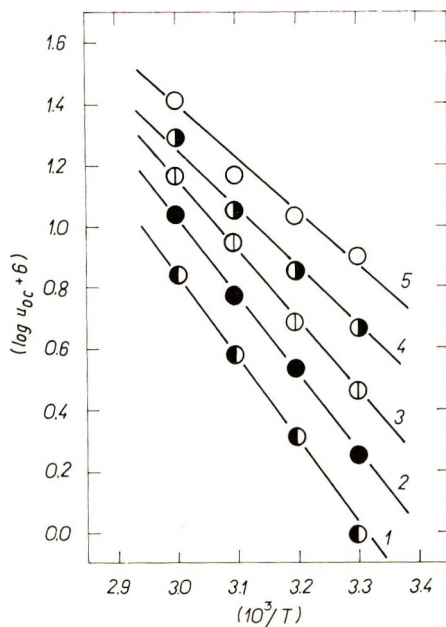


Fig. 5. Rate of dissolution of PVC in cyclohexanone as a function of temperature: (●) fraction 1; (●) fraction 2; (⊙) fraction 3; (●) fraction 4; (○) fraction 5.

82°C for PVC. This trend can also be observed from the data in Figures 2 and 3.

The experimentally determined dependence of the induction period t_0 for dissolution on temperature (Fig. 4) is in good agreement with eq. (4). The calculated apparent activation energies of swelling for PVC in cyclohexanone for the given ranges of molecular weight and temperature are between 9 and 14 kcal/mole.

Comparatively good agreement of experimental results for the depen-

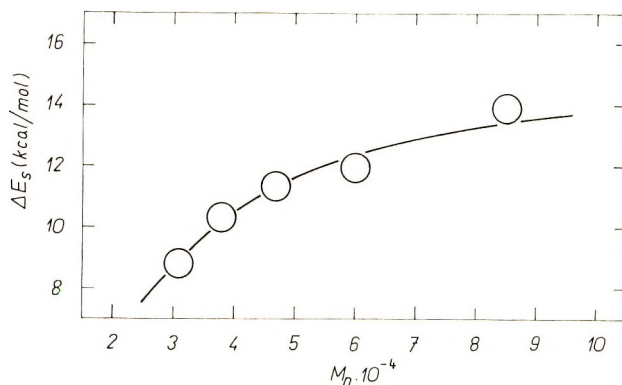


Fig. 6. Apparent activation energy of swelling of PVC in cyclohexanone as a function of molecular weight.

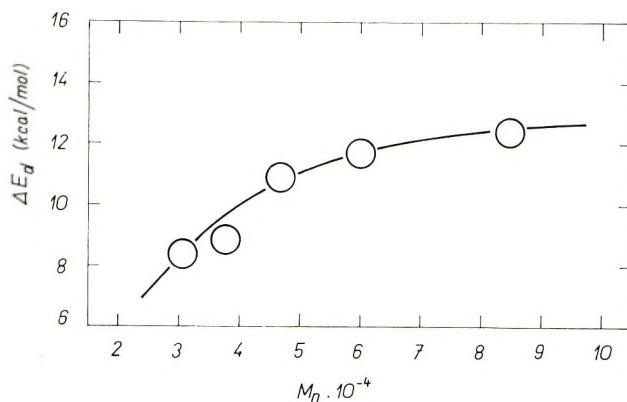


Fig. 7. Apparent activation energy of dissolution of PVC in cyclohexanone as a function of molecular weight.

dence of the rate of dissolution on temperature is evident from Figure 5. The calculated apparent activation energies of dissolution of PVC in cyclohexanone are between 8 and 12 kcal/mole.

The dependence of apparent activation energies ΔE_s and ΔE_d on the number-average molecular weight of PVC (Figs. 6 and 7) indicates that the chain ends make a greater contribution to the swelling and dissolution than the interior of the polymer chains.

TABLE II
The Parameter α as a Function of Temperature

Temperature, °C	α	
	Calcd from $t_Q = t_Q(M)$	Calcd from $u_{OC} = u_{OC}(M)$
30.0	2.2	3.8
40.0	1.9	3.0
50.0	1.8	2.8
60.0	1.8	2.6

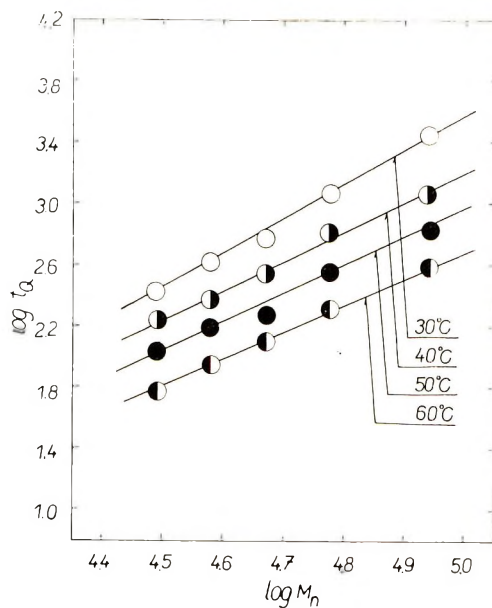


Fig. 8. Induction period for dissolution of PVC in cyclohexanone as a function of molecular weight.

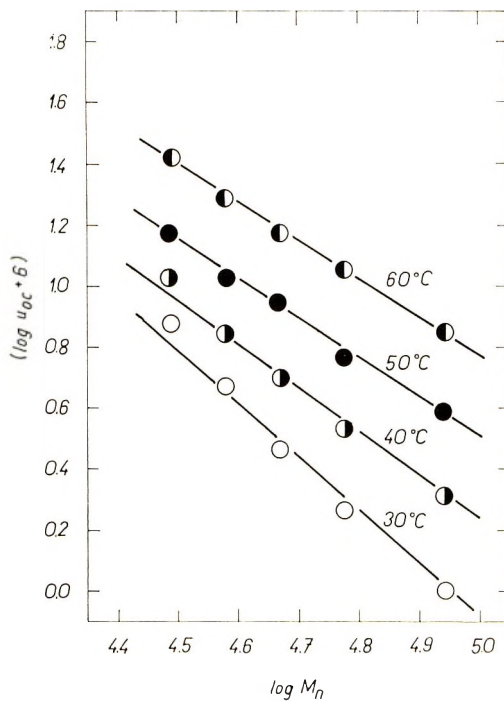


Fig. 9. Rate of dissolution of PVC in cyclohexanone as a function of molecular weight.

From the comparison of apparent activation energies of swelling and dissolution of polymers, it follows that the latter are smaller by about 0.8 kcal/mole. The initial arrangement of the macromolecular coils in the surface of a sample may have a considerable effect on these quantities as different values are sometimes obtained for the interior part of the sample. The dissolution of PVC, especially in poor solvents, varies with the method of film preparation. In going from poor solvents to good solvents, the polymer coil in solution expands. The deformation of the polymer chain network produces changes in chain conformations with a concomitant change in the potential energy of this network. The magnitude of the apparent activation energies of swelling and of dissolution, according to the current viewpoint, are connected with the transition of polymer chain segments from a low-energy to a high-energy state. In the swelling of the polymer many segments of the polymer chain are displaced from their original positions in the lattice by the solvent molecules. In the course of this process, some of the displaced segments or their neighbors will be forced to assume conformationally higher energy states. This effect influences the magnitude of the apparent activation energies of swelling and dissolution. From Figures 6 and 7 it follows that the activation energy is constant or independent of the molecular weight for $\bar{M}_n > 100,000$.

Values of $\log t_Q$ and $\log u_{OC}$ are plotted against $\log \bar{M}_n$ in Figures 8 and 9, respectively. However, the slope of the straight line through the data points represents α . The temperature dependence of α is given in Table II.

We would like to thank Professor Vojtech Kellö for his interest in this work and for the facilities placed at our disposal. We wish to express our deep gratitude to Professor H. Odani, Dr. L.-O. Sundelöf and Dr. T. E. Gunter from the Institute of Physical Chemistry University of Uppsala for critical discussion of this paper.

References

1. C. Robinson, *Proc. Roy. Soc. (London)*, **A204**, 339 (1950).
2. A. Smiegelskas and E. Kirkendall, *Trans. AIME*, **171**, 130 (1947).
3. F. Asmussen and K. Ueberreiter, *Kolloid-Z.*, **185**, 1 (1962).
4. K. Ueberreiter and F. Asmussen, *J. Polym. Sci.*, **23**, 75 (1957); *ibid.*, **57**, 187, 199 (1962).
5. S. Glasstone, K. J. Laidler, and H. Eyring, *The Theory of Rate Processes*, McGraw-Hill, New York, 1941.
6. L. Valko, *Chem. Zvesti*, **15**, 1 (1961).
7. L. Valko and L. Lapčík, *Sborník Chem. fak. SVŠT*, **1967**, 47.
8. V. P. Shanbhag and J. Öhman, *Arkiv Kemi*, **9**, 163 (1968).
9. J. G. Kirkwood, R. L. Baldwin, P. I. Dunlop, L. J. Gosting and G. Kegeles, *J. Chem. Phys.*, **33**, 1505 (1960).
10. K. Ueberreiter and F. Asmussen, *Makromol. Chem.*, **44-46**, 324 (1961).
11. L. Lapčík and L. Valko, *Chem. Zvesti*, **20**, 489 (1966).
12. F. Danusso, G. Moraglio, and S. Gazzera, *Chim. Ind. (Milan)*, **12**, 883 (1954).
13. I. Corbiere, P. Terra, and R. Paris, *J. Polym. Sci.*, **8**, 101 (1952).
14. F. Bueche, *Physical Properties of Polymers*, Interscience, New York, 1962.

Received March 10, 1970.

Revised September 15, 1970.

Analysis of Small-Angle X-Ray Diffraction from Polymers

D. R. BUCHANAN,*

Phillips Petroleum Company, Bartlesville, Oklahoma 74003

Synopsis

The Fourier transform method of Vonk and Kortleve for the analysis of small-angle x-ray diffraction (SAXRD) from semicrystalline polymers has been compared with a modified direct method, originally due to Tsvankin. SAXRD data for three melt-crystallized polyethylene samples have been analyzed in terms of the mean true periodicity, mean crystal length, and mean length of amorphous segments. The two methods of analysis yield substantially equivalent results for all three samples. Calibration curves for the Tsvankin analysis are tabulated, and the relative merits of the two methods of analysis are discussed. With either method, information about the diffracting structure may be deduced that is not available from a simple measurement of the position of the SAXRD maximum. In fact, direct application of the Bragg law to any but the sharpest maximum yields a spacing (the long period) that lacks direct physical significance.

INTRODUCTION

The small-angle x-ray diffraction (SAXRD) pattern of a semicrystalline polymer is usually characterized by the appearance of one, and sometimes several, intensity maxima at angles 2θ between ca. 0.05 and 2.0° . Straight-forward application of Bragg's equation to the angular positions of these maxima leads to the conclusion that the periodicities in electron density that are responsible for the scattering correspond to units of size ca. 1500 – 50 Å. Difficulties with this simple approach fall into two classes: first, the sizes calculated do not agree with those inferred from other experiments, especially electron microscopy, and often the same size cannot be calculated from what appear to be first-order and second-order diffraction maxima;¹ second, utilization of only the position of the SAXRD maximum wastes the other information inherent in the experiment, particularly that about the distribution of intensity within the scattering pattern.

These points were first treated by Rheinhold et al.,² who showed that a model based on the linear paracrystal³ was able to predict SAXRD patterns in which the scattering maxima were shifted out of the positions given by the Bragg equation. With the use of an asymmetric distribution function for the lamellar thickness, scattering curves were calculated in which the positions of the first-order and second-order maxima differed by factors of other

* Present address: Phillips Fibers Corporation, Greenville, South Carolina 29602.

than two. These results encouraged the expectation that physically realistic sizes might be obtained from experimental SAXRD data that were analyzed properly.

A procedure for more complete analysis of experimental SAXRD intensity distributions was developed by Tsvankin,⁴ in which the scattering to be expected from a variety of related supermolecular structures was calculated. The theoretical curves were analyzed with respect to the positions and widths of the first-order maxima, and "calibration" curves were constructed. These curves were used in conjunction with the same data from experimental scattering curves to compute average values of the true periodicity of a superlattice composed of alternating "crystalline" and "amorphous" segments, average lengths of the segments, and a one-dimensional linear "crystallinity" for the superlattice. Crystal lengths calculated in this manner have been found to correspond quite closely with those estimated from wide-angle x-ray diffraction profile broadening in oriented nylon 66⁵ and also with step heights measured from electron micrographs of polyethylene single-crystal mats.⁶ Such an analysis also has been applied to other studies.⁷⁻⁹

An alternative treatment of SAXRD data involves calculation of the Fourier transform of the experimental scattering curve to yield a correlation function proportional to the self-convolution of the electron density fluctuation within the sample. Such a procedure has been investigated by Vonk and Kortleve,^{10,11} who suggested that differences between experimental correlation functions and those calculated from a model could be more readily interpreted in terms of the model than if the scattering curve itself were used. The Vonk-Kortleve method differs from that of Tsvankin principally in the way in which the observed scattering curve is compared with the theoretical scattering curve for an assumed model.

It is the purpose of this paper to present calibration curves for the full analysis of SAXRD data by a modified Tsvankin technique and to compare the results obtained by this method with those obtained by the Vonk-Kortleve technique with the same data. The relative merits of the two methods are discussed.

ANALYSIS OF THE DIRECTLY OBSERVED DIFFRACTION: TSVANKIN METHOD

Tsvankin⁴ assumed the following model of the superlattice in oriented polymer fibers.

A fiber is composed of parallel fibrils with the regions of higher and lower electron density alternating regularly along the fibril. The regions of lower electron density correspond to amorphous segments of the fibril, while those of higher electron density correspond to crystals. Scattering from such an assembly may be calculated from the projection of the electron density within the fibril onto the fiber axis.

The distribution of crystal sizes (as projected onto the fiber axis) is rec-

tangular, with mean size (or length) a and limits of $(a - \Delta)$ and $(a + \Delta)$. A long period c is defined as the mean projected distance between crystal centers, while a mean length of noncrystalline material (amorphous length) is given by $c - a$.

In general, the diffracted intensity from a system of N crystals of different lengths (i.e., with different structure amplitudes F , where F is the Fourier transform of the electron density distribution within a crystal) is given by

$$I \propto N(|\bar{F}^2| - |\bar{F}|^2) + |\bar{F}|^2 \left(N + \sum_{i \neq k}^N \sum \exp\{i\mathbf{s} \cdot \mathbf{z}_{ik}\} \right) \quad (1)$$

Here $|\mathbf{s}| = 4\pi \sin\theta/\lambda$ is the diffraction vector, and \mathbf{z}_{ik} is the vector from the center of the i th crystal to that of the k th. In eq. (1) the first term arises from differences in scattering power among the individual crystals and was assumed to be constant by Tsvankin. The second term of eq. (1) describes scattering from the lattice of crystalline and amorphous regions, and is responsible for the occurrence of maxima in the scattering pattern at scattering angles other than zero. Tsvankin showed that this second term can be represented by

$$|\bar{F}|^2 I_1 = |\bar{F}|^2 \left(N + \sum_{i \neq k}^N \sum \exp\{i\mathbf{s} \cdot \mathbf{z}_{ik}\} \right) \quad (2)$$

where

$$I_1 = (\beta^2 y^2 + \beta^2 y^4 - \sin^2 \beta y) / (\sin^2 \beta y + \beta^2 y^2 + \beta^2 y^4 - 2\beta y \cos \alpha y \sin \beta y + 2\beta y^2 \sin \alpha y \sin \beta y) \quad (3)$$

The following substitutions have been made in the derivation of (3):

$$\begin{aligned} y &= sl = 2\pi l \sin 2\theta / \lambda \\ \alpha &= a/l \\ \beta &= \Delta/l, \\ l &= c - a \end{aligned} \quad (3a)$$

where the mean long period is represented by c , the mean crystal length by a , the mean amorphous length by $l = c - a$, and the dispersion of crystal lengths about the mean value by 2Δ .

In order to evaluate eq. (2), the scattering amplitude F must be obtained. Tsvankin assumed that the projection onto the fiber axis of the electron density within a crystal could be represented by a trapezoidal function such as that shown in Figure 1. If $\epsilon = \delta/x$,

$$F = \int_0^{\epsilon x} (z/\delta) \exp\{iyz/l\} dz + \int_{\epsilon x}^{(1-\epsilon)x} \exp\{iyz/l\} dz + \int_{(1-\epsilon)x}^x [(a-z)/\delta] \exp\{iyz/l\} dz \quad (4)$$

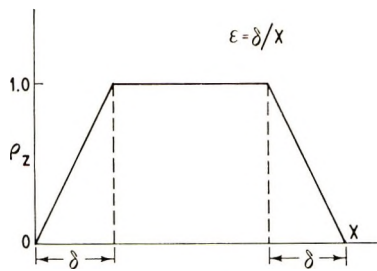


Fig. 1. Relative electron density ρ_z within a crystal of length x .⁴

Since

$$\bar{F} = (1/2\Delta) \int_{a-\Delta}^{a+\Delta} F(x) dx \quad (4a)$$

and

$$|\bar{F}|^2 = |\bar{F}| \cdot |\bar{F}^*| \quad (4b)$$

the result was obtained that

$$|\bar{F}|^2 = \frac{\alpha^2}{\epsilon^2(\alpha y)^4} \left(\left\{ \frac{\sin \beta y}{\beta y} [\cos(1 - \epsilon)\alpha y - \cos \alpha y] + \cos \epsilon \alpha y - 1 \right\}^2 + \left\{ \frac{\sin \beta y}{\beta y} [\sin(1 - \epsilon)\alpha y] + \sin \epsilon \alpha y \right\}^2 \right). \quad (5)$$

Theoretical scattering curves can thus be computed from eqs. (3) and (5) as functions of $y = 2\pi l \sin \theta / \lambda$ for variations of the parameters $\alpha = a/l$, $\beta = \Delta/l$, and ϵ . It is, however, more convenient to vary β/α , α , and ϵ , as these parameters may be interpreted more easily in terms of the model. Thus, α is a measure of the crystal packing density along the fiber axis, $\beta/\alpha = \Delta/a$ characterizes the dispersion of crystallite lengths about the mean value, and ϵ is a measure of the sharpness of the transition between crystalline and amorphous regions (cf. Fig. 1). Moreover, it is convenient to choose $c(\sin 2\theta)/\lambda = (1 + \alpha)y/2\pi$ as the independent variable in order to facilitate comparisons of the mean long-period c with the position of the primary maximum.

Scattering curves calculated in this manner indicate that (1) for constant β/α , large values of α lead to the sharpest intensity maxima and also to second-order maxima, while smaller values of α are associated with scattering curves that show single, very broad, poorly defined maxima; (2) for constant α , the sharpest maxima occur for low values of β/α . In general, the position of the primary maximum does not correspond to $c(\sin 2\theta)/\lambda = 1$, but is displaced to $c(\sin 2\theta)/\lambda > 1$ for most values of β/α . For sufficiently large β/α , the primary maximum is displaced to $c(\sin 2\theta)/\lambda < 1$. For those cases in which two maxima are observed, their positions usually are related by factors other than exactly two.

In order to establish relations between the calculated scattering curves and experimental SAXRD data, it is necessary to establish "calibration curves" based on the calculated scattering. Tsvankin did this for $\beta/\alpha = 0.2$ and for several values of ϵ . He noted that the shape of the scattering curve was relatively insensitive to the value of ϵ chosen; a nonzero value, however, seems necessary for consistency with morphological evidence that sharp boundaries between crystalline and amorphous regions are unlikely.

The peak positions and widths based on the calculated scattering curves are expressed in terms of a $c(\sin 2\theta)/\lambda$ scale for the diffraction vector. Equivalent quantities may be obtained from experimental SAXRD data which, however, are referred to a $(\sin 2\theta)/\lambda$ scale for the diffraction vector. For consistency, a linear background, defined similarly to that for the calculated curves, i.e., from the points of tangency on either side of the maximum, should be subtracted from the experimental data. In Tsvankin's notation, the calculated and experimental peak positions are X_m and d , respectively, while the calculated and experimental half-widths are p and q , respectively. They are related by

$$p = cq$$

$$X_m = c/d$$

and

$$p/X_m = dq = \psi(p)$$

Thus, the quantity $\psi(p)$ relates the calculated and experimental curves. This relation is accomplished through calibration curves which relate (1) p to $\psi(p)$; (2) p to $k = \alpha/(l + \alpha)$; and (3) p to X_m . Note that k is a crystallinity-like quantity, expressing the linear crystallinity along the fibril axis. There will be a set of calibration curves for every value of the parameter, β/α . If values of d and q are known from experiment and a value for β/α is assumed, then $\psi(p)$ is known, and p , X_m , and k may be obtained from the calibration curves. From these parameters the mean long period c , the mean crystallite length a , and the mean amorphous length l may be obtained from

$$c = X_m d$$

$$a = kc$$

$$l = c - a$$

It is evident that, in order to analyze an experimental scattering curve in this manner, it is necessary to choose *a priori* a value for β/α , corresponding to the expected dispersion of crystal lengths about the mean value. In some cases, information necessary for this choice may be available from other sources, such as wide-angle x-ray diffraction (WAXRD) estimates of size-average crystal length in the direction of the fiber axis,^{5,12} or from electron microscopy.^{6*} In general, however, it is necessary to choose values for

β/α arbitrarily. Reasonable choices appear to lie in the range 0.2 to 0.5, corresponding to size dispersions of 20–50% about the mean size.

ANALYSIS OF THE DIRECTLY OBSERVED DIFFRACTION: MODIFIED TSVANKIN METHOD

In the Tsvankin treatment of diffraction from the crystalline-amorphous superlattice, the first term of eq. (1) was neglected on the basis of the assumption that it was essentially constant throughout the angular interval in the vicinity of the primary diffraction maximum, and, therefore, would have no effect on the position or the shape of the maximum. In the course of assessing the validity of this assumption, it has been found that a somewhat different expression for $|\bar{F}|^2$ from that derived by Tsvankin was appropriate for the calculation. Therefore, new expressions for $|\bar{F}^2|$ and $|\bar{F}|^2$ and an evaluation of the continuous scattering from the assembly of crystals, proportional to $|\bar{F}^2| - |\bar{F}|^2$, are presented below.

Calculation of $|\bar{F}|^2$

For the distribution of electron density within a crystal shown in Figure 1, F is given by eq. (4), \bar{F} by eq. (4a), and $|\bar{F}|^2$ by eq. (4b). On substitution of eqs. (3a) into eq. (4) and with the additional relations

$$1/\delta s^2 = a/\epsilon(\alpha y)^2$$

and

$$\exp\{ik(A + B)\} - \exp\{ik(A - B)\} = 2 \sin k B (i \cos k A - \sin k A)$$

eq. (4b) becomes

$$|\bar{F}|^2 = \frac{a^2}{\epsilon^2(\alpha y)^4} \left\{ \left[\frac{\sin(1 - \epsilon)\beta y}{(1 - \epsilon)\beta y} \cos(1 - \epsilon)\alpha y + \frac{\sin\epsilon\beta y}{\epsilon\beta y} \cos\epsilon\alpha y - \frac{\sin\beta y}{\beta y} \cos\alpha y - 1 \right]^2 + \left[\frac{\sin(1 - \epsilon)\beta y}{(1 - \epsilon)\beta y} \sin(1 - \epsilon)\alpha y + \frac{\sin\epsilon\beta y}{\epsilon\beta y} \sin\epsilon\alpha y - \frac{\sin\beta y}{\beta y} \sin\alpha y \right]^2 \right\} \quad (6)$$

This result clearly differs from that obtained by Tsvankin [eq. (5)]. The extent of the difference is shown in Figure 2, in which $|\bar{F}|^2$, calculated from eqs. (5) and (6), is plotted as a function of $c(\sin 2\theta)/\lambda$ for selected values of the parameters α and β/α ($\epsilon = 0.2$ throughout). The discrepancy is largest for large β/α and for small α , i.e., for large dispersions of crystal length about the mean and/or for small crystal packing densities in the direction of the fibril axis.

* The size-average crystal length and the mean (number-average) crystal length together define the breadth of an assumed unimodal distribution function. It is shown below that the mean crystal length is relatively insensitive to changes in β/α for a rectangular distribution function.

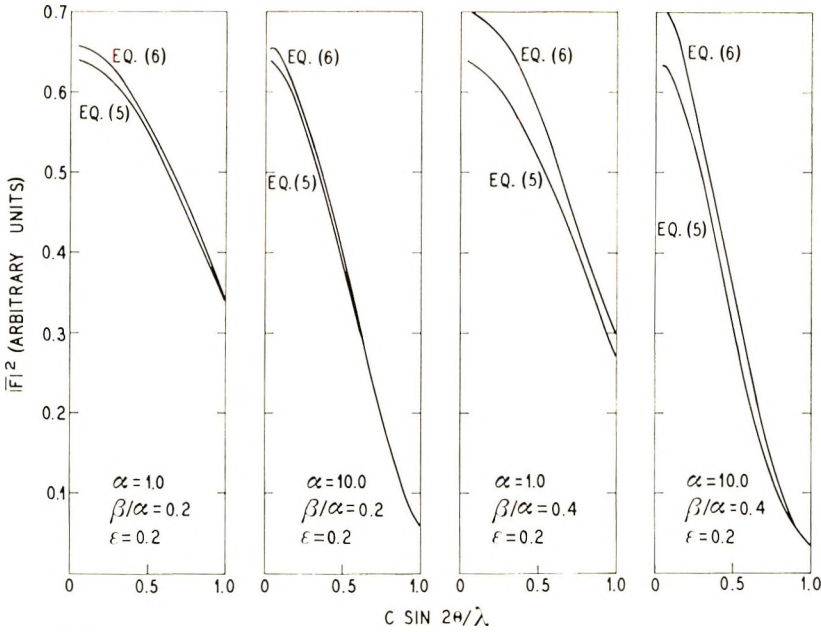


Fig. 2. $|F|^2$ as a function of $c \sin 2\theta/\lambda$ calculated from eq. (5), the original Tsvankin⁴ expression, and from eq. (6), a modified expression.

Calculation of $|F^2|$

Again, F is given by eq. (4). Integration and formation of the product $F \cdot F^*$ yields the result:

$$F^2 = \frac{1}{\delta^2 s^4} \left\{ 4 + 2 \cos[yx(1 - 2\epsilon)/l] - 4 \cos(yx\epsilon/l) - 4 \cos[yx(1 - \epsilon)/l] + 2 \cos(yx/l) \right\} \quad (7)$$

For $|F^2|$ we have

$$|F^2| = (1/2\Delta) \int_{a-\Delta}^{a+\Delta} F^2(x) dx \quad (7a)$$

and the same substitutions used in the derivation of eq. (6) transform eq. (7a) to:

$$|F^2| = \frac{\alpha^2}{\epsilon^2(\alpha y)^4} \left[4 + 2 \frac{\sin(1 - 2\epsilon)\beta y}{(1 - 2\epsilon)\beta y} \cos(1 - 2\epsilon)\alpha y - 4 \frac{\sin(1 - \epsilon)\beta y}{(1 - \epsilon)\beta y} \times \cos(1 - \epsilon)\alpha y - 4 \frac{\sin\epsilon\beta y}{\epsilon\beta y} \cos\epsilon\alpha y + 2 \frac{\sin\beta y}{\beta y} \cos\alpha y \right] \quad (8)$$

Evaluation of the Continuous Scattering

The first term of eq. (1), $|\bar{F}^2| - |\bar{F}|^2$, is obtained from eqs. (6) and (8). It represents the continuous scattering from the assembly of crystals. In

TABLE I
 Tsrankin Parameters for the Construction of Calibration Curves, Based on Eqs. (1), (3), (6), and (8)

p	$\beta/\alpha = 0.1$			$\beta/\alpha = 0.2$			$\beta/\alpha = 0.3$			$\beta/\alpha = 0.4$			$\beta/\alpha = 0.5$		
	$\psi(p)$	X_m	k												
0.0	0.0	1.025	0.942	0.0	1.000	1.000	0.0	0.947	1.000	0.0	0.865	—	0.0	0.725	—
0.1	0.102	1.025	0.873	0.102	1.002	0.927	0.102	0.948	0.990	0.110	0.868	1.000	0.132	0.727	—
0.2	0.196	1.032	0.805	0.196	1.013	0.845	0.205	0.958	0.898	0.220	0.875	0.982	0.260	0.738	—
0.3	0.288	1.046	0.744	0.288	1.030	0.769	0.306	0.970	0.815	0.326	0.884	0.877	0.383	0.746	—
0.4	0.377	1.065	0.691	0.381	1.048	0.708	0.400	0.987	0.744	0.436	0.898	0.790	0.507	0.755	—
0.5	0.456	1.092	0.641	0.465	1.070	0.654	0.485	1.006	0.682	0.536	0.918	0.718	0.623	0.770	1.000
0.6	0.529	1.124	0.596	0.547	1.102	0.610	0.569	1.033	0.624	0.637	0.938	0.655	0.736	0.795	0.847
0.7	0.595	1.162	0.558	0.619	1.135	0.568	0.646	1.060	0.580	0.727	0.967	0.597	0.835	0.822	0.721
0.8	0.656	1.209	0.523	0.687	1.170	0.533	0.718	1.090	0.538	0.813	0.993	0.549	0.921	0.855	0.622
0.9	0.712	1.255	0.495	0.757	1.211	0.502	0.784	1.128	0.503	0.885	1.028	0.506	0.994	0.899	0.542
1.0	0.763	1.303	0.470	0.801	1.252	0.470	0.844	1.166	0.470	0.952	1.065	0.470	1.056	0.938	0.478

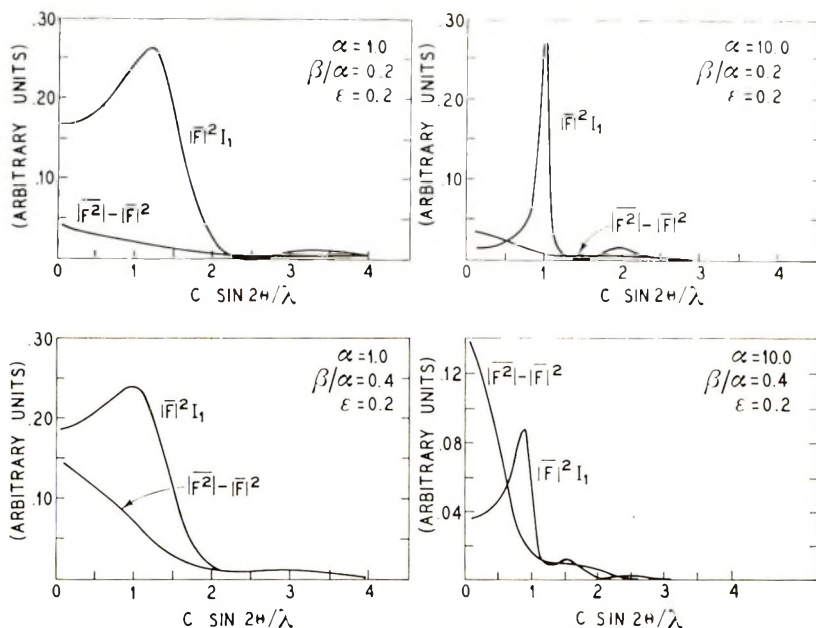


Fig. 3. Two components of the theoretical SAXRD curve, $|\bar{F}|^2 I_1$ and $|\bar{F}|^2 - |\bar{F}|^2$, calculated as functions of $c(\sin 2\theta)/\lambda$ from eqs. (3), (6), and (8).

Figure 3, the contribution to the total scattering from this term is compared with that from the second term of eq. (1), the diffraction from the crystal-amorphous superlattice obtained through eqs. (3) and (6). It can be observed that, especially for large β/α , the continuous scattering represents a significant fraction of the total scattering, even for large α . Since the continuous scattering varies quite significantly in the region of the primary diffraction maximum, it will also contribute to the shape of the maximum and should be included in the calculations which lead to the calibration curves. Data for the construction of calibration curves with $\beta/\alpha = 0.1, 0.2, 0.3, 0.4,$ and 0.5 , all for $\epsilon = 0.2$, are presented in Table I. They are based on the complete form of eq. (1) and were calculated with eqs. (3), (6), and (8).

ANALYSIS OF THE FOURIER TRANSFORM OF THE OBSERVED DIFFRACTION: VONK-KORTLEVE METHOD

Vonk and Kortleve (VK) assumed a model of crystal-amorphous supermolecular structure that is substantially identical with that assumed by Tsvankin, i.e., a structure consisting of alternating layers of "crystalline" (high electron density) and "amorphous" (low electron density) material, and considered small-angle scattering in the direction perpendicular to the layers. In place of a rectangular crystal-length distribution, however, VK assumed a log normal distribution. (In both instances, the choice of distribution function apparently was made to facilitate computation, rather than to express a fundamental preference for a particular form.)

Although the fundamental concepts are similar, the VK technique differs markedly in execution from that of Tsvankin. VK proposed that the Fourier transform of an experimental SAXRD curve would be more readily interpretable, when analyzed in terms of a model, than would the directly observed curve. As a result, they compared the Fourier transform of the observed scattering curve with a calculated correlation function given by [eq. (14) of VK¹⁰]:

$$\gamma(x) = \frac{\Phi}{1 - \Phi} \left\{ \frac{1}{\Phi^2} \int_x^\infty (X_C - X) P_C(X_C) dX_C + P_{CAC} \right. \\ \left. + P_{CACAC} + \dots - 1 \right\} \quad (9)$$

In eq. (9), C is the mean thickness of crystalline layers, A is the mean thickness of amorphous layers, and $\Phi = C/(C + A)$ is a crystallinity-like parameter. The quantities, P_{CAC} , P_{CACAC} , etc., are functions of convolution products of the distribution functions, P_C and P_A , for the distribution of the thickness of crystalline layers and of amorphous layers, respectively, about their mean values. There are four adjustable parameters implicit in eq. (9): C and ΔC , which describe the log-normal distribution of crystalline layer thicknesses; and A and ΔA , which describe the log-normal distribution of amorphous layer thicknesses. In practice, VK found that a good fit with the experimental correlation function could be obtained if $\Delta A/A$ was assumed to be equal to $\Delta C/C$. In this case, the number of adjustable parameters implicit in eq. (9) is reduced to three. Also, the average periodicity, $B = C + A$, may be obtained directly from the position of the first maximum in the experimental correlation function.

COMPARISON OF METHODS

Data (Fig. 4) for three Marlex 6050 polyethylene samples (Phillips Petroleum Company) reported by Vonk and Kortleve¹¹ have been analyzed by the modified Tsvankin technique and compared with the Fourier transform analysis of VK. The SAXRD data were corrected for the effects of slit-smearing.¹³ A comparison of results is shown in Table II.

In general, the agreement between the two methods is quite good, especially if the difference in assumed crystal length distribution functions is taken into account. The mean crystal lengths derived by the Tsvankin analysis are effectively independent of the value assumed for β/α , and differ from those deduced by VK by 13, 6, and 3% for samples 1A, 1B, and 1C, respectively. The values for the other parameters, mean long period and mean amorphous length, depend significantly on β/α in the Tsvankin analysis. The values of $\Delta C/C$ from the VK analysis suggest that values for β/α between 0.3 and 0.4 are most appropriate for these samples. With this assumption, fair agreement between the two methods is also observed for the mean long periods and mean amorphous lengths, with best agreement

TABLE II
Analysis of SAXRD Data for Melt-Crystallized Polyethylene (Marlex 6050)

Parameter and notation ^a	Sample 1A			Sample 1B			Sample 1C					
	Tsvankin			Tsvankin			Tsvankin					
	$\beta/\alpha =$ 0.2	$\beta/\alpha =$ 0.3	$\beta/\alpha =$ 0.4	VK ^b	$\beta/\alpha =$ 0.2	$\beta/\alpha =$ 0.3	$\beta/\alpha =$ 0.4	VK ^b	$\beta/\alpha =$ 0.2	$\beta/\alpha =$ 0.3	$\beta/\alpha =$ 0.4	VK ^b
Observed long period	481	481	490	490	365	365	360	360	274	274	274	315 ^c
$(d) [D_1], \text{\AA}$	0.00095	0.00095	—	—	0.00135	0.00135	—	—	0.00199	0.00199	0.00199	—
Half-width of primary maximum $(q), \text{\AA}^{-1}$	1.07	1.00	—	—	1.08	1.01	—	—	1.10	1.02	0.92	—
Product of (d) and (q) (dq)	1.07	1.00	0.90	—	1.08	1.01	0.91	—	1.10	1.02	0.92	—
Peak shift factor (X_m)	514	481	434	445	394	368	332	320	302	281	252	240
Mean periodicity $(c) [B], \text{\AA}$	338	337	335	390	251	249	248	265	184	180	179	175
Mean crystal length (thickness) $(a) [C], \text{\AA}$	135	202	268	240	100	150	202	180	74	108	144	135
Breadth of distribution function, $(2\Delta) [\Delta C], \text{\AA}$	175	144	98	55	143	119	84	55	118	101	73	65
Mean amorphous segment length $(l) [A], \text{\AA}$	70	86	78	35	57	72	68	35	47	61	58	50
Breadth of distribution function $[\Delta A], \text{\AA}$	0.66	0.70	0.77	0.88	0.64	0.68	0.75	0.83	0.61	0.64	0.71	0.72
Linear crystallinity $(k) [\Phi]$	0.40	0.60	0.80	0.61	0.40	0.60	0.80	0.68	0.40	0.60	0.80	0.77
Relative breadth of crystal length distribution function $(2\beta/\alpha) [\Delta C/C]$	0.40	0.60	0.80	0.61	0.40	0.60	0.80	0.68	0.40	0.60	0.80	0.77

^a () Tsvankin notation, [] Vonk-Kortleve notation.

^b Data of Vonk and Kortleve¹¹ (Table 2).

^c Apparently an erroneous result.

^d Assumed to be given by $(2\beta/\alpha)/l$ for the Tsvankin analysis.

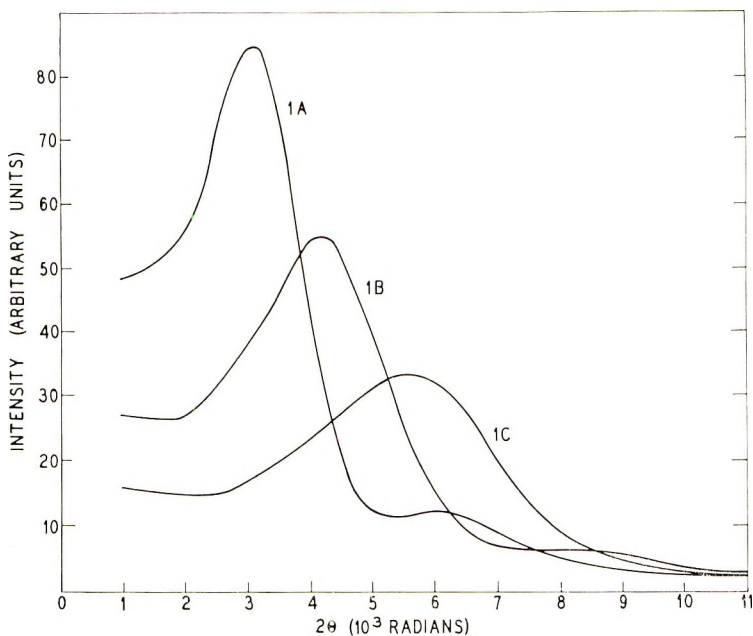


Fig. 4. Experimental SAXRD curves from melt-crystallized polyethylene, corrected for slit-smearing effects.¹¹

for sample 1C. Naturally this agreement also implies agreement for the linear crystallinities derived by the two methods.

It should be noted that the two methods of analysis produce best agreement for sample 1C, for which the broadest SAXRD maximum was observed, and agree least well for sample 1A, for which the sharpest SAXRD maximum was found. At least part of the discrepancy in results for sample 1A may be attributed to the difficulty of fitting the observed correlation function for a sharp SAXRD maximum in terms of the VK model, as was illustrated by VK in their Figure 5.¹¹ That the Tsvankin method can provide accurate crystal lengths from a sharp SAXRD maximum has been demonstrated for solution-grown polyethylene single crystals.⁶ However, the mean crystal length in this case was significantly smaller (110 Å) than that for sample 1A (335 Å), so that the effects of both a narrow maximum and a long period as large as that for sample 1A have not been evaluated for the Tsvankin analysis.

DISCUSSION AND CONCLUSIONS

The two methods of analysis of SAXRD data discussed here differ not only in execution, but also in a significant detail of the assumed model, the shape of the distribution of crystal lengths. While the choice of direct or Fourier analysis of the diffraction profile would not be expected to affect the results of such an analysis, at least in principle, it is indeed surprising that

the choice of crystal-length distribution (rectangular versus log-normal) should have so little influence on the values of the parameters.

There seems to be no fundamental reason to prefer one analysis over the other. The Tsvankin technique is usable with or without a computer, in the latter case with calibration curves constructed from the data of Table I. However, it suffers from the serious disadvantage that prior knowledge of β/α , the breadth of the crystal length distribution, is required for its full utilization. On the other hand, reliable mean crystal lengths, which do not vary appreciably with β/α in the range 0.1 to 0.5, may be obtained without such an assumption. On the basis of this and previous work,⁵ it seems reasonable to expect β/α to lie between 0.3 and 0.4 for most melt-crystallized polymer samples. However, direct estimation of β/α from a combination of SAXRD and WAXRD data or from SAXRD and electron microscope data is still desirable, if possible.

A significant advantage of the VK technique is that the equivalent of the Tsvankin β/α , i.e., $\Delta C/C$, is estimated independently in this analysis. The VK technique does require the use of a computer and, more importantly, appears to be less reliable for sharp diffraction maxima than for broader maxima. For many melt-crystallized polymers, however, sufficiently broad maxima may be observed for the VK technique to be used without difficulty. In such cases, the direct estimation of the breadth of the crystal-length distribution that can be obtained makes this a very powerful technique.

With either the Tsvankin or the VK analysis, information about the diffracting structure may be deduced that is not available from a simple measurement of the position of the SAXRD maximum. In fact, direct application of the Bragg law to any but the sharpest maximum yields a spacing (the long period) that lacks direct physical significance. While the Tsvankin and VK methods of analysis are not sensitive enough to distinguish between different crystal-length distributions, the agreement between structural parameters deduced from them, and the agreement previously noted between parameters deduced from the Tsvankin analysis and from WAXRD or electron microscopy, support the assertion that these parameters do have physical significance, and, therefore, have real value in the characterization of semicrystalline polymers.

A portion of this work was done while I was employed by Chemstrand Research Center, Inc. I wish to thank them, and also Phillips Petroleum Company, for permission to publish this paper.

References

1. P. H. Geil, *Polymer Single Crystals*, Interscience, New York, 1963.
2. C. Rheinhold, E. W. Fischer, and A. Peterlin, *J. Appl. Phys.*, **35**, 71 (1964).
3. R. Hosemann and S. N. Bagchi, *Direct Analysis of Diffraction by Matter*, North-Holland, Amsterdam, 1962.
4. D. Ya. Tsvankin, *Polym. Sci. USSR*, **6**, 2304, 2310 (1964).
5. J. H. Dumbleton, D. R. Buchanan, and B. B. Bowles, *J. Appl. Polym. Sci.*, **12**, 2067 (1968).

6. D. R. Buchanan and R. L. Miller, *J. Polym. Sci. B*, **5**, 771 (1967).
7. Yu. A. Zubov and D. Ya. Tsvankin, *Polym. Sci. USSR*, **6**, 2358 (1964).
8. D. R. Buchanan and J. H. Dumbleton, *J. Polym. Sci. A-2*, **7**, 113 (1969).
9. J. H. Dumbleton, *Polymer*, **10**, 539 (1969).
10. C. G. Vonk and G. Kortleve, *Kolloid Z. Z. Polym.*, **220**, 19 (1967).
11. G. Kortleve and C. G. Vonk, *Kolloid Z. Z. Polym.*, **225**, 124 (1968).
12. D. R. Buchanan, R. L. McCullough, and R. L. Miller, *Acta Cryst.*, **20**, 922 (1966).
13. A. Dijkstra, G. Kortleve, and C. G. Vonk, *Kolloid Z. Z. Polym.*, **210**, 121 (1966).

Received August 12, 1970

Revised October 27, 1970

Adhesion of Viscoelastic Materials to Rigid Substrates. III. Energy Criterion for Failure

A. N. GENT* and A. J. KINLOCH,
*Department of Materials, Queen Mary College,
University of London, England*

Synopsis

Measurements are described of the strength of a model adhesive joint subjected to (1) tensile rupture, with the interface containing a small unbonded region of varying size, and (2) pure shear deformation, in the form of a partly unbonded sheet. These, and previous measurements of resistance to peeling separation, are all shown to be consistent with an energy criterion for adhesive failure. The characteristic failure energy per unit area of interface has been determined for the model adhesive material as a function of the effective rate of detachment, over a wide range covering almost the entire spectrum of viscoelastic response. The values obtained are found to increase from levels only slightly higher than thermodynamic considerations would predict, i.e., 10^2 – 10^3 ergs/cm², at low rates of crack propagation, up to a value of about 10^6 ergs/cm² at high rates when the material responds in a glasslike manner. These results suggest that the failure energy has two components: the (reversible) work of adsorption and the (irreversible) work of deformation of the adhesive in effecting separation.

INTRODUCTION

The resistance to separation by peeling and the breaking stress in tension have recently been determined for a simple viscoelastic adhesive spread on a rigid substrate.^{1,2} Both measures of adhesion have been shown to vary with rate of deformation of the adhesive and with temperature in accordance with the Williams, Landel, and Ferry rate-temperature equivalence, indicating that the observed strength reflects a viscoelastic property of the adhesive rather than a thermodynamic one, such as heat of wetting the substrate. However, the two measures show striking differences at equivalent rates of deformation of the adhesive. The peel resistance is greater for thicker adhesive layers, whereas the tensile strength is lower. Also, the peel strength is enhanced by high extensibility or ductile flow of the adhesive but the tensile strength is much less influenced. These differences have been shown to be qualitatively in accord with a single failure criterion, that a critical strain energy density is needed locally to cause bond failure.² This criterion is a special case of Griffith's criterion for the fracture of solids,³ which may be expressed as follows: fracture occurs when suffi-

* Present address: The University of Akron, Akron, Ohio 44304.

cient energy is released by growth of the fracture plane to supply the energy requirements of the new fracture surfaces.

The energy released comes from stored elastic or potential energy of the loading system and can in principle be calculated for any type of testpiece. The energy required for fracture, per unit area of new surface, is found to be largely independent of the type of testpiece and the way in which stresses are applied to it, and may thus be regarded as a characteristic measure of strength. It is not usually equal to the thermodynamic surface energy, as Griffith originally supposed, but is found to be some orders of magnitude larger due to additional energy consumed in irreversible processes around the fracture front.⁴⁻⁸ Indeed, for viscoelastic solids the fracture energy depends strongly on the speed at which fracture propagates and upon temperature, in the same way that the mechanical energy absorption of these materials depends upon rate of deformation and temperature.^{7,9}

We now examine the applicability of a similar energy criterion to the failure of adhesive joints, using the same combination of a simple viscoelastic adhesive and an inert rigid substrate as before, as a model adhesive system. Three types of testpiece have been employed: (1) simple extension, with a small non-adhering region of length $2c$ present initially as a model flaw (Fig. 1); (2) pure shear, as shown schematically in Figure 2; (3) peeling separation (Fig. 3). (The results obtained previously are used in this case.) These test arrangements have been chosen because although the applied forces to cause bond failure are quite different it is a relatively simple matter to deduce the fracture energy from them in each case. They are, in fact, virtually the same as those employed by Rivlin and Thomas⁵ to establish the validity of a fracture energy criterion for the rupture of vulcanized rubber. Indeed, the relations derived by Rivlin and Thomas for the fracture energy T per unit area of growth of a fracture plane need little if any alteration to apply to the failure energy θ of a soft adhesive adhering to a rigid substrate:

simple extension:

$$\theta = kcW_b \quad (1)$$

pure shear:

$$\theta = h_0W_b \quad (2)$$

peeling:

$$\theta = P/t_0 \quad (3)$$

Here W_b is the strain energy per unit volume at rupture; k is a numerical factor given to good approximation by $\pi/\lambda_b^{1/2}$,¹⁰ where λ_b is the extension ratio at rupture; $h_0(t_0)$ is the unstrained height (thickness) of the adhesive, and P is the peel force per unit width of the adhesive layer. These relations do not require that the adhesive be linearly elastic. They are therefore more generally applicable than others (for example, Griffith's original relation³ for cohesive rupture in simple extension) which assume linearly elastic behavior.

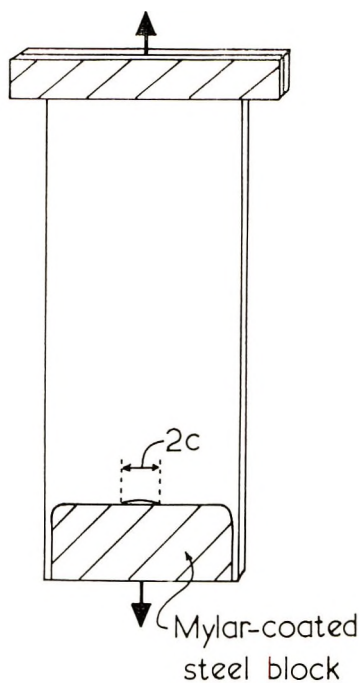


Fig. 1. Sketch of simple extension testpiece.

That an energy criterion applies to the failure of adhesive joints is not in itself a novel proposal; it is implicit in Rivlin's discussion of the work of peeling¹¹ and has been stated explicitly by Williams in a treatment of stress singularities at interfaces.^{12,13} Experimental measurements of the failure energy for epoxy adhesives have been reported by Ripling et al.,^{14,15} Malyshev and Salganik,¹⁶ and Jemain and Ventrice.¹⁷ It is particularly noteworthy that Malyshev and Salganik obtained similar values for the failure energy with the use of three different test arrangements, because this strongly supports the proposed energy criterion for adhesive failure. Apart from this, however, no critical examination of an energy criterion is known to the present authors. Also, these earlier measurements were all carried out under relatively uniform conditions so that the failure energy itself was substantially constant. Correlation with other properties of the adhesive and substrate was therefore not feasible.

In contrast, by suitably varying the rate of separation and the temperature of test, the strength of adhesion of the model viscoelastic substance used in the previous investigations in this series can be altered by orders of magnitude.^{1,2} It is therefore in principle possible to test the applicability of an energy criterion for failure over the entire experimentally accessible range. Moreover, the variation observed in the characteristic failure energy with rate of separation and temperature should throw light on the basic mechanisms of adhesion. The experiments described below were carried out with these aims in view.

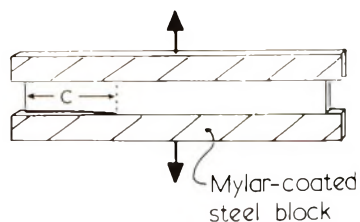


Fig. 2. Sketch of pure shear testpiece.

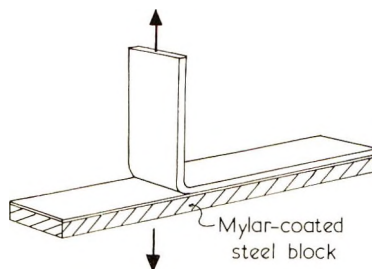


Fig. 3. Sketch of peel testpiece.

EXPERIMENTAL

The material employed as a model viscoelastic adhesive was a rubbery copolymer of butadiene and styrene (60:40, Ameripol 1513, Goodrich-Gulf Chemicals, Inc.), with a glass transition temperature T_g of -40°C . In order to crosslink the material later, 0.5 wt-% of dicumyl peroxide (Di-Cup R, Hercules Powder Company) and 1 wt-% of phenyl- β -naphthylamine were added to it initially on an open mill. It was then pressed into a flat sheet in contact at one edge with the chosen substrate, a layer of poly(ethylene terephthalate) film (Type A Mylar, 0.0075 cm thick, E. I. du Pont de Nemours and Co.), and lightly crosslinked in this position by heating the assembly for 10 min at 100°C followed by 15 min at 150°C .

The Mylar film was supported rigidly by a steel backing plate to which it was firmly cemented by a thin layer of a mixture of 75% of a polyester adhesive (46970) and 25% of a modified isocyanate curing agent (RC-S05), both supplied by E. I. du Pont de Nemours and Co. Satisfactory bonding was obtained by heating the combination for 8 h at 130°C .

Simple Extension

In some preliminary experiments with straight interfaces and small central cracks having a length $2c$ of less than 1 cm, failure was found to occur at the edges of the interface rather than at the crack. These edge failures were due to high stress concentrations set up at the corner of the adhesive sheet. They were eliminated by rounding the edges of the Mylar-coated steel endpieces to a radius of 0.32 cm and carrying the adhesive sheet past them in the form of two thin extensions, 0.15 cm wide, as shown in Figure 1. For simplicity, the other end of the adhesive sheet was gripped in a metal clamp.

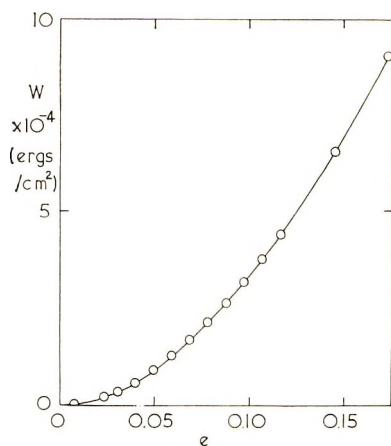


Fig. 4. Representative relation between strain energy density W and fractional extension e . Rate of strain, 1.6×10^{-4} sec⁻¹; temperature, 20°C. Note: ordinate should read (ergs/cm³).

The adhesive sheets were 10.5 cm long, 5.1 cm wide, and 0.3 cm thick. An initial separation zone was created in the center of the adhering face by levering the sheet away from the substrate with a sharp tool. Cracks were inserted in this way with lengths $2c$ ranging from about 0.3 cm to 1.5 cm, a value of about 1 cm being employed for most of the experiments. These crack lengths were found to be sufficiently small to make no significant difference to the elastic properties of the sheet. A master curve for the strain energy W per unit volume as a function of the degree of extension e was therefore obtained for a sheet with no crack, by integrating the experimental relation between tensile force and extension, and used subsequently to deduce approximate values of W_b at which failure occurred from measurements of the extension e_b at failure for sheets containing cracks. A typical experimental relation between W and e is shown in Figure 4.

Pure Shear

A thin sheet of the model adhesive material was prepared in the same way as for the simple extension testpiece, but sandwiched between two parallel Mylar-coated metal strips (Fig. 2). The sheet was 10 cm wide, 1 cm high, and about 0.3 cm thick. The initial separation zone had a length c between 2 and 5 cm long. Values of the strain energy density W_b at which failure occurred were obtained from the experimental relation between applied force and displacement up to the point at which the separation zone started to grow. The corresponding volume of material was assumed to be bounded by the adhering region in Figure 2, i.e., the nonadhering region of length c was assumed to be completely unstrained.

Care was taken to keep the metal endpieces parallel to each other as they were pulled apart.

Constant-Load and Constant-Strain Experiments

Although most of the experiments were carried out at a constant rate of strain, some measurements were made in simple extension under a constant load and in pure shear under a constant displacement. A predetermined load or displacement was applied rapidly to the testpiece and then the rate at which the initial crack grew was measured. These constant load and constant displacement measurements are represented in the figures by crosses to distinguish them from the results obtained at constant rate of strain, although no significant difference was noticed between the results from these different test procedures.

RESULTS

Simple Extension; Effect of Crack Length

Testpieces containing cracks of various lengths were stretched at a constant rate of strain, $1.6 \times 10^{-4} \text{ sec}^{-1}$, until the initial crack was seen to grow by a distance of about $5 \times 10^{-3} \text{ cm}$. The strain energy density W_b at this point was determined from the corresponding extension e_b , as described in the preceding section. The values obtained were found to decrease sharply as the length $2c$ of the initial zone of separation increased. When they were plotted against the reciprocal of c , reasonably satisfactory linear relations were obtained, passing through the origin (Fig. 5). This variation of W_b with crack length indicates that the adhesion failure energy θ is independent of crack length, eq. (1); it is given by k times the slope of linear relations like those of Figure 5, where k is approximately π at the low strains (<0.1)

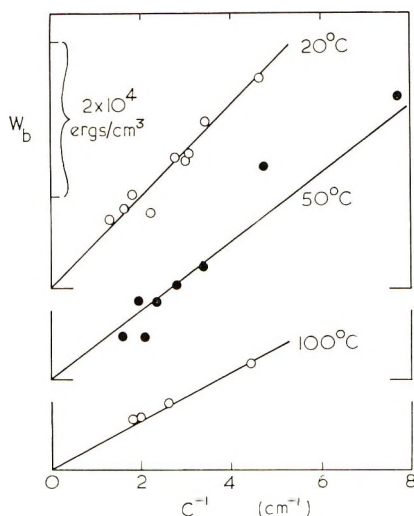


Fig. 5. Experimental relations between strain energy density W_b at the start of crack propagation and the crack half-length c for simple extension testpieces. Rate of strain, $1.6 \times 10^{-4} \text{ sec}^{-1}$.

employed in these experiments. Thus, the linear relations shown in Figure 5 give strong support to the hypothesis that adhesive failure is governed by an energy criterion. Values of the characteristic energy were obtained from them of 1.9×10^4 ergs/cm² at 20°C, 1.4×10^4 ergs/cm² at 50°C, and 1.0×10^4 ergs/cm² at 100°C.

Simple Extension ; Effect of Rate and Temperature

Clearly the characteristic failure energy varies with temperature, decreasing as the temperature is increased. Other experiments showed that θ varied with the rate of extension $\dot{\epsilon}$, increasing with increasing rate. These observations point to a viscoelastic effect. The appropriate variable to characterize the rate of failure propagation should be the rate \dot{c} at which the tip of the separation zone propagates, rather than the rate $\dot{\epsilon}$ at which the testpiece is extended. Indeed, some measurements were carried out under constant strain conditions, $\dot{\epsilon} = 0$, as described above. Measurements were therefore made in all cases of the rate \dot{c} of crack tip propagation in the early stages of growth, as soon as the strain energy density, W_b was sufficiently large to cause observable growth. Corresponding values of failure energy θ were calculated from W_b and the initial crack half-length c by means of eq. (1).

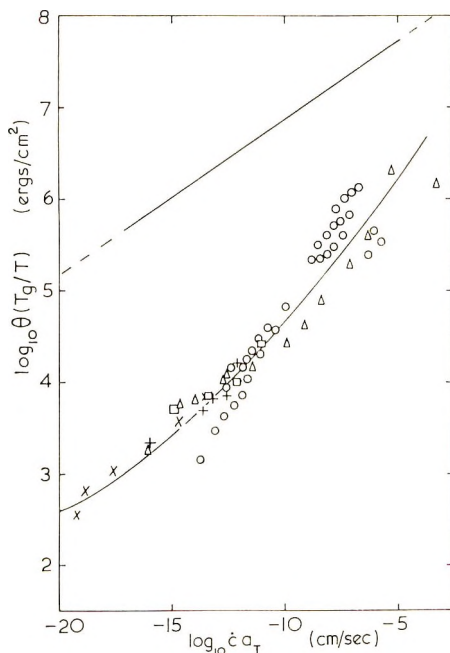


Fig. 6. Adhesive failure energy θ vs. effective rate of crack propagation at T_g for cross-linked Ameripol 1513 against a Mylar substrate: (Δ) simple extension testpieces, stretched at constant rate; (\times) simple extension testpieces, under constant load; (\square) pure shear testpieces, stretched at constant rate; ($+$) pure shear testpieces, under constant strain; (\circ) peel testpieces; (upper curve) tear energy vs. rate of tear.^{9,21}

Measurements were made over a wide range of temperature, from -40°C to $+100^{\circ}\text{C}$. The observed rate of propagation \dot{c} was reduced to an equivalent rate $\dot{c}a_T$ at a reference temperature T_s by the Williams, Landel, and Ferry rate-temperature equivalence for simple viscoelastic materials,¹⁸ where the reduction factor a_T is given by

$$\log a_T = -C_1(T - T_0)/(C_2 + T - T_0)$$

C_1 and C_2 being constants. For simplicity, the glass transition temperature T_0 of the polymer is employed here as a reference temperature, so that C_1, C_2 take the values 17.5 and 52°C .¹⁸

Experimentally determined values of θ are plotted in Figure 6 against the reduced rate of crack propagation $\dot{c}a_T$. They have been multiplied by the temperature ratio T_0/T , in accordance with previous work^{18,19} on other failure processes in viscoelastic materials, although the physical significance of this factor is obscure. Its effect is small, however, and none of the conclusions would have been altered if this correction had been omitted.

All the measurements are seen to lie on a single curve, although they correspond to widely differing rates and temperatures. Thus the failure energy θ appears to depend strongly upon the rate of crack propagation \dot{c} and upon temperature, but only as a result of viscoelastic processes within the polymer. The success of the Williams, Landel, and Ferry reduction scheme provides conclusive evidence for this.

Pure Shear; Effect of Rate and Temperature

Similar measurements were made by using pure shear testpieces (Fig. 2), both at constant rate of strain and also by rapidly extending them to a fixed strain. The values obtained for the failure energy θ , calculated by means of eq. (2), are plotted in Figure 6 against the reduced rate of crack propagation $\dot{c}a_T$. Again, the measurements at different rates and temperatures were found to be successfully combined into a single relation by means of the Williams, Landel, and Ferry rate-temperature equivalence for simple viscoelastic materials. Moreover, the present results from testpieces of quite different elastic characteristics are in good agreement with those obtained previously using simple extension testpieces, confirming the applicability of an energy criterion to the failure of an adhesive joint.

Peeling Separation; Effect of Rate and Temperature

Results were obtained previously¹ for the peel force P per unit width required to separate the same material (although crosslinked to a somewhat higher degree) from a Mylar substrate. They have been recalculated in terms of the failure energy θ , by means of eq. (3) and are also plotted in Figure 6 against the reduced rate of propagation of the peel front, $\dot{c}a_T$. They are seen to agree fairly well with the results from simple extension and pure shear experiments, except for the lowest values which correspond to extremely small peel forces of the order of 1 g and are probably rather in-

accurate. The way in which forces are applied to cause peeling separation are, of course, quite different from the two previous test methods, so that the general agreement obtained again between the values of failure energy θ at equivalent rates of crack propagation gives further support to the energy criterion for adhesion failure.

DISCUSSION AND CONCLUSIONS

The agreement between quite different methods of measurement indicates that the failure of adhesion between lightly crosslinked Ameripol 1513 and Mylar film is indeed governed by an energy criterion. A characteristic amount of energy θ per unit area of interface is required to bring about separation, whatever the form of the testpiece. However, previous work has shown that the failure energy is much smaller if the adhesive is prevented from deforming.¹ The failure energy criterion thus applies only to test methods which involve a similar degree of local deformation of the adhesive in the vicinity of the separation zone. This is likely to be the case when the substrate is rigid and the adhesive layer is thick, but it will require careful examination under other circumstances.

The importance of the viscoelastic response of the adhesive is shown by the dependence of failure energy upon rate of propagation of the failure zone and temperature, in close agreement with the Williams, Landel, and Ferry relationship for simple viscoelastic materials. A similar result has been demonstrated for the dependence of sliding friction upon speed of sliding and temperature;²⁰ in this case the energy expended in deforming a viscoelastic material up to the point at which adhesive bonds break appears to be the dominant term in the observed frictional work. Similarly, it may be concluded that deformation energy is the dominant term in the observed failure energy for an adhesive joint. Indeed, this conclusion is probably valid for all adhesives, irrespective of the mode of deformation and energy dissipation within them.

The way in which the failure energy θ depends upon the effective rate of propagation of the failure zone, Figure 6, is of particular interest. On thermodynamic grounds one would expect the work of separation to be of the same order as simple surface energies, i.e., about 10–100 ergs/cm². The experimental results are seen to decrease with decreasing rate of propagation, reaching a value of only 300 ergs/cm² at the lowest effective rate employed in the present experiments, 10⁻²⁰ cm/sec. This dependence on rate is clearly consistent with a lower limit for θ of the thermodynamically predicted amount at still lower rates of propagation, although further measurements are necessary to establish whether such a lower limit does exist and what its magnitude might be.

For comparison, the upper full curve in Figure 6 represents the tear energy for a similar polymer to the present adhesive plotted against the rate of tear propagation at T_g .^{9,21} The tear energy is also seen to decrease with decreasing rate, approaching a value only about 10 times the theo-

retical value for breaking carbon-carbon chain molecules in a typical rubbery polymer, about 10^4 ergs/cm², at the lowest rate.²²

Thus, both for cohesive rupture and adhesive failure, the failure energy at extremely low rates of failure is not much larger than would be expected on equilibrium thermodynamic grounds. As the rate of failure is increased, the measured failure energy in both cases increases by orders of magnitude, presumably reflecting energy dissipation when deformations take place under nonequilibrium conditions.

The authors gratefully acknowledge support from the Science Research Council of Great Britain in the form of a Senior Visiting Fellowship (A.N.G.) and a Research Studentship (A.J.K.). They are also indebted to Professor E. H. Andrews, Queen Mary College, University of London, and A. G. Thomas, Visiting Professor at the University of Akron, for helpful comments.

References

1. A. N. Gent and R. P. Petrich, *Proc. Roy. Soc. (London)*, **A310**, 433 (1969).
2. A. N. Gent, *J. Polym. Sci. A-2*, **9**, 283 (1971).
3. A. A. Griffith, *Phil. Trans. Roy. Soc. (London)*, **A221**, 163 (1921).
4. E. Orowan, *Proceedings of the Symposium on Fatigue and Fracture of Metals*, Wiley, New York, 1950, p. 139.
5. R. S. Rivlin and A. G. Thomas, *J. Polym. Sci.*, **10**, 291 (1953).
6. G. R. Irwin, *Structural Mechanics*, J. N. Goodier and N. J. Hoff, Eds., Pergamon Press, New York, 1960.
7. H. W. Greensmith, L. Mullins, and A. G. Thomas, *Chemistry and Physics of Rubberlike Substances*, L. Bateman, Ed., Maclaren, London, 1963, Chap. 10.
8. E. H. Andrews, *Fracture in Polymers*, Oliver and Boyd, London, 1968.
9. A. N. Gent and A. W. Henry, *Proceedings of the International Rubber Conference, Brighton, 1967*, Maclaren, London, 1968, p. 193.
10. G. J. Lake, private communication.
11. R. S. Rivlin, *Paint Technol.*, **9**, No. 106, 1 (1944).
12. M. L. Williams, *Proc. 5th U.S. Natl. Congr. Appl. Mech.*, **1966**, 451.
13. M. L. Williams, *J. Appl. Polym. Sci.*, **13**, 29 (1969).
14. E. J. Ripling, S. Mostovoy and R. L. Patrick, *Recent Developments in Adhesion Science* (ASTM Materials Science Series), STP 360, 5 (1964).
15. E. J. Ripling, S. Mostovoy and R. L. Patrick, *Materials Res. Stand.*, **4**, 129 (1964).
16. B. M. Malyshev and R. L. Salganik, *Int. J. Fracture Mech.*, **1**, 114 (1965).
17. W. A. Jemain and M. B. Ventrice, *J. Adhesion*, **1**, 190 (1969).
18. J. D. Ferry, *Viscoelastic Properties of Polymers*, Wiley, New York, 1961.
19. R. F. Landel and R. F. Fedors, in *Rupture Processes in Polymeric Solids*, B. Rosen, Ed., Interscience, New York, 1964, Chap. IIIB.
20. K. A. Grosch, *Proc. Roy. Soc. (London)*, **A274**, 21 (1963).
21. L. Mullins, *Trans. Inst. Rubber Ind.*, **35**, 213 (1959).
22. G. J. Lake and A. G. Thomas, *Proc. Roy. Soc. (London)*, **A300**, 108 (1967).

Received October 15, 1970

Dynamic Mechanical and Dielectric Relaxations of Polystyrene Below the Glass Temperature

OKIMICHI YANO and YASAKU WADA, *Department of Applied Physics, Faculty of Engineering, University of Tokyo, Bunkyo-ku, Tokyo, Japan*

Synopsis

Dynamic mechanical and dielectric properties of various kinds of polystyrene, including bulk-polymerized, monodisperse, isotactic, and thermally degraded samples, have been measured below the glass temperature to 4°K. Five relaxation processes are found, designated β , γ , γ' , δ , and ϵ in order of descending temperature. The β peak (350°K at 10 kHz) is attributed to the local oscillation mode of backbone chains and the γ peak (180°K at 10 kHz) to rotation of phenyl groups. The γ' peak (100°K at 10 kHz) is observed only in dielectric properties of the bulk-polymerized sample and is assigned to weak polar bonds, such as oxygen bonds in the chain. The δ peak (55°K at 10 kHz) which is prominent in dynamic mechanical properties is interpreted in terms of lattice defects due to a syndiotactic diad inserted between isotactic sequences in a chain or vice versa. The ϵ peak (ca. 25°K at 10 kHz) is first reported in the present work, but the mechanism involved is not yet clear.

Introduction

Relaxation processes in amorphous polymers in the glassy state have been widely studied for a number of polymers by dynamic mechanical, dielectric, and NMR techniques. Below the glass transition temperature where segmental motion is frozen, a considerable amount of local motion in the form of rotation or rotational oscillation may be present, each mode corresponding to a relaxation process at characteristic temperature and frequency.

A local relaxation mode, or anharmonic rotational oscillation of parts of backbone chains, is the most general among various mechanisms,^{1,2} and the associated loss peak appears just below the glass temperature in most polymers without side chains; in addition, side-chain relaxations appear in polymers with side chains,³ poly(methyl methacrylate) for example. For long side chains with multiple degrees of freedom, this relaxation is often separated into two peaks.⁴

At lower temperatures, the relaxations due to methyl-group rotation are observed in dynamic mechanical measurements as well as in NMR absorption. The methyl-group relaxation has been theoretically analyzed by Tanabe et al.,⁵ and satisfactory agreement has been attained between theory and experiment with respect to relaxation strength and relaxation time.

In addition to these typical relaxation processes, polymers in the glassy state exhibit a variety of relaxations originating from defects in chemical

structure such as those associated with chain ends, branches, imperfect tacticity, and also from low molecular weight impurities, including absorbed water.

Polystyrene can be obtained in atactic and isotactic forms. The molecular weight distribution is easily found by gel-permeation chromatography, and narrow-distribution samples of any molecular weight may be prepared by living polymerization. For these reasons, polystyrene is particularly suitable for the investigation of effects of tacticity, molecular weight, heterojunctions, and other molecular factors on the relaxation behavior.

Relaxation processes in polystyrene have been investigated by dynamic mechanical,⁶⁻²⁰ dielectric,²¹⁻²⁵ and NMR techniques.²⁶⁻³³ According to previous studies, at least three relaxations appear below the glass temperature.

According to Schmieder and Wolf,⁶ a mechanical loss peak is found at 325°K for 8 Hz, which seemingly corresponds to the NMR narrowing at around 350°K observed by Odajima.²⁶ This peak will be designated the β peak in the following. The β peak is separated from the α peak (the primary relaxation above the glass temperature) only at low frequencies and merges into the α peak at high frequencies.

The γ peak was observed at 132°K for 1 Hz in dynamic-mechanical data by Illers⁸ and Baccaredda¹⁵ on polystyrene and *para*-substituted halogen derivatives. The peak seems to correspond to the gradual narrowing of NMR absorption spectra in the vicinity of 200°K.³¹

At temperatures below 70°K, a prominent loss peak (designated as the δ peak in this paper) has been observed in dynamic mechanical measurements by Sinnott¹³ and by Woodward and co-workers.^{17,20} This peak was found in both atactic and isotactic samples.

Other authors³⁴ have indicated the existence of small peaks which have not been definitely assigned to any of the above classifications. The data of the various authors are often scattered, probably because of variations in sample preparation.

In the present study, dynamic-mechanical and dielectric measurements have been made over a wide range of temperature from 4°K to the glass temperature on three kinds of polystyrene, namely, a bulk-polymerized atactic sample, a monodisperse atactic one, and an isotactic one. The observed relaxation processes, as well as results in the literature, are classified into five groups, the β , γ , γ' , δ , and ϵ peaks in order of descending temperature. Molecular mechanisms involved with each process will be proposed. The third peak is denoted γ' because it is observed only for bulk-polymerized samples in dielectric measurements and seems, as will be described in detail in a later section, to come from weak polar bonds in backbone chain.

Experimental Techniques

The composite oscillator method at 34 and 152 kHz was used in dynamic-mechanical measurements. This method proved to be very suitable for low-temperature measurements because of the small size of specimen re-

quired. The method consists essentially of measuring the resonant frequency and the width of the resonant curve of the composite oscillator made by cementing the circular-rod specimen to a quartz torsional resonator of the the same diameter as the specimen. Details of principles and practice have been described in a previous paper.³⁵

Two quartz resonators were used, 6 mm and 5 mm in diameter for 34 and 152 kHz, respectively. Epoxy resin and silicone of 10^6 centistokes viscosity were used as adhesives above and below 100°K , respectively. The length of the specimen was adjusted so as to make the resonance frequency of the composite oscillator coincide with that of the quartz resonator within 5%. All the measurements were performed in the fundamental mode of the specimen rod.

A block diagram of the electronic circuit for the composite oscillator method is shown in Figure 1. To balance out the clamped admittance of the resonator, a bridge-circuit was used in which the capacitor C_1 and the conductance shifter G could be so adjusted as to eliminate the resonator admittance or the admittance at off-resonance frequency.³⁶ Only the motional current, which is a maximum at the mechanical resonant frequency f , was indicated on the voltmeter. The value of f and the half-value width Δf of the resonant curve were measured by the electronic counter.

The values of f and Δf of the rod specimen were calculated by using the equations:

$$f = f_2 - (f_1 - f_2)(m_1/m) \quad (1)$$

$$\Delta f = [1 + (m_1/m)]\Delta f_2$$

where m is the mass, subscripts 1 and 2 stand for the quartz resonator and the composite oscillator, respectively, and quantities without a subscript represent values for the specimen alone. The complex shear modulus of the specimen is then calculated from the equations:

$$G' = (2lf/n)^2\rho \quad (2)$$

$$G'' = (\Delta f/f)G'$$

where l is the length of the specimen, n the mode number ($n = 1$ through the present study), and ρ the density of the specimen. The density at low-temperatures was estimated from the value at room temperature and the thermal expansion coefficient reported by Zakin et al.³⁷

Dielectric constant and loss at frequencies from 30 Hz to 100 kHz were measured with a transformer bridge³⁶ (Ando Denki TR-10). The specimen film was 150–250 μ in thickness and silver electrodes, 5.3 cm² in area, were vacuum-deposited on both surfaces.

The structure of the cell used for dielectric measurements above 200°K has been described elsewhere.³⁸ The cell was immersed in a liquid bath, and the temperature of the specimen was measured by a Cu-Constantan thermocouple near the specimen. Water and methanol-Dry Ice mixture

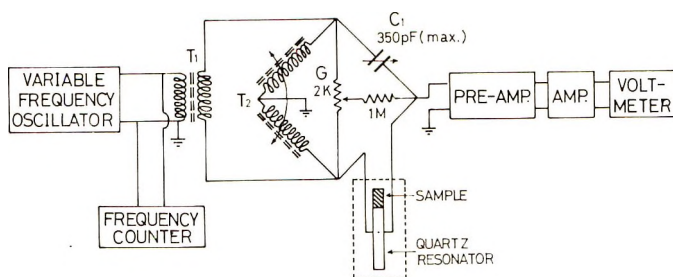


Fig. 1. Block diagram of the composite oscillator method.

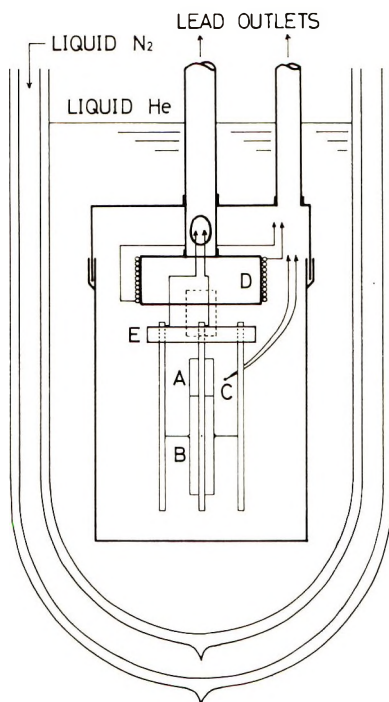


Fig. 2. Schematic drawing of the cryostat: (A) specimen; (B) quartz resonator; (C) thermocouple; (D) copper block with heater winding; (E) Teflon plate.

were used as the bath media above and below room temperature, respectively.

Below 250°K , the cryostat illustrated in Figure 2 was used for both mechanical and dielectric measurements. In Figure 2, the arrangement for the composite oscillator method is illustrated. The jacket surrounding the specimen was sealed with Wood's metal and helium gas was introduced into it to insure good thermal contact. The temperature of the specimen was measured with a Cu-constantan thermocouple.

Mechanical and dielectric measurements were carried out with temperature increasing, the heating rate being about 1°C per 3–10 min.

Samples

Samples as listed in Table I were used in this study. Sample APS was prepared from Styron 666 (Asahi Dow Chem. Co.) by precipitating the polymer several times with methanol from a benzene solution and then thoroughly drying the precipitate *in vacuo* at 100°C.

TABLE I
Polystyrene Samples

Symbol	Type	Molecular weight \bar{M}_v	Density, g/cm ³ (25°C)
APS	Atactic	2.4×10^5	1.050
MPS	Monodisperse	4.1×10^5	1.051
IPS	Isotactic	9.2×10^5	1.071
APpfs	Atactic poly- <i>p</i> -fluorostyrene		
DPS-1	Thermally degraded at 280°C for 0.5 hr		
DPS-2	Thermally degraded at 280°C for 3.5 hr		

Sample MPS obtained from Pressure Chemical Co. was characterized by a weight-average to number-average molecular weight ratio $\bar{M}_w/\bar{M}_n \leq 1.06$, indicating a relatively narrow distribution.

Isotactic polystyrene was polymerized from monomer dissolved in *n*-hexane with $\text{Al}(\text{C}_2\text{H}_5)_3\text{-TiCl}_3$ as a catalyst. The polymer thus obtained was purified, and the fraction insoluble in MEK but soluble in toluene was used as sample IPS. The sample was proved to be isotactic by infrared spectroscopy. The crystallinity of IPS was estimated from density to be 28%.

Poly-*p*-fluorostyrene was bulk-polymerized at 80°C without initiator. A fractionated polymer was used as sample APpfs.

Thermally degraded polystyrenes, samples DPS-1 and DPS-2, were prepared by heating APS samples at 280°C for 0.5 and 3.5 hours, respectively.

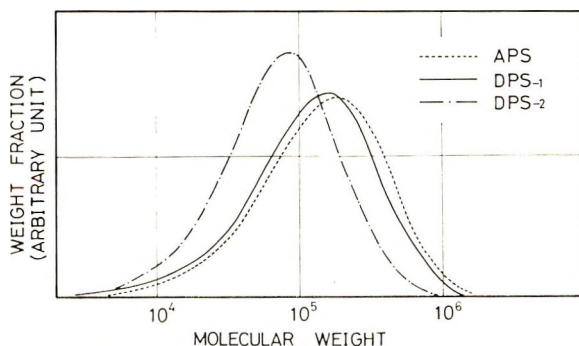


Fig. 3. Molecular weight distribution of atactic polystyrene (APS) and thermally degraded polystyrenes (DPS-1 and DPS-2).

The heat treatment was effected in a glass tube in which air had been replaced by nitrogen gas. The tube was steadily evacuated to 10^{-3} mm Hg during heat treatment to avoid the effect of humidity and oxygen. In the upper part of the tube outside the furnace, a trace of volatile material was deposited. In the case of heat treatment for 3.5 hr, the deposit was a highly viscous liquid. The residue was used as the sample. The molecular weight distribution of samples APS, DPS-1, and DPS-2, as measured by the gel-permeation chromatography is shown in Figure 3.

The samples were molded *in vacuo* into circular rods or pressed into film at 50°C above the glass temperature. The IPS sample was molded or pressed just above the melting point and then slowly cooled.

Overall Behavior

Figure 4 represents the relaxation map of polystyrene, in which frequencies corresponding to temperatures of mechanical and dielectric loss peaks, NMR narrowing, and minimum of the spin-lattice relaxation time are plotted against reciprocal absolute temperature. Six relaxations called α , β , γ , γ' , δ , and ϵ , in the order of descending temperature, are clearly indicated. Activation energies obtained from the slopes of the lines in Figure 4 are 30, 9, 2.7, and 1.6 kcal/mole for the β , γ , γ' , and δ processes, respectively.

Above the glass temperature, the α relaxation is the primary relaxation due to segmental motion, and the temperature dependence of the relaxation time is of the WLF type.³⁹ In Figure 5, in which the dielectric constant and loss at high temperatures are shown, the primary relaxation is observed above 350°K . The peak in sample MPS is at a higher temperature than in sample APS, in which the low molecular weight component acts as a plasticizer. A dielectric loss peak due to sorbed water was observed between the β and γ peaks by Okamoto et al.,³⁴ but this peak was not found in the present study.

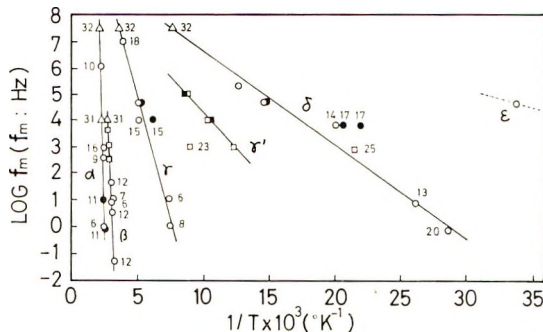


Fig. 4. Relaxation map of polystyrene: (O, ●) mechanical loss peaks, (□, ■) dielectric loss peaks, and (Δ, ▲) NMR narrowing and T_1 -minima, for (O, □, Δ) atactic and (●, ■, ▲) isotactic polymers. Numbers refer to references. Points without numbers are from the present work.

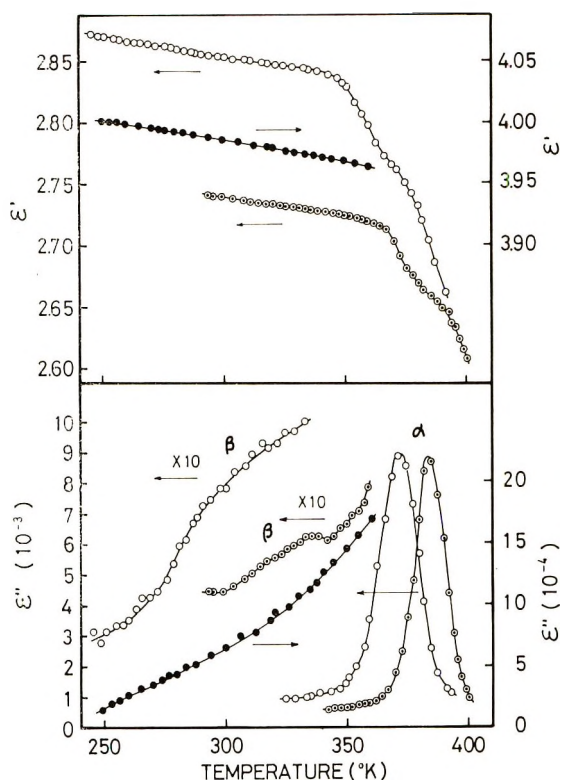


Fig. 5. Dielectric constant and dielectric loss of samples: (○) APS, 110 Hz; (◊) MPS, 110 Hz; (●) IPS 300 Hz.

The β Relaxation

Polystyrene has a β relaxation immediately below the primary relaxation. The β relaxation appears in both dynamic mechanical and dielectric loss. The NMR narrowing around 350°K may be attributed to the β process. The β peak merges into the α peak when measured at high frequencies.

Some authors have assigned the β process to the rotation of phenyl groups. Illers and Jenckel,⁷ among others, suggested that the molecular motion responsible for the β relaxation is the rotation of some phenyl groups possessing less steric hindrance than the majority. Vol'kenshtein and his co-workers,^{40,41} who measured the NMR narrowing of spectra of fluorine nuclei in polyfluorostyrenes, observed the narrowing for *ortho*-substituted and *meta*-substituted polymers but no narrowing for the *para*-substituted polymer in the temperature range of the β relaxation. This result favors the interpretation by Illers and Jenckel.

However, there is evidence indicating that rotational vibration of backbone chains occurs in the β relaxation region. As is readily seen in Figure 5, the β relaxation appears in dielectric loss at 340°K for MPS and around 320°K for APS as a shoulder on the α peak. Rotation of phenyl groups would result in no change in polarization and hence no dielectric relaxation.

On the contrary, the rotation of a segment of the backbone chain results in a change of polarization if the vector sum of dipoles of phenyl groups in the segment does not vanish. This assumption is consistent with the fact that, in isotactic PS, the β relaxation is not pronounced, as Figure 5 shows. A perfect 3_1 helix in isotactic PS might exhibit no resultant dipole.

The amount of narrowing of the second moment of NMR absorption spectra in the β relaxation region is about 2–3 gauss²,²⁶ which is reasonable for the rotation of the backbone chain. According to Tanaka et al.,⁴² the β narrowing was observed in the NMR spectra of fluorine nuclei in poly-*p*-fluorostyrene, in contrast to the data of Vol'kenshtein.

As has been mentioned above, many polymers without long side-chains exhibit in general a relaxation due to the rotation of backbone segments, which was called by Okano¹ the "local relaxation mode." Large-amplitude rotational vibrations of backbone segments become incoherent among neighboring chains. When the polymer is strained, the distance between chains is changed, and the distribution of rotational displacement goes to a new equilibrium with a corresponding relaxation time. The β relaxation of polystyrene, the local mode relaxation, is therefore attributed to the anharmonic character of the interchain potential for rotational motion of backbone chain.

According to Moraglio and Danusso,⁴³ a peculiar variation is observed in the thermal expansion of polystyrene around 50°C. Bianchi and Rossi⁴⁴ found an irregularity in the internal pressure in the temperature interval from 47 to 55°C. Wunderlich and Bodily⁴⁵ also found small peaks of specific heat for polystyrene at 29° and 52°C. These results seem, however, to have no direct relation to the β relaxation, because, when it is measured at low frequency, the relaxation is observed below these anomalous temperatures.

The γ Relaxation

Figures 6–8 illustrate the real and imaginary parts of the complex shear modulus at 34 kHz for samples APS, MPS, and IPS. The peak around 200°K corresponds to the γ relaxation. The γ peak has been found by Schmieder and Wolf⁶ at 133°K (11.3 Hz) for atactic PS and by Illers and Jenckel⁸ at 132°K (1 Hz).

The γ peak does not appear in dielectric measurements as can be seen in Figure 9, which includes the temperature range of the γ peak. The minimum in the spin-lattice relaxation time at 260°K observed by Hunt et al.³² corresponds to the γ peak.

Illers and Jenckel⁸ have attributed this peak to the torsional motion of methylene sequences formed in the backbone chain by head-to-head or tail-to-tail coupling on the basis of the fact that this peak does not exist in isotactic PS. The present result reveals, however, that sample MPS, which was prepared by anionic polymerization and hence is expected to have no heterojunctions, exhibits the γ peak clearly.

The fact that the γ peak does not appear in dielectric loss suggests the

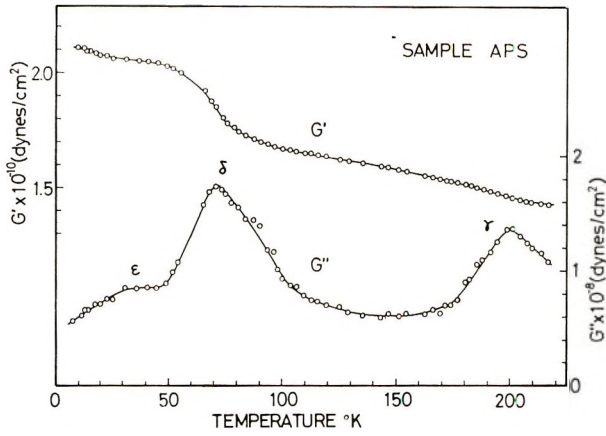


Fig. 6. Complex shear modulus vs. temperature for sample APS at 34 kHz.

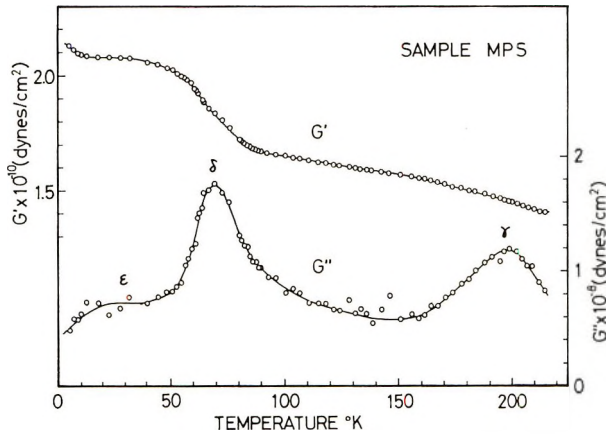


Fig. 7. Complex shear modulus vs. temperature for sample MPS at 34 kHz.

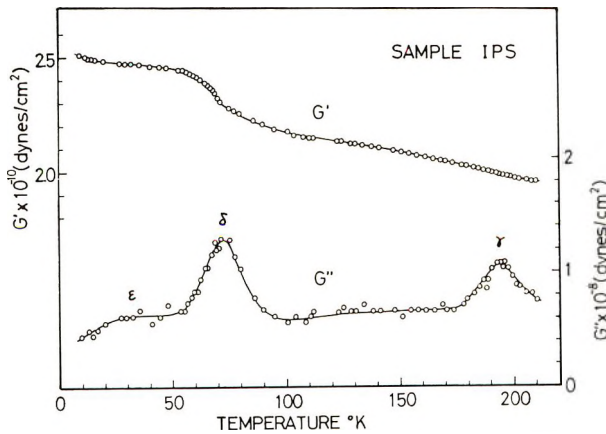


Fig. 8. Complex shear modulus vs. temperature for sample IPS at 34 kHz.

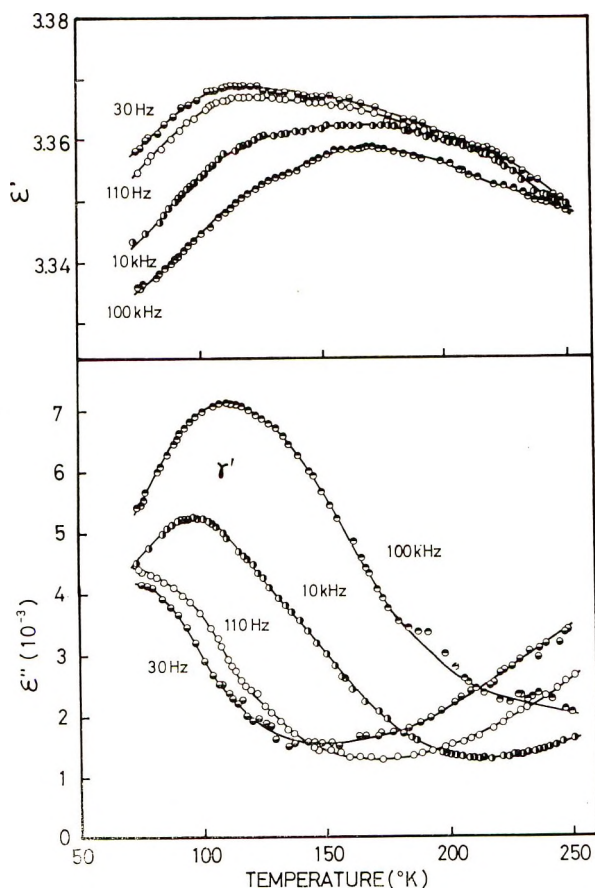


Fig. 9. Dielectric constant and dielectric loss vs. temperature for sample APS at various frequencies.

peak may be attributed to the rotation of phenyl groups around the bond to the backbone chain. Even sample APpFS does not show the γ peak in dielectric loss (Figure 10).

The NMR narrowing of PS in the γ region amounts to about 1 gauss^{2,31} which is reasonable for phenyl rotation. According to Odajima et al.,³¹ the narrowing occurs in *para*-substituted polystyrene but does not in the *ortho*- and *meta*-substituted polymers, probably because of a hindering effect in the latter cases.

The mechanism of the mechanical relaxation due to phenyl group rotation may be similar to that due to methyl group rotation described by Tanabe et al.⁵ The amplitude of fluctuation of a phenyl group should depend on strain, but this process is characterized by a relaxation time because the energy must be exchanged between the phenyl group and the backbone chain. The peak height is smaller in isotactic than atactic PS, probably because phenyl groups in an atactic chain exert strong interactions with other phenyl groups or backbone chains. This is also supported by the fact that the loss-maximum in isotactic PS shifts to lower temperature.

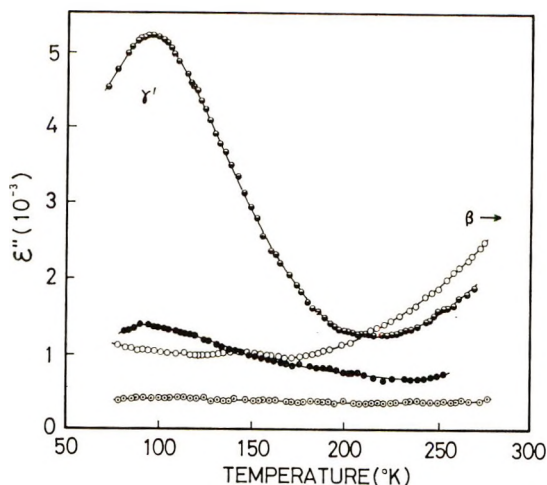


Fig. 10. Dielectric loss at 10 kHz for samples: (●) APS; (●) IPS; (○) MPS; (○) APpFS.

The temperature for the γ peak in PS is higher than that for methyl group relaxations in various other polymers because the phenyl group is more bulky than the methyl group.

The γ' Relaxation

Figure 9 represents the dielectric constant and dielectric loss at various frequencies as a function of temperature for sample APS, and Figure 10 gives the dielectric loss at 10 kHz for APS, MPS, IPS, and APpFS. Only sample APS exhibits a prominent loss peak around 97°K, which is designated here as the γ' peak. Results in Figure 11, which gives the loss for thermally degraded PS, indicate that the γ' peak almost disappears with heat treatment at 280°C for 30 min, during which, as is shown in Figure 3, the molecular weight distribution shifts only slightly to lower values. The γ' peak was not observed in dynamic mechanical measurement even for APS, as can be seen in Figure 6.

These facts suggest that the γ' relaxation may originate from polar groups introduced into molecules during bulk polymerization. As is well known,⁴⁶ polystyrene which has been thermally polymerized in bulk has various types of weak bonds: heterojunctions or head-to-head (tail-to-tail) junctions, oxygen bonds such as $(-C-O-O-C-)$, polar chain ends and so on.

In general, such a defect may have a dipole moment and result in a dielectric relaxation. The strength of the relaxation

$$\Delta\epsilon = \epsilon_0 - \epsilon_\infty$$

is given according to the two-state model as⁴⁷

$$\Delta\epsilon = \frac{4\pi N\mu^2}{3kT} \left(\frac{n^2 + 2}{3} \right)^2 \left(\frac{3\epsilon_0}{2\epsilon_0 + \epsilon_\infty} \right) \frac{K}{(1 + K)^2} \quad (3)$$

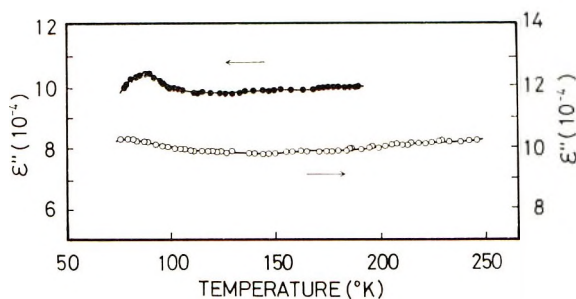


Fig. 11. Dielectric loss at 10 kHz for samples: (●) DPS-1; (○) DPS-2.

where ϵ_0 and ϵ_∞ are the dielectric constants at sufficiently low and high frequencies, respectively, N is the number of defects per unit volume, μ is the dipole moment difference between the two states (expressed as the moment *in vacuo*), and n is the refractive index. The equilibrium constant K between the two states is expressed by

$$K = \exp\{-\Delta G^\circ/RT\} \quad (4)$$

where ΔG° is the standard free energy difference between the two states. The value of $\Delta\epsilon$ was estimated from the experimental curve of ϵ'' versus $1/T$ by the approximate equation,³⁸

$$\Delta\epsilon \approx (2\Delta H/\pi R)\epsilon_{\max}'' \left[\left(\frac{1}{T_1} \right) - \left(\frac{1}{T_2} \right) \right] \quad (5)$$

where ΔH is the activation energy and T_1 and T_2 are temperatures at which ϵ'' falls to half ϵ_{\max}'' .

If heterojunctions were the cause of the γ' relaxation, N would have to be very large because the dipole moment of phenyl group and hence μ may be small for a heterojunction. This contradicts the observation that the γ' peak disappears after slight degradation by heat treatment.

To interpret the observed strength of the γ' peak of APS, μ must be taken to be fairly large. If μ is assumed to be 2.3 D, which is reasonable for oxygen bonds, the density of defects is calculated from eq. (3) as one per 200 monomer units, which may be a reasonable estimate. In this calculation, ΔG° is estimated as 350 cal/mol from the dependence of $\Delta\epsilon$ on T observed in Figure 9, and hence K as 0.2 at 97°K from eq. (4). In fact, infrared spectroscopy of the volatile components from the thermal degradation revealed the existence of carbonyl groups.

The δ Relaxation

As illustrated in Figures 6–8, polystyrene exhibits a prominent mechanical loss peak, designated the δ peak at 70°K. The existence of this relaxation was first pointed out by Sinnott.¹³ He reported a small loss maximum for atactic PS by using free oscillation of a torsion pendulum (5.59 Hz, 38°K). Crissman and McCammon¹⁴ have found the δ peak with

a longitudinal vibration apparatus (6294 Hz, 48°K). The spin-lattice relaxation time T_1 of polystyrene has been measured by Hunt et al.³² as a function of temperature. The T_1 versus temperature curve exhibits a minimum around 130°K, which probably corresponds to the δ peak as illustrated in the relaxation map in Figure 4. McCammon et al.²⁵ found that the δ peak in dielectric loss was very slight.

The effect of tacticity on the mechanical δ peak is not so appreciable but, as can be seen in Figures 6–8, the peak is narrow and the peak height is low in the isotactic sample. Similar results have been obtained by Crissman, Woodward, and Sauer.¹⁷

In Figure 12, the shear modulus and loss modulus of sample APS at 152 kHz are shown. It can be seen, by comparison with Figure 6, that the peak shifts to higher temperature with increasing frequency and the peak height increases with increasing temperature.

In Figure 13, the observed G'' value as a function of $1/T$ is compared with the theoretical curve for a single relaxation time which was calculated by the equations,

$$G'' = G_{\max}'' [2\omega\tau / (1 + \omega^2\tau^2)] \quad (6)$$

$$\tau = \tau_0 \exp\{\Delta H/RT\}$$

where τ_0 was determined so that $\omega\tau = 1$ at the temperature of the loss maximum and ΔH was taken as 1.6 kcal/mol. The results indicate that the δ peak of atactic sample has a broad distribution of relaxation times but the distribution is narrowed in the isotactic sample.

Mechanical relaxations are in general classified into thermal relaxations and volume relaxations.⁴⁸ The term "volume" has a broad meaning here and includes volume change and other types of strain such as shear.

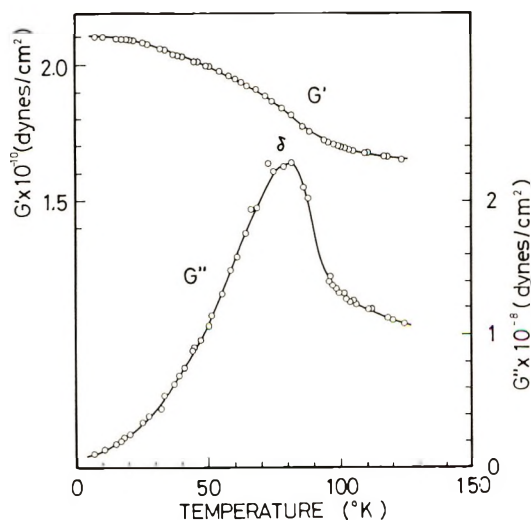


Fig. 12. Complex shear modulus of sample APS vs. temperature at 152 kHz.

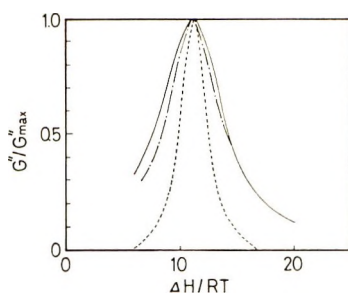


Fig. 13. Shape of the δ peak for samples: (—) APS and (- · -) IPS compared with (- -) theoretical curve for a single relaxation.

The thermal relaxation is caused by the relaxation of specific heat of a degree or degrees of freedom in the system. If we consider a vibrational degree of freedom of polystyrene with frequency ν , the specific heat due to this mode is given by

$$\delta C = R \left(\frac{h\nu}{kT} \right)^2 \frac{\exp\{h\nu/kT\}}{[\exp\{h\nu/kT\} - 1]^2} \quad (7)$$

where h is Planck's constant and k is Boltzmann's constant. At low temperatures where the δ peak occurs, however, δC is usually very small. In order to account for the observed peak height of the δ peak on the basis of thermal relaxation of a vibrational mode, the frequency ν would have to be assumed as low as 10 cm^{-1} , which is an order of magnitude too low to be realized. Furthermore, the fact that the δ peak occurs in shear deformation in which temperature is kept constant is evidence that the relaxation is not thermal.

In the following we consider a volume relaxation caused by motion of defects between two states, 1 and 2 (the two-state model). The general theory of volume relaxation⁴⁸ gives the relaxation strength r as

$$\begin{aligned} r &= (G_\infty - G_0)/G_\infty \\ &= (NG_0/kT)(\Delta v)^2 [K/(1 + K)^2] \end{aligned} \quad (8)$$

where G_∞ and G_0 are instantaneous and equilibrium moduli, respectively, N is the number of defects per unit volume, and Δv is the deformation of the system when a defect moves from state 1 to state 2, and K has the same significance as in eq. (4).

For evaluation of r , the following approximation, similar to that of eq. (5), was used³⁸

$$\Delta G = G_\infty - G_0 \approx (2\Delta H/\pi R)G_{\text{max}}''[(1/T_1) - (1/T_2)] \quad (9)$$

From the data in Figures 6 and 12, values of r for sample APS at two temperatures can be obtained by eq. (9) as $r = 0.037$ at 70°K and $r = 0.041$ at 80°K . Since Δv and N are independent of temperature, ΔG° and consequently K are obtained as $\Delta G^\circ = 300 \text{ cal/mole}$ and $K = 0.1$ at 70°K .

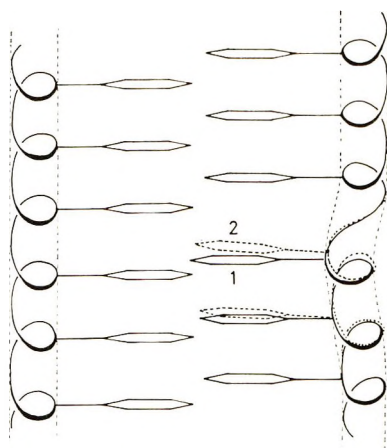


Fig. 14. Schematic representation of disorder in the vicinity of a syndiotactic diad in the isotactic chain. Numbers 1 and 2 represent states 1 and 2, respectively.

The problem of the defect entity responsible for the δ relaxation is still open. A speculative model of the defect is presented in the following.

In the case of perfectly isotactic polystyrene, for example, molecules in the crystal take on a 3_1 helical conformation and each helix is surrounded by three neighbors.⁴⁹ Phenyl groups are successively arranged, and a strong intermolecular interaction exists through van der Waals force between phenyl groups. In the glassy phase, the arrangement may be locally similar to that in the crystal but, when a defect of tacticity such as $(\dots d d l l l \dots)$ is introduced into a chain in the process of polymerization, the helical conformation of the chain in the glassy phase must change sense at the defect point, with a resulting misfit of phenyl groups with the surrounding chains. The phenyl group in the disordered region may be in a complicated potential field and have, therefore, one or more metastable states which correspond to state 2 in the above two-state model. The transition of a phenyl group between the states 1 and 2 accompanies the deformation of the backbone helix and hence the strain of the bulk system. Figure 14 represents schematically the disordered region; the phenyl group is assumed to be most stable at the position 1 where the intrachain potential is at a minimum and have a metastable state 2 where the interchain potential is at a minimum.

We cannot say anything quantitative about the molecular arrangement of the disordered region but, on the basis of this model, Δv in eq. (8) should be a fraction of the volume of a phenyl group. If we assume one defect per 20 monomer units, N is $3.12 \times 10^{20} \text{ cm}^{-3}$. This leads with the observed values of r and K to $\Delta v = 26 \times 10^{-24} \text{ cm}^3$ from eq. (8), which corresponds to one-sixth of the volume of a phenyl group. According to Flory, Mark, and Abe,⁵⁰ an isotactic vinyl polymer has such defects in 5–10% concentration.

The tacticity defect model presented above for the δ relaxation can explain qualitatively the observed facts as follows: (1) the peak height is small in the isotactic sample, in which the defect density may be small; (2)

the δ peak is specific to polystyrene and its derivatives because the relaxation is brought about by strong interaction between phenyl groups; (3) only a small relaxation is observed in dielectric loss because the phenyl group has a small dipole moment; (4) according to Frosini and Woodward,²⁰ uniaxially stretched polystyrene shows a smaller δ peak when twisted around the stretching axis. This appears reasonable because, in the present model, the transition of the phenyl group results in a deformation of the chain axis (Fig. 14) and hence torsion around the chain axis is less effectively coupled with the motion in the defect region.

Crissman et al.¹⁷ have observed mechanical loss peaks similar to the δ peak of polystyrene in polystyrene derivatives: at 50°K for poly-*o*-methylstyrene, 35°K for polyvinyltoluene rich in the *meta*-substituent, and at 20°K for poly- α -methylstyrene. The peak height is greatest for polystyrene and decreases in the above order. According to our model for the γ' and δ peaks, however, the relaxations are related to defects of chemical structure introduced in the course of polymerization; and hence, a direct correlation between monomer structure and peak height or peak position would hardly be expected.

In general, defects or disorder in chemical structure of polymers may result in low-temperature relaxations. If the molecular mechanism is established, the study of relaxation may afford a new tool for physical analysis of the defects.

TABLE II
Relaxation processes in polystyrene

Symbol	Temperature at 10 kHz, °K	Activation energy, kcal/mole	NMR	Mechanical	Dielectric	Mechanism
α	400	WLF-type	+	+	+	Segmental motion of backbone chain
β	350	30	+	+	+	Local oscillation mode of backbone chain
γ	180	9	+	+	0	Rotation of phenyl group
γ'	97	2.7	0	0	+	Polar defects such as oxygen bonds
δ	55	1.6	+	+	0	Defects in tacticity
ϵ	(25)			+		

A recent study of T_1 for monodisperse polystyrenes by Connor³³ revealed that a minimum of T_1 appears near the δ relaxation region and the strength is inversely proportional to the degree of polymerization. In a mechanism that he proposed, the butyl endgroup of monodisperse polystyrene is responsible for the T_1 minimum. This may not be, however, related to the δ peak in the present study because the δ peak appears in samples APS and IPS which have no butyl groups at chain ends.

The ϵ Relaxation

The curves in Figures 6–8 indicate a new peak, the ϵ peak, which appears as a shoulder on the low temperature side of the δ peak. The existence of this peak is also confirmed from the asymmetry of the δ peak observed by Crissman et al.,¹⁷ when the loss modulus is replotted against $1/T$. As is seen in Figure 12, the ϵ peak shifts to high temperature with increasing frequency and merges into the δ peak. The molecular motion giving rise to the ϵ peak is not yet clear.

Conclusions

Conclusions of the present work are listed in Table II. A plus sign in the table indicates that the relaxation is distinct and the zero that the relaxation is weak or missing.

The authors wish to express their thanks to Y. Kawamura of this laboratory for his assistance in obtaining some of the data and to Dr. K. Iimura of the Science University of Tokyo for providing us with the Zielger-Natta catalyst.

References

1. N. Saito et al., *Solid State Physics*, Vol. 14, F. Seitz and D. Turnbull, Eds., Academic Press, New York, 1963, p 387.
2. Y. Wada et al., in *U.S.-Japan Seminar in Polymer Physics (J. Polym. Sci., C, 15)*, R. S. Stein and S. Onogi, Eds., Interscience, New York, 1966, p. 101.
3. J. Heijboer, *Brit. Polym. J.*, **1**, 3 (1969).
4. Y. Kawamura, S. Nagai, J. Hirose, and Y. Wada, *J. Polym. Sci. A-2*, **7**, 1559 (1969).
5. Y. Tanabe, J. Hirose, K. Okano, and Y. Wada, *Polym. J.*, **1**, 107 (1970).
6. K. Schmieder and K. Wolf, *Kolloid-Z.*, **134**, 149 (1953).
7. K. H. Illers and E. Jenckel, *Rheol. Acta*, **1**, 322 (1958).
8. K. H. Illers and E. Jenckel, *J. Polym. Sci.*, **41**, 528 (1959).
9. R. A. Wall, J. A. Sauer, and A. E. Woodward, *J. Polym. Sci.*, **35**, 281 (1959).
10. R. Kono, *J. Phys. Soc. Japan*, **15**, 718 (1960).
11. S. Newman and W. P. Cox, *J. Polym. Sci.*, **46**, 29 (1960).
12. K. H. Illers, *Z. Elektrochem.*, **65**, 679 (1961).
13. K. M. Simmott, *SPE Trans.*, **2**, 65 (1962).
14. J. M. Crissman and R. D. McCammon, *J. Acoust. Soc. Am.*, **34**, 1703 (1962).
15. M. Baccaredda, E. Butta, and V. Frosini, *J. Polym. Sci. B*, **3**, 189 (1965).
16. A. E. Woodward, in *Transitions and Relaxations in Polymers (J. Polym. Sci. C, 14)*, R. F. Boyer, Ed., Interscience, New York, 1966, p. 89.
17. J. M. Crissman, A. E. Woodward, and J. A. Sauer, *J. Polym. Sci. A*, **3**, 2693 (1965).
18. J. Hirose and Y. Wada, *Repts. Progr. Polym. Phys. Japan*, **9**, 287 (1966).

19. G. Goldbach and G. Rehage, *Kolloid-Z.*, **216**, 56 (1967).
20. V. Frosini and A. E. Woodward, *J. Polym. Sci. A-2*, **7**, 525 (1969).
21. A. J. Curtis, *SPE Trans.* **2**, 82 (1962).
22. S. Saito and T. Nakajima, *J. Appl. Polym. Sci.*, **2**, 93 (1959).
23. T. Hara, M. Nozaki, and S. Okamoto, *Japan. J. Appl. Phys.*, **6**, 1138 (1967).
24. V. Adamec, *J. Polym. Sci. B*, **6**, 687 (1968).
25. R. D. McCammon, R. G. Saba, and R. N. Work, *J. Polym. Sci. A-2*, **7**, 1721 (1969).
26. A. Odajima, J. Sohma, and M. Koike, *J. Phys. Soc. Japan*, **12**, 272 (1957).
27. W. P. Slichter, *Makromol. Chem.*, **34**, 67 (1959).
28. W. P. Slichter, *SPE J.*, **15**, 303 (1959).
29. R. Kosfeld, *Kolloid-Z.*, **172**, 182 (1960).
30. R. P. Gupta, *J. Polym. Sci.*, **54**, S20 (1961).
31. A. Odajima, J. A. Sauer, and A. E. Woodward, *J. Polym. Sci.*, **57**, 107 (1962).
32. B. I. Hunt, J. G. Powles, and A. E. Woodward, *Polymer*, **5**, 323 (1964).
33. T. M. Connor, *J. Polym. Sci. A-2*, **8**, 191 (1970).
34. M. Nozaki, K. Shimada, and S. Okamoto, *Japan. J. Appl. Phys.*, **9**, 578 (1970).
35. K. Yamamoto and Y. Wada, *J. Phys. Soc. Japan*, **12**, 374 (1957).
36. R. H. Cole and P. M. Gross Jr., *Rev. Sci. Instr.*, **20**, 252 (1949).
37. J. L. Zakin, R. Simha, and H. C. Hershey, *J. Appl. Polym. Sci.*, **10**, 1455 (1966).
38. K. Tsuge, *Japan. J. Appl. Phys.*, **3**, 588 (1964).
39. M. L. Williams, R. F. Landel, and J. D. Ferry, *J. Amer. Chem. Soc.*, **77**, 3701 (1955).
40. R. A. Abdrashitov, N. M. Bazhenov, M. V. Vol'kenshtein, A. I. Kol'tsov, and A. S. Khachaturov, *Vysokomol. Soedin.*, **5**, 405 (1963); **6**, 1871 (1964).
41. M. V. Vol'kenshtein, A. I. Kol'tsov, and A. S. Khachaturov, *Vysokomol. Soedin.*, **7**, 296 (1965).
42. K. Tanaka, O. Yano, S. Maru, and R. Nagao, *Repts. Progr. Polym. Phys. Japan*, **12**, 379 (1969).
43. G. Moraglio and F. Danusso, *Polymer*, **4**, 445 (1963).
44. U. Bianchi and C. Rossi, *Polymer*, **4**, 447 (1963).
45. B. Wunderlich and D. M. Bodily, *J. Appl. Phys.*, **35**, 103 (1964).
46. G. G. Cameron and G. P. Kerr, *Europ. Polym. J.*, **4**, 709 (1968).
47. C. P. Smyth, *Dielectric Behavior and Structure*, McGraw-Hill, New York, 1955.
48. J. Lamb, *Physical Acoustics*, Vol. 2A, W. P. Mason, Ed., Academic Press, New York, 1964, p. 203.
49. G. Natta, P. Corradini, and I. W. Bassi, *Nuovo Cimento*, **15**, 68 (1960).
50. P. J. Flory, J. E. Mark, and A. Abe, *J. Amer. Chem. Soc.*, **88**, 639 (1966).

Received June 23, 1970

Revised October 9, 1970

Thermodynamic and Conformational Properties of Polystyrene. III. Dilute Solution Studies on Branched Polymers

G. C. BERRY, *Mellon Institute, Carnegie-Mellon University, Pittsburgh, Pennsylvania 15213*

Synopsis

Light-scattering and viscometric measurements on dilute solutions of five branched polystyrene polymers are reported. The data include studies in decalin as a function of temperature, including the theta temperature, and in toluene. The results for the radius of gyration and the second virial coefficient are not in accord with the two parameter random-flight model. Possible causes of this discrepancy are considered. It is shown that the intrinsic viscosity of branched chains is not uniquely determined by the radius of gyration.

INTRODUCTION

Investigations on branched polymers afford a degree of freedom lacking in studies on linear polymers: the average segment density of the polymer coil can be altered independently of its radius of gyration by variation of the structural parameters of the branched macromolecules. This additional degree of freedom can complicate the analysis of experimental data, but it can also offer an additional probe for the investigation of the fundamental properties of macromolecules. Despite the undeniable importance of chain branching on polymer properties, relatively few experimental data can be found on the dilute solution properties of well characterized, model, branched polymers.¹⁻⁶ Comparatively, more examples of attempts to characterize branched polymers of unknown structure by the use of theories on dilute solution properties can be found. In this investigation, parts of which were discussed in an earlier preliminary report,⁶ we seek to extend our previous studies (Parts I and II of this series⁷) on the dilute solution properties of polystyrene prepared by anionic polymerization to include data on two types of branched polymers: (1) two different regular-star branched chains comprising several arms of equal length, each with one end connected to a common branch node; and (2) two different random-comb branched chains, each with branches of equal length attached at random intervals to a much longer backbone molecule. Light scattering data on the radius of gyration (s^2) at the Flory temperature Θ and on the temperature coefficient of the second virial coefficient A_2 for

temperatures near Θ will be presented. In addition, light scattering data on $\langle s^2 \rangle$ and A_2 at temperatures greater than Θ will be given. The intrinsic viscosity $[\eta]$ of the branched polymers will also be considered at Θ and at temperatures greater than Θ .

THEORETICAL BACKGROUND

For convenience, we have gathered in the following sections certain theoretical considerations pertinent to the analysis of data to be considered. However, these sections are not intended to serve as an exhaustive review of the material. The random-flight chain model has been used to calculate properties of unperturbed branched chains including the mean square radius of gyration $\langle s^2 \rangle_0$,^{1,8-15} the intrinsic viscosity $[\eta]_0$,¹⁶ the translational friction factor Ξ_0 ,^{9,13,17} and certain light scattering properties.^{15,18,19} Here and in the following, the subscript zero denotes properties of the unperturbed chain, i.e., under conditions such that the second virial coefficient A_2 is zero (cf. seq.). The first-order perturbation theory^{20,21} has been used to calculate A_2 and $\langle s^2 \rangle / \langle s^2 \rangle_0$ ²⁵⁻²⁶ in terms of the two parameters $n^2\beta$ and nb_0^2 , where n is the number of effective statistical chain-segments characterized by a mean-square length b_0^2 and pairwise mutually excluded volume β . In addition to the parameter nb_0^2 , the calculation of $[\eta]_0$ and Ξ_0 involves a segmental friction factor ζ_0 .

Random-Flight Chain Parameters

Presently available theories have not related β , n , b_0^2 or ζ_0 in any satisfactory way to molecular parameters of the real chain. It is assumed that interchain and intrachain interactions are characterized by the same parameter β . The excluded volume integral β is given formally in terms of a potential $u(\mathbf{r})$ for the pairwise interactions of the random-flight segments by the integral

$$\beta = \int_{(\epsilon)} [1 - \exp \{ -u(\mathbf{r})/kT \}] d\mathbf{r} \quad (1)$$

Although β is sometimes thought of only in terms of polymer-polymer interactions, the function $u(\mathbf{r})$, representing the mean potential of average force between two segments separated by the vector distance \mathbf{r} , includes polymer-solvent and solvent-solvent interactions as well, and may not even be centrosymmetric.²⁷

The use of an arbitrary centrosymmetric function for the potential $u(\mathbf{r})$ with a hard core volume $\beta_0 = 4\pi r_0^3/3$ (e.g., infinite u for $r \leq r_0$), and a weak attraction such that $|u(r)| \ll kT$ for $r > r_0$ yields

$$\beta = \beta_0(1 - \Theta/T) \quad (2)$$

with

$$\Theta = k^{-1} \int_1^\infty x^2 \{ -u(x) + [u^2(x)/2kT] - \dots \} dx$$

where

$$x = r/r_0$$

Attempts to use a more precise formulation for $u(r)$ to deduce Θ or β_0 in terms of molecular parameters, or to assess the temperature dependence of β for $T \gg \Theta$ are beyond the scope of the random-flight model.²⁷ The simple temperature dependence of β given by eq. (2) can be obtained from phenomenological considerations certainly valid when T is very near Θ . The conclusion⁷ that eq. (2) was, in fact valid for data on linear polystyrene in decalin for temperatures up to $\Theta + 100^\circ\text{K}$ has recently been challenged,²⁸ and the revised relation

$$\beta = \beta_0[(1 - \Theta/T) + 2.5 \ln(\Theta/T)] \quad (3)$$

suggested as a substitute for that system on the consideration that there must be a lower critical solution temperature at $T > \Theta$ somewhere in the vicinity of the critical temperature of decalin. Definitive discrimination between eqs. (2) and (3) on the basis of the data on linear polystyrene in decalin does not appear possible.

There is nothing in the definition of β that indicates that β should depend on chain branching. To be sure, in principle the function $u(r)$ could vary with some parameter such as the segment density of the chain, and so depend on chain branching. This possibility, which is usually ignored, will be considered further in the following. Similarly, n and b_0^2 are usually taken as invariants of the chain configuration.

Radius of Gyration

Random-flight chain statistics predict that for a branched chain with n segments of mean-square length b_0^2

$$\langle s_{br}^2 \rangle_0 = g \langle s_l^2 \rangle_0 \quad (4)$$

where, as usual,

$$\langle s_l^2 \rangle_0 = 1/6 n b_0^2$$

and where g is a numerical constant that depends on chain geometry.^{1,8-15} Here, and in the following, the subscripts br and l will denote branched and linear chains, respectively. Subscripts will be suppressed where no confusion is possible. For regular-star and random-comb branched polymers, it has been shown¹⁵ that

$$g = \lambda + 2\lambda(1 - \lambda^2)f^{-1} + (1 - \lambda)^3(3f - 2)f^{-2} \quad (5)$$

with f the number of branches per molecule, and $1 - \lambda$ the fraction of material in the branches of the molecule ($\lambda = 0$ for regular stars). Since eq. (5) obtains for combs with exactly f randomly spaced branches on each molecule, in principle it should be modified to account for the random number of branches placed on the backbone chains during the actual coupling step; but this modification^{12,15} has negligible effect on the estimate for

g for the samples of interest here. Equation (5) can be approximated to within 1% for $f > 4$ (and to within 4% for all f) by the simpler expression

$$g = \lambda + (1 - \lambda)^{7/3}(3f - 2)f^{-2} \quad (6)$$

Here, and in the following, we will reserve the symbol g to denote the parameter calculated by random-flight statistics, as opposed to a ratio of experimentally determined radii of gyration. Inasmuch as $n\lambda$ is the number of segments in the chain backbone, Eqs. (4), (5) and (6) show that $\langle s_{br}^2 \rangle_0$ can be given in an alternate form useful for the analysis of data on comb polymers:

$$\langle s_{br}^2 \rangle_0 = \langle s_r^2 \rangle_0 [1 + \lambda^{-1}(1 - \lambda)^{7/3}(3f - 2)f^{-2}] \quad (7a)$$

where the subscript r refers to the backbone polymer. Thus, if λ is near unity, this relation predicts a radius for the branched chain essentially the same as that of the backbone polymer used in the grafting step in the preparation of the branched molecule, even though the molecular weight of the molecule is increased by grafting on the branches. This can provide a useful internal check on the effect of branching on $\langle s_{br}^2 \rangle_0$ since, if $\langle s_r^2 \rangle_0$ is measured separately (before the grafting step), the expected value of $\langle s_{br}^2 \rangle_0$ can be calculated without recourse to molecular weight measurements and use of the relation between $\langle s_r^2 \rangle_0$ and M . Moreover, any effects of molecular weight polydispersity of the backbone polymer on $\langle s^2 \rangle$ as determined by light scattering are suppressed by comparison of $\langle s_{br}^2 \rangle_0$ with $\langle s_r^2 \rangle_0$.

In a similar way, for star polymers, we can write

$$\langle s_{br}^2 \rangle_0 = \langle s_f^2 \rangle_0 [(3f - 2)/f] \quad (7b)$$

where $\langle s_f^2 \rangle_0$ is the radius of gyration of a single branch determined before the coupling reaction.

The first-order perturbation theory²¹ has been used to calculate the effect of small excluded volume β on $\langle s^2 \rangle$ with a result analogous to that for linear chains^{25, 26}

$$\langle s^2 \rangle = \langle s^2 \rangle_0 (1 + a_1 z + \dots) \quad (8)$$

where

$$z = (3/2\pi n b_0^2)^{3/2} n^2 \beta \quad (9)$$

The constant a_1 depends on the branched chain structure but is not a single-valued function of g . Thus, approximate relations of the type^{1, 29, 30}

$$\langle s^2 \rangle = \langle s^2 \rangle_0 \mathcal{S}(g, z) \quad (10)$$

where \mathcal{S} is some function unspecified here, cannot be expected to be generally valid. Since $a_{1, br} > a_{1, l}$, it follows that chain dimensions ought to expand more rapidly with increasing z for branched chains than for linear molecules, at least for small z . The approximate relation for $\alpha^2 \equiv \langle s^2 \rangle / \langle s^2 \rangle_0$ established experimentally³¹ and theoretically³²

$$\alpha^2 = 1 + a_1(z/\alpha^3)h(z/\alpha^3) \quad (11)$$

with

$$h(z/\alpha^3) = 0.508\{1 + 0.969[1 + 7.84a_1(z/\alpha^3)]^{-2/3}\}$$

should not necessarily be expected to hold for branched chains with $h(z/\alpha^3)$ unchanged. The conformation averaged value of the radius of gyration given by eq. (11) was calculated from the relation

$$\langle s^2 \rangle = \frac{\int s^2 F(s^2) \exp \{-E(s^2)/kT\} ds^2}{\int F(s^2) \exp \{-E(s^2)/kT\} ds^2}$$

with

$$E(s^2) = 2\pi kT\beta \int \rho^2(r|s) dr$$

where $\rho(r|s)$ is the segment distribution about the center of mass, averaged over all conformations with a given s , and $F(s^2)$ is the distribution of s for the unperturbed chain. An approximate function $F(s^2)$ designed to reproduce the first few averages $\langle s^{2m} \rangle_0$ was used in calculations of $\langle s^2 \rangle$ for the linear chain. The weighting function was taken to be

$$E(s^2) = \sigma a_1 kT z \langle s^2 \rangle_0^{3/2} s^{-3}$$

where $\sigma^{-1} = \langle s^2 \rangle_0^{3/2} \langle s^{-3} \rangle_0 - \langle s^2 \rangle_0^{1/2} \langle s^{-1} \rangle_0$ can be calculated from the approximate function $F(s^2)$ to give σ the value 1.185 for linear chains. To the first approximation in the calculation of $\langle s_{br}^2 \rangle$ one might try to use the same function $F(s^2)$ as that employed for linear chains, but use the values of a_1 appropriate to the branched chain in the assessment of the weighting function $E(s^2)$. In essence, this means that, to this approximation, α should be given by eq. (11) provided the correct value of a_1 is used.

Second Virial Coefficient

The second virial coefficient can be given in terms of the two parameters in the random-flight model by³¹

$$A_2 = (N_a \beta n^2 / 2M^2) F'(z) \quad (12)$$

with

$$F'(z) = 1 - b_1 z + \dots \quad (13)$$

where b_1 is a constant that depends on chain structure (e.g., linear or branched). The parameter b_1 has been calculated for certain star and comb-branched chains with the general result that $b_{1,br} > b_{1,l}$, but that $b_{1,br}$ is not a single-valued function of g .^{9,22-24} This result indicates that $A_{2,br}$ will be less than $A_{2,l}$ at least for small z .

Equation (13) is limited to small values of z but can be used as an aid in determining the temperature dependence of the excluded volume integral β for β near zero, that is, for T near the Flory temperature Θ . In this limit, we can assume with generality that

$$\beta = \beta_0(1 - \Theta/T)$$

where β_0 and Θ are independent of temperature and molecular weight. Thus for Θ/T near unity, we write

$$\lim_{T \rightarrow \Theta} \frac{\partial A_2}{\partial(1 - \Theta/T)} = \left(\frac{n^2}{2M^2} \right) N_a \beta_0 = 4\pi^{3/2} N_a \beta_0$$

where, for convenience, we have defined the parameter B_0 for later use. Estimates of B_0 determined in this way can be used to calculate values of z for each temperature of measurement and finally values of $F'(z)$ by means of a suitable approximate theory. These data can then be used to obtain a refined estimate of β_0 by use of the relation

$$\lim_{T \rightarrow \Theta} \frac{\partial[A_2/F'(z)]}{\partial(1 - \Theta/T)} = 4\pi^{3/2} N_a B_0 \quad (14)$$

This procedure, which helps to remove some of the curvature from the plots in the vicinity of $(1 - \Theta/T)$ near zero, has been used previously in the analysis of data on linear polystyrene in *cis*-decalin.⁷ First and final estimates of B_0 determined in this way may differ by 10–30%, depending on the molecular weight and type of branching.

Approximate theories must be used to correlate A_2 if $b_1 z$ exceeds ca. 0.1, since the series $F'(z)$ is very poorly convergent, and exact calculation of its higher-order terms presents unsurmountable difficulties. These theories generally lead to a relation of the type

$$A_2 M^2 \langle s^2 \rangle^{-3/2} = 4\pi^{3/2} N_a (z/\alpha^3) F(z/\alpha^3) \quad (15a)$$

Of these, the expression

$$(z/\alpha^3) F(z/\alpha^3) = (1/2 b_1 \rho g^{3/2}) [1 - \exp \{-2b_1 \rho (z/\alpha^3)\}] \quad (15b)$$

where $\rho = (\alpha/\alpha_2)^3$ with $\alpha^5 - \alpha^3 = (a_1/k_1)(\alpha_2^5 - \alpha_2^3)$ is a relation that has been found useful in the correlation of data on linear polymers,³¹ (of course, with g equal to unity). Here, α_2 is the average expansion factor of the dimension of a chain in a bimolecular cluster, a_1 and b_1 are the coefficients introduced above, and k_1 is a coefficient that depends on chain configuration.

In the limit of large z (very good solvent) eqs. (15) reduce to the result:

$$\lim_{z \rightarrow \infty} A_2 M^2 \langle s^2 \rangle^{-3/2} \equiv \Psi = 4\pi^{3/2} N_a / 2\rho b_1 g^{3/2} \quad (16)$$

where $\rho = (a_1/k_1)^{3/6}$ in the limit of large z . A value of 4.0×10^{24} has been found for linear polystyrene, giving ρ the value 2.43.⁷ To a first approximation, one might suspect that Ψ is independent of molecular structure. Detailed calculations of b_1 , however, show that

$$b_{1,br} \leq b_{1,l} g^{-3/2}$$

where the equality holds only in the limit for certain lightly branched structures,²³ so that in general Ψ depends on the branched structure.

Moreover, Ψ cannot be a single-valued function of g , since b_1 is not. These considerations mean that correlations of the type

$$A_{2,br}/A_{2,l} = (\langle s_{br}^2 \rangle / \langle s_l^2 \rangle)^{3/2}$$

sometimes suggested^{1,30} (the ratios taken at constant molecular weight) cannot be generally valid.

Hydrodynamic Properties

The hydrodynamics of the random-flight branched chains have been explored less exhaustively than have the thermodynamics. The steady-flow intrinsic viscosity of nondraining random-flight star-branched chains is given by¹⁶

$$[\eta]_0 = \frac{3^{1/2} \pi^{3/2} N_a \langle s_l^2 \rangle_0^{3/2}}{2M} \sum \frac{1}{\lambda_k'} \quad (17)$$

where the λ_k' are eigenvalues different for each branched polymer. Numerical calculation of $\Sigma(1/\lambda_k')$ has been carried out for four branched structures: one unsymmetrical and three symmetrical star-branched molecules (as well as for linear chains, of course). If these numerical results are expressed in terms of the theoretical parameter g as

$$\Sigma(1/\lambda_k') = 0.586g^\gamma$$

e.g. such that

$$[\eta_{br}]_0 / [\eta_l]_0 = g^\gamma \quad (18)$$

then γ is approximately 0.44 for the symmetrical star polymers and 0.54 for the one unsymmetrical case investigated. The numerical results were given in terms of g with the hope that the exponent γ might be invariant with branched structure, and it was suggested that $\gamma = 1/2$ might be the best choice for use with all branched structures,¹⁶ or that

$$[\eta_{br}]_0 = [\eta_l]_0 g^{1/2} \quad (19)$$

By contrast, subsequent calculations of the translational friction coefficient Ξ_0 for the nondraining random-flight chain show that $\Xi_{0,br}/\Xi_{0,l}$ is not proportional to g^μ with a value of μ invariant to the branch structure.^{13,17} In fact, μ tends toward $1/2$ for comb-branched polymers as the ratio of the branch length to the backbone length tends toward zero ($\mu = 1/2$ being equivalent to $m = 3/2$), but no constant value of μ could correlate the data on all symmetrical star-branched polymers.

It seems likely that a similar situation will exist for the ratio $[\eta_{br}]_0/[\eta_l]_0$, with this ratio (1) tending toward $g^{3/2}$ in the limit of comb molecules with short branches and long backbones, (2) about equal to $g^{1/2}$ for star-branched polymers, and (3) somewhere between these limits for other structures, with a value sensitive to details of the chain configuration.

First-order perturbation calculations of branched random-flight chains have not been carried out, but one can anticipate that these will yield the type of relation found for linear chains³⁴

$$[\eta] = [\eta]_0[1 + p(h)z + \dots] \quad (20)$$

with $p(h)$ dependent on branching and the hydrodynamic interaction parameter

$$h = (s/6\pi\eta_0)(2\pi\langle s^2 \rangle_0)^{-1/2}N \quad (21)$$

We must assume that $p(h)$, like a_1 , will not be a unique function of g . As with linear chains,⁷ we can eliminate z between expressions for $[\eta]/[\eta]_0$ and $\alpha^3 \equiv (\langle s^2 \rangle / \langle s^2 \rangle_0)^{3/2}$ to obtain the result

$$([\eta]/[\eta]_0 - 1 = [2p(h)/3a_1](\alpha^3 - 1) \quad (22)$$

where terms of order $(\alpha^3 - 1)^2$ are suppressed. Of course, one hopes that eq. (22) will be adequate for a wider range in z than either eq. (8) or (20). The random-flight model yields 0.81 for $2p(h)/3a_1$ in the limit of large h . Data on linear polystyrene suggest that $2p(H)/3a_1$ increases with increasing M to a value near unity at high M .⁷

Exclusion Chromatography

It is generally accepted that the separation mechanism in exclusion chromatography depends on the size of the pores in the porous substrate relative to some dimension of the macromolecule. It has been suggested³⁵ on the basis of empirical evidence that the product $[\eta]M$ will characterize data on the elution volume V to give a $[\eta]M$ versus V function for a given chromatographic column that is independent of molecular weight, chain branching, or the chemical nature of the polymer or solvent. Data to support this conclusion are available for a variety of linear polymers and some branched polymers in thermodynamically good solvents. In a theoretical treatment of star-shaped random-flight chains, it was found that the partition function K , and hence the elution volume, could not be precisely represented as any simple relation involving g , but that the quantity $\langle s^2 \rangle_0 g^{1/3}$ appeared to correlate the data as well as any such function.³⁶ Since $[\eta_{br}]_0 \approx [\eta_l]_0 g^{1/2}$ for random-flight star-branched molecules, this prediction agrees well with the observed correlation of V with $M[\eta]$ (albeit the empirical correlation was made in good solvents). In particular, the parameter $\langle s_{br}^2 \rangle_0$ was not found to correlate with K for the diverse star-branched structures investigated theoretically.

EXPERIMENTAL

Materials

Solvents were prepared as described in Part I.⁷ The A branched polymers were prepared by Mr. T. Altares, utilizing the synthesis procedure outlined elsewhere.³⁷ In this method, preparation of the star and comb

polymers is accomplished by coupling polystyryllithium to a previously prepared multiply chloromethylated molecule. Thus, star-branched polymers were prepared by coupling polystyryllithium to chloromethylated benzene. An anionically prepared polystyrene was lightly chloromethylated to make the backbone molecule of the comb polymer. An excess of the polystyryllithium was used in all preparations to ensure complete conversion of the chloromethylated groups. In consequence, the final product was always contaminated with uncoupled linear polymer with the molecular weight of the branches on the branched polymer. The linear polymer was separated from the branched polymer by a fractional precipitation using benzene as the solvent and methanol as the nonsolvent. The branched polymer was then further fractionated to remove the high and low molecular weight "tails" from its distribution, the middle fraction being used for these studies. The molecular weights of the component molecules of the branched chain and other parameters determined in dilute solution are given in Table I. The sedimentation velocity profile of the chloromethylated backbone precursor molecule was compared with that of the unfractionated polymer to be certain that no degradation occurred during the chloromethylation reaction. In addition, the sedimentation velocity profile was very useful in showing that sample A-48; 2 was not contaminated by molecules with 2, 3, 5, or more arms as the presence of these is easily distinguished in the ultracentrifuge.

TABLE I
 Linear Polymers Used in Preparation of Branched Species

Pre-cursor polymer	Used in branched polymer	$M_w \times 10^{-4}$	$\langle s^2 \rangle_0 \times 10^{-2}, \text{cm}^2$ ^a	$[\eta]_0, \text{dl/g}^a$	$[\eta], \text{dl/g}^b$	$M_v \times 10^{-4}^c$
A-18	A-53; 2 A-68; 4	133	9.90 ^d	0.98	(2.85) ^e	—
A-48-C	A-48; 2	39.4	3.05	—	—	—
A-51-C	A-51	—	—	—	0.308	5.6
A-68-C	A-68; 4	—	—	—	0.54	12.0
A-53-C	A-53; 2	—	—	—	0.175	4.60

^a Measured at the Flory theta temperature in cyclohexane.

^b Measured at 25°C in toluene.

^c Deduced from $[\eta]$ in toluene and the correlations in Part II.

^d A value of $10^{12}\langle s^2 \rangle = 23.3 \text{ cm}^2$ would be expected in toluene according to the data in Part I.

^e Deduced from M_w and the correlation in Part II.

Light Scattering

Light-scattering measurements were carried out with the apparatus and methods described in Part I.⁷ Calculations with the random-flight chain model¹⁵ show that in cases of interest here the simple Debye expression from the reciprocal scattering function $P^{-1}(u)$ for linear chains is an adequate approximation to the more complicated relation for $P^{-1}(u)$, provided that

$\langle s_{br}^2 \rangle$ is used in place of $nb^2/6$ in the definition of u . Thus, $P^{-1}(u)$ can be approximated by

$$P^{-1}(u) = (2/u^2)[u - 1 + \exp\{-u\}] \quad (23)$$

where

$$u = (4\pi n/\lambda)^2 \langle s_{br}^2 \rangle \sin^2(\theta/2)$$

The form of eq. (23) suggests that plots of $[c/R(u,c)]^{1/2}$ versus u and concentration c be extrapolated to $u = 0$ and $c = 0$, as first proposed in Part I of this series, to aid in the calculation of the derivatives $\partial[c/R(0,c)]^{1/2}/\partial c$ and $\partial[c/R(u,0)]^{1/2}/\partial u$ that yield the second virial coefficient $\Gamma_2 = A_2M$ and the mean-square radius of gyration $\langle s^2 \rangle$, respectively.

The effect of the heterogeneity in molecular weight caused by the variation in the number of branches per molecule on the comb-branched chains does not seriously affect $\langle s^2 \rangle_{LS}$ in this case, although

$$\langle s^2 \rangle_{LS} = \frac{\sum \langle s^2 \rangle_i M_i W(M_i)}{\sum M_i W(M_i)} \quad (24)$$

is usually very sensitive to heterogeneity. We have

$$\langle s^2 \rangle_i \approx kM'_i$$

where M' is the molecular weight of the backbone molecule of the i th species. Since the backbone polymers are narrowly distributed anionic polymers, $\langle s^2 \rangle_{LS}$ is approximately given by

$$\langle s^2 \rangle_{LS} \approx kM'$$

irrespective of the polydispersity in the number of branches per molecule.

Intrinsic Viscosity

Viscometric measurements were carried out with the apparatus described in Part II. The concentric cylinder viscometer was used with samples A-53; 2 and A-68; 4. The suspended-level Ubbelohde viscometer was used with sample A-48; 2. The double extrapolation of η_{sp}/c and $\ln \eta_{rel}/c$ described in Part II was used to analyze these data.

Exclusion Chromatography

The Waters gel-permeation chromatograph was used with columns with 3×10^6 , 1.5×10^5 , 10^4 , and 10^3 Å ratings. The columns were placed in the order given, with the 3×10^6 Å column at the efflux end. The elution volume V_{peak} corresponding to the maximum in the refractive index was determined from the recorder output and correlated with $\log[\eta]M$ for linear polystyrenes in both toluene and 2-butanone (the latter being only a moderately good solvent³¹). In all cases, 0.1 ml injections of a 0.5 g/dl solution were used with a 1 ml/min flow rate. Measurements were made on the $4\times$ attenuation scale and peak height averaged 20% of full scale.

Repeated injections over the time period used for these studies gave reproducible elution volumes to within ± 0.12 ml or better for some of the samples. All elution volumes represent averages of at least three separate injections, and sometimes more. One sample was injected at intervals to be certain the column did not change. No appreciable effect on V_{peak} was noted when the flow rate was reduced to 0.5 ml/min.

RESULTS

Data at the Flory Temperature

Molecular parameters of the various precursor molecules used to synthesize the branched chains are collected in Table I. The structural parameters of the various polymers studied are given in Table II, together with some theoretical parameters specific to each structure. Unless stated otherwise, all molecular weights were determined from light scattering studies at the Flory temperature. As with linear polymers, we define the Flory temperature operationally as the temperature at which A_2 vanishes. Values of Θ , $[\eta]_0$, and $\langle s^2 \rangle_0$ are recorded in Table III, together with the parameters measured in toluene. (Here the subscripts zero denote values at $T = \Theta$.) Values of B_0 in *cis*-decalin are also included in Table III.

The experimental values of $\langle s_{br}^2 \rangle_0$ are compared with values calculated with the theoretical parameter g in Table IV. Equation (7b), the measured value of $\langle s_s^2 \rangle_0$, and the number of branches per molecule, $f = M/M_s$, were used to compute $\langle s_{br}^2 \rangle_0$ for the star polymer A-48; 2. Equation (7a), the measured values of $\langle s_r^2 \rangle_0$, $\lambda = M_r/M$, and

$$f = (M - M_r)/M_s$$

were used to compute $\langle s_{br}^2 \rangle_0$ for the comb polymers.

The exponents m calculated from experimental molecular size data according to the relation

$$[\eta_{br}]_0/[\eta_l]_0 = (\langle s_{br}^2 \rangle_0/\langle s_l^2 \rangle_0)^m \quad (25)$$

for three comb polymers and one star polymer are given in Table IV. We remark that the value of γ from eq. (18) and experimental intrinsic viscosities is smaller than m and close to $1/2$ in those cases where $\langle s_{br}^2 \rangle_0/g$ is found to exceed $\langle s_l^2 \rangle_0$ for chains with the same molecular weight. We do not regard this as of fundamental significance, however, since in most cases the proximity of γ to $1/2$ appears to be the result of compensating deviations from the prediction of the random-flight theory. Since m appears to be sensitive to the detailed molecular structure, it appears that a correlation of the type of eq. (25) should be used only as a rough approximation.

Data in Good Solvents

The dependence of Γ_2 , $\langle s^2 \rangle/\langle s^2 \rangle_0$, and $[\eta]$ of the branched polymers in *cis*-decalin on temperature is illustrated in Figures 1, 2, and 3. As with linear polymers, the rate of increase of Γ_2 , $\langle s^2 \rangle$, and $[\eta]$ with T decreases as

TABLE II
Structural Parameters of Branched Polystyrene

Polymer	f	$M_s \times 10^{-4}$ (branch)	$M_r \times 10^{-4}$ (backbone)	$M \times 10^{-4}$ (polymer)	g [eq. (5)]	a_1 [eq. (8)] ^a	b_1 [eq. (13)] ^b
				Star-branched			
OW ^c	3	11.2	—	34.8	0.778	1.298	3.28
A-48; 2	4	40.0	—	19.0	0.625	1.342	3.87
A-51	6	5.6 ^d	—	33.0	0.444	1.449	5.39
				Comb-branched			
A-53; 2	24	4.6 ^d	133	250	0.561	2.15	5.19
A-53; 3	21	4.6 ^d	133	223	0.593	—	—
A-68; 4	22	12.0 ^d	133	395	0.395	2.69	7.22

^a a_1 is 1.276 for linear chains.

^b b_1 is 2.865 for linear chains.

^c Data taken from reference 3.

^d Determined viscometrically in toluene through the relation $[\eta] = 1.08 \times 10^{-4} M^{0.716}$, cf. Part II.

TABLE III
Dilute Solution Parameters at the Flory Temperature and in Toluene

Polymer	Solvent ^a	$M \times 10^{-4}$	$(s^2) \times 10^{12}$, cm ²	$[\eta]$, dl/g	θ , °C	$B_0 \times 10^{26}$, cm ³ -mol ² /g ²	$\Gamma \equiv A_2 M$, cm ³ /g
OW ^b	C	34.8	—	0.44	34.8	—	—
	T	—	—	0.98	—	—	115
A-48; 2	D	192	8.56	0.79	12.2	—	—
	C	185	8.03	0.82	—	2.03	—
A-51	T	187	21.0	2.27	—	—	380
	D	36.3	—	—	10.2	1.85	—
	C	32.4	—	—	—	—	—
Star-branched							
A-53; 2	D	265	14.0	0.90	12.2	1.20	—
	C	251	13.1	0.96	—	—	—
A-53; 3	T	232	37.3	3.35	—	—	404
	D	223	13.3	—	—	—	—
A-68; 4	D	407	18.0	0.98	14.3	0.73	—
	C	387	17.5	—	36.1	0.50	—
	T	388	53.3	3.72	—	—	520
Comb-branched							

^a Solvents: D, *cis*-decalin at $T = \theta$; C, cyclohexane at $T = \theta$; T, toluene at 12°C.

^b Data on this polymer are taken from reference 3.

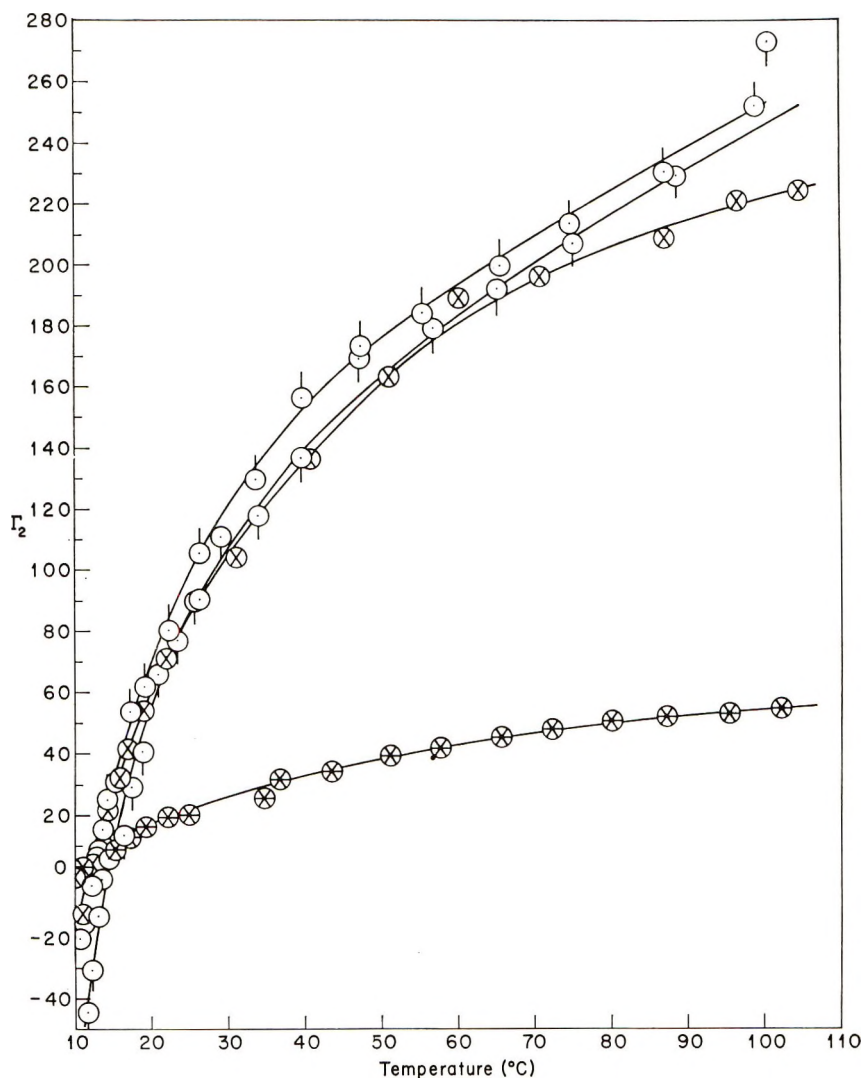


Fig. 1. Second virial coefficient Γ_2 (cc/g) as a function of temperature for branched polystyrenes in *cis*-decalin: (○) A-53;2; (◐) A-68;4; (⊗) A-48;2; (⊙) A-51.

TABLE IV
Comparison of Dilute Solution Parameters of Branched and Linear Chains

Polymer	Structure	$\Theta_{br} - \Theta_l$	$\frac{B_{0,br}}{B_{0,l}}$	$\frac{\langle s_{br}^2 \rangle_0}{g \langle s_l^2 \rangle_0}$	$\frac{[\eta_{br}]_0}{[\eta_l]_0}$	m
OW	Star	0	0.62	—	0.85	—
A-48; 2	Star	0	1.00	1.08	0.75	0.60
A-51	Star	-2	0.90	—	—	—
A-53; 2	Comb	0	0.59	1.33	0.73	1.06
A-68; 4	Comb	+2	0.36	1.55	0.60	1.03

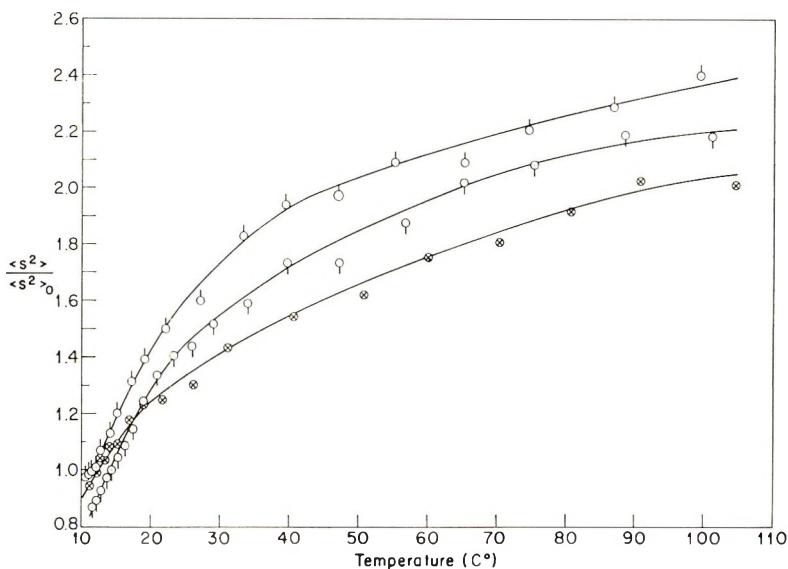


Fig. 2. Expansion factor $\langle s^2 \rangle / \langle s^2 \rangle_0$ as a function of temperature for branched polystyrenes in *cis*-decalin. Symbols are defined in the caption for Figure 1.

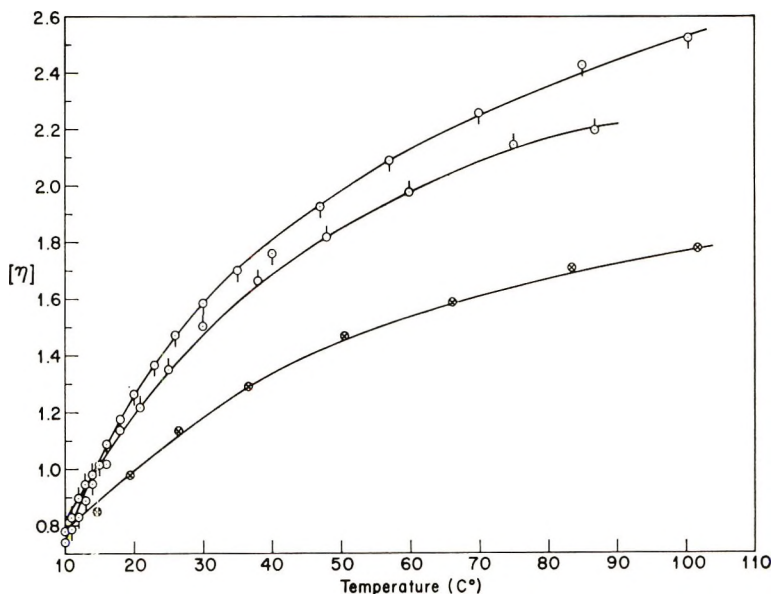


Fig. 3. Intrinsic viscosity $[\eta]$ as a function of temperature for branched polystyrene in *cis*-decalin. Symbols are defined in the caption for Figure 1.

T increases, but in some cases the temperature coefficient did not become as small at 100°C as that for linear polystyrene in this solvent. Further increase in T would not appreciably increase the factor $(1 - \Theta/T)$ important in determining the interaction parameter z . As in Part I,⁷ we have ex-

licitly neglected any temperature dependence of the unperturbed radius of gyration $\langle s^2 \rangle_0$, and set $\langle s^2 \rangle_0$ equal to the value of $\langle s^2 \rangle$ at $T = \Theta$ for all T . Similarly, $[\eta]_0$ is set equal to $[\eta]$ at $T = \Theta$ for all T .

Values of Γ_2 , $\langle s^2 \rangle$, and $[\eta]$ for solutions of the branched polymers in toluene are given in Table III. As with linear polystyrene,⁷ we expect these parameters to be independent of temperature since Θ for polystyrene in toluene is far below our range of measurement.

DISCUSSION

Random-Flight Parameters and the Unperturbed Dimension

Values of B_0 listed in Table III were computed with eq. (14) by using the relation given in eq. (16) and the values of b_1 appropriate for the branched structure²²⁻²⁴ to calculate $F'(z)$. The values of B_0 are unexpectedly different from each other, and most are smaller than the value 2.03×10^{-28} cm³-mole²/g² found for linear polystyrene in *cis*-decalin. The experimental values of $\langle s_{br}^2 \rangle_0$ are generally not in accord with estimates calculated with the random-flight model; in only one instance in Table IV are the calculated and experimental values of $\langle s_{br}^2 \rangle_0$ identical within experimental error. Moreover, the values of Θ and B_0 found for this polymer are also equal to values found for linear chains. In all other instances, $B_{0,br}$ is less than $B_{0,l}$, $\langle s_{br}^2 \rangle_0$ is greater than that calculated, and for two polymers the Θ is slightly different from that for linear polymers. It will be noted in Table IV that although Θ is relatively unaffected by branching, B_0 is markedly lower than the value for linear chains for some of the branched chains. Similar behavior has been reported previously for a star-branched polystyrene polymer.³ By contrast, studies³⁸ on some comb-branched poly(methyl methacrylate) gave a 10°C depression of Θ . In another study⁵ of comb-branched polystyrene,⁶ Θ was found to increase monotonically from a value 10°C below Θ_l for linear chains to a value near Θ_l as the molecular weight of the branches increased. In the latter two cases the frequency of branching was much greater than in our work. Values of B_0 were not given for the comb polymers, but the data on the polystyrene suggest that B_0 is decreased by branching.

It appears that the correlation between calculated and measured values of $\langle s_{br}^2 \rangle_0$ and, to some extent, between $B_{0,br}$ and $B_{0,l}$ bears a close relation to the fraction of segments near branch nodes in the molecule. That is, $\langle s^2 \rangle_0$ and B_0 are within experimental error of their "expected" value for the star-branched sample A-48; 2, which has long branches, whereas B_0 is larger than expected for the star-branched polymers A-51 and OW,³ which have relatively short branches. The values of B_0 and $\langle s^2 \rangle_0$ for the polymers appear to approach the expected values as the length of the branches is decreased, with other structural parameters of the chain held (nearly) constant. As we have seen, in terms of the random-flight model, the observed decrease in B_0 can be traced to one, or both, of the parameters n and β_0 of the equivalent random-flight chain. It appears probable that the enhanced segment density of the branched structures relative to their linear

homologs is the source of the observed effect. The responsible structural feature of branched chains may be the concentration of segments in the vicinity of branch nodes that cannot be "diluted" to a value characteristic of linear chains. The data suggest that in the cases examined here at least, this enhanced segment concentration may not appreciably affect the longer-range features of the intersegmental potential $u(\mathbf{r})$ inasmuch as Θ is not affected strongly by the kind of branching studied here (although Θ apparently is affected by branched structures with still greater segment concentrations about branch nodes^{5,38}).

It is of interest at this point to note that β might, in principle, be dependent on details of the chain conformation not usually considered. Thus, $u(\mathbf{r})$ could depend on the instantaneous density of segments in the neighborhood of the segment pair under consideration. This raises the specter of an average β for intramolecular interactions (affecting, say, the radius of gyration) that differs in magnitude from the average β for intermolecular interactions. We note that data on a linear homopolymer in a binary solvent have been interpreted to mean that β for intrachain and interchain interactions differ, presumably owing to preferential solvent absorption.³⁹

The deviation between measured and calculated values of $\langle s_{br}^2 \rangle_0$ might also be understood on the basis of the increased segment density of the branched molecules in the vicinity of the branch node. We do not believe that $\langle s_{br}^2 \rangle_0$ is augmented by short-range interference effects on the potential for rotational isomers of groups in the immediate vicinity of the branch node, but rather that the augmented segment density in a fairly large (say, 30 Å radius) volume about each branch node causes a chain expansion. The Flory temperature, after all, represents the temperature for which a delicate balance between repulsive and attractive interchain interactions has been achieved. There is no *a priori* reason to believe that the chain dimensions must necessarily be independent of chain structure at this temperature (even though this is a consequence for the two parameter random-flight model).

Although the effects on B_0 and on $\langle s_{br}^2 \rangle_0$ appear to be related to details of the segment density, we do not know how to correlate this relation in a general way. In the following, we will assume that a random-flight model still obtains for the branched chain, but that the segment length b_0 is altered by the augmented segment density. We will also assume that β_0 is unaltered by chain expansion in response to an increase in temperature, although there is no reason to believe this must be the case. It might even be more reasonable to suppose that $b_{0,br}$ and $\beta_{0,br}$ should tend toward $b_{0,l}$ and $\beta_{0,l}$, respectively, as the chain expands and relieves some, if not all, of the effects of the augmented segment density.

The Kuhn equivalent chain⁴⁰ is sometimes used to evaluate the individual parameters n , β_0 , and b_0 from the observable parameters $n^2\beta_0$ and nb_0^2 . In this model, the length nb_0 is made to correspond to the actual "stretched-out" molecular length. This condition can be restated as

$$b_{br}b_{0,br} = n_l b_{0,l}$$

for branched and linear chains of the same mass chains. With this constraint, it is easy to show that

$$\frac{b_{0,br}}{b_{0,l}} = \frac{n_l}{n_{br}} = \frac{1}{g} \frac{\langle s_{br}^2 \rangle_0}{\langle s_l^2 \rangle_0}$$

where $\langle s_l^2 \rangle_0$ is the radius of a linear chain with the same molecular weight as the branched chains. Thus, in this interpretation the equivalent branched chain must have fewer, but longer, segments than its linear homolog with the same molecular weight if the last term on the right is experimentally greater than unity. According to this model, the phenomenological parameter $B_0 \propto n^2\beta_0$ must be decreased by branching if $\langle s_{br}^2 \rangle_0$ is increased, and by the factor $(n_l/n_{br})^2$ if β_0 is unaffected by branching. The data in Table IV are in partial agreement with this prediction, suggesting that the hard-core excluded volume β_0 itself may indeed be little affected by branching.

Behavior of A_2 and $\langle s^2 \rangle$

Analysis of the data in *cis*-decalin for $T > \Theta$ is complicated by the uncertainties in the evaluation of $n^2\beta$ and nb_0^2 appropriate at these temperatures. This problem is more severe than the similar one encountered in studies on linear polystyrene, since here there is no comparable way to assess the assumed temperature dependence of β . Data for $A_2M^{1/2}$ versus $M^{1/2}(1 - \Theta/T)$ could be tested for uniqueness for a range of M and T with linear samples without regard to the functional form of the correlation. For branched chains, however, the relation between these two variables depends on chain structure. In the following, two of the methods by which we shall examine the data minimize the importance of the assignments of $n^2\beta$ and nb_0^2 . This analysis is meant to show that branching does indeed augment the chain expansion and depress the second virial coefficient as predicted theoretically for the random-flight chain.

Elimination of z between eqs. (8) and (12) yields a relation that is found to apply farther from theta conditions than does either relation alone for linear chains and which avoids the need to know $n^2\beta$ (but not nb_0^2):

$$\frac{\langle s^2 \rangle}{\langle s^2 \rangle_0} = 1 + \frac{a_1}{4\pi^{3/2}N_a(\langle s_l^2 \rangle_0/M)^{3/2}} A_2M^{1/2} + \dots \quad (26)$$

Here the only parameter in the coefficient of $A_2M^{1/2}$ formally dependent on the branched structure is a_1 . Values of a_1 have been calculated for symmetrical combs (comb polymers with f branches of equal length spaced equidistantly along the backbone) and for star molecules.^{25,26} We assume that the calculation of a_1 can be used with negligible error here. Plots of measured values of $\langle s_{br}^2 \rangle / \langle s_{br}^2 \rangle_0$ versus $A_2M^{1/2}$ are shown in Figure 4. Values of a_1 and b_1 calculated for symmetrical branched structures are given in Table II.

The data lie approximately on straight lines, and show that $\langle s_{br}^2 \rangle / \langle s_{br}^2 \rangle_0$ is larger than the corresponding ratio for linear chains at given $A_2M^{1/2}$, in

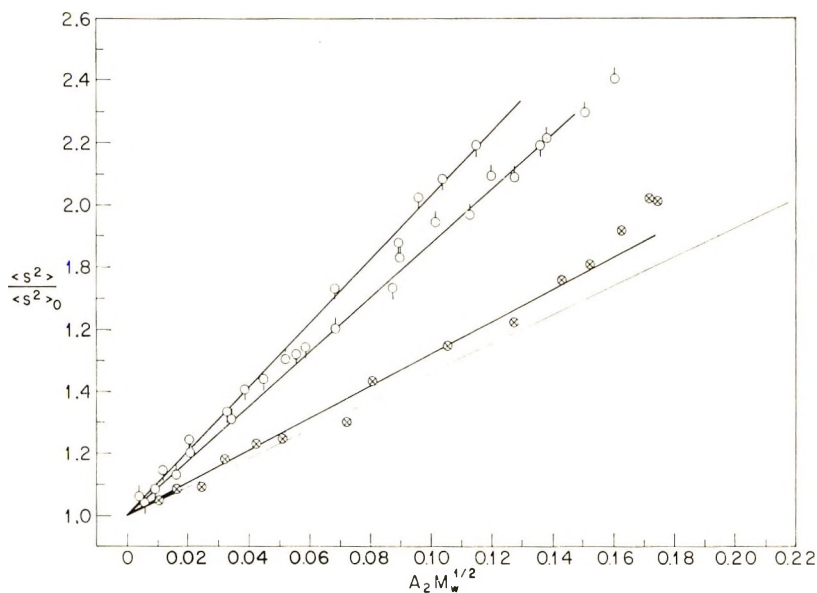


Fig. 4. Expansion factor $\langle s^2 \rangle / \langle s^2 \rangle_0$ vs. $A_2 M_w^{1/2}$ for various branched polystyrenes in *cis*-decalin. Symbols are defined in the caption for Figure 1. The light line is the experimental correlation found for linear polystyrene in *cis*-decalin.⁷

accord with theory. Quantitative agreement of the data with the linear relation between $\langle s^2 \rangle / \langle s^2 \rangle_0$ and $A_2 M_w^{1/2}$ using theoretical values of a_1 is not quite achieved, however, in contrast with the behavior of linear polystyrene⁷ (cf. Table V). For example, estimates of $(\langle s^2 \rangle / \langle s^2 \rangle_0) - 1$ from $A_2 M_w^{1/2}$ by use of eq. (26) are respectively ca. 15% and 5% less than experimental determinations for samples A-53; 2, and A-68; 4, whereas the calculated and experimental values for sample A-48; 2 are in reasonable agreement. It is not clear whether these deviations are caused by the neglect of higher-order terms in eq. (26) or by other effects related to the deviation of $\langle s_{br}^2 \rangle_0 / g$ and $B_{0,br}$ from their anticipated values. We remark that the closest agreement between observed and calculated values of the slope in Figure 4 is achieved if $\langle s_l^2 \rangle_0 / M$ is taken as the value found in Part I for linear chains, rather than as $\langle s_{br}^2 \rangle_0 / gM$. This suggests that the unexpected chain expansion encountered at the Flory temperature may be compensated as the temperature is increased; but it is not altogether consistent to use $\langle s_l^2 \rangle_0 / M$ in computing the slope on the right-hand side of eq. (26) and $\langle s_{br}^2 \rangle_0$ on the left-hand side in computing $\langle s^2 \rangle / \langle s^2 \rangle_0$.

The data on A_2 and $\langle s^2 \rangle$ as functions of temperature for temperatures above the Flory temperature can be used to estimate $B_0 (\langle s^2 \rangle_0 / M)^{-3/2}$ if (1) a temperature dependence for B is assumed, and (2) relations between $\langle s^2 \rangle / \langle s^2 \rangle_0$ and z and between A_2 and z are used. In the following analysis, we will assume that the simple relation $B = B_0(1 - \Theta/T)$ can be used for our analysis, and that eqs. (11) and (15) can be used to correlate $\langle s^2 \rangle$

TABLE V
Comparison of Observed and Calculated Constants in Equation (26)

Polymer	Structure	$a_1/[4\pi^{3/2}N_a(\langle s_l^2 \rangle_0/M)^{3/2}]$		
		Obs.	Calcd ^a	Calcd ^b
A-48; 2	Star	5.16	4.76	4.26
A-53; 2	Star	6.90	7.65	5.00
A-68; 4	Star	10.25	9.64	4.98
	Linear	4.45	4.54	—

^a Calculated with $\langle s_l^2 \rangle_0/M$ from Part I.

^b Calculated from $\langle s_{br}^2 \rangle_0$ with $\langle s_l^2 \rangle_0/M = \langle s_{br}^2 \rangle_0/gM$.

and A_2 with z . Clearly, such an analysis is not definitive, since we have no certain procedure to assess either assumption. Our purpose will be satisfied if the analysis confirms the peculiar behavior of B_0 found by analysis of the temperature dependence of A_2 near Θ .

In the analysis of $\langle s^2 \rangle / \langle s^2 \rangle_0$, one need only determine the proportionality constant between z and $M^{1/2}(1 - \Theta/T)$ to achieve a "best" fit of eq. (11) with the data. The values of a_1 given in Table II were used in this correlation. This is a trial-and-error procedure, but the result converges rapidly. The proportionality constant so determined is the interaction parameter $B_0(\langle s_l^2 \rangle_0/M)^{-3/2}$ sought. The curves in Figure 5 were computed in this way with the interaction parameters listed in column 3 of Table VI.

TABLE VI
Comparison of Thermodynamic Interaction Parameters
Determined by Different Methods

Polymer	Structure	$10^3 z$		$B_{0,br}(\langle s_l^2 \rangle_0/M)^{-3/2} \times 10^3$ ^a	$B_{0,br}(\langle s_{br}^2 \rangle_0/gM)^{-3/2} \times 10^3$ ^a
		From eq. (11)	From eq. (27)		
A-48; 2	Star	10.3	9.5	9.8	8.6
A-51	Star	—	8.8	8.8	—
A-53; 2	Comb	12.2	5.5	5.7	3.7
A-68; 4	Comb	5.8	3.0	4.6	1.8

^a $B_{0,br}$ from Table III.

Similarly, a trial-and-error numerical analysis with eqs. (15) together with the experimental values of α can be used to analyze the data on A_2 to determine the interaction parameter. [Equation (11) was used to calculate values of α for sample A-51, since none could be determined directly by light scattering.] Thus, recasting in a form more suitable for analysis, eq. (15) is

$$A_2 M^{1/2} = 4\pi^{3/2} N_a (\langle s_l^2 \rangle_0 / M)^{3/2} \alpha_2^3 \frac{1 - \exp\{-2b_1 z / \alpha_2^3\}}{2b_1} \quad (27a)$$

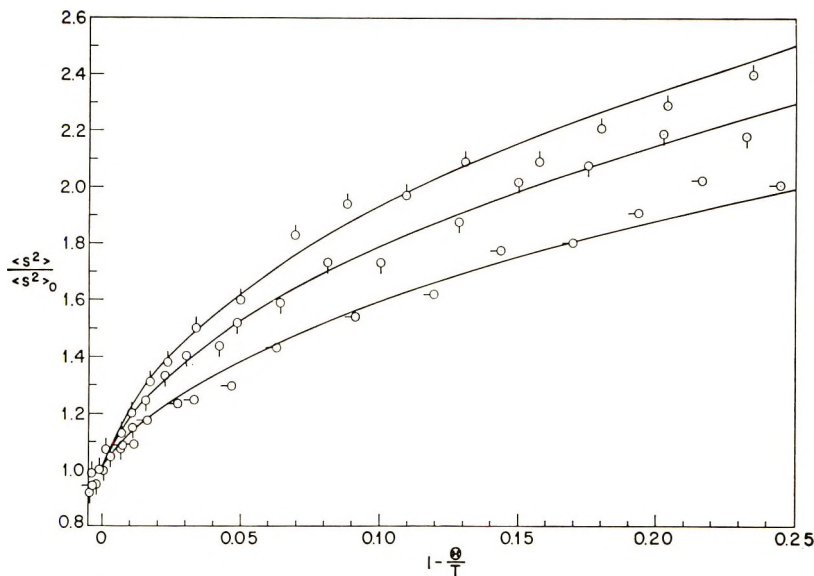


Fig. 5. Expansion factor $\langle s^2 \rangle / \langle s^2 \rangle_0$ versus $1 - \Theta/T$ for various branched polystyrenes in *cis*-decalin. The curves were calculated with eq. (11) and the proportionality factors between z and $M^{1/2}(1 - \Theta/T)$ listed in Table VI.

where α_2 is determined from the experimental values of α according to the relation

$$\alpha_2^5 - \alpha_2^3 = (k_1/a_1)(\alpha^3 - \alpha^3) \quad (27b)$$

Values of b_1 and a_1 given in Table II were used in the analysis, together with $\langle s_l^2 \rangle_0/M = 7.6 \times 10^{-16}$ given in Part I. Here, k_1/a_1 is treated as an adjustable parameter. Its value can be estimated from the data in the good solvent toluene, since at large z the relation for A_2 reduces to

$$\lim_{z \rightarrow \infty} A_2 M^{1/2} = 4\pi^{3/2} N_a (\langle s_l^2 \rangle_0 / M)^{3/2} \alpha^3 (k_1/a_1)^{3/5} / 2b_1 \quad (28)$$

and so allows an estimate of k_1/a_1 . The value $k = 3.10$ was found for linear polystyrene in Part I. The curves in Figure 6 were computed with the interaction parameters listed in Table VI (column 4), together with the values of k_1/a_1 listed in Table VII.

TABLE VII
Molecular Parameters Used in the Analysis of A_2 with Equation (27)

Polymer	Structure	b_1	k_1	k_1/a_1	g	$\Psi \times 10^{-24}$
A-48; 2	Star	3.86	3.98	2.92	0.625	7.5
A-51	Star	5.39	7.25	5.00	0.444	10.7
A-53; 2	Comb	5.19	7.32	3.40	0.561	6.4
A-68; 4	Comb	7.22	13.45	5.00	0.395	9.8
	Linear	2.865	3.10	2.43	1	4.0

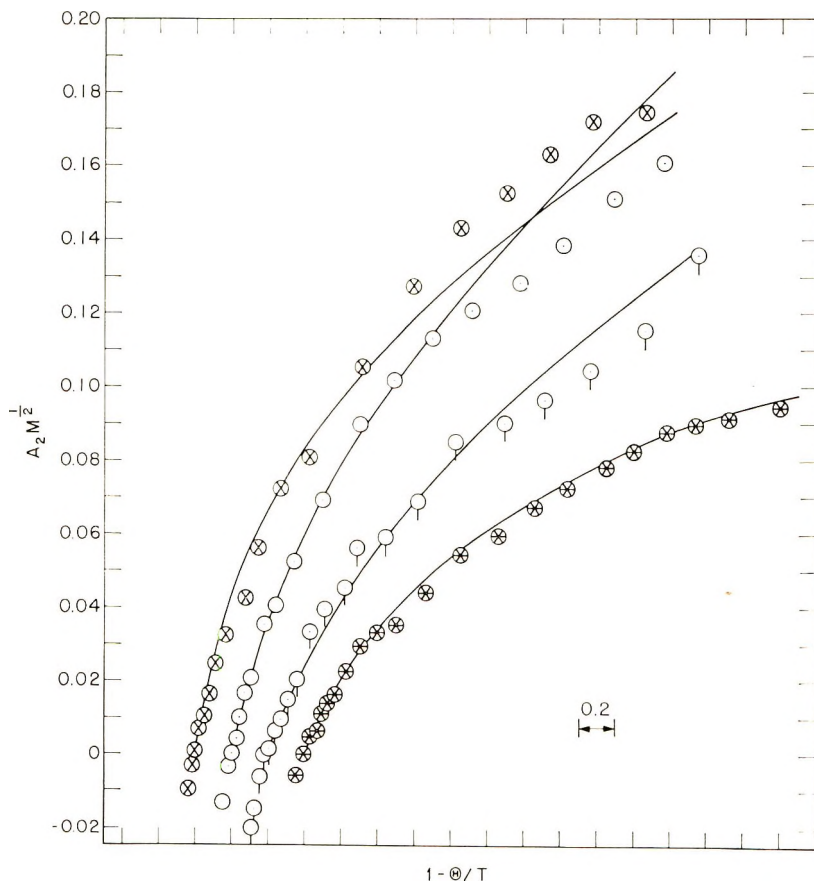


Fig. 6. Plots of the function $A_2M^{1/2}$ vs. $(1 - \Theta/T)$ for various branched polystyrenes in *cis*-decalin. The curves were calculated with eq. (27) using the proportionality factors between z and $M^{1/2}(1 - \Theta/T)$ and the parameters k_1 listed in Tables VI (column 4) and VII, respectively.

The data on the interaction parameter deduced from eqs. (11) and (27) given in column 3 and 4 of Table VI are in qualitative agreement with the results obtained from the analysis of the temperature dependence of A_2 near the Flory temperature given in columns 5 and 6 of Table VI. For example, all three methods show that the interaction parameter for sample A-68; 4 is considerably less than the value for linear polystyrene. The overall results suggest that the interaction parameter of the branched polymers may tend to the value observed for linear chains as the temperature increases. Thus, the values deduced from eq. (11) tend to be the largest values determined, and the use of eq. (11) tends to emphasize the values of $\langle s^2 \rangle / \langle s^2 \rangle_0$ at temperatures above Θ .

Values of k_1 , k_1/a_1 , and Ψ [see eq. (16)] deduced by the analysis of the data on A_2 are gathered in Table VII. It is seen that both k_1 and the ratio k_1/a_1 depend on chain structure according to our analysis. That is, the

expansion of the molecular dimensions of chains in a bimolecular cluster is enhanced more by branching than is the expansion due only to intramolecular interaction. Like a_1 , k_1 is not a unique function of g , although the ratio k_1/a_1 might nearly be so. The data in Table VII can be correlated by $k_1/a_1 = 2.43 g^{-0.70}$ to give k_1 to within $\pm 10\%$. The deviation of Ψ from its value 4.0×10^{24} for linear polymers is, in part, a consequence of the deviation of k_1/a_1 from 2.43.

It is of interest to examine the use of eqs. (11) and (15) with data in very good solvents, such as toluene. Values of α can be calculated from eq. (26) by using measured values of A_2 , and from eq. (11) by using the proportionality constant $z/M^{1/2} = 5.3 \times 10^{-3}$ found for linear polystyrene. Values of α so determined agree with experimental values within 3% for samples A-48; 2 and A-53; 2, and within 7% for sample A-68; 4. It may be that the proportionality constant 5.3×10^{-3} is too large in the latter case. For large z , the function $h(z/\alpha^3)$ attains its limiting value 0.508 for both branched and linear chains, so, according to eq. (11), α should be given by

$$\lim_{\alpha \rightarrow \infty} (\alpha_{br}/\alpha_l) \approx \left\{ \frac{a_{1,br}}{a_{1,l}} \right\}^{1/5} \quad (29)$$

Experimental values of α_{br}/α_l in toluene agree reasonably with those calculated with eq. (29), with the largest deviation (10%) again found for sample A-68; 4. Similarly, use of eq. (28) in the limit of large z yields

$$\lim_{z \rightarrow \infty} (A_{2,br}/A_{2,l}) = 1.17 a_1^{3/5}/b_1 g^{0.42}.$$

Even this approximate relation will not have general utility, since $a_1^{3/5}/b_1$ is not a unique function of g and is only known for a limited class of branched structures.

Intrinsic Viscosity

The data in Table IV show that the exponent m in eq. (25) is not invariant with the branched-chain structure. This result does not disagree with calculations of $[\eta]_0$ based on the random-flight chain model since the existing calculations all pertain to one class of structure. The data seem to be in accord with the suggestion made above that m should tend toward $1/2$ for star-branched structures, and toward $3/2$ for comb-branched structures with very short branches. Further, it seems that an appropriate m might well be nearer unity than $1/2$ for randomly branched polymers such as those prepared by high conversion of free radically polymerized polymers.

The data in *cis*-decalin with $T > \Theta$ are plotted in Figure 7 according to Eq. (22). Reasonably linear plots are obtained, giving values of $2p(h)/a_1$ listed in Table VIII, which are all less than the value 1.0 found for linear polystyrene and 0.81 predicted by first-order perturbation calculations for the random-flight model. Values of $p(h)$ calculated with a_1 given in Table II are also listed in Table VIII. According to these estimates, chain branching never increases $p(h)$ as much as it does a_1 , and can actually cause

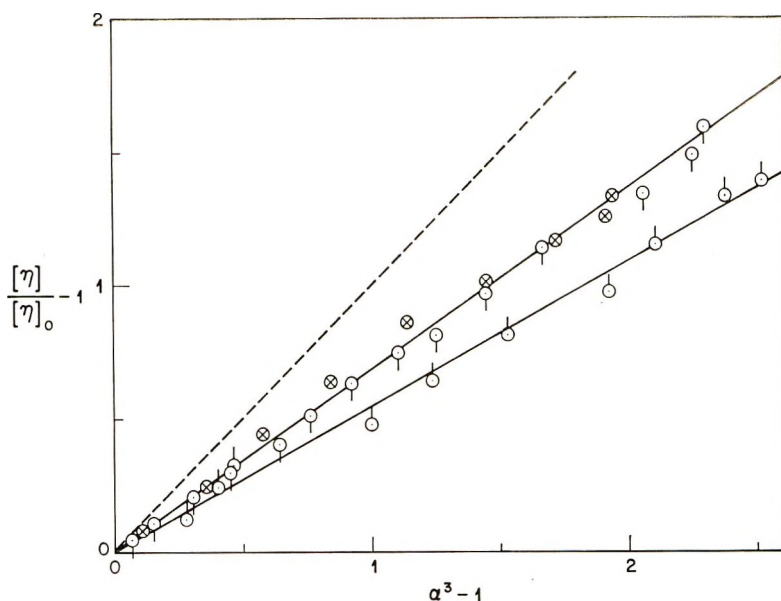


Fig. 7. Plots of the function $([\eta]/[\eta]_0) - 1$ vs. $(\langle s^2 \rangle / \langle s^2 \rangle_0)^{1/2} - 1$ for various branched polystyrenes in *cis*-decalin. Symbols are defined in the caption for Figure 1.

a decrease in $p(h)$. In other words, insofar as the excluded volume is concerned, the hydrodynamic radius is not augmented as much by branching as is the radius of gyration.

Values of $[\eta]/[\eta]_0$ in toluene can be computed with eq. (22), the experimental values of α , and the values of $p(h)/a_1$ deduced from the data in *cis*-decalin. These results are compared with the measured values of $[\eta]/[\eta]_0$ in Table VIII. The reason for the large (25%) discrepancy between measured and calculated values of $[\eta]/[\eta]_0$ for sample A-53; 2 is unknown.

A correlation of $[\eta]$ with $A_2 M^{1/2}$ has been suggested as an element in a method of estimating chain branching.³⁰ This correlation is obtained by

TABLE VIII
Viscometric Parameters of Branched Polystyrene

Polymer	Structure	$\frac{2p(h)^a}{3a_1}$	$p(h)^b$	$([\eta]/[\eta]_0)$	
				Calcd with eq. (22) ^c	Measured ^c
A-48; 2	Star	0.69	1.39	2.84	3.04
A-53; 2	Comb	0.55	1.78	2.98	3.72
A-68; 4	Comb	0.66	2.67	3.77	3.79

^a From Figure 8 and Eq. (22).

^b $2p(h)/3a_1$ was found to be 1.0 for high molecular weight linear polystyrene in decalin, so that $p(h) = 1.91$, cf. Part II.

^c $[\eta]$ in toluene.

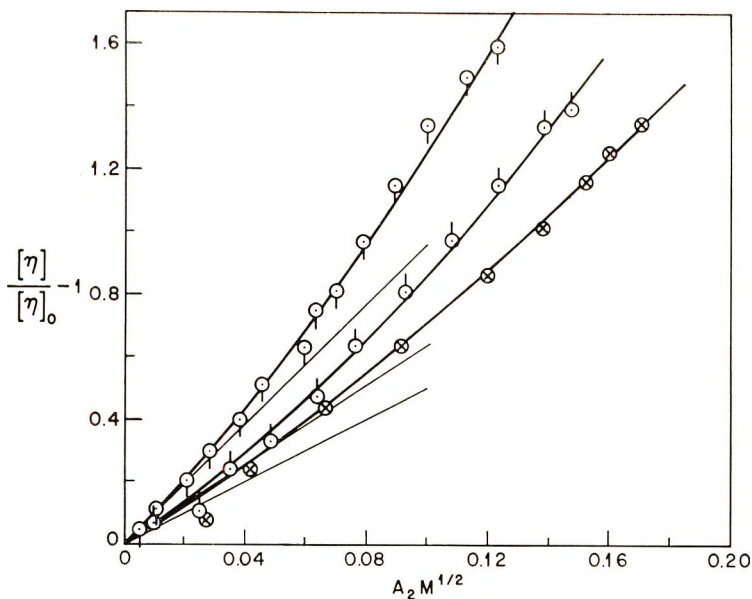


Fig. 8. Plots of the function $([\eta]/[\eta]_0) - 1$ vs. $A_2M^{1/2}$ for various branched polystyrenes in *cis*-decalin. Symbols are defined in the caption for Figure 1.

the elimination of z between series expansions of $[\eta]/[\eta]_0$ and $A_2M^2\langle s^2 \rangle_0^{-3/2}$ to give

$$[\eta]/[\eta]_0 - 1 = \{p(h)/[4\pi^{3/2}N_a(\langle s_l^2 \rangle_0/M)^{-3/2}]\} A_2M^{1/2} \quad (31)$$

where higher order terms in $A_2M^{1/2}$ are suppressed. Figure 8 shows that such a plot is not linear, rendering it unsatisfactory for purposes of extrapolation. The light lines give the initial tangents calculated with the values of $p(h)$ listed in Table VIII and $\langle s_l^2 \rangle_0/M = 7.6 \times 10^{-18.7}$.

Curiously, $([\eta]/[\eta]_0) - 1$ does seem to be linear in $A_2M^{1/2}$ for values of $A_2M^{1/2}$ greater than ca. 0.1. However, extrapolation of these data to $A_2M^{1/2} = 0$ would yield low values of $[\eta]_0$.

Another type of correlation is of interest for the data in toluene. We assume that in this (nearly) athermal solvent, α varies only slowly with z , so that any deviation between α for branched and linear chains can be neglected, to allow a direct comparison to be made of $[\eta_{br}]$ and $\langle s_{br}^2 \rangle$ with the respective parameters for linear chains. If we represent this correlation as

$$[\eta_{br}]/[\eta_l] = (\langle s_{br}^2 \rangle / \langle s_l^2 \rangle)^\nu \quad (32)$$

ν should be greater than m , inasmuch as $\langle s^2 \rangle / \langle s^2 \rangle_0$ is augmented more by branching than is $[\eta]/[\eta]_0$. Further, ν should be greater for those branch structures that give larger α_1 . In effect, ν combines diverse, and perhaps, opposing, effects in to one parameter. Values of ν are of the order 1.1–1.4

for the polymers investigated here, compared to values of m between 0.6 and 1.1 (cf. Table IV). Examples of studies on model branched structures, for which both $[\eta_{br}]/[\eta_l]$ and $\langle s_{br}^2 \rangle / \langle s_l^2 \rangle$ are determined in good solvents, are sparse. Data on some comb-branched poly(vinyl acetate) polymers are displayed in Figure 9, together with the data obtained in this study and curves calculated with $\nu = 1/2, 1,$ and $3/2$. Lack of correlation with any

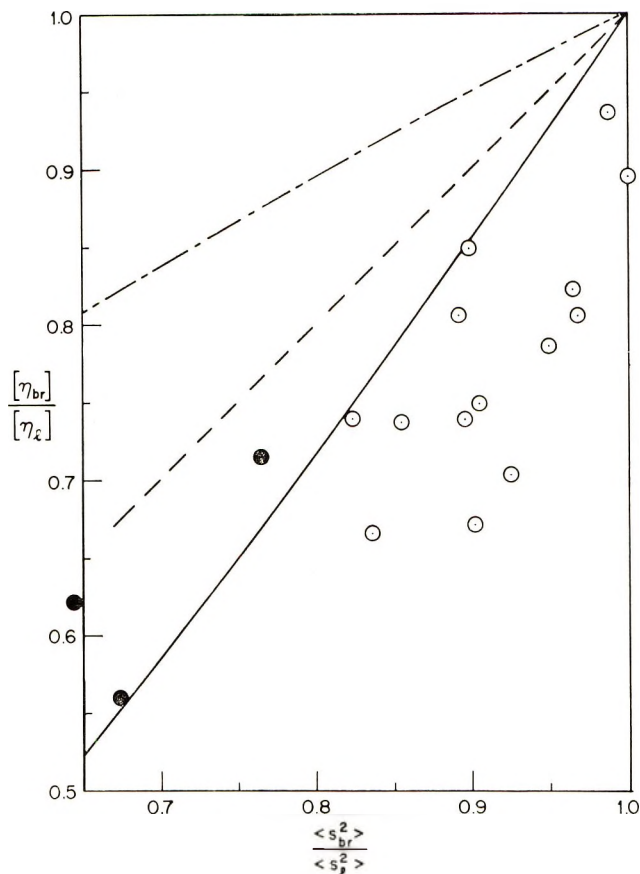


Fig. 9. $[\eta_{br}]/[\eta_l]$ as a function of $\langle s_{br}^2 \rangle / \langle s_l^2 \rangle$ for various branched polymers: (●) polystyrenes in toluene examined in this study; (○) various comb-branched poly(vinyl acetates) in a good solvent; (---) ν [eq. (32)] = $1/2$; (- -) $\nu = 1$; (—) $\nu = 3/2$.

single value of ν is evident, and it is also evident that $\nu = 1/2$ would provide a very poor fit to the data. By contrast, correlation of $[\eta_{br}]/[\eta_l]$ with g^μ is best made with $\mu = 0.67$ for the data on poly(vinyl acetate) (data on $\langle s_{br}^2 \rangle_0 / \langle s_l^2 \rangle_0$ are not available for this system). These results perhaps illustrate the futility of attempts to correlate $[\eta_{br}]/[\eta_l]$ with $\langle s_{br}^2 \rangle / \langle s_l^2 \rangle$ alone. Apparently considerably more information on the detailed chain structure is required than is afforded by the radius of gyration.

Exclusion Chromatography

Plots of $\log [\eta]M$ versus V_{peak} and $\log \langle s^2 \rangle_{LS}$ versus V_{peak} for branched and linear polystyrenes are given in Figure 10. It is clear that no choice can be made between $M[\eta]$ and $\langle s^2 \rangle$ as correlating parameters with V_{peak} based on these data. This implies that $M[\eta]$ is a function of $\langle s^2 \rangle$ for these data, which is verified in Figure 11. Data on $M[\eta]$ versus $\langle s^2 \rangle$ on linear and comb-branched poly(vinyl acetates) are also shown in Figure 11. Since $\log M[\eta]$ is linear in $\log \langle s^2 \rangle$ for both the polystyrene and the poly(vinyl

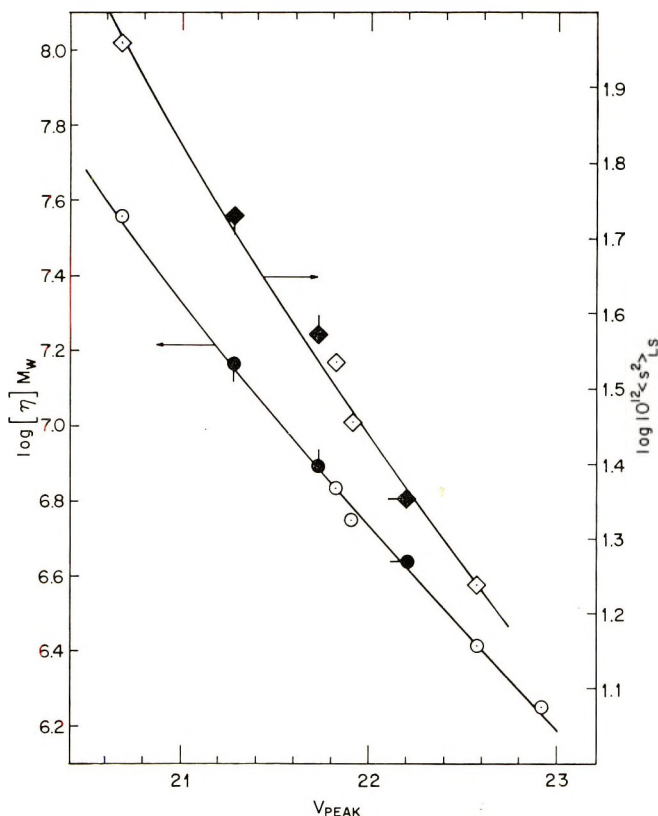


Fig. 10. Plots of $\log M[\eta]$ and $\log \langle s^2 \rangle_{LS}$ vs. the peak elution volume V_{peak} for linear and branched polystyrenes in decalin.

acetate) samples, it is tempting to assume that such a relation might be generally valid in good solvents. (Such a correlation does not obtain at the Flory temperature.) However, data of Chiang⁵ on branched polystyrene do not exhibit this behavior: these polymers generally contain many more branches per molecule than is characteristic of the samples used in Figure 11. In addition, for these highly branched polymers, $\log M[\eta]$ could be correlated with V_{peak} by the relation used for linear polystyrene.⁴²

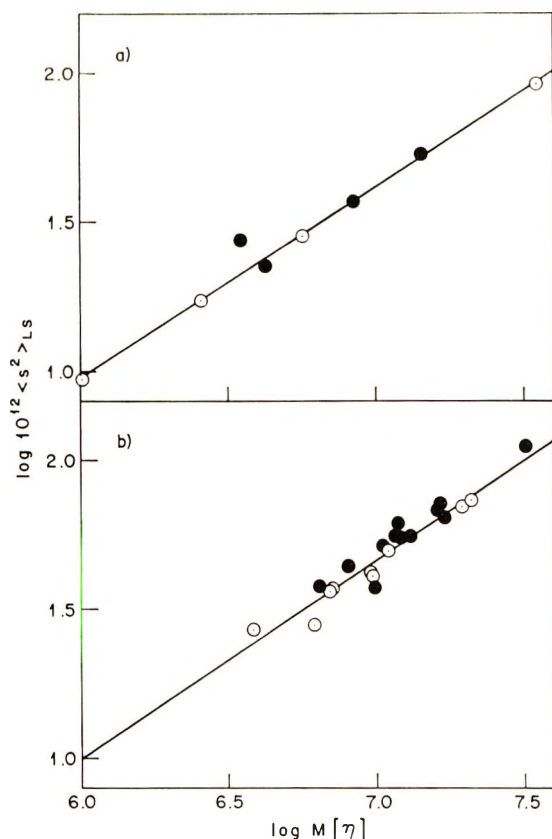


Fig. 11. Plots of $\log M[\eta]$ vs. $\log \langle s^2 \rangle$ for linear and branched polymers: (a) polystyrene; (b) poly(vinyl acetate) from reference 1.

CONCLUSIONS

This investigation on a relatively few branched polymers has not led to definitive, general correlations. It has been shown that the parameters B_0 and nb_0^2 are not necessarily independent of chain branching for a homologous series, but may depend in some unspecified way on the segment density of the coil. The theoretical prediction that excluded volume effects cause greater expansion of branched chains than of linear chains at equivalent thermodynamic conditions, appears to be qualitatively, and nearly quantitatively, corroborated. Similarly, the predicted decrease in A_2 caused by branching is in reasonable accord with experiment. It appears that in both of these correlations the effect depends on more details of the chain structure than are held in the single parameter g .

Similarly, the reduction of $[\eta]_0$ caused by chain branching does not correlate simply with g , contrary to many attempts to find such a correlation. Moreover, it appears that effects of chain expansion do not affect $[\eta_{br}]/[\eta_{br}]_0$ as much as they affect $\langle s_{br}^2 \rangle / \langle s_{br}^2 \rangle_0$. A correlation between these parameters is discussed. In toluene solution $M[\eta]$ is a single-valued func-

tion of $\langle s^2 \rangle$ for the samples studied, so that no discrimination can be made $M[\eta]$ or $\langle s^2 \rangle$ as controlling parameters in exclusion chromatography.

This study was supported in part by the Air Force Materials Laboratory, Research and Technology Division, Wright-Patterson Air Force Base, under Contract No. AF 33(615)-3884.

References

1. G. C. Berry, L. M. Hobbs, and V. C. Long, *Polymer*, **5**, 31 (1964).
2. G. C. Berry and T. G. Fox, *J. Amer. Chem. Soc.*, **86**, 3540 (1964).
3. T. A. Orofino and F. Wenger, *J. Phys. Chem.*, **67**, 566 (1963).
4. G. V. Schulz, *Z. Physik. Chem.*, **B43**, 25 (1939).
5. R. Chiang, *J. Polym. Sci.*, **36**, 91 (1959).
6. G. C. Berry, paper presented at IUPAC International Symposium on Macromolecular Chemistry, Tokyo-Kyoto, 1966, Preprint XI-144.
7. G. C. Berry, *J. Chem. Phys.*, **44**, 4550 (1966); *ibid.*, **46**, 1338 (1967).
8. B. H. Zimm and W. H. Stockmayer, *J. Chem. Phys.*, **17**, 1302 (1949).
9. W. H. Stockmayer and M. Fixman, *Ann. N. Y. Acad. Sci.*, **57**, 334 (1953).
10. M. Wales, P. A. Marshall, and S.-G. Weissberg, *J. Polym. Sci.*, **10**, 229 (1953).
11. J. S. Ham, *J. Chem. Phys.*, **26**, 625 (1957).
12. T. A. Orofino, *Polymer*, **2**, 295, 305 (1961).
13. M. Kurata and M. Fukatsu, *J. Chem. Phys.*, **41**, 2934 (1964).
14. G. R. Dobson and M. Gordon, *J. Chem. Phys.*, **41**, 2389 (1964).
15. E. F. Casassa and G. C. Berry, *J. Polym. Sci. A-2*, **4**, 881 (1966).
16. B. H. Zimm and R. W. Kilb, *J. Polym. Sci.*, **37**, 19 (1959).
17. G. C. Berry, *J. Polym. Sci. A-2*, **6**, 1551 (1968).
18. H. Benoit, *J. Polym. Sci.*, **11**, 507 (1953).
19. Yu. Ya. Kolbovskii, *Vysokomol. Soedin.*, **2**, 1375 (1960).
20. B. H. Zimm, *J. Phys. Chem.*, **14**, 164 (1946).
21. M. Fixman, *J. Chem. Phys.*, **23**, 1656 (1955).
22. E. F. Casassa, *J. Chem. Phys.*, **37**, 2176 (1962).
23. E. F. Casassa, *J. Chem. Phys.*, **41**, 3213 (1964).
24. E. F. Casassa and Y. Tagami, *J. Polym. Sci. A-2*, **6**, 63 (1968).
25. G. C. Berry and T. A. Orofino, *J. Chem. Phys.*, **40**, 1614 (1964).
26. G. Tanaka and H. Yamakawa, *J. Chem. Phys.*, **46**, 3689 (1967).
27. W. H. Stockmayer, *Makromol. Chem.*, **35**, 54 (1960).
28. B. E. Eichinger, *J. Chem. Phys.*, **53**, 561 (1970).
29. O. B. Ptitsyn and Y. E. Eizner, *Zh. Fiz. Khim.*, **32**, 2464 (1950).
30. W. R. Krigbaum and Q. A. Trementozzi, *J. Polym. Sci.*, **28**, 295 (1958).
31. G. C. Berry and E. F. Casassa, *J. Polym. Sci., Part D*, **4**, 1 (1970).
32. P. J. Flory and S. Fisk, *J. Chem. Phys.*, **44**, 2243 (1966).
33. C. D. Thurmond and B. H. Zimm, *J. Polym. Sci.*, **22**, 495 (1956).
34. M. Kurata and H. Yamakawa, *J. Chem. Phys.*, **29**, 311 (1958).
35. Z. Grubisic, P. Rempp, and H. Benoit, *J. Polym. Sci. B*, **5**, 753 (1967).
36. E. F. Casassa and Y. Tagami, *Macromolecules*, **2**, 14 (1969).
37. T. Altares, Jr., D. P. Wyman, V. R. Allen, and K. Meyersen, *J. Polym. Sci. A-2*, **3**, 4131 (1965).
38. M. Wales and H. Coll, *Ann. N. Y. Acad. Sci.*, **164**, 102 (1969).
39. A. Dondos and H. Benoit, *Europ. Polym. J.*, **4**, 561 (1968).
40. W. Kuhn, *Kolloid-Z.*, **68**, 2 (1934).
41. P. J. Flory, *Principles of Polymer Chemistry*, Cornell Univ. Press, Ithaca, N. Y. 1953.
42. D. D. Freyss, Ph.D. Thesis, University of Strasbourg, France, 1968.

Received September 16, 1970

Revised October 14, 1970

Laser-Raman Spectra of Vinyl Chloride-Vinylidene Chloride Copolymers

M. MEEKS, *Dow Chemical Company, Midland, Michigan 48640*
and J. L. KOENIG, *Division of Macromolecular Science,*
Case Western Reserve University, Cleveland, Ohio 44106

Synopsis

Several copolymers as well as homopolymers of vinylidene chloride and vinyl chloride have been examined by Raman spectroscopy. Probabilities of concentrations of monomer sequences have been calculated from known reactivity ratios. Surface scattering intensities at some frequencies were found to be linearly proportional to specific microstructure concentrations. Normalization of scattering intensities was accomplished using the intensity of the CH_2 asymmetric stretching mode at 2926 cm^{-1} , which is common to all samples examined. Good correlation was found for the concentrations of comonomer sequences {B}, {BB}, {BBB}, {AA} and {AAAA} in which A denotes vinylidene chloride and B vinyl chloride.

Introduction

Laser-excited Raman spectrometers have recently been used in the study of problems in the vibrational spectroscopy of a number of polymers. Of the chlorine containing polymers, both poly(vinyl chloride) (PVC) and poly(vinylidene chloride) (PVDC) studies have been reported. Koenig and Druessedow¹ have obtained Raman spectra and have observed polarized lines in PVC consistent with its extended syndiotactic conformation. Raman scattering of PVDC has been studied by Hendra and Mackenzie² and they have confirmed the structure of this polymer as proposed by Miyazawa and Ideguchi.³ The infrared spectra of several of these copolymers have been published by Narita et al.,⁴ who found good correlation between the absorbance at 1206 cm^{-1} and the vinyl chloride content of the copolymers below 25%. The CH deformation mode of the vinyl chloride in the infrared has been found by Enomoto⁵ to appear at various frequencies depending upon the combination of monomer units on either side of the vinyl chloride unit.

Raman scattering patterns of these copolymers have not hitherto been obtained nor has a study of the relation between concentrations of monomer sequences and scattering intensities been undertaken. It is the purpose of this paper to present laser-Raman scattering spectra of PVC, PVDC, and several copolymers of the monomer pair and show the existence of linear relations between concentrations of monomer sequences in these copolymers and scattering intensities at certain frequencies.

Experimental

The Raman patterns were excited with the 4880 Å line of an argon ion laser by using a filter of bandwidth 30 Å. Frequency scanning was done by a Spex 1400 double monochromator. A pulse counting system with thermoelectrically cooled photomultiplier tube served as a detection system. Intensities of scattering were recorded on a strip-chart recorder. The peak heights at particular frequencies were measured under the following conditions: source, 0.168 ($\pm 10\%$) W; scan speed, 45 cm⁻¹/min; slit, 0.110 μ (mechanical), 5.4 cm⁻¹ (spectral, 5145 Å); time constant, 4 sec.

Amplifier gain was set as a compromise between excess noise level and peak height acceptable for accurate measurement. These settings, while not the same for each sample examined, were the same for pairs of peaks whose intensity ratios were used in the correlation. The scattering ratios were found to be independent of amplifier gain for the above conditions. The greatest difficulty in making accurate peak height measurements was the instability of the laser beam intensity. The scatter of data points obtained in the following correlations is believed due primarily to this factor.

Both homopolymers and all copolymers used in this study were prepared by free-radical initiation with isopropyl peroxydicarbonate and monomers suspended in water at 52°C in a small batch reactor. The resulting powder was screened through a 100-mesh sieve and pressed into an opaque disk at 40,000 psi at room temperature. Front-surface scattering patterns were obtained with a defocused laser beam. Since fluorescence was not a problem in these measurements, no other sample preparation or treatment was necessary. Any fluorescence which did occur could be eliminated by exposure for a short period of time to the laser beam. No heat stabilizers were used to prevent thermal degradation.

Calculation of Copolymer Microstructures

A theory for the prediction of comonomer sequence distributions from copolymerization kinetics has been developed by Ito and Yamashita.⁶ This method was used by Yamashita et al.⁷ to calculate probabilities of occurrence (concentration) of various dyad and tetrad sequences in copolymers of vinylidene chloride and vinyl chloride. They found good correlation between the calculated values of dyad and tetrad sequences and values obtained by NMR. These investigators found no evidence for a copolymerization mechanism involving the penultimate group in the chain end. For the terminal model, they have calculated, using the NMR data, reactivity ratios of 4.5 ± 0.5 for vinylidene chloride and 0.16 ± 0.03 for vinyl chloride. These ratios are in excellent agreement with reactivity ratios obtained⁸ by an independent method. Therefore, the values 4.0 for vinylidene chloride and 0.20 for vinyl chloride will be used in our calculations.

In another paper, Yamashita et al.⁹ also report good agreement between calculated and NMR results on dyads and tetrads in vinylidene chloride-vinyl acetate polymers. Their method will therefore be considered suffi-

ciently accurate for our calculations and will be used in the following discussions. While these authors report no calculations for triads, because NMR is not sensitive to these sequences for these polymers, the concentration of triads will be calculated here and a relation shown with Raman scattering intensities.

The method of Meyer and Lowry¹⁰ gives the relation between mole fraction of total monomers converted to polymer at a given time to the instantaneous mole-fraction composition, f_A (vinylidene chloride) and f_B (vinyl chloride) of unreacted monomer. A plot of this relation for f_B is shown in Figure 1. The value of X defined by

$$X = f_A/f_B \quad (1)$$

can be readily obtained at any degree of conversion. The probability of occurrence of the sequence BA is

$$P_2\{BA\} = P\{B\}P\{A/B\}$$

where $P\{A/B\}$ denotes the probability that an A follows a B and $P\{B\}$ is the instantaneous vinyl chloride content of the copolymer being formed for the terminal model. The conditional probabilities are given by

$$P\{A/B\} = 1 - P\{A/A\} = 1/(1 + r_A X) \quad (2)$$

$$P\{B/A\} = 1 - P\{B/B\} = 1/[1 + (r_B/X)] \quad (3)$$

where monomer unit r_A and r_B are the reactivity coefficients for chain ending in A and B respectively. The instantaneous copolymer composition is easily determined by use of the familiar copolymerization equation from the known monomer composition. However the terminal model requires that $P\{A/xB\}$, $P\{A/xA\}$, $P\{B/xA\}$, $P\{B/xB\}$ all be independent of

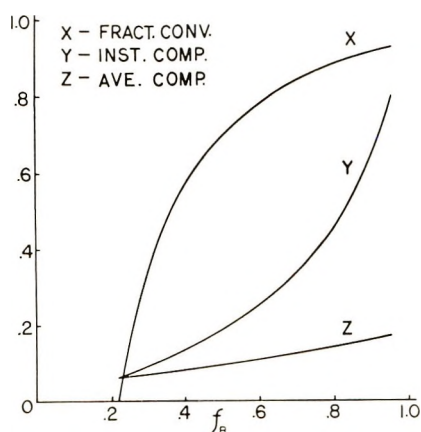


Fig. 1. Calculated mole fraction converted, instantaneous copolymer composition and average copolymer composition as a function of mole fraction of vinyl chloride in unreacted monomer. Initial monomer feed composition, 22% vinyl chloride.

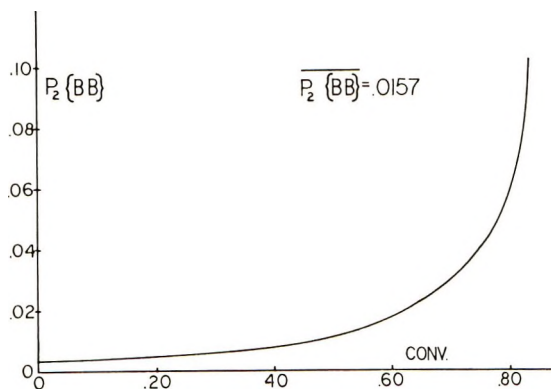


Fig. 2. Instantaneous dyad concentration as a function of mole fraction converted ($f_B^0 = 0.22$).

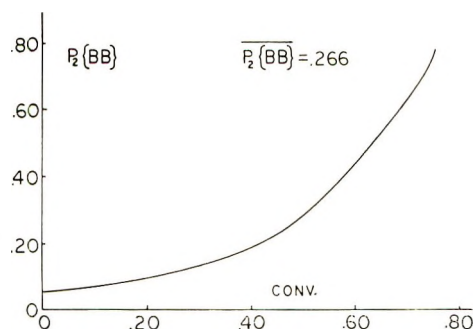


Fig. 3. Instantaneous dyad concentration as a function of mole fraction converted ($f_B^0 = 0.61$).

whether x represents A or B. Thus in the case of triads the probability of the triad AAA becomes

$$P_3\{AAA\} = P\{A\}P\{A/A\}^2$$

In a similar manner, the instantaneous probability or concentration of any sequence can be calculated. A plot of the instantaneous concentration of

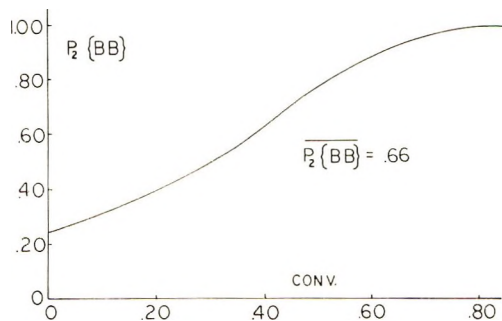


Fig. 4. Instantaneous dyad concentration as a function of mole fraction converted ($f_B^0 = 0.825$).

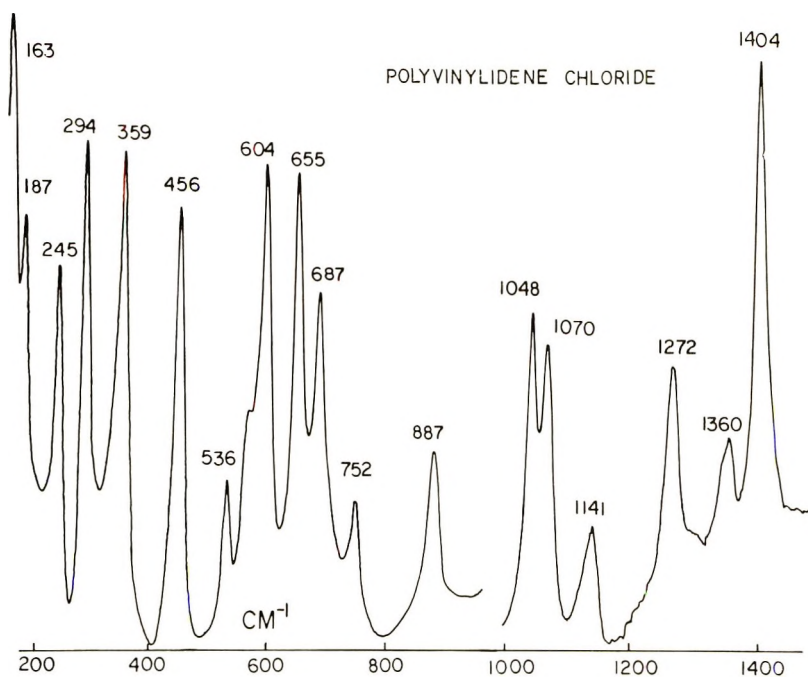


Fig. 5. Raman spectrum of poly(vinylidene chloride).

the sequence versus mole fraction conversion, when integrated over the entire course of reaction and divided by the total mole fraction of monomer converted, will give the total sequence concentration at any degree of conversion for the copolymer. The total mole fraction will be distinguished from the instantaneous concentrations by a horizontal bar ($\overline{P_n\{\dots\}}$). Three such curves for various initial monomer compositions are shown in Figures 2-4 in which the total concentrations are also indicated. At low initial concentration of vinyl chloride (22 mole-%) the curve rises sharply at high conversions for the BB dyad. The high initial concentration of vinylidene chloride prevents formation of long vinyl chloride sequences in-

TABLE I
Calculated Comonomer Sequence Concentrations and
Initial Vinyl Chloride Monomer Content

f_B^0	Conv.	$\overline{P_1\{B\}}$	$\overline{P_2\{BB\}}$	$\overline{P_3\{BBB\}}$	$\overline{P_2\{BA\}}$	$\overline{P_2\{AA\}}$	$\overline{P_4\{AAAA\}}$
0		0	0	0	0	1.00	1.00
0.22	0.83	0.13	0.015	0.0035	0.22	0.77	0.60
0.46	0.59	0.26	0.0062	0.016	0.39	0.55	0.31
0.61	0.75	0.49	0.27	0.16	0.47	0.27	0.10
0.74	0.85	0.69	0.51	0.41	0.36	0.13	0.028
0.83	0.87	0.80	0.66	0.56	0.28	0.057	0.020
0.90	0.91	0.89	0.80	0.72	0.19	0.024	0.010
1.00		1.00	1.00	1.00	0	0	0

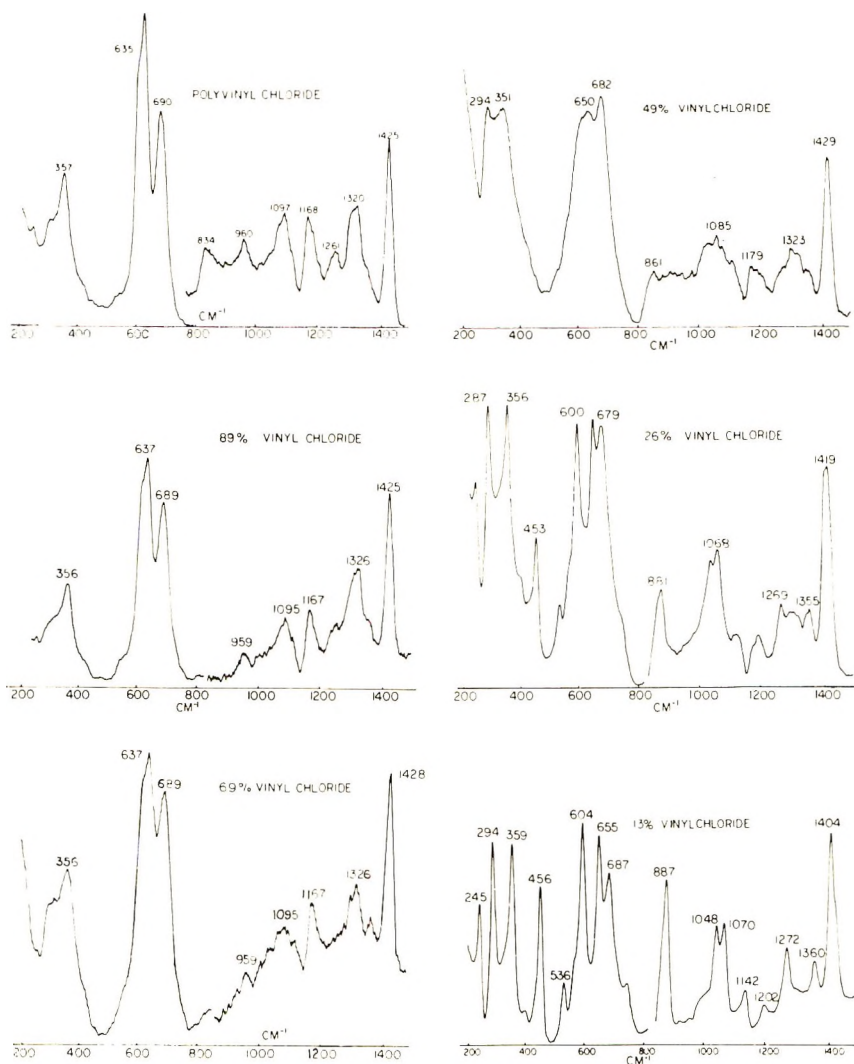


Fig. 6. Raman spectra of poly(vinyl chloride) and copolymers containing 89, 69, 49, 26, and 13% vinyl chloride.

initially. However, at higher initial vinyl chloride concentration (82.5%), the vinylidene chloride is consumed early in the polymerization so that the vinyl chloride dyad concentration approaches unity at 80% conversion. The calculated total sequence concentrations of the various copolymers discussed in this paper are summarized in Table I. For any given initial monomer concentration the total sequence concentrations are dependent upon the total mole fraction of monomers converted to polymer. The conversion for each copolymerization is therefore noted in the table.

The dyad probability $P\{BA\}$ shows an interesting trend. The probability of its formation increases as the second monomer is added to the poly-

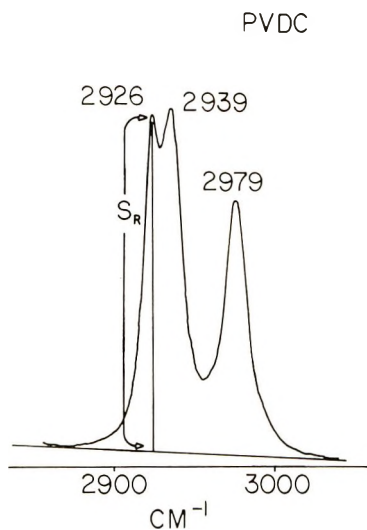


Fig. 7. Raman spectrum of poly(vinylidene chloride), carbon-hydrogen stretching region.

merization and a maximum in concentration would be expected. This is seen to occur at about 0.5 mole fraction of vinyl chloride in the copolymer.

Raman Spectra of VDC-VC Copolymers

The scattering pattern of the homopolymer, vinylidene chloride, is shown in Figure 5. Those for poly(vinyl chloride) and some copolymers studied are shown in Figure 6, in which are plotted scattering intensities against Raman shifts. Some of the stronger lines observed in all of these patterns are the C—Cl stretch frequencies ($600\text{--}700\text{ cm}^{-1}$). Of great importance in this study is the CH_2 stretching region ($2900\text{--}3000\text{ cm}^{-1}$), of which three examples are shown in Figures 7–9.

We cannot determine the number of scattering units by thickness measurements as in conventional infrared spectroscopy, since in this work Raman scattering is measured from the surface of the samples. The number of scattering units must be known if quantitative relationships are to be studied by this method. An internal standard in the scattering material would serve as a reference for the normalization of scattering intensities of peaks used in this quantitative study. Fortunately, the materials examined contain such reference in the CH_2 group which is present in the same molar ratio in vinyl chloride, vinylidene chloride and all the copolymers. The CH_2 deformation mode is seen at 1404 cm^{-1} in PVDC but increases by about 20 cm^{-1} in some of the copolymers, its position being apparently influenced by the number of chlorine atoms on adjacent carbon atoms. This shift has also been observed by Enomoto and Satoh in the infrared.¹¹ The CH_2 asymmetric stretching frequency is seen at 2926 cm^{-1} and remains at that frequency in all the homopolymers and copolymers examined. It is

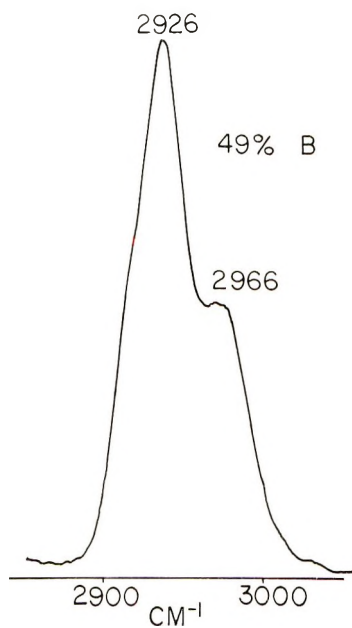


Fig. 8. Raman spectrum of copolymer containing 49% vinyl chloride, carbon-hydrogen stretching region.

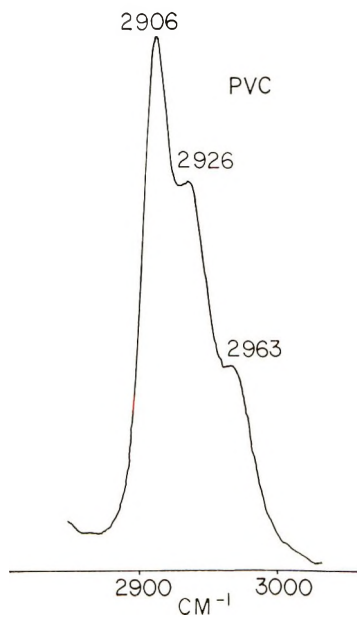


Fig. 9. Raman spectrum of poly(vinyl chloride), carbon-hydrogen stretching region

therefore the frequency of choice as a scattering reference in these observations.⁶ That is, the scattering intensity S at each analytical frequency was divided by the intensity S_R at 2926 cm^{-1} for the particular scan of each

sample. The method of measuring the reference intensity S_R is shown in Figure 7. Scattering intensities at other frequencies are measured by using a baseline method in a similar manner.

Results and Discussion

It is expected from theory that the scattering intensity will be linear with respect to concentration of the specific scattering comonomer sequences. Careful examination of the patterns obtained revealed several such relations with the calculated comonomer sequence concentration.

The first of the correlations to be discussed is that with the total vinyl chloride content of the polymers. It is shown in Figure 10 for the peak at 2906 cm^{-1} in the carbon-hydrogen stretching region. This line is not observed in the infrared, but the infrared absorption at 1205 cm^{-1} has been found to correlate with vinyl chloride content of the copolymers only up to 25%.⁴ Figure 10 clearly shows a linear relation to 100% vinyl chloride content. All of the points shown on this and following curves are averages of four measurements, the uncertainty for the ratios was calculated from the expression

$$\pm (S/S_R)[(\Delta S/S) + (\Delta S_R/S_R)] \quad (5)$$

where ΔS and ΔS_R denote the total ranges of the sets of four measurements. It is noteworthy that the point indicated by the triangle falls on the line. Polymerization of this sample was accomplished at constant monomer composition throughout the polymerization by continuous addition of monomer. Integration of the instantaneous concentration of the sequences in this sample is thus avoided. No peaks in the spectra could be observed with intensity proportional to the vinylidene chloride content of the polymers. This is of no consequence, given the vinyl chloride content.

The dyad concentration $\overline{P}_2\{\text{BB}\}$ deduced from kinetics was also found to be proportional to scattering, as is shown in Figure 11 for the 1320 cm^{-1} peak, which results from the CH_2 wagging motion. This line has not been observed in the infrared but does show good correlation in the Raman.

The Raman peak at a frequency of 1167 cm^{-1} is due to the C—C stretching mode. In some papers on the infrared absorption of PVC this mode is not reported, in others it is observed as very weak. Its intensity in Raman scattering is proportional to the calculated $\overline{P}_3\{\text{BBB}\}$ in these copolymers, as is readily seen in Figure 12. NMR does not have sufficient resolution to permit observation of this triad.

In all of the spectra examined no correlation was found with sequences containing both A and B in any combination. It has been pointed out in Table I that the dyad concentration $\overline{P}\{\text{BA}\}$ increases from zero in each homopolymer to a maximum in the copolymer containing equal mole fractions of the two. No scattering peak was found to respond in this manner. However, a carbon-chlorine stretching line at 687 cm^{-1} goes through a minimum at this copolymer composition. This rather trivial relation is shown

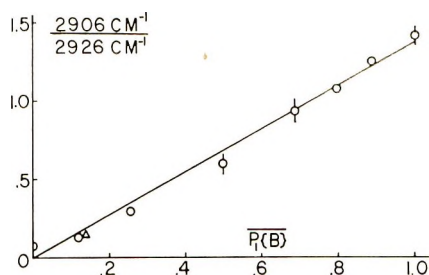


Fig. 10. Raman scattering intensity as a function of total vinyl chloride content of the copolymer, $\overline{P_1\{B\}}$.

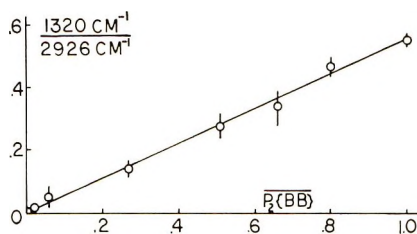


Fig. 11. Total vinyl chloride dyad concentration $\{P_2\overline{BB}\}$ vs. Raman scattering intensity.

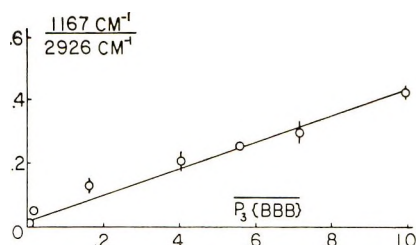


Fig. 12. Total vinyl chloride triad concentration as a function of Raman scattering intensity, $P_3\{BBB\}$.

in Figure 13, where the scattering ratios are plotted against $1 - \overline{P_2\{AB\}}$. In PVDC ($P\{A\} = 1$), the ratio is high (here plotted as circles) and decreases with increased $P\{B\}$ to about 50%, at which point the ratio increases (here plotted as squares) to a maximum in PVC ($P\{B\} = 0$). The significance of $1 - \overline{P_2\{AB\}}$ is obvious from the relation

$$\overline{P_2\{AA\}} + \overline{P_2\{BB\}} + \overline{P_2\{AB\}} + \overline{P_2\{BA\}} = 1 \quad (6)$$

in which $\overline{P_2\{AB\}} = \overline{P_2\{BA\}}$. In spite of the rather poor quantitative aspect of this plot, values for $2\overline{P_2\{AB\}}$ can be readily obtained from the total of $\overline{P_2\{AA\}}$ and $\overline{P_2\{BB\}}$. Apparently, the scattering coefficients for the $\overline{P_2\{AA\}}$ and $\overline{P_2\{BB\}}$ are sufficiently different for this mode to reflect the combination of the dimer.

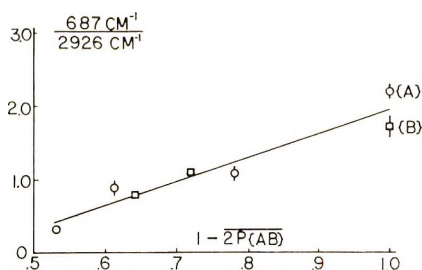


Fig. 13. The function $1-2P_2\{\overline{AB}\}$ vs. intensity of Raman line at 687 cm^{-1} .

Linear plots for some vinylidene chloride sequences have been observed, as shown in Figure 14 for $P_2\{\overline{AA}\}$ and the carbon-hydrogen stretch frequency at 2979 cm^{-1} . This appears to be the peak observed in the Raman spectrum by Hendra and Mackenzie² and reported at 2984 cm^{-1} . From this curve and the one for $P_2\{\overline{BB}\}$, values for $2P_2\{\overline{AB}\}$, can be obtained. The constant-composition sample is also shown.

No correlation could be found for the vinylidene chloride triad AAA, but a good relationship for the tetrad concentration $P_4\{\overline{AAAA}\}$ is shown in Figure 15. Here again the constant-composition copolymer falls on the line. Three of the copolymers examined have so little of these tetrad sequences that they do not appear on the curve. This scattering has a frequency of 887 cm^{-1} , characteristic of the homonuclear carbon-carbon stretching for which the Raman effect is so well suited.

The scattering ratios are specific for a given sequence, as is illustrated in Figure 16 in which $P_1\{\overline{A}\}$, $P_2\{\overline{AA}\}$, and $P_3\{\overline{AAA}\}$ are all plotted against scattering at 2979 cm^{-1} . The dyad concentration is seen to be linear, whereas the other two plots deviate greatly from linearity.

An effort to describe the precision of the measurements of the various sequences in this study is illustrated in Table II. The slopes of the $P_n\{\dots\}$ versus S curves are denoted as K_n . The errors in S are the averages of all points on the curve and based on the average deviation from the average of four measurements. The errors in S are multiplied by K_n to determine the sensitivity $\Delta P_n\{\dots\}$ of the measurements of $P_n\{\dots\}$.

TABLE II
Calculated Errors of Measurement for Various Microstructures

	K_n	$\Delta P_n\{\dots\}$
$\overline{P_1\{B\}}$	1.36	± 0.02
$\overline{P_2\{BB\}}$	0.56	± 0.12
$\overline{P_3\{BBB\}}$	0.46	± 0.10
$\overline{P_2\{AA\}}$	0.52	± 0.05
$\overline{P_4\{AAAA\}}$	1.24	± 0.06

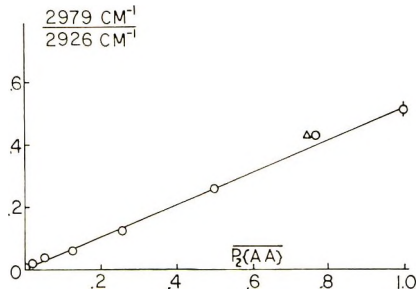


Fig. 14. Raman scattering intensity as a function of the vinylidene chloride dyad concentration $\overline{P}_2\{AA\}$.

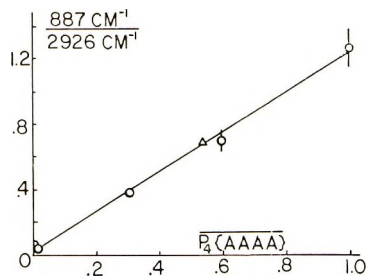


Fig. 15. $\overline{P}_4\{AAAA\}$ vs. Raman scattering intensity.

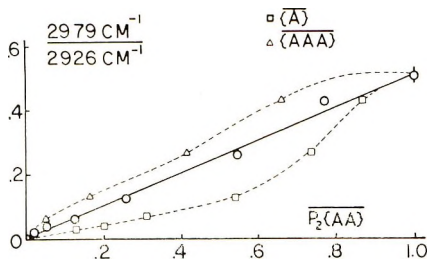


Fig. 16. Vinylidene chloride sequence concentrations $\overline{P}_1\{A\}$, $\overline{P}_2\{AA\}$ and $\overline{P}_3\{AAA\}$ plotted against Raman scattering at 2979 cm^{-1} .

Conclusions

The first study of copolymers by Raman scattering has shown that quantitative correlations exist between certain scattering intensities and calculated concentrations of microstructures in copolymers. Theory predicts these relations to be linear and experiment shows this is indeed the case. Some of the frequencies used for analysis are not observed in the infrared. Triad concentrations are detected which cannot be measured by NMR. This suggests that Raman spectroscopy may generally be applicable to the study of the microstructure of copolymers.

The authors are grateful to J. L. Garner for his helpful assistance in the synthesis of the polymers used in this study.

One of us (M. R. M.) expresses appreciation to the Dow Chemical Co. for the opportunity for a period of study and research at the Division of Macromolecular Science at Case Western Reserve University.

References

1. J. L. Koenig and D. Druesedow, *J. Polym. Sci. A-2*, **7**, 1075 (1969).
2. P. J. Hendra and J. R. Mackenzie, *Spectrochim. Acta*, **25A**, 1349 (1969).
3. T. Miyazawa and Y. Ideguchi, *J. Polym. Sci. B*, **3**, 541 (1965).
4. S. Narita, S. Ichinoke, and S. Enomoto, *J. Polym. Sci.*, **36**, 389 (1959).
5. S. Enomoto, *J. Polym. Sci.*, **55**, 95 (1961).
6. K. Ito and Y. Yamashita, *J. Polym. Sci. A*, **3**, 2165 (1965).
7. Y. Yamashita, K. Ito, H. Ishii, S. Hoshino, and M. Kai, *Macromolecules*, **1**, No. 6, 529 (1968).
8. M. Meeks and J. L. Garner, Dow Chemical Co., unpublished data.
9. Y. Yamashita, K. Ito, S. Ikuma, and H. Kada, *J. Polym. Sci. B*, **6**, 219 (1968).
10. V. E. Meyer and G. G. Lowry, *J. Polym. Sci. A*, **3**, 2843 (1965).
11. S. Enomoto and S. Satoh, *Kolloid-Z. Z. Polym.*, **29**, 12 (1967).

Received June 11, 1970

Revised October 27, 1970

Determination of the Pressure Coefficient and Pressure Effects in Capillary Flow

RICHARD C. PENWELL and ROGER S. PORTER,
Polymer Science and Engineering, and STANLEY MIDDLEMAN,
Chemical Engineering and Polymer Science and Engineering,
University of Massachusetts, Amherst, Massachusetts 01002

Synopsis

General expressions for determining the pressure coefficient and axial distribution of the viscosity and pressure in capillary flow are derived for Newtonian and shear-thinning fluids. The pressure-dependent viscosity model is obtained from the WLF equation as derived from Doolittle's free volume theory. The model has also been derived from Eyring's hole theory for viscosity. Poiseuille's equation is modified to correct for the pressure effect on viscosity. A Newtonian, low-molecular-weight polystyrene and a shear-thinning, high-molecular-weight polystyrene were tested in an Instron capillary rheometer. The axial velocity distribution was found to be negligibly affected by pressure whereas the viscosity was shown to increase markedly with a decrease in volume. The resulting pressure effects on the viscosity of both samples were analyzed by using the derived expressions.

INTRODUCTION

Several investigators have recently suggested that under certain conditions, pressure can effectively influence the capillary flow of amorphous polymers.¹⁻⁸ The phenomenon generally appears as an unexpected increase in pressure or stress with increasing shear rate. The effect becomes more pronounced with the use of longer capillaries and lower melt temperatures. In particular, the increase in apparent viscosity with increasing capillary shear rate for a Newtonian fluid and for a shear-thinning polystyrene has been attributed to the effect of pressure in decreasing the free volume available for flow.^{1,2}

A form of the WLF equation derivable from Doolittle's free volume expression has been used to determine the pressure dependence of viscosity.² At a particular shear rate and temperature, an average viscosity based on an average pressure can be calculated. To determine the average pressure, a linear pressure drop down the capillary was assumed.^{1,2} However, if the viscosity is pressure-dependent, the axial pressure distribution is expected to be nonlinear.⁸⁻¹⁰ The calculated average pressure would then depend on the nonlinearity of the pressure drop over the capillary length.

The present work is an attempt to calculate the effect of pressure in capillary flow and to apply the results to the capillary flow of polystyrene of low and high molecular weight. Initially, a pressure-dependent model for the viscosity is chosen which can be obtained from the WLF equation and Eyring hole theory^{11,12} and which, when combined with the momentum equation, provides a reasonable solution to the problem. A general method for determining the pressure coefficient in the model is given. It is thus possible to calculate the pressure and viscosity at any axial position in a capillary and the average pressure and viscosity at each shear rate. This has been done for both a low (Newtonian) and a (shear-thinning) high molecular weight polystyrene. A pressure-corrected version of Poiseuille's equation is also presented and compared with experimental data.

EXPERIMENTAL

Samples

The narrow distribution polystyrene samples used in the tests were obtained from the Pressure Chemical Company, Pittsburgh, Pennsylvania. The sample of 20,400 molecular weight (sample 20.4K) has $\bar{M}_w/\bar{M}_n \leq 1.06$ and the sample of 670,000 molecular weight (670K) has $\bar{M}_w/\bar{M}_n \leq 1.10$.

Capillary Measurements

For the study on the low-molecular-weight polystyrene, a tungsten carbide capillary, 0.030 in. in diameter and 1.007 in. long, was used in an Instron capillary rheometer. A capillary 0.050 in. in diameter and 1.964 in. long was used for the high molecular weight sample. The test temperatures were 140°C for the 20.4K polystyrene and 165°C for the 670 K polystyrene. Pressure losses in the barrel and the kinetic energy correction were negligible for these tests.² An end correction based on data taken with other capillaries was applied to the data of the high molecular weight sample.²

Cone-and-Plate Measurements

A Weissenberg rheogoniometer (Model No. 17) was used to measure the apparent viscosity as a function of shear rate for the two polystyrenes at atmospheric pressure. Measurements were made by using a 5.0 cm plate and a 2° cone angle. The samples were inserted into the rheogoniometer at their respective test temperatures. Therefore, the time required for thermal equilibration had little effect on degradation.¹³

DISCUSSION

It has been previously suggested and illustrated that pressure can influence the flow of amorphous polymers in capillary viscometry.^{1-3,14,15} If the test temperature is in a region where the flow is determined by the

probability of sufficient free volume being available, then the glass transition can be significantly shifted at high pressures.¹⁶⁻²⁰ The WLF equation has been used successfully to predict an average viscosity increase with pressure by insertion of the shift in the glass transition temperature, T_g .² The shift in T_g has been calculated by using an average pressure of an assumed linear pressure drop in the capillary.² Since the viscosity is pressure-dependent, this may have been a limiting assumption. One possible way of determining the variation in the average pressure is to select a pressure-dependent viscosity model and solve the appropriate component of the momentum equation.

Model for a Pressure-Dependent Viscosity

The model selected for the pressure-dependent viscosity should be the simplest possible for the realistic solution of the problem. The WLF equation has been used previously to calculate the pressure dependence of apparent viscosity. It is:

$$\log \eta/\eta_0 = -C_1(T - T_g)/(C_2 + T - T_g) \quad (1)$$

where T_g is the glass transition temperature, T is the test or reference temperature, η_0 is the viscosity at T_g , and C_1 and C_2 are usually considered constants for a given material.

By using the following equation for the pressure dependence of T_g , an increase in the apparent viscosity can be calculated with increasing pressure;

$$T_g = T_{g0} + A_1P \quad (2)$$

where T_{g0} is the glass transition at atmospheric pressure, $A_1 = \partial T_g/\partial P$, and P is the pressure.

Inserting eq. (2) into eq. (1) gives:

$$\eta = \eta_0 \exp \left\{ 2.303[(A_2 + A_3P)/(A_4 - A_1P)] \right\} \quad (3)$$

where $A_2 = -C_1(T - T_{g0})$, $A_3 = C_1A_1$, and $A_4 = C_2 + T - T_{g0}$. At low pressures ($P < 200$ bars), A_1P will be a small percentage of A_4 and as a first approximation can be ignored. Equation (3) then simplifies to the form

$$\eta = \eta_0 e^{bP} \quad (4)$$

where $\eta_0 = \eta_0 e^{2.303A_2/A_4}$ and $b = 2.303 A_3/A_4$. To obtain an estimate of η_0 and b , consider the following values for low-molecular-weight polystyrene at 140°C:² $\eta_0 \approx 10^{13}$ poise, $T_{g0} = 90^\circ\text{C}$, $C_1 = 14.4$, $C_2 = 36.2$, and $A_1 = 0.028$.¹⁸ The values of η_0 and b are found to be 4.36×10^4 poise and 1.07×10^{-2} bars⁻¹, respectively. The zero shear viscosity of this sample at 140°C is 4.0×10^4 poise, which is in good agreement with the value calculated for η_0 .² Since C_2 is pressure-dependent, the expression for b indicates that it will decrease in value with increasing temperature and pressure.

A relation equivalent to eq. (4) has been previously and independently derived through considerations of the Eyring hole theory for viscosity.^{11,12}

The parameter b in eq. (4) is equal to v_h/RT where v_h equals the volume of the holes. Using the compressibility data for polystyrene of Maxwell and Matsuoka,²¹ Hirai and Eyring evaluated v_h .¹² With their value for v_h , b is found to be $4.43 \times 10^{-3} \text{ bars}^{-1}$ at 140°C , which should be considered only an estimate.

Equation 4 should thus be a reasonable approximation describing the pressure dependence of viscosity. Indeed this empirical form has been used previously for this purpose.^{3,7,8,22,22a} At extreme pressures, it would be expected to fail owing to its derivation from the WLF equation and from the assumptions made in the Eyring hole theory.^{11,12} For high pressures, eq. (3) could possibly be used, it being noted that A_4 may also vary with increasing pressure.

Continuity Constitutive and Momentum Equations

Equation (4) has been established as a reasonable model for pressure-dependent viscosity. It can therefore be used for problems] of isothermal, compressible, Newtonian, and shear-thinning capillary flows. Heat generation and its effect on the temperature and velocity profiles in both the radial and axial directions of a capillary have been well discussed for both Newtonian and non-Newtonian liquids.²³⁻²⁹ Considering these previous results and the conditions of the present tests, the assumption of an isothermal problem appears acceptable.

Gerrard et al.^{28,29} have discussed the adiabatic and isothermal flow of a Newtonian fluid. They used a fluid with a previously determined pressure-temperature relation. One consequence of their numerical solution was the calculated, nonlinear pressure drop down the capillary. Duvdevani and Klein have studied the pressure effect in the capillary flow of polyethylene by using the pressure-viscosity relation of eq. (4).³ Expressions were derived for the shear stress at the entrance and exit which were subsequently used to determine the pressure coefficient. As the pressure coefficient of viscosity for polyethylene is much less than that for polystyrene, they were able to incorporate a limiting series expansion (assuming $b\Delta P < 1$) into their solution involving regression analysis. Brenschede and Klein also used eq. (4) in their determination of the pressure coefficient and of the error involved by neglecting the pressure dependence of viscosity.⁷ An iterative technique was used as one means of determining the pressure coefficient. They found that the volume change due to the compressibility of the melt is insignificant when considering a possible pressure effect on the flow rate.

The present discussion is an attempt to determine general expressions for the pressure-dependent flow behavior of Newtonian and shear-thinning polymers whose viscosities are given by eq. (4) and for which the following assumptions apply: steady-state flow; no gravitational effects; no slip at the boundary; $v_\theta = \tau_{r\theta} = \tau_{z\theta} = 0$ in terms of cylindrical coordinates (r, θ, z) (from considerations of the symmetry); and $v_r = 0$ (fully developed flow).

The equation of continuity is represented by;

$$D\rho/Dt = -\rho(\nabla \cdot \mathbf{v}) \quad (5)$$

where D/Dt is the material derivative, ρ the density, and \mathbf{v} the velocity field. With the given assumptions, eq. (5) reduces to

$$\partial(\rho v_z)/\partial z = 0 \quad (6)$$

By rearranging eq. (6), the following equivalent form is obtained:

$$d(\ln \rho) = d(\ln v_z) \quad (6a)$$

This states that the relative axial change of v_z is equal to the relative change in density. For polystyrene, the expected change in density with pressure would be approximately 1%.² Therefore, the axial velocity distribution will be negligibly dependent on pressure and the assumption of incompressible flow in the calculation of the velocity field for polystyrene is reasonable. To determine the relative effect of pressure on viscosity a similar procedure can be applied to eq. (4). With $V = V_0 + \beta P$, where β is the compressibility coefficient, the relative change in viscosity with density is;

$$d(\ln \eta) = (-b/\beta\rho)d(\ln \rho) \quad (7)$$

Inserting average values for the parameters of polystyrene into eq. (7) indicates that the relative change in viscosity would be approximately 80 times the relative change in density.

The momentum equation is represented by;

$$\rho D\mathbf{v}/Dt = -\nabla p - [\nabla \cdot \boldsymbol{\tau}] - \rho\mathbf{g} \quad (8)$$

where $\boldsymbol{\tau}$ is the stress tensor, \mathbf{g} is the gravitational field, and the other parameters are as defined previously. The z component of eq. (8) reduces to

$$0 = -\frac{\partial P}{\partial z} + \frac{1}{r} \frac{\partial}{\partial r} (r\tau_{rz}) \quad (9)$$

The constitutive equation for a Newtonian fluid is

$$\boldsymbol{\tau} = 2\eta_0(^{1/2}\nabla\mathbf{v} + ^{1/2}\nabla\mathbf{v}^T) - (^{-2/3}\eta_0 + \kappa)(\nabla \cdot \mathbf{v})\boldsymbol{\delta} \quad (10)$$

where η_0 is the zero shear viscosity, κ is the bulk viscosity and the other parameters are as defined previously. In cylindrical coordinates, eq. (10) gives

$$\tau_{rz} = \eta_0(\partial v_z/\partial r) \quad (11)$$

when the given assumptions are applied.

The substitution of eqs. (4) and (11) into eq. (9) and separation of the variables gives;

$$-\frac{1}{\eta_0} e^{-bP} \frac{\partial P}{\partial z} = C = \frac{1}{r} \frac{\partial}{\partial r} \left(r \frac{\partial v_z}{\partial r} \right) \quad (12)$$

With atmospheric pressure as a reference, C is given by

$$C = -(1/b\eta_0L)(1 - e^{-b\Delta P}) \quad (13)$$

From eqs. (12) and (13), the velocity distribution is found to be

$$v = \frac{1 - e^{-b\Delta P}}{b\Delta P} \left\{ \frac{\Delta PR^2[1 - (r^2/R^2)]}{4\eta_0L} \right\} \quad (14)$$

The velocity distribution is modified from the classical result by the pressure correction term $(1 - e^{-b\Delta P})/b\Delta P$, which is also applicable to Poiseuille's law as given below:

$$\eta_0 = (\pi\Delta PR^4/SLQ)[(1 - e^{-b\Delta P})/b\Delta P] \quad (15)$$

With eqs. (12) and (13) the following expression for the axial pressure distribution is obtained.

$$P = \ln [e^{-b\Delta P} + (1 - e^{-b\Delta P})z/L] - b \quad (16)$$

From this, the pressure gradient is given as

$$\partial P/\partial z = -(1 - e^{-b\Delta P})/\{bL[e^{-b\Delta P} + (1 - e^{-b\Delta P})z/L]\} \quad (17)$$

The average pressure is given by

$$\bar{P} = \int_0^L P dz/L \quad (18)$$

Substituting eq. (16) for P and defining $\xi = z/L$ and $\delta = e^{b\Delta P} - 1$ gives

$$\bar{P} = \Delta P - \frac{1}{b} \int_0^1 \ln [1 + \delta\xi] d\xi \quad (19)$$

By expansion of the logarithm and integration, eq. (18) becomes

$$\bar{P} = \Delta P + \frac{1}{b} \sum_{i=1}^n \frac{\delta^i (-1)^i}{i(i+1)} \quad (20)$$

Equation (20) is valid only when $b\Delta P < 1$ and the number of terms included in the series depends on how much less than unity $b\Delta P$ is. If $b\Delta P > 1$, then \bar{P} must be found by numerical integration of the P versus z curve.

The average flow rate, can be calculated and compared to either the measured flow rate or the flow rate calculated from the plunger motion.

$$Q = \pi R^4(1 - e^{-b\Delta P})/8b\eta_0L \quad (21)$$

Determination of the Pressure Coefficient b

To determine the parameter b in eq. (4), the actual Newtonian viscosity η_0 , given by eq. (15), and the uncorrected viscosity η° are used. The uncorrected viscosity η° is given by Poiseuille's law as $\eta^\circ = \pi\Delta PR^4/SLQ$. The volume flow rate can be calculated from the plunger speed V_p and the cross section πR_p^2 , so that

$$\eta^\circ = \Delta PR_c^4/SL_c R_p^2 V_p \quad (22)$$

where the subscripts c and p refer respectively to the capillary and reservoir dimensions. Functions ϕ and θ can be defined as

$$\begin{aligned}\phi &= \eta_0/\eta^\circ \\ \theta &= \phi_1/\phi_2\end{aligned}\quad (23)$$

where the subscripts refer to capillaries and reservoirs of different sizes.

Combining eqs. (22) and (23) gives

$$\begin{aligned}\theta &= \phi_1/\phi_2 \\ &= \eta_1^\circ/\eta_2^\circ \\ &= \frac{\Delta P_2 L_{c_1} V_{p_1} R_{p_1}^2 R_{c_2}^4}{\Delta P_1 L_{c_2} V_{p_2} R_{p_2}^2 R_{c_1}^4} \\ &= KC_1 V_R\end{aligned}\quad (24)$$

where $K = \Delta P_2/\Delta P_1$,

the ratio of plunger speeds is

$$V_R = V_{p_1}/V_{p_2}$$

and

$$C_1 = \frac{L_{c_1} R_{p_1}^2 R_{c_2}^4}{L_{c_2} R_{p_2}^2 R_{c_1}^4}$$

is a geometrical factor.

Combining eqs. (15) and (23) yields

$$\theta = K[(1 - e^{-b\Delta P_1})/(1 - e^{-bK\Delta P_1})] \quad (25)$$

and equating eqs. (24) and (25) gives

$$C_1 V_R = \frac{1 - e^{-b\Delta P_1}}{1 - e^{-bK\Delta P_1}} \quad (26)$$

Equation (26) is a general expression for determining the pressure coefficient of a Newtonian fluid. If one capillary is used in the same rheometer C_1 is unity and b can be determined in the following manner. For convenience, the pressure required for flow at the lowest shear rate can be used as the reference pressure ΔP_1 . From earlier calculations, an estimate of b is available. Therefore, a suitable range of values for $b\Delta P_1$ can be selected. The range of K values can also be determined from the experimental data by using ΔP_1 as the reference pressure. For different values of K , V_R can be calculated as a function of $b\Delta P_1$. Since the velocity ratios are predetermined, it is convenient to plot this information with K and $b\Delta P$ as variables, as shown in Figure 1. From experimental values of K and V_R ($n = 1$), $b\Delta P_1$ and therefore b can be determined. Although one curve is sufficient to determine b , several can be used to calculate any possible

change in b with increasing pressure. For low molecular weight polystyrene at 140°C, b was found to be 5.51×10^{-3} bars $^{-1}$. The variation in b over the pressure range studied was approximately 10%. A second means of determining b is to calculate η° by using eq. (22) and then eq. (4):

$$b = \ln (\eta^\circ / \eta_0) / P \quad (27)$$

Modifications for a Shear-Thinning Polymer

By a separation of the pressure and shear rate dependence of the apparent viscosity, the problem becomes similar to the Newtonian case. The power law expression

$$\tau = K' \dot{\gamma}^n \quad (28)$$

is assumed applicable at atmospheric pressure. The corrected shear rate $\dot{\gamma}$ is obtained from the measured shear rate times a factor of $(3n + 1)/4n$.³⁰ Equation (4) now becomes

$$\eta = \eta_{\text{atm}} e^{bP} = K' \dot{\gamma}^{n-1} e^{bP} \quad (29)$$

By following the same procedure as before, eq. (9) can be solved and eq. (13) now becomes

$$C = (e^{-b\Delta P} - 1) / bK'L \quad (30)$$

For a single capillary, the expression for determining b is

$$V_R^n = (1 - e^{-b\Delta P_1}) / (1 - e^{-bK\Delta P_1}) \quad (31)$$

where V_R is the ratio of the plunger speeds and $K = \Delta P_2 / \Delta P_1$. The expressions for P , $\partial P / \partial z$, and \bar{P} remain the same.

The procedure for determining the pressure coefficient b is identical to that for the Newtonian case. The Weissenberg rheogoniometer was used to obtain the data at atmospheric pressure required to calculate the power-law exponent n . Figure 1 was used to calculate a value of 2.90×10^{-3} for the pressure coefficient of the high molecular weight polystyrene.

RESULTS

A study of the low molecular weight polystyrene at 140°C was performed in an Instron rheometer with a capillary 0.030 in. in diameter and 0.922 in.-long. At this temperature and in the shear rate range studied, a negligible capillary end correction and extrudate expansion have been reported.²

For the low molecular weight polystyrene, the pressure coefficient had values of 5.51×10^{-3} and 5.54×10^{-3} bars $^{-1}$ as calculated by eqs. (26) and (27), respectively. Figure 2 represents the axial pressure distribution, given by eq. (16), at various shear rates. The deviation from a linear pressure drop increases with increasing shear rate. The greater the non-linearity in the pressure drop, the greater is the deviation of the average pressure

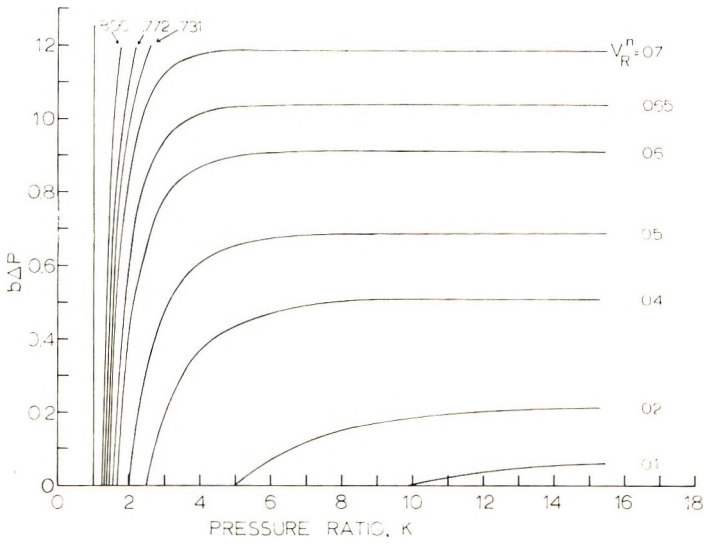


Fig. 1. General curve for the determination of the pressure coefficient of Newtonian and shear-thinning fluids.

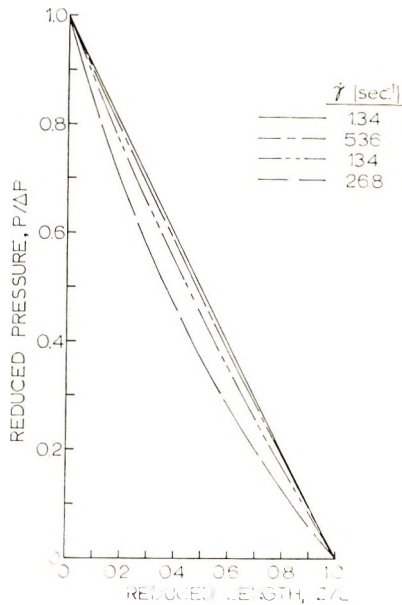


Fig. 2. Axial pressure distribution of the low molecular weight (20,400) polystyrene (20.4K) for several shear rates at 140°C; capillary length = 0.922 in., diameter 0.030 in.

from $\Delta P/2$. The magnitude will affect the value of the average viscosity calculated by using eq. (3). The variation in the average pressure with the total pressure is illustrated in Figure 3. At low pressure, the average is

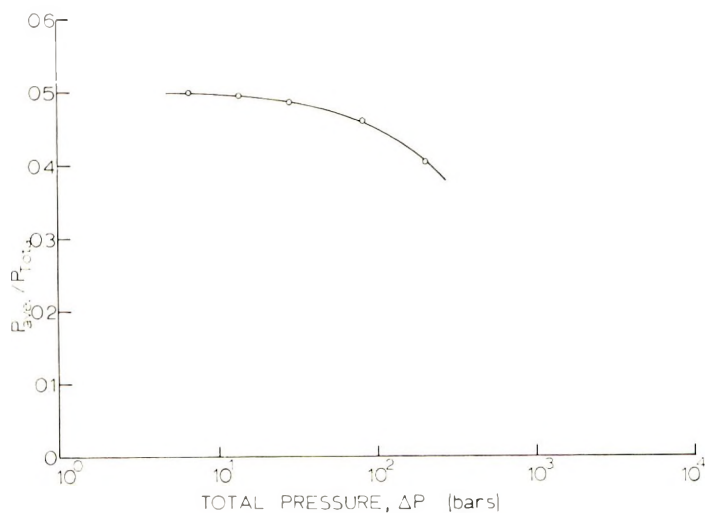


Fig. 3. Average pressure as a function of the total pressure drop for the 20.4K polystyrene at 140°C.

adequately represented by $\Delta P/2$ but decreases significantly from this value at higher pressures.

With a pressure-dependent viscosity, an appreciable change in viscosity with total pressure and axial position can be anticipated. The magnitude of this variation is illustrated in Figure 4, in which the apparent viscosity is plotted as a function of the axial distance at various shear rates. These curves may be integrated to obtain an average viscosity which can be compared to the viscosity calculated by eq. (4) by using an average pressure. This comparison is made in Table I which also includes the viscosity calculated as the stress/shear rate.

TABLE I
Pressure-Dependent Viscosity for Low Molecular Weight
Polystyrene at 140°C^a

$\dot{\gamma}$, sec ⁻¹	ΔP_{Total} , bars	$\Delta P_{Average}$, bars	$\eta_a \times 10^{-4}$, poises		
			Calcd from $\tau/\dot{\gamma}$	From Fig. 3 ^b	From eq. (4)
1.34	6.71	3.34	3.95	4.02	4.02
2.68	13.86	6.84	4.08	4.10	4.10
5.36	28.57	13.91	4.20	4.27	4.27
13.4	82.57	38.18	4.86	4.90	4.88
26.8	205.7	83.95	6.05	6.47	6.29

^a Capillary diameter = 0.030 in., length = 0.922 in.

^b Numerically integrated.

The corrected version of Poiseuille's equation presented in eq. (15) predicts the Newtonian behavior of a polymer with a pressure-dependent

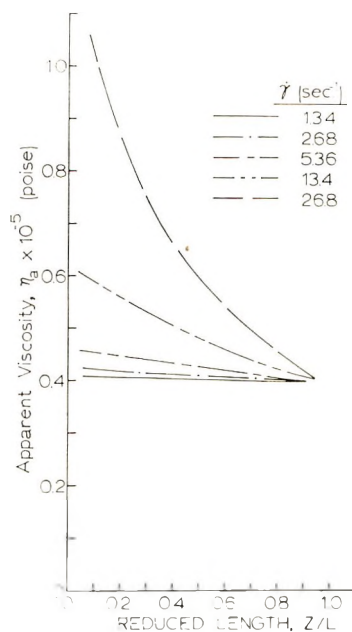


Fig. 4. Axial variation in viscosity at several shear rates for the 20.4K polystyrene at 140°C; capillary length = 0.922 in., diameter = 0.030 in.

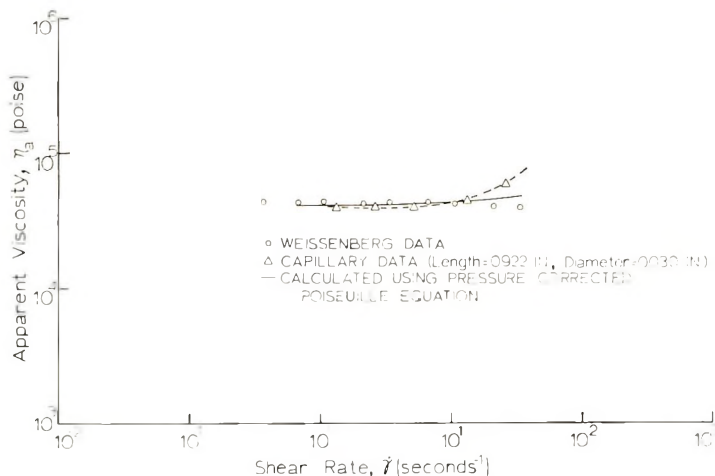


Fig. 5. Comparison of (Δ) Instron and (O) Weissenberg data with (—) data calculated from the pressure-corrected Poiseuille equation; 20.4K polystyrene at 140°C.

viscosity. Figure 5 is a comparison of the viscosity calculated from eq. (15) and the viscosity obtained from measurements in the Instron and Weissenberg rheometers. The Weissenberg data, taken at atmospheric pressure, are Newtonian within the range studied. The capillary data deviate from Newtonian behavior with increasing shear rate, reflecting the pressure dependence of the viscosity. The calculated curve is Newtonian with a

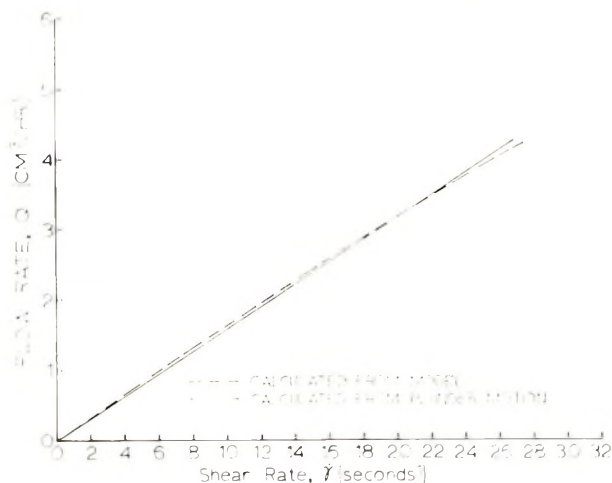


Fig. 6. Comparison of the flow rate (—) calculated from the plunger motion and (---) the pressure-corrected flow rate equation: 20.4K polystyrene at 140°C.

slight increase in viscosity at the highest shear rates. The deviation of eq. (15) at higher shear rates is possibly a consequence of the limitations stated in deriving the pressure-dependent viscosity model from eq. (3).

Figure 6 is a comparison of the pressure-corrected flow rate [eq. (21)] and the flow rate calculated from the plunger motion of the Instron rheometer. It has been previously observed that no appreciable difference exists between measured flow rates and those calculated from the plunger motion.² The flow rate calculated with eq. (21) begins to deviate at higher shear rates, again indicating that the limits of the model have been exceeded.

It may be reasonably assumed that the pressure effect is independent of shear-thinning. Thus flow data on the high molecular weight polystyrene may be treated by the approach used for the Newtonian case. Data from the Weissenberg rheogoniometer were used to evaluate the power-law exponent, n having a value of 0.19. Figure 1, a graphical representation of eq. (31), was used to evaluate the pressure coefficient, b having a value of 2.90×10^{-3} bars.⁻¹ An appropriate end correction had been previously applied to the capillary data.²

The axial pressure distribution is given in Figure 7 for several shear rates at 165°C. The deviation from a linear pressure drop is not as great as for the low molecular weight polystyrene. This is a consequence of the lower value of the pressure coefficient obtained for the high molecular weight polystyrene. The value of $\Delta P/2$, used previously in calculations involving an average pressure, does not appear to cause serious error.

Figure 8 represents the axial variation of viscosity at shear rates of 1, 40, and 150 sec.⁻¹ As with the low molecular weight polystyrene, the viscosity varies considerably with the axial position and total pressure. Average values of the viscosity obtained from Figure 8 are within 1% of the values calculated with eq. 4 and the calculated average pressure.

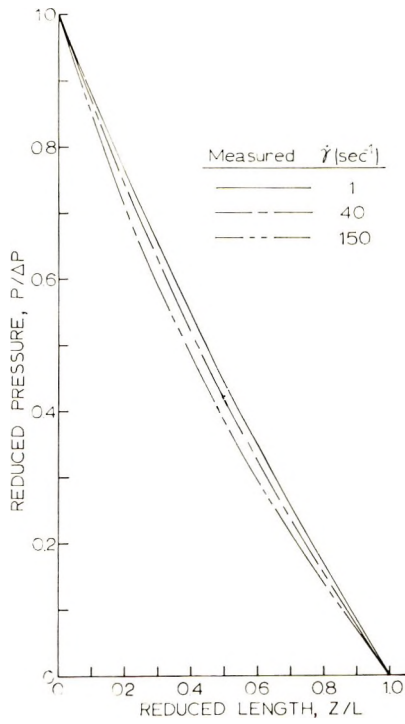


Fig. 7. Axial pressure distribution of the high molecular weight (670,000) polystyrene (670K) at 165°C for various shear rates; capillary length = 1.964 in., diameter = 0.050 in.

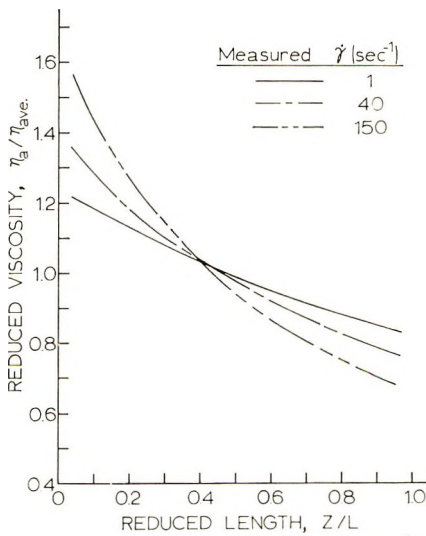


Fig. 8. Axial variation in viscosity at several shear rates for the 670K polystyrene at 165°C; capillary length = 1.964 in., diameter = 0.050 in.

SUMMARY

The influence of pressure on the viscosity in capillary flow has been discussed for Newtonian and shear-thinning fluids. A model for pressure-dependent viscosity, derivable from Doolittle's free volume equation and the Eyring hole theory for viscosity, was combined with the momentum equation to derive general expressions for determining the pressure coefficient and the axial pressure and viscosity distributions. From these, an average pressure and viscosity can be determined.

The resulting expressions were applied to a Newtonian, low molecular weight polystyrene and a shear-thinning, high molecular weight polystyrene. From a consideration of the continuity equation, the axial velocity was found to be negligibly affected by pressure for the test conditions used. The axial pressure distributions for both the low and high molecular weight samples were nonlinear at moderate shear rates, resulting in average capillary pressures less than $\Delta P/2$. The viscosities averaged over several intervals of the capillary agreed well with the viscosities calculated by using an average pressure representing the entire capillary. Values calculated by using the pressure-corrected flow rate and Poiseuille equations agreed well with the experimental data.

Acknowledgment

The authors wish to express appreciation for financial support to the Paint Research Institute (RCP) and to the U. S. Army-Durham (DAH CO4-68-C-0028), (RSP).

References

1. R. C. Penwell and R. S. Porter, *J. Appl. Polym. Sci.*, **13**, 2427 (1969).
2. R. C. Penwell and R. S. Porter, *J. Polym. Sci., A-2* **9**, 463 (1971).
3. I. Duvdevani and I. Klein, *SPE J.*, **23**, 41 (1967).
4. K. Ito, *Repts. Progr. Polym. Phys. Japan*, **12**, 131 (1969).
5. G. A. Toelke, C. G. Gogas, and J. A. Biesenberger, *SPE 13th Antec*, **1967**, 98.
6. D. P. Thomas and R. S. Hagan, *Polym. Eng. Sci.*, **9**, 164 (1969).
7. E. Brenschede and J. Klein, *Rheol. Acta*, **8**, 71 (1969).
8. V. Semjonow, *Rheol. Acta*, **4**, 133 (1965).
9. B. C. Sakiadis, *AIChE J.*, **8**, 317 (1962).
10. T. Arai, I. Suzuki, and N. Akino, *Proc. Fujihara Mem. Fac. Eng. Keio Univ. Tokyo*, **20**, 39 (1967).
11. S. Glasstone, K. Laidler, and H. Eyring, *The Theory of Rate Processes*, McGraw-Hill, New York, 1941, p. 512.
12. N. Hirai and H. Eyring, *J. Polym. Sci.*, **37**, 51 (1959).
13. K. Arisawa and R. S. Porter, *J. Appl. Polym. Sci.*, **14**, 879 (1970).
14. R. L. Ballman, *Nature*, **202**, 288 (1964).
15. A. K. Van der Vegt and P. P. A. Smit, S.C.I. Monograph No. 26, Soc. Chem. Ind., London, 1967, p. 313.
16. A. Miyake and M. Sakakibara, *Repts. Progr. Polym. Phys. Japan*, **6**, 93 (1963).
17. R. W. Warfield, *J. Appl. Chem.*, **17**, 263 (1967).
18. G. Gee, *Polymer*, **7**, 177 (1966).
19. A. J. Matheson, *J. Chem. Phys.*, **44**, 695 (1966).
20. A. Eisenberg, *J. Phys. Chem.*, **67**, 1333 (1963).
21. B. Maxwell and S. Matsuoka, *SPE J.*, **27**, 13 (1957).

22. E. Kuss, *Chem. Ing. Technol.*, **37**, 465 (1965).
- 22a. S. Y. Choi and O. Nakajima, *Proc. Fifth Int. Cong. Rheol.* **4**, 287 (1970).
23. H. L. Toor, *AIChE J.*, **4**, 319 (1958).
24. H. C. Brinkman, *Appl. Sci. Res.*, **A2**, 120 (1950).
25. R. B. Bird, *SPE J.*, **11**, 35 (1955).
26. H. L. Toor, *Ind. Eng. Chem.*, **48**, 922 (1956).
27. R. E. Gee and J. B. Lyon, *Ind. Eng. Chem.*, **49**, 956 (1957).
28. J. E. Gerrard, F. E. Steidler, and J. K. Appeldoorn, *Ind. Eng. Chem. Fund.*, **4**, 332 (1965).
29. J. E. Gerrard, F. E. Steidler, and J. K. Appeldoorn, *Ind. Eng. Chem. Fund.*, **5**, 260 (1966).
30. S. Middleman, *The Flow of High Polymers*, Interscience, New York, 1968, p. 15.

Received July 13, 1970

Electronic States at Defects in Infinite Polyenes

A. H. BEGG and D. PUGH, *Department of Pure and Applied Chemistry, University of Strathclyde, Glasgow, C1, Scotland*

Synopsis

The electronic states localized at defects in a polyene chain with alternating bond lengths have been investigated in the Hückel approximation by direct computation on large rings. The defects considered include substitutional impurities and bond distortions. None of the cases treated seem likely to be thermally activated donor or acceptor centers, but several examples of deep or shallow traps for electrons in the conduction band are found.

INTRODUCTION

The system $(-\text{CH}=\text{CH}-)_n$ exhibits behavior which is probably characteristic of a wide class of polymers.¹ As a consequence of the alternation of the bond lengths the electronic energy states of the π -electrons are grouped into two energy bands separated by an energy gap, the lower band being full and the upper one empty. The states therefore resemble those found in solid-state semiconductors. This similarity is probably less superficial than that of an infinite system of apparently equal bonds to a metal. The possibilities of distortion of a linear system when empty states lie immediately above filled ones are obviously considerable^{2,3} and probably invalidate the analogy between such a system and a metal. In the case of alternating bond lengths, however, no difficulties arise near the Fermi surface, and it seems to be acceptable to apply to the system concepts derived from the theory of semiconductors.

One such concept is that of an electron state localized at a defect in the chain with energy lying in the region of the gap in the energy spectrum of the perfectly periodic structure. The importance of such states, especially in relation to electronic transport along the chain, is clear, and the effects to be expected can again be seen from analogies with conventional semiconductor theory.

A simple case of such defect states was treated by Pople and Walmsley,⁴ and more recently an application of the Green's function method of Slater and Koster,⁵ has been made to the polyene chain in the Hückel approximation by Kventsel and Kruglyak.⁶ The last named authors derive various conditions for the existence of localized states but restrict their treatment to cases where only the resonance integral or the Coulomb integral (but not both) changes at a defect. The method of Kventsel and Kruglyak⁶ could no doubt be extended to more complicated cases, but

multiple of $2\pi/a$ is identical with that for k ; it is therefore sufficient to consider only solutions in the range, $-\pi/a \leq k < \pi/a$. This region of "k-space" is the first Brillouin zone of the chain.

LOCALIZED STATES

Localized states can exist only if there is some defect in the perfect translational periodicity at which they can be localized. Such a defect will not necessarily produce a localized state but may do so if the perturbation of the potential is sufficiently great. If the change in the potential is appreciable only over a few atoms, the wave function of the localized state will extend into a region where the chain has reverted to its translational symmetry. In this region the localized state eigenfunction must satisfy the equations determining the solution in the perfectly periodic chain. However, solutions corresponding to complex k can now be admitted in such a way that the exponential variation involved is always a decay away from the defect. In the general case, k can lie anywhere in the complex plane, but it can be shown that, in the particular case where only nearest-neighbor interactions are included, the localized states in the energy gap will always have k of the form,

$$k = (\pi/a) + i\lambda \quad (2)$$

and those above or below the entire band system will have $k = \lambda$.

The parameter λ determines the rate of decay of the localized wavefunction at large distances from the defect. This is given by $e^{-\lambda r}$, where r is the distance from the defect.

The energy function outside the bands can be written in terms of λ as,

$$\epsilon(\lambda) = \alpha \pm (\beta_1^2 + \beta_2^2 \pm 2\beta_1\beta_2 \cosh \lambda a)^{1/2} \quad (3)$$

giving

$$\cosh \lambda a = \mp (\epsilon - \alpha)^2 \pm (\beta_1^2 + \beta_2^2)/2\beta_1\beta_2 \quad (4)$$

where the upper sign refers to states in the gap and the lower to states below the lower band or above the upper band.

In the gap $(\beta_1 - \beta_2) < \epsilon < (\beta_2 - \beta_1)$ and over this range of ϵ , $\cosh \lambda a$ has its maximum value when $\epsilon = \alpha$. Therefore, λ is greatest and the state localized over the smallest region at the center of the gap. The localization gets less towards the edges of the gap, until $\lambda = 0$ at the band edges. At the center of the gap

$$\cosh \lambda a = (\beta_1^2 + \beta_2^2)/2\beta_1\beta_2$$

and the value of λ determined by this equation gives the greatest degree of localization for any state in the gap irrespective of the nature of the defect.

The particular λ and ϵ values in a given case are determined in principle by solving the Schrödinger equation over the defect region in such a way that the "boundary conditions" when the solution extends into the un-

disturbed region are satisfied. Pople and Walmsley⁴ have solved the problem in this way for the case where the defect consists of a pair of equal bonds. In more general cases, when the region of perturbation becomes a little larger and the symmetry is not as simple, the equations involved in the direct approach become rather complicated. The simplicity of the matrix elements in the Hückel method is lost, and a transcendental equation for ϵ in terms of λ is obtained. Similar difficulties occur in the Green's function method.⁶

We have made a direct computation on finite rings of 40 to 56 atoms containing various types of defects. The specification of the parameters at the defects can then be made in accordance with the usual rules of Hückel theory without regard to the extent of the perturbation from perfect translational symmetry.

CHOICE OF PARAMETERS FOR THE PERFECT CHAIN

An average value of β appropriate for use in calculations of excited states can be obtained from data for the lowest π - π^* transitions of the first few members of the polyene series. Streitwieser⁸ recommends a value of 2.62 eV. The gap width, $2(\beta_1 - \beta_2)$ is related to the limiting value of the first π - π^* transition for infinite chain length, and Salem⁷ has estimated a value of 2.19 eV for this quantity. To obtain β_1 and β_2 separately requires one more equation. Evidently, β must lie between β_1 and β_2 , and it therefore seems reasonable to relate β to some kind of average of β_1 and β_2 . If the arithmetic mean

$$\beta = (\beta_1 + \beta_2)/2$$

is used, we obtain

$$\beta_1 = -3.17$$

$$\beta_2 = -2.07$$

If the geometric mean

$$\beta^2 = \beta_1\beta_2$$

is used, we get

$$\beta_1 = -3.23$$

$$\beta_2 = -2.13$$

The particular kind of average used does not therefore seem to be critical. The reason is that the difference, $\beta_1 - \beta_2$, is fairly small ($< 1/2$) compared to the average value. We have chosen to use the geometric mean, since this implies a stronger dependence of β on bond length. In the perfect chain therefore the upper and lower limits of the full band are -1.1 and -5.36 eV, respectively, and those of the empty band 5.36 and 1.1 eV. The computer program was checked by using it to calculate the energy levels in the undisturbed rings when all the eigenvalues were found to lie within the limits of the bands as given alone.

TYPES OF DEFECT AND CHOICE OF PARAMETERS

We are concerned mainly with situations where the polyene chains are in some kind of solid matrix, either crystalline or noncrystalline. In this type of situation we should expect that the introduction of well separated "point" defects into the system would have no long-range effects on the structure of the chain. We have therefore thought it reasonable to assume in all cases that changes in parameters are confined to the immediate vicinity of the defect.

We have considered three types of defect: (1) substitution for a hydrogen (substituents: Cl); (2) substitution for a carbon (substituents: N, O, B); (3) "misfits" in the alternating system (three short or three long bonds in sequence and two equal bonds).

In cases (1) and (2) we adopt the scheme summarized by Streitwieser⁸ for including a heteroatom X in a Hückel calculation. The Coulomb integral on the heteroatom is given by eq. (5):

$$\alpha_x = \alpha_0 + h_x \beta_0 \quad (5)$$

We take $\beta_0 = 2.62$ eV.

On atoms close to the heteroatom we make corrections to the Coulomb integrals via an auxiliary inductive parameter, i.e.

$$h_n = \delta^n h_x \quad (6)$$

where n is the number of bonds between X and the atom in question. Following Streitwieser we take $\delta = 0.1$. Only the correction for the case $n = 1$ is found to have an appreciable effect, but it has been included in the calculation for $n = 1, 2$.

The resonance integrals for the bonds ending on the heteroatom are modified by the equation,

$$\beta' = k_{ex} \beta$$

where β is β_1 or β_2 for a substitution in the chain and β_0 for an H substitution. The parameters h and k are taken from Streitwieser.

In case (2) the assumption that the overall system of bond alternations along the chain is not interrupted by the substitution is dependent on the chain being embedded in a solid matrix and therefore subject to external

TABLE I
Hückel Parameters for Substituents^a

	X	h_x	k_{ex}	α'	β_1'	β_2'	β_{xy}
Substituted for C	N	0.5	0.8	-1.31	-2.58	-1.70	—
	O	2.0	0.9	-5.24	-2.91	-1.92	—
	B	-1.0	0.7	2.62	-2.26	-1.49	—
Substituted for H	Cl	2.0	0.4	-5.24	-3.23	-2.13	-1.05

^a α' is the Coulomb integral on the substituent X and β_1' and β_2' are the modified values of the resonance integrals for the bonds ending on X. The last line refers to a substitution in the Y position, when X = C. The α' value then refers to the Y position.

constraints which maintain the overall conformation. Under these circumstances we can regard the heteroatom as a simple substitution for a carbon atom without any large-scale rearrangement of the bonding in the chain.

The values of the parameters used are shown in Table I, the energy levels and the corresponding λ value obtained with the maximum ring size in Table II, and the electron-density distributions in Table III. Some comments on the results are made in the next section. The case of the oxygen substitution is described in more detail as a typical example.

TABLE II
Energy and Extension of States Localized at Substituents^a

Substituent	States below the full band		States in the gap	
	ϵ	λa	ϵ	λa
N	—	—	1.02	0.16
O	-7.35	1.7	0.47	0.36
B	—	—	-0.63	0.34
Cl	-5.86	0.88	—	—

^a λa is calculated from eq. (4).

TABLE III
 π -Electron Densities near Substituents

Substituent	Atom ^a							
	Y	X	1 ₊	2 ₊	3 ₊	1 ₋	2 ₋	3 ₋
N	—	1.25	0.82	1.00	0.94	1.02	0.98	1.00
O	—	1.72	0.83	1.02	1.00	1.05	1.00	1.00
B	—	-0.33	0.98	0.97	0.97	0.98	0.98	1.00
Cl	1.99	0.86	0.94	0.97	0.99	0.69	0.85	0.92

^a The atoms are specified in the notation illustrated in Fig. 1.

RESULTS

Oxygen

Two localized states are found, one in the gap at 0.47 eV and the other below the lower band at -7.35 eV. The convergence of these energies on the values quoted as the ring size is increased from 42 to 56 atoms leads to a value of ± 0.01 as an estimate of the accuracy with which the results for an infinite chain are being reproduced.

By counting the number of states found in the various regions of the spectrum we are led to the conclusion that the state at -7.35 eV can be regarded as split off the lower band by the perturbation and that the state at 0.47 eV is split off the upper band; i.e., both bands contain one fewer state. Since oxygen contributes one extra π -electron to the conjugated system the state in the gap will contain one electron. The gap state is too far removed from either of the band edges to act as a donor or acceptor state. However, if we are interested in the common case where electronic transport properties are studied by injecting electrons into the conduction band of the polymer from a metal cathode, then the half-filled gap state

could have an important role as a low-lying trap for conduction electrons. This state might therefore be classified in solid state terminology as a deep trap.

The electron density is asymmetric about the O atom as a consequence of the preservation in the calculation, of the fundamental asymmetry of the alternating chain. It should be noted that to calculate the electron distribution it is necessary to know the wave function of the full localized state below the lower band.

Nitrogen

A localized state is produced in the gap near the bottom of the upper band. The decay of the atomic orbital coefficients and the variation of the eigenvalue with ring size have been investigated closely in this case to confirm that this is a genuine localized state and does not belong to the upper band. The state is empty and therefore provides a shallow trap.

Chlorine

One π -orbital from the chlorine atom replacing an H atom is included in the conjugated system. It is found that a localized state is produced below the lower band which is in this case an additional state and accommodates the two extra π -electrons. No state appears in the gap. According to Koster and Stater,⁵ this behavior can be found only when Coulomb and resonance integrals near the defect are simultaneously changed. It might have been expected that an electrophilic substituent like Cl might also have split a state off the bottom of the upper band to give a gap state. The absence of such a state indicates that an isolated chlorine impurity has little effect on the electronic behavior along the chain. The same conclusion should apply *a fortiori* to Br and I.

Bond Distortions

Pople and Walmsley⁴ dealt with the case where one of the shorter bonds is omitted. There are then two long bonds in sequence, and the whole chain is symmetric about the atom on which the two adjacent long bonds meet. In this case they deduced that a localized level is found in the gap.

Kventsel and Kruglyak⁶ have deduced formulae which give the energy levels when the resonance integral for one bond is varied. Of three cases described here, the second and third are covered by their formulae, and the computer results in these cases merely confirm their analysis.

There is a certain arbitrariness about introducing bond distortions which

TABLE IV
Bond Distortions

Type of distortion ^a	Energies of localized states, eV
1	1.003, -1.003
2	1.026, -1.026
3	-0.956, 0.956

^a Type 1, two equal bonds with resonance integral β_0 ; type 2, three equal short bonds; type 3, three equal long bonds.

might arise as a result of external influences on the chain, and we have therefore chosen what we consider to be three extreme examples of altered bonds to examine the maximum effects which might be observed.

In the first case we have taken two successive equal bonds with a resonance integral equal to 2.62 eV. In the second case we assume that there are three equal short bonds in sequence; in the third case we assume that there are three equal long bonds.

The results are shown in Table IV. In each case a pair of localized states is produced in the gap symmetrically placed in energy about $\epsilon = \alpha$ each one being ca. 0.1 eV from one of the band edges. These energy differences between localized state and band edge are of the same order as those found by Pople and Walmsley⁴ for the case of a mismatch. However, it seems likely that bond distortions would normally be much smaller than those we have considered. This is because the defects considered here are strictly localized and do not necessitate a displacement of the whole chain as in the case of Pople and Walmsley. We therefore suggest that variations in the bond lengths to which linear chains (as opposed to three-dimensional crystals) are subject will produce a spectrum of localized states in the energy gap extending from the band edges to an energy of about 0.1 eV into the gap.

CONCLUSION

We have examined, sometimes admittedly in a heuristic manner, a variety of possible defects in an infinite linear chain with alternating bond lengths. None of the structures considered has produced states suitably occupied and suitably placed in energy to act as thermally activated donors and acceptors. In a number of cases, traps close to the band edges are likely to exist, and in the case of oxygen, a deep trap near the middle of the gap. The maximum degree of localization of any state in the gap is determined by the factor $\exp\{-0.42\}$ which gives the rate of decay at the center of the gap. It is hoped that these computations will serve as a guide for more accurate self-consistent calculations on polymer molecules with alternating bond lengths.

References

1. H. A. Pohl, in *Electrical Conduction Properties of Polymers* (*J. Polym. Sci. C*, **17**), A. Rembaum and R. F. Landel, Eds., Interscience, New York, 1967, p. 13.
2. H. C. Longuet-Higgins and L. Salem, *Proc. Roy. Soc. (London)*, **A251**, 172 (1959).
3. Y. Ooshika, *J. Phys. Soc. Japan*, **14**, 747 (1959).
4. J. A. Pople and S. H. Walmsley, *Mol. Phys.*, **5**, 15 (1962).
5. G. F. Koster and J. C. Slater, *Phys. Rev.*, **95**, 1167 (1954).
6. G. F. Kventzel and Y. A. Kruglyak, *Theoret. Chem. Acta*, **12**, 1 (1968).
7. L. Salem, *Molecular Orbital Theory of Conjugated Systems*, Benjamin, New York, 1966.
8. A. Streitwieser, *Molecular Orbital Theory for Organic Chemists*, Wiley, New York, 1961.

Received September 11, 1970

Revised November 12, 1970

Generalizations of the Diffusion Equation

P. F. LESSE, *C.S.I.R.O. Division of Forest Products,
Melbourne, Victoria, Australia 3205*

Synopsis

The mass flux entering the Fick's diffusion equation is considered as an arbitrary analytical function of concentration, concentration gradient, and of the gradient of concentration gradient. The restrictions imposed on the flux by the principle of material objectivity are stated and briefly discussed.

INTRODUCTION

The transport of small organic molecules in polymers appears to depend very strongly on temperature and the activity of the penetrant. It has been suggested that, for low penetrant activities and high temperatures, concentration-independent (Fickian) diffusion usually takes place, whereas for high activities and low temperatures (below the glass temperature) case II diffusion is observed.^{1,2} These regions are separated by domains of anomalous (time-dependent) diffusion and concentration-dependent diffusion (i.e. diffusion which can be described by Fick's equation with diffusivity dependent on time or concentration). To describe the characteristic features of case II diffusion there has been proposed a generalization of Fick's diffusion equation³ which was solved⁴ and the solution was found to be in agreement with experimental investigations.⁵ The generalization consisted of adding a term dependent on concentration to Fickian mass flux J so that the new flux J' is

$$J' = -D(c) \frac{\partial c}{\partial x} + B(c)Sc$$

where c is concentration of penetrant $D(c)$, $B(c)$ are functions of concentration, and S is constant.

In this paper I try to find the restrictions imposed by the principle of material objectivity^{6a,7a,8a} or material indifference on a mass flux which is concerned to be an arbitrary analytical function of concentration, concentration gradient and of the gradient of concentration gradient.

General Form of Objective Flux of Mass

Fick's diffusion equation is obtained by combining the equation of conservation of mass with an assumption

$$\rho_\alpha u_\alpha = -D \text{grad } \rho_\alpha$$

where ρ_α is the density of the diffusing component α , u_α is its diffusion velocity and $D(\rho_\alpha)$ is the diffusivity.^{6b}

The quantity $J_\alpha = \rho_\alpha u_\alpha$ is called the flux of mass of component α .

The equation of conservation of mass subject to the usual assumptions of the diffusion theory (uniform total density and negligible mean velocity of the mixture^{6c} can be written:

$$(\partial c_\alpha / \partial t) + \operatorname{div} J_\alpha = 0$$

where $c_\alpha = (\rho_\alpha / \sum \rho_\alpha)$ is the concentration of component α .

From the definition of the flux J_α it follows that it is an objective quantity which is invariant with respect to changes of the frame of reference or observer. The requirements of invariance with respect to the frame of reference was formulated as a principle of material objectivity or material frame indifference.^{6d, 8a}

Let us assume that the flux J_α in a very general theory of diffusion is a function of concentration, concentration gradient, and of the gradient of concentration gradient:

$$J_\alpha = J_\alpha(c_\alpha, \operatorname{grad} c_\alpha, \operatorname{grad} \operatorname{grad} c_\alpha) \quad (1)$$

The principle of material frame indifference requires that the equation

$$QJ_\alpha = J_\alpha(c_\alpha, Q \operatorname{grad} c_\alpha, Q \operatorname{grad} \operatorname{grad} c_\alpha Q^T)$$

be valid for any orthogonal tensor Q and its transpose Q^T . Vector-valued functions having this property are called isotropic.^{7b, 8b}

Any isotropic function of the type (1) can be represented in the form^{8c}

$$J_\alpha = (\phi_0 I + \phi_1 \operatorname{grad} \operatorname{grad} c_\alpha + \phi_2 \cdot [\operatorname{grad} \operatorname{grad} c_\alpha]^2) \operatorname{grad} c_\alpha \quad (2)$$

where I is the unit tensor and ϕ_0 , ϕ_1 , ϕ_2 are the functions of concentration, of the three invariants of the tensor $\operatorname{grad} \operatorname{grad} c_\alpha$ and of invariants $\operatorname{grad} c_\alpha \cdot \operatorname{grad} c_\alpha$, $\operatorname{grad} c_\alpha \cdot \operatorname{grad} \operatorname{grad} c_\alpha \cdot \operatorname{grad} c_\alpha$, $\operatorname{grad} c_\alpha \cdot (\operatorname{grad} \operatorname{grad} c_\alpha)^2 \cdot \operatorname{grad} c_\alpha$.

We have thus arrived at the following conclusion:

Any objective function J_α given by equation (1) can be represented by eq. (2).

Discussion

Let us consider a special case

$$J = J(c, \operatorname{grad} c) \quad (3)$$

From eq. (2) it follows:

$$J = \phi_0(c, \operatorname{grad} c \cdot \operatorname{grad} c) \cdot \operatorname{grad} c$$

If ϕ_0 can be developed in power series in $\operatorname{grad} c \cdot \operatorname{grad} c$ we obtain:

$$J = [\psi_0(c) + \psi_1(c) \operatorname{grad} c \cdot \operatorname{grad} c + \psi_2(c)(\operatorname{grad} c \cdot \operatorname{grad} c)^2 + \dots] \operatorname{grad} c \quad (4)$$

If c_α is a function of only one coordinate x , say,

$$J_x = \psi_0(c)(\partial c/\partial x) + \psi_1(c)(\partial c/\partial x)^3 + \psi_2(c)(\partial c/\partial x)^5 + \dots \quad (4a)$$

The first term obviously corresponds to Fickian diffusion; on the other hand, the assumptions of the type

$$J_x = \psi(c)(\partial c/\partial x)^n \quad n = 2, 3, \dots \quad (4b)$$

can also be found in the literature, and the corresponding process was named n -diffusion.⁹

It follows from eq. (4a) that only odd n are compatible with material objectivity.

The generalizations of Fick's equation based on equations of the type (3) thus lead to polynomial n -diffusion (with odd n).

On the other hand, a flux J' of the type

$$J' = f_1(c) \text{ grad } c + f_2(c)$$

cannot be obtained from eq. (2), and hence it should be incompatible with the requirement of material objectivity.

Let us consider the more general case including the dependence on $\text{grad grad } c$.

By developing the functions $\varphi_0, \varphi_1, \varphi_2$ in eq. (2) in power series in the above-mentioned invariants we obtain:

$$J = w_1(c) \text{ grad } c + w_2(c) \text{ grad grad } c \cdot \text{grad } c + w_3(c) \text{ tr}(\text{grad grad } c) \cdot \text{grad } c + \dots \text{ (more complicated terms)} \quad (5)$$

where the $\text{tr}(\quad)$ term denotes the trace (sum of diagonal components) of a tensor.

This becomes in the one dimensional case

$$J_x = w_1(c) \frac{\partial c}{\partial x} + [w_2(c) + w_3(c)] \frac{\partial^2 c}{\partial x^2} \frac{\partial c}{\partial x} + \dots \text{ (more complicated terms)} \quad (5a)$$

which is a different type of generalization.

Both eqs. (4a) and (5a) appear to lead to nonlinear generalizations of Fick's diffusion equations even if $\psi_0, \psi_1, \dots, w_1, w_2, \dots$ do not depend on concentration. We have therefore to conclude that the only objective flux which can lead to linear diffusion equations is the "classical" $J = -D \text{ grad } c$ and the simple generalizations based on equations of the type (1) are hence not very advantageous. On the other hand, there are exact generalizations of the Fick's equation derived by using the laws of rational mechanics and thermodynamics to be found in the literature.¹⁰⁻¹³

References

1. H. B. Hopfenberg and H. L. Frisch, *J. Polym. Sci. B*, **7**, 405 (1969).
2. T. Alfrey Jr., E. F. Gurnee, and W. G. Lloyd, in *Perspectives in Polymer Science J. Polym. Sci. C*, **12**), E. S. Proskauer, E. H. Immergut, and C. G. Overberger, Eds., Interscience, New York, 1966, p. 249.
3. H. L. Frisch, T. T. Wang, and T. K. Kwei, *J. Polym. Sci. A-2*, **7**, 879 (1969).
4. T. T. Wang and T. K. Kwei, *J. Polym. Sci. A-2*, **7**, 2019 (1969).
5. T. K. Kwei and H. M. Zupko, *J. Polym. Sci. A-2*, **7**, 867 (1969).
6. C. Truesdell and R. A. Toupin, in *Encyclopaedia of Physics*, S. Flügge, Ed., Vol. III/1, Springer, Berlin-Göttingen-Heidelberg, 1960, (a) p. 702; (b) Sect. 159, 295; (c) p. 706; (d) Sect. 293.
7. D. C. Leigh, *Nonlinear Continuum Mechanics*, McGraw-Hill, New York, 1968, (a) p. 143; (b) p. 70.
8. C. Truesdell and W. Noll, in *Encyclopaedia of Physics*, S. Flügge, Ed., Vol. III/3, Springer, Berlin-Heidelberg-New York, 1965, (a) Sect. 19; (b) Sect. 8; (c) p. 35.
9. J. R. Philip, *Austral. J. Phys.*, **14**, 1 (1961).
10. I. Müller, *Arch. Rational Mech. Anal.*, **28**, 1 (1968).
11. A. E. Green and P. M. Naghdi, *Int. J. Eng. Sci.*, **3**, 231 (1965).
12. A. E. Green and J. E. Adkins, *Arch. Rational Mech. Anal.*, **15**, 235 (1967).
13. M. J. Crochet and P. M. Naghdi, *Int. J. Eng. Sci.*, **4**, 283 (1966).

Received July 27, 1970

Revised October 8, 1970

NOTES

**Calculation of Long-Chain Branching Distribution
from Combined GPC, Sedimentation, and
Intrinsic Viscosity Experiments**

We have presented a method¹ for the determination of long-chain branching distribution from concurrent gel-permeation chromatography (GPC) and sedimentation velocity experiments. In the method, a two-dimensional distribution function is used; the calculation is therefore cumbersome and tedious. For a special class of branched samples this long method can be avoided. We describe in the following a simplified calculation scheme.

In sedimentation velocity experiments the relation among sedimentation constant S , hydrodynamic radius at theta temperature R , and molecular weight M , is given by

$$S = K_s M / R \quad (1)$$

where K_s is a constant. For linear molecules at the theta temperature, M is proportional to R^2 :

$$M = K_r R^2 \quad (2)$$

and hence

$$S = K_s K_r^{-0.5} M^{0.5} \quad (3)$$

Equation (3) is the relation used for correlating molecular weight and sedimentation constant of linear molecules. If the polymer contains branches we may only obtain an apparent molecular weight M_s from this relation, thus:

$$M_s = S^2 / K_s^2 K_r \quad (4)$$

In GPC experiments the retention volume is a measure of the hydrodynamic volume² of the chains in solution. We shall assume as we did before¹ that there is a one-to-one correspondence between the hydrodynamic volume in a good solvent and that in a theta solvent regardless of the degree of branching. Using the calibration curve for linear molecules, if the chains are branched, we may obtain from GPC another apparent molecular weight M_r :

$$M_r = K_r R^2 \quad (5)$$

The hydrodynamic radius in eq. (5) now is the hydrodynamic radius for the branched chain in a theta solvent. If the sample is monodisperse, we may thus obtain from sedimentation velocity and GPC experiments two distinct apparent molecular weights. Substituting eqs. (4) and (5) in eq. (1) we obtain the true molecular weight M , for the sample

$$M = (M_r M_s)^{0.5} \quad (6)$$

For linear samples we have the identities

$$M_r = M = M_s$$

and for branched samples

$$M_r < M < M_s$$

A parameter h used by Stockmayer and Fixman³ to relate experimental results to branched-chain statistics is the ratio

$$h = R/R_L \quad (7)$$

where R_L is the hydrodynamic radius of a linear chain having the same molecular weight as the branched chain. From eqs. (2) and (6) we find that

$$R_L^2 = (M_r M_s)^{0.5} / K_r \quad (8)$$

By combining eqs. (5), (7), and (8) we obtain

$$h^2 = (M_r / M_s)^{0.5} \quad (9)$$

For a polydisperse sample we obtain from GPC a distribution of apparent molecular weight M_r . Let $F(M_r)$ denote such a distribution function. Similarly from sedimentation velocity measurement we obtain a distribution $G(M_s)$ of the apparent molecular weight M_s . For linear polydisperse samples these two distribution functions are the same and identical with the true molecular weight distribution $W(M)$. For branched samples these three distribution functions are different.

We may construct two integral distributions, $F_1(M_r)$ and $G_1(M_s)$, for the apparent molecular weights M_r and M_s :

$$F_1(M_r) = \int_0^{M_r} F(M_r) dM_r \quad (10)$$

$$G_1(M_s) = \int_0^{M_s} G(M_s) dM_s \quad (11)$$

As the distribution functions $F(M_r)$ and $G(M_s)$ are normalized, $F_1(M_r)$ and $G_1(M_s)$ both vary from 0 to 1. Let subscript 1 and 2 represent two incremental amounts of material in the sample. If we have for any two incremental amounts when

$$(M_r)_2 > (M_r)_1$$

the relation

$$(M_s)_2 > (M_s)_1$$

then each and every point on $F_1(M_r)$ will represent the same increment of material as that represented by the corresponding point on $G_1(M_s)$. This condition is likely to be satisfied for samples in which the degree of branching increases monotonically with molecular weight. If branching does not increase monotonically with molecular weight then we will definitely find in the sample incremental amounts of material for which the order of the apparent molecular weights is reversed.

If the above condition is satisfied then we may compute, using eqs. (6) and (9), the corresponding true molecular weight M and the parameter h^2 for every point on the integral distribution curves. The relation between h^2 and M is thus obtained. From the chain statistics provided by Stockmayer and Fixman we may obtain the distribution of branching as a function of M . An integral distribution of true molecular weight can also be easily constructed as illustrated in Figure 1. The distribution of true molecular weight $W(M)$ can be obtained by differentiation.

Recently, GPC units equipped with automatic viscometers have been reported by Meyerhoff⁴ and by Goedhard and Opschoor.⁵ The formulation given above can be used to calculate branching distribution from concurrent intrinsic viscosity and GPC experiments. For linear chains the relationship between molecular weight and intrinsic viscosity is given by the Mark-Houwink relation

$$[\eta] = KM^\alpha \quad (12)$$

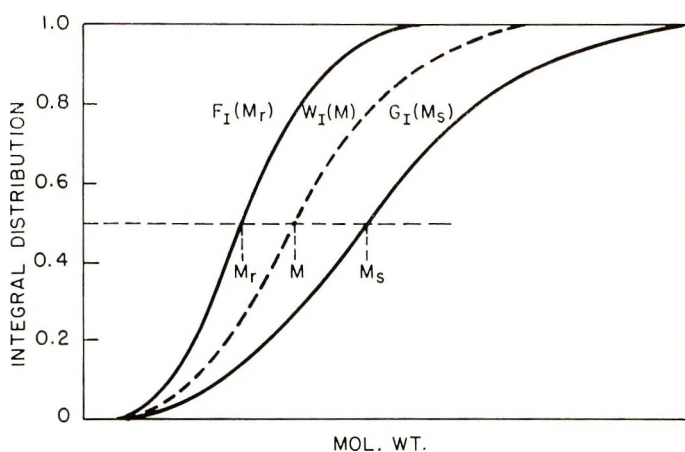


Fig. 1. Method of constructing the integral molecular weight distribution function $W_I(M)$.

An apparent molecular weight M_e can be computed from eq. (12) for monodisperse branched samples,

$$M_e = ([\eta]/K)^{1/\alpha} \quad (13)$$

In GPC experiments Grubisic, Rempp, and Benoit² have shown that the product $M[\eta]$ is a function of the retention volume. For linear chains this product can be expressed as $KM^{\alpha+1}$. For branched samples the relation between the apparent GPC molecular weight M_r and the true molecular weight is thus

$$M = KM_r^{\alpha+1}/[\eta] \quad (14)$$

From eqs. (13) and (14) we obtain

$$M = M_r(M_r/M_e)^\alpha \quad (15)$$

For linear chains we have now the identities

$$M = M_r = M_e$$

and for branched chains

$$M > M_r > M_e$$

For the present data system it is more convenient to use the parameter g to relate experimental data with branched chain statistics. The parameter g is defined as the ratio of the unperturbed mean square radii of the branched and linear chains of identical molecular weight. Zimm and Kilb⁶ have derived the relation between g and intrinsic viscosity as

$$g^{1/2} = [\eta]/[\eta]_L \quad (16)$$

where $[\eta]_L$ is the intrinsic viscosity of a linear chain having the same molecular weight as the branched chain. Combining eqs. (12), (13), and (15), we obtain

$$g^{1/2} = (M_e/M_r)^{(\alpha+1)\alpha} \quad (17)$$

For the polydisperse samples we may construct the integral distributions of the GPC apparent molecular weight M_r and the viscosity apparent molecular weight M_e . If the degree of branching in the sample increases monotonically with molecular weight we may

again have the one-to-one correspondence between the two integral distributions. Equations (15) and (17) can now be used to construct the distribution of branching and the true molecular weight distribution function.

The condition required for a branched sample to be treated by this simplified method is not a very restrictive one. Many chain-branching mechanisms do promote more branches for chains of higher molecular weight in the sample. Low-density polyethylene is an excellent example.

References

1. L. H. Tung, *J. Polym. Sci. A-2*, **7**, 47 (1969).
2. Z. Grubisic, P. Rempp, and H. Benoit, *J. Polym. Sci. B*, **5**, 753 (1967).
3. W. H. Stockmayer and M. Fixman, *Ann. N. Y. Acad. Sci.*, **57**, 334 (1953).
4. G. Meyerhoff, paper presented at the 159th American Chemical Society Meeting, Houston, February 1970.
5. D. Goedhart and A. Opschoor, *J. Polym. Sci. A-2*, **8**, 1227 (1970).
6. B. H. Zimm and R. W. Kilb, *J. Polym. Sci.*, **37**, 19 (1959).

L. H. TUNG

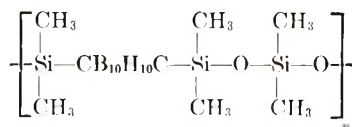
Physical Research Laboratory
The Dow Chemical Company
Midland, Michigan 48640

Received August 17, 1970

Revised October 19, 1970

***Ultrasonic Propagation in the Vicinity of the Glass
Transition of a Poly(Carborane Siloxane)***

Measurements were made of ultrasonic propagation in a poly(metacarborane siloxane) as a function of temperature and frequency. The polymer used in these measurements had the structure:



The polymer was crosslinked but had no fillers.

Two specimens were used, one $5 \times 5 \times 1.34$ cm in size and the other $5 \times 5 \times 2.67$ cm. Ultrasonic measurements were made by using the liquid-immersion technique.¹ The specimen was held between two transducers, all immersed in an ethylene glycol-water mixture. Pulses of ultrasound were sent from one transducer to the other and measurements were made of the time of flight and amplitude of the pulses with and without the specimen in the path of the sound beam. From a knowledge of the speed of sound in the immersion liquid, the longitudinal speed of sound and absorption in the specimen were calculated.

Results of these measurements as a function of temperature at 650 kHz are shown in Figure 1. Two changes in slope of the speed of sound curve are observed. The lower temperature change is observed at -38°C , close to the reported² dilatometric glass transition temperature. The position of this change in slope did not vary with frequency. The higher temperature change in Figure 1 occurs at 2°C and shifts to -1°C at 240 kHz and to -9°C at 92 kHz. Using these values on an Arrhenius plot of log frequency versus reciprocal temperature yields an activation energy of 25 kcal/mole. While the result is not as accurate, a similar plot using the absorption peak yields an activation energy of 20 kcal/mole.

The lower temperature change in slope is related to the change in thermal expansion coefficient at the glass transition temperature, as pointed out by Work.³ It has been shown^{3,4} that the temperature at which the slope changes is the glass transition temperature and is independent of frequency.

As clearly pointed out for liquids,⁵ the bulk modulus is made up of two parts: a lattice spacing part and a structural rearrangement part. Structural rearrangements take a finite amount of time (the relaxation time) to occur, and therefore this part of the modulus is frequency dependent. Furthermore, the structural relaxation time depends on the temperature of the material. The higher temperature change in slope is the point at which the structural relaxation time becomes small compared to the period of the sound wave. Thus, the frequency dependence of this point is related to the temperature dependence of the relaxation time. Assuming the relationship is of the Arrhenius type, our measurements above yield the activation energy for structural rearrangements.

Although the data below the glass transition is scarce (because the immersion liquid solidified in this region), we can estimate the slope of the sound speed below -38°C . Below the glass transition, the slope of the sound speed is approximately -4.3 m/sec $^\circ\text{C}$, while above 2°C the slope is -6.95 m/sec $^\circ\text{C}$. We define β , the temperature coefficient of the sound speed u , as

$$\beta = -(1/u)(\partial u/\partial T)_p \quad (1)$$

We recall that Rao⁶ found a simple relation between β and the thermal expansion coefficient, α . Rao found empirically that for many liquids

$$n \equiv \beta/\alpha = 3 \quad (2)$$

In applying Rao's rule to polymers, Wada⁴ found that while n might be greater than 10,

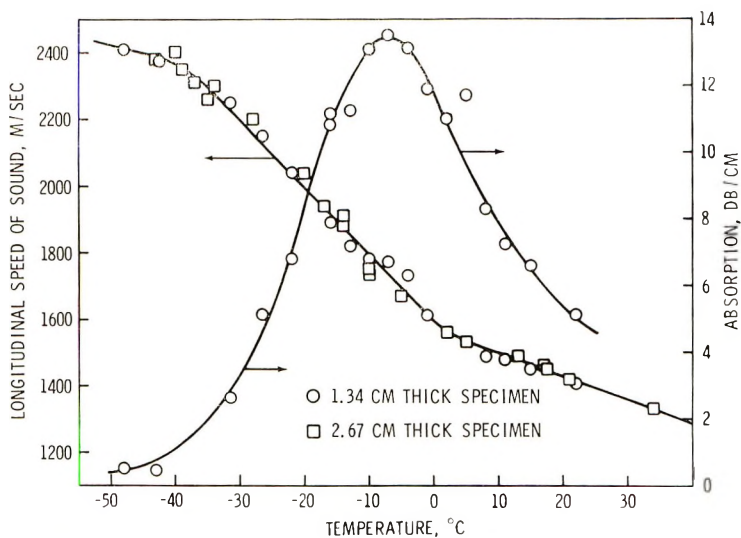


Fig. 1. Ultrasonic properties of a poly(carborane siloxane) at 650 kHz: (○) 1.34 cm thick specimen; (□) 2.67 cm thick specimen.

it had the same value just above the glass transition, n^+ , and just below, n^- . Wada's rule is therefore

$$n^- = n^+ \quad (3)$$

Table I illustrates Wada's rule. Data for the first four polymers were taken from Wada's paper. The n values are approximately the same above and below the glass transition even though they vary by a factor of three from polymer to polymer. [Schuyer⁷ has suggested that high values of n result from using the longitudinal speed of sound in eq. (1) rather than the bulk speed of sound, as Rao used. These considerations do not affect the results here, as we are not interested in the magnitude of n , only in the comparison of n above and below the glass transition.] Also in Table I are our β values obtained from measurements on isotactic polypropylene, which measurements were made to check

TABLE I
Values of n for Various Polymers^a

Polymer	$\beta \times 10^4, \text{deg}^{-1}$	$\alpha \times 10^4, \text{deg}^{-1}$	$n = \beta/\alpha$
Polystyrene	9.4	2.2	4.3
	23.8	5.3	4.5
Poly(methyl methacrylate)	14.5	3.4	4.3
	24.2	5.1	4.7
Nylon 6	32	2.6	12.5
	49	3.9	12.5
Poly(vinyl chloride)	28	3.4	8.3
	57	5.7	10.0
Polypropylene	26	2.4	10.8
	58	6.8	8.5
Carborane	18	4.3	4.2
	30	8.3	3.6

^a For each polymer, the upper row gives the values below the glass transition and the lower row the values above the glass transition.

our experimental technique. The glass transition temperature we determined for polypropylene was 15°C, in good agreement with the value of approximately 20°C determined⁸ for the noncrystallized isotactic chains in polypropylene. Also, the measured sound speed as a function of temperature for polypropylene is in satisfactory agreement with measurements made by Wada⁸ and by Eby.⁹ The α values for polypropylene in Table I are literature¹⁰ values for atactic polypropylene. The values of n are fairly close, showing that polypropylene is another polymer which obeys Wada's rule.

Our measured values of β for the carborane are given in the last line of Table I, along with literature values² for α . The β values were calculated by using the sound speed at the glass transition temperature, 2350 m/sec, and the slopes below -38°C and above 2°C. As can be seen, the carborane polymer also obeys Wada's rule.

The specimens used were supplied by the Olin Mathieson Chemical Corporation, New Haven, Connecticut. This work was sponsored by the Office of Naval Research.

References

1. Y. Maeda, *J. Polym. Sci.*, **18**, 87 (1955).
2. L. H. Sperling, S. L. Cooper, and A. V. Tobolsky, *J. Appl. Polym. Sci.*, **10**, 1725 (1966).
3. R. N. Work, *J. Appl. Phys.*, **27**, 69 (1956).
4. Y. Wada and K. Yamamoto, *J. Phys. Soc. Japan*, **11**, 887 (1956).
5. T. A. Litovitz and T. Lyon, *J. Acoust. Soc. Amer.*, **30**, 856 (1958).
6. M. Rao, *J. Chem. Phys.*, **9**, 682 (1941).
7. J. Schuyer, *J. Polym. Sci.*, **36**, 475 (1959).
8. Y. Wada, Y. Hotta, and R. Suzuki, in *Macromolecular Chemistry, Tokyo-Kyoto 1966* (*J. Polym. Sci. C*, **23**), I. Sakurada and S. Okamura, Eds., Interscience, New York, 1968, p. 583.
9. R. K. Eby, *J. Chem. Phys.*, **37**, 2785 (1962).
10. E. Passaglia and G. M. Martin, *J. Res. Nat. Bur. Stand.*, **68A**, 273 (1964).

BRUCE HARTMANN
JACEK JARZYNSKI*

U.S. Naval Ordnance Laboratory
White Oak, Silver Spring, Maryland 20910

Received July 14, 1970

Revised November 17, 1970

* Also affiliated with American University, Washington D.C. 20016.

INFORMATION FOR CONTRIBUTORS

This Journal Does Not Carry a Page Charge for Contributions

1. Manuscripts should be submitted to H. Mark, Polytechnic Institute of Brooklyn, 333 Jay Street, Brooklyn, New York 11201, or for Part A-1 (Polymer Chemistry) to C. G. Overberger, Department of Chemistry, University of Michigan, Ann Arbor, Michigan 48104, or for Part A-2 (Polymer Physics) to T. G. Fox, Mellon Institute, Pittsburgh, Pennsylvania 15213. Address all other correspondence to Periodicals Division, Interscience Publishers, John Wiley & Sons, Inc., 605 Third Avenue, New York, New York 10016.
2. It is the preference of the Editors that papers be published in the English language. However, if the author desires that his paper be published in French or German, it is necessary that a particularly complete and comprehensive English synopsis be furnished.
3. Manuscripts should be submitted in triplicate (one *original*, two carbon copies), typed *double space* throughout and on one side of each sheet only, on a *heavy* grade of paper with margins of at least one inch on all sides.
4. A short synopsis (maximum length 200 words) is required for papers in Parts A-1 and A-2. No synopsis is published for Part B or for "Notes" in Parts A. This synopsis should be carefully prepared, for it is automatically the source of most abstracts. The Synopsis should be a summary of the entire paper; not the conclusions alone.
5. The paper should be reasonably subdivided into sections and, if necessary, subsections. Please refer to any issue of this *Journal* for examples.
6. The references should be numbered consecutively in the order of their appearance and should be complete, including authors' initials and—for unpublished lectures or symposia—the title of the paper, the date, and the name of the sponsoring society. Please compile references on a separate sheet at the end of the manuscript. Abbreviations of journal titles should conform to the practices of *Chemical Abstracts*.
7. Please supply numbers and titles for all tables. All table columns should have an explanatory heading.
8. It is particularly important that all figures be submitted in a form suitable for reproduction. Good glossy photographs are required for halftone reproductions. For line drawings (graphs, etc.), the figures must be drawn clearly with India ink on heavy white paper, Bristol board, drawing linen, or coordinate paper with a very light blue background. The India ink lettering of graphs must be large, clear, and "open" so that letters and numbers do not fill in when reduced for publication. It is the usual practice to submit drawings that are twice the size of the final engravings; the maximum final size of figures for this *Journal* is $4\frac{1}{2} \times 7\frac{1}{2}$ inches.
It is the author's responsibility to obtain written permission to reproduce material which has appeared in another publication.
If in doubt about the preparation of illustrations suitable for reproduction, please consult the publisher at the address given above in paragraph 1 and ask for a sample drawing.
9. Please supply legends for all figures and compile these on a separate sheet.
10. Authors are cautioned to type—wherever possible—all mathematical and chemical symbols, equations, and formulas. If these must be handwritten, please print clearly and leave ample space above and below for printer's marks; please use only ink. All Greek or unusual symbols should be identified in the margin the first time they are used. Please distinguish in the margins of the manuscript between capital and small letters of the alphabet wherever confusion may arise (e.g., k, K, κ). Please underline with a wavy line all vector quantities. Use fractional exponents to avoid root signs.
The nomenclature sponsored by the International Union of Chemistry is requested for chemical compounds. Abbreviations should follow the American Chemical Society *Handbook for Authors*. Chemical bonds should be correctly placed, and

JOURNAL OF POLYMER SCIENCE

- double bonds clearly indicated. Valence is to be indicated by superscript plus and minus signs.
11. Authors will receive 50 reprints of their articles without charge. Additional reprints can be ordered and purchased by filling out the form attached to the galley proof. Page proofs will not be supplied.
 12. No manuscript will be returned following publication unless a request for return is made when the manuscript is originally submitted.

Manuscripts and illustrations not conforming to the style of the *Journal* will be returned to the author for reworking, thus delaying their appearance.

The *Journal of Polymer Science* publishes results of fundamental research in all areas of high polymer chemistry and physics. The *Journal* is selective in accepting contributions on the basis of merit and originality. It is not intended as a repository for unevaluated data. Preference is given to contributions that offer new or more comprehensive concepts, interpretations, experimental approaches, and results. Part A-1 *Polymer Chemistry* is devoted to studies in general polymer chemistry and physical organic chemistry. Contributions in physics and physical chemistry appear in Part A-2 *Polymer Physics*. Contributions may be submitted as full-length papers or as "Notes." Notes are ordinarily to be considered as complete publications of limited scope.

Three copies of every manuscript are required. They may be submitted directly to the editor: For Part A-1, to C. G. Overberger, Department of Chemistry, University of Michigan, Ann Arbor, Michigan 48104; and for Part A-2, to T. G. Fox, Mellon Institute, Pittsburgh, Pennsylvania 15213. Three copies of a short but comprehensive synopsis are required with every paper; no synopsis is needed for notes. Books for review may also be sent to the appropriate editor. Alternatively, manuscripts may be submitted through the Editorial Office, c/o H. Mark, Polytechnic Institute of Brooklyn, 333 Jay Street, Brooklyn, New York 11201. All other correspondence is to be addressed to Periodicals Division, Interscience Publishers, a Division of John Wiley & Sons, Inc., 605 Third Avenue, New York, New York 10016.

Detailed instructions on preparation of manuscripts are given frequently in Parts A-1 and A-2 and may also be obtained from the publisher.

Coming soon from Wiley-Interscience—

The Second Edition of the Most Comprehensive Book in the Field of Polymer Science

TEXTBOOK OF POLYMER SCIENCE

Second Edition

By FRED W. BILLMEYER, JR., *Rensselaer Polytechnic Institute*

In the last 50 years, the field of polymer science has developed into a discipline essential to most aspects of our modern technology. Because this development has been so rapid, it has been difficult for educational systems and texts to keep pace. *Textbook of Polymer Science* was originally published in 1962 to help fill this gap, and this new Second Edition continues to supply up-to-date information on the field.

To up-date the original treatment of the theory and practice of all major phases of polymer science, engineering, and technology, the author has made extensive revisions and additions throughout the entire work.

Part I:

An introduction to concepts and characteristics of macromolecules, Part I now includes material on solubility parameters, free-volume theories of polymer solution thermodynamics, gel-permeation chromatography, vapor-phase osometry, and scanning electron microscopy.

Part II:

The advances gained from new data on the crystalline nature of polymers are now treated in a thorough discussion of the structure and properties of bulk polymers.

Part III:

The format and content of Part III, concerned with polymerization kinetics, have been revised to include recent advances and new references, as well as further data and explanations of recently discovered processes.

Part IV:

The material on commercially important polymers has been rearranged, and now includes information on aromatic heterochain, heterocyclic, ladder, and inorganic polymers.

Part V:

The comprehensive discussion of polymer processing in Part V now includes many new references for plastics, fiber, and elastomer technology.

1971 In Press

wiley

WILEY-INTERSCIENCE

a division of JOHN WILEY & SONS, Inc.

605 Third Avenue, New York, New York 10016

In Canada: 22 Worcester Road, Rexdale, Ontario

1 6 N.A. 2514